TRANSPORT PHENOMENA IN ESTUARIES

A Dissertation

Submitted to the Graduate Faculty of the
Louisiana State University and
Agricultural and Mechanical College
in partial fulfillment of the
requirements for the degree of
Doctor of Philosophy

in

The Department of Chemical Engineering

by

Simon Hacker
B,S, in Chem. Engr., Louisiana State University, 1969
M,S. in Chem. Engr., Louisiana State University, 1971

August, 1973

EXAMINATION AND THESIS REPORT

Candidate: Simon Hacker

Major Field: Chemical Engineering

Title of Thesis: Transport Phenomena in Estuaries

Approved:

Ralph W. Pike
Major Professor and Chairman

James L. Graham
Dean of the Graduate School

EXAMINING COMMITTEE:

Philip A Bryant

Bent Hilbert

D P Harrison

Frank A. Iddings

Date of Examination:

April 9, 1973

TO MARTHA

ACKNOWLEDGMENTS

The author is obliged to Dr. Ralph W. Pike for providing the. opportunity to participate in this research project. His guidance and encouragement during the course of this work are deeply appreciated.

Financial support is gratefully acknowledged from the Louisiana State University Sea Grant Program, a part of the National Sea Grant Program which is maintained by the National Oceanic and Atmospheric Administration of the U.S. Department of Commerce.

Gratitude is expressed to the Louisiana State University Sea Grant personnel, especially Mr. Ed Bishop and many others, for the help given during the field data gathering period of this work. The field data made available by Mr. Barney Barrett of the Louisiana Wild Life and Fisheries is highly prized. The time available in the Computer Research Center's IBM 360/65 is appreciated. The author also wished to thank the Dr. Charles E. Coates Memorial Fund, donated by George H. Coates, for financial assistance in the preparation of the manuscript.

Sincere appreciation is extended to Mr. John F. Balhoff for his help and general expertize, Mr. James Callender for his assistance in computer graphics, to Mr. Hasit Trivedi for checking the formulas used, to Ms. Ann Von Brock, Ms. Julianne Justi, Ms. Debbie Blanchard, Ms. Evelyn Jeansonne, and to Ms. Eleanor S. Thibodeaux for their typing under trying conditions.

TABLE OF CONTENTS

PAGE

APPENDICES PAGE

LIST OF TABLES

LIST OF FIGURES

FIGURE PAGE

FIGURE PAGE

FIGURE PAGE

ABSTRACT

Two-dimensional, time-dependent transport equations were developed that predict velocity profiles, tidal fluctuations, and temperature and salinity profiles as a function of time for a coastal bay-salt marsh system when environmental conditions, tidal variations at the passes and fresh water flows into the system are specified. The equations were solved on a digital computer for the Barataria Bay region of coastal Louisiana.

It was found that the Hydrodynamic Model accurately predicted the dynamics of tidal fluctuations and velocity profiles in the Barataria Bay system for marsh areas as well as open waters of the bay. Verification of the analysis was made by comparing with experi¬ mental data measured in the bay and by comparing with results obtained by other investigators in similar bays.

The Energy Transport Model was found to accurately predict the time-varying temperature distributions in the Barataria Bay system for marsh areas as well as open waters of the bay. Verification of the analysis was made by comparing with experimental data measured in the bay and by comparing with results obtained by other investigators in similar bays.

The Materials Transport Model was found to accurately predict the time varying salinity distributions in the Barataria Bay system for marsh areas as well as open waters of the bay. Verification of the analysis was made using comparisons of computed daily-average salinity distributions with measured salinity distributions reported in the literature.

Results are reported for the dynamics of tidal fluctuations, velocity profiles, and salinity and temperature distributions for conditions encountered in May of a typical year (1970). This information demonstrated the range of capability of the analyses and provided a set of reference solutions from the models.

Analysis of the effect of high fresh-water runoff was studied with the models to simulate conditions encountered in a "wet-year." Results were obtained that show the shift in salinity profiles due to increased fresh-water flow into the bay system.

Analysis of the effect of a cold-front was studied with the models to simulate this type of environmental condition that is encountered in early spring and is detrimental to the commercially important species in the bay system. Results show that the effect of the cold front on the water temperature at typical water depths can amount to a 10°F drop within several hours.

Analysis of the effect of a tidal surge from a hurricane like Hurricane Camille was studied. Results are reported that show the shift in salinity distributions as compared with typical conditions and show the high salinity Gulf waters moved into the upper reaches of the estuary.

For the typical conditions studied, it was found that the model reaches a quasi-steady state in three to five tidal cycles. This is in agreement with results of other investigations.

The transport equations were time-averaged, and the terms that arise from the time-averaging were evaluated for the x-component of the equation of motion. It was found that these terms arising from the time-averaging cannot be neglected if the equations are solved since their sum is of the same order of magnitude as the largest other term in the time-averaged equations.

Computer programs of the models are given in a form that can be readily used by engineers and scientists for studies of ecological, design, e.g. salinity control for fisheries management. Users manuals are included with the programs for ease in applying the programs.

NOMENCLATURE

Arabic Characters

A	=	Dimensional Constant = 1,($L^{1/2}$ /T)
B	=	Bowen ratio, dimension less
C	=	Chezy Coefficient ($L^{1/2}$/t)
C*	=	equilibrium concentration, moles/L^3
C_A	=	species A concentration, moles/L^3
C_p	=	heat capacity at constant pressure, per unit mass, L^2/t^2T
D	=	depth of water, D = h + L, L
$\overset{*}{D}_A$	=	binary diffusivity of species A in water, L^2 /t
$\overset{*}{D}_{AX}$	=	diffusivity (x-direction) of species A, L^2 /t
B_{AX}	=	dispersion coefficient (x-direction) of species A, L^2 /t
$\overset{*}{D}_{AY}$	=	diffusivity (y-direction) of species A, L /t
B_{AY}	=	dispersion coefficient (y-direction) of species
E	=	internal energy
E_v	=	rate of evaporation, L/t
e_a	=	water vapor pressure in air, M/L^2
e_s	=	water vapor pressure at surface, M/L^2
F	=	coriolis force parameter
F_n	=	function of
f,f_1,f_2	=	friction factors, dimensionless
g	=	gravitational acceleration, L/t^2

g_i = body force per unit mass of component i, L/t^2

H = E + pVol = enthalpy, ML^2/t^2

h = distance between reference plane and bottom

j_i = mass flux of i relative to mass average velocity, M/L^2t

J_i = molar flux of species i by diffusion, moles/$L\,t^2$

K_i = mass transfer coefficient of species i, moles/tL^2

K, K_1, k*= wind friction coefficients, dimensionless

k = thermal conductivity, $ML/t^3\,T$

L = water height above mean sea level, L

m = total number of species in system

M_i = molecular weight of i, M/mole

N = empirical evaporation constant, See Eq. 3.107, $M^{-1}\,L^2$

n = roughness factor, dimensionless

n_i = mole fraction of species i

p = pressure, M/L^2

P_a = air pressure, M/L^2

$\vec{Q}$ = average discharge rate, L^3/tL

Q = magnitude of the average discharge rate, = $(u^2+v^2)^{1/2}$, L^3/tL

q = heat flux by conduction, ML^2/t^3

q_s = heat flux through the surface of the water, ML^2/t^3

q_{rad} = heat flux by total incoming radiation from the sky, ML^2/t^3

q_{ref} = heat flux by reflection by the water surface, ML^2/t^3

q_w = heat flux by radiation of the water surface, ML^2/t^3

q_e = heat flux due to evaporation, ML^2/t^3

q_c = heat flux due to convection at the water surface, ML^2/t^3

R	=	rainfall rate, L/t
R_h	=	hydraulic radius, L
R_i	=	molar rate of production of species i, moles/tL^3
R_i	=	mass rate of production of species i, M/tL^3
S_A	=	concentration of species A
Se	=	energy slope, dimensionless
SS	=	Sink and Source term
t	=	time, t
T	=	absolute temperature, T
T_{wb}	=	wet bulb temperature, T
v,u,w	=	mass average velocity, L/t
V,U	=	average velocity, L/t
Vol	=	specific volume, L^3/M
W	=	wind velocity, L/t
W_c	=	critical wind velocity, L/t
x	=	rectangular coordinate, L
X	=	wind friction force in the x-direction, M/L^2
y	=	rectangular coordinate, L
Y	=	wind friction force in the y-direction, M/L^2
z	=	rectangular coordinate, L

Greek Characters

α	=	bottom friction factor, dimensionless
β	=	bottom friction correction factor, dimensionless
Δ	=	forward difference operator
δ	=	wind friction constant, dimensionless

$\bar{\bar{\delta}}$ = unit tensor, dimensionless

ε = emissivity, dimensionless

η_i = wind friction factor, dimensionless

θ = angle of wind velocity vector and x-axis, degrees

λ = latent heat of vaporization, L^2/t

μ = viscosity, M/L^3

$\bar{\bar{\pi}}$ = pressure tensor, M/t^2L

ρ = density, M/L^3

σ = Stephen-Boltzman constant, M/t^3T^4

τ = viscous stress, M/t^2L

$\bar{\bar{\tau}}$ = viscous stress tensor, M/t^2L

ϕ = friction force per volume, M/L^3

ω_i = mass friction of I, dimensionless

Overlines

^ = per unit mass

~ = partial molal

$\overline{\quad}$ = averages

$\rightarrow$ = vector quantity

= = tensor quantity

' = instantaneous deviation from the average

Subscripts

A,i = species in the system

a, air = air above body of water under study

b = bottom of lake, benthos

c	=	convection
E	=	Energy
ev	=	evaporation
f	=	at final time
j,k	=	integer position
0	=	at time zero
r, rain	=	rainfall
s	=	surface of the lake
w	=	water
x,y,z	=	rectangular coordinate axes

Superscripts

b, bottom	=	bottom
eddy	=	refers to eddy flow
l, laminar	=	refers to laminar flow
s	=	surface
t, turb	=	refers to turbulent flow

CHAPTER I

INTRODUCTION AND BACKGROUND

Introduction

The purpose of this dissertation is to develop a mathematical model of the momentum, energy, and mass transfer of an estuarine bay system[1]. Particular emphasis will be given to the application of this mathematical model to the Barataria Bay System. This chapter will serve as a

[1] An estuary may be defined as a "semi-enclosed coastal body of water which has a free connection with the open sea and within which seawater is measurably diluted with fresh water derived from land drainage". (Ref. 1.2)

general introduction to the subject of estuarine system analysis and will establish the appropriate ground work for further development in subsequent chapters.

The chapter will consist of three parts: the first will be a discussion of the importance and difficulties of modeling estuarine bays; the second part will be a brief overview of estuarine analysis; and the conclusion will consist of a statement on the objectives of this present research.

The Importance of Modeling Estuarine Bay System

Due to the pressures generated by the population explosion, there is today an ever increasing need for the use of estuarine resources as fountains of economic opportunities, food, and recreational centers. However, this exploitation is not as simple as the use of other physiographical areas; the estuary is a most delicate environment. It terms of primary productivity (Ref. 1.1) it is more efficient than grasslands (nutrient rich, water poor) and oceans (nutrient poor, water rich) due to its ideal balance of constituents. Shallow coastal waters and semi-enclosed areas of the sea can be characterized as always more viable in productivity than the waters of open oceans in the same latitudes. Estuaries are nutrient traps and thus provide a surplus of usable fuel to the life it supports. However, just as they accumulate nutrients, they can, and do accumulate pollutants (Ref 1.2). This characteristics, coupled to the high rate of primary productivity gives the estuary its delicate balance.

Coastal waters and estuaries are of great importance to the world population that uses these waters in a variety of ways, some of which are in conflict. Ever since antiquity, seaports have been the centers of civilization. In the United States, more than half the population lives in the coastal states, including those bordering the Great Lakes. A major share of the world's marine fisheries is obtained from coastal waters, and estuaries are essential as breeding grounds for many species of coastal fishes as well as serving as home for many seafood delicacies. Unfortunately, these waters are also used for the disposal of the waste products of civilization; a use conflicting with fisheries and recreational demands that exist in these areas. The pollution of many estuaries is so intense that some species have been locally eliminated while others are unfit for human consumption (Ref. 1.3).

The state of Louisiana is a good example to show the importance of estuaries to the economy of coastal states. Forty-five percent of Louisiana's surface consists of coastal and flood plain wetlands. This area contains eighty percent of the state's manufacturing capability and seventy-five percent of its population. Most of the state oil, sulfur, and salt production come from offshore and coastal waters. Louisiana contains more than five million acres of coastal marshes, swamps, and estuaries. As more than two million of these acres are considered to be important habitat areas for fish and wildlife, Louisiana ranks first among all states in area of important estuarine habitat. Shrimp utilize the estuaries as nursery grounds, and Louisiana consistently ranks first or second in shrimp production. In 1969, the state had a production of more than a million pounds of headless shrimp having a dockside value In excess of $33,400,000. Louisiana, the

only state where oysters are harvested the year round, supplies twenty percent of the total U.S. market. Ten to fifteen million pounds of oysters are produced annually. The total annual value of all fishery operations is in the $100 to $150 million range, and total production of all species often exceeds one billion pounds annually. Fur and meat products provided by animals of the estuarine habitat are a several-million-doliar per year business (Ref. 1.4).

The importance of the salt marshes cannot be denied. Nevertheless, man is slowly but surely encroaching on these previously untouchable areas. Airports, highways and residential developments are sprouting around estuaries, and thus, this delicate system is threatened and something must be done. Here, the alarmist steps in and announces the unavoidability of the coming doom unless something is done immediately. The eco-politician, in order to protect his office from the wave of public furor, gives money to the nearest scientist so that he can do something to save the estuaries. The nearest scientist is, unfortunately, a botanist-zoologist-ecologist who has spent his life applying his abilities to the estuaries. His work in the marsh is best summarized by Hitchcock (Ref. 1.5):

> ---"collecting, weighing and measuring every plant and animal from specific areas that had been previously staked out in square meters".

So with new and extensive funding, the botanist-zoologist-ecologist multiplies his previous efforts. Clearly, extensive cataloging is not the total answer to the problem. The complexity of an ecosystem, the estuary in particular, is staggering; and the best way to cope with this difficulty is to use systems analysis. This approach is so obvious that many of the present studies on environmental phenomena are based on systems analysis. However, several other factors have made system analysis the panacea of problems in environmental management; the oversupply of systems analysts caused by the aerospace business breakdown and the willingness of government to fund this type of research have significantly contributed to the proliferation of natural systems modeling and analysis.

Until recently, man considered the growth of population, industry and gross national product to be the goal of civilization. Now recognition is being given to the fact that uncontrolled growth leads to disaster. The key to the best management of our resources lies in good planning (Refs. 1.5, 1.6, 1.7). Increasing are the ranks of those who recognize that the stresses placed upon the environment are such that nature cannot recover without help. It is not too late to save the undamaged environments and to recover some of the lost quality of the damaged environments. In spite of his magnificent achievements, the man of today, in contradistinction of past civilizations which are called primitive and savage by the egocentric western culture, has not learned to live in harmony with his environment. Unless he does, he will have the dubious honor of joining, prematurely, the fraternity of the extinct.

Estuarine Analysis

In our so called “laissez-faire” society, industry has always tried to maximize its profit. To do so, it has turned to the use of optimization techniques. Today's complicated processes are not amenable to "off the cuff" optimization, so industry has resorted to the use of powerful analytical tools in order to obtain the answers to its problems. One of these is the mathematical model. A mathematical model is a set or sets of related equations in which the important variables of the system to be studied are included. Once a system is described by an adequate mathematical model, it can be studied by the manipulation of the model rather than by actual experimental work. For example, if a change in the independent variables is known, it is possible to predict the behavior of the system being modeled. Workers in industry use mathematical models of processes in order to predict optimum working conditions and hence to maximize profits. This same idea can be applied to the management of natural environments.

There are living and nonliving factors in a natural environment. From the integration of these factors, an ecosystem results. In other words, an ecosystem is a complex of organisms and environment forming a functioning whole in nature. As the reader can realize, because of the great number of varying parameters and relationships existing in a given ecological system, development of an exact mathematical model of even the sma1lest, simplest ecosystem is a monumental task. However, quite often a simplified mathematical model using only important parameters can be developed which will adequately describe the system for the purpose under investigation.

In the mathematical modeling of aquatic ecological systems, the modeling of the abiotic component (the nonliving environment) is important. The abiotic factor plays a more important role in the aquatic ecological system than in its terrestrial counterpart. The physical (abiotic) model is combined with the biological model to form the complete mathematical model of the given aquatic environment. One example of this is the systems analysis for Barataria Bay (see Fig. 1.1). Optimization techniques can be used with the complete mathematical model; thus, the meaningful management decisions that are so badly needed today, can be made on the region of interest.

Statement of Objectives

The main objective of the current study is to develop a mathematical model of the transport phenomena that occur in estuarine bays, with particular emphasis on the Barataria Bay System. Specifically, the following models will be developed:

1. A Hydrodynamic Model that will describe velocity profiles and tidal fluctuations in the region of study.

2. An Energy Transport Model that will describe temperature distributions and energy transport.

3. A Materials Transport Model that will be used to describe salinity distribution and mass transport in the estuary. Also this model, with proper data, can be used to describe the

transport of any given species such as dissolved oxygen (DO), biological oxygen demand (BOD), and phytoplankton.

These models will be subsequently refined and coupled to other models, as shown in Fig.1.1, to obtain an overall model of Barataria Bay.

The following chapter will consist of a detailed review of previous literature on estuarine analysis, and a critique on previous models will be presented.

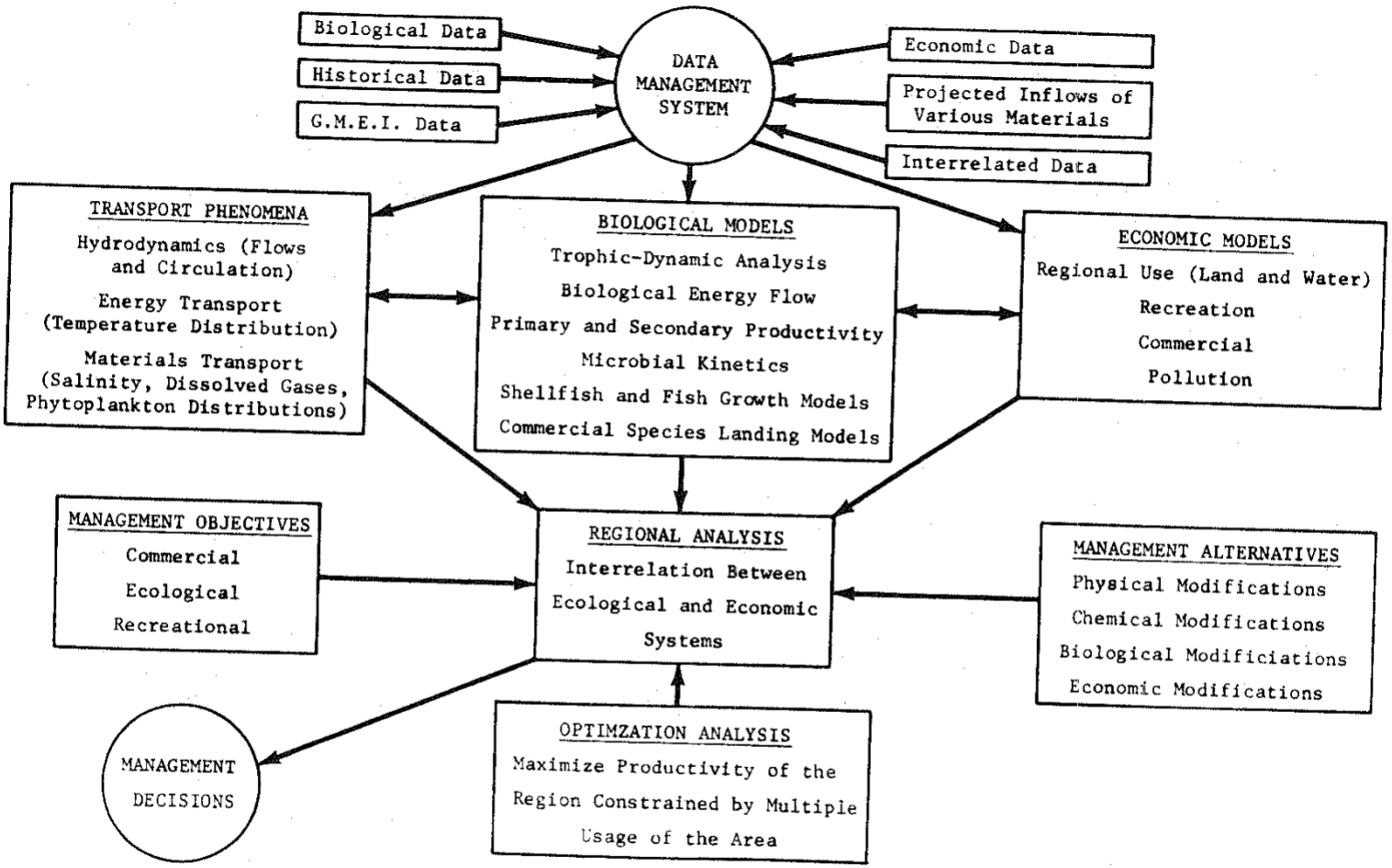

Figure 1.1. Systems Approach for Quantitative Regional Analysis. (Ref. 1.9)

REFERENCES

1.1 Patten, B. C. , Ed,, Systems Analysis and Simulation in Ecology, Academic Press, New York, New York (1971).

1.2 Russell-Hunter, W. D. , Aquatic Productivity, The MacMillan Company, New York, New York (1970).

1.3 Matthews, W. H., F. E. Smith and E. D. Goldberg, Eds., Man's Impact on Terrestrial and Oceanic Ecosystems, The M.I.T. Press, Cambridge, Mass, (1971).

1.4 Van Lopik, J. R., "Graduate Study in Marine Science at Louisiana State University", Coastal Studies Bulletin No. 6, Louisiana State University, Baton Rouge, La. (1971).

1.5 Hitchcock, S. W., Can We Save Our Salt Marshes?, National Geographic, Vol. 141, No. 6, pp. 729-765 (June 1972).

1.6 Brahtz, J. F., Ocean Engineering, John Wiley and Sons, Inc. New York, New York (1968).

1.7 Brahtz, J. F, , Ed. Coastal Zone Management, John Wiley and Sons, Inc., New York, New York (1972).

1.8 Watt, K. E., Ecology and Resource Management, McGraw-Hill Inc., New York, New York (1970).

1.9 Hacker, S., R. W. Pike and B. Wilkins, Jr., "Analysis of the Energy, Mass and Momentum Transfer in the Louisiana Coastal Marsh Region", Coastal Sutdies Bulletin No. 6, Louisiana State University, Baton Rouge, Louisiana (1971).

CHAPTER II

A REVIEW OF PREVIOUS ANALYSES IN ESTUARINE SYSTEMS

Introduction

It is the purpose of this chapter to review the previous works on estuarine analysis that have significant relationship with the current work. To introduce this subject in the proper perspective, the first part of this chapter will be a description of the historic development of the equations used to model two-dimensional estuarine transport phenomena. The second part will consist of a

discussion on the existing work on two-dimensional-time dependent models followed by a brief discussion on works for one-dimensional models. The fourth part will consist of a prediction on the possible future of estuarine modeling, and the chapter will be concluded with a statement of the contributions that the current work will make to the state of the art.

Historic Development of the Two-Dimensional Estuarine Systems Transport Phenomena Equations

The general equations that describe transport phenomena have long been known and are commonly found in the pertinent literature (Ref. 2.1). However, application of these equations to the estuarine bays in question without any simplifying assumptions are beyond the power of existing analytical or numerical methods to arrive at a solution. The first and most logical modification is to reduce the curse of dimensionality by assuming that the phenomena under study is characterized by two-dimensional behavior. In the case of shallow estuaries, this assumption is justifiable. The vast expanses of brackish waters that cover several hundred square miles of estuarine systems found commonly in the East and Gulf Coasts of the United States are seldom deeper than twenty feet, and depths greater than these are only found in proximity of the connection between the estuary and the ocean. The modeling of the momentum transport of shallow waters with a two-dimensional hydro-dynamic model was first proposed by Hansen in 1938 (Ref. 2.3). However, the computer hardware necessary to effectively carry out the numerical techniques needed to arrive at a solution was not available at the time. With passing time, the necessary computers became available and the models first proposed in 1936 came into being and the predecessor of today's estuarine models was presented by Hansen in 1956 (Ref. 2.4). All of the existing hydrodynamic models for shallow waters, or long-wave equations as they are sometimes called, derive from Hansen's model. As time progressed, so did the number of hydrodynamic models presented in the literature. Models were presented by Platzman in 1958 (Ref. 2.5), Miyazaki (Ref. 2.6) and Unoki and Isozaki (Ref. 2.7), both in1963, a further refinement by Hansen (Ref. 2.8) in 1966, Leendertse (Ref. 2.9) in 1967 and Reid and Bodine (Ref. 2.10) in 1968.

As the modeling of natural systems increased due to ecological concern, hydrodynamic models, which previously were only used to model storm surges, were used as a basis for an overall transport phenomena model in estuaries. The first suggestion of this idea in the literature was a proposed Systems Analysis of Galveston Bay in a report by TRACOR (Ref. 2.11) in 1968. Later on, based on the assumptions made earlier by Hanson, two-dimensional energy and species transport model derivations were presented by Leendertse (Ref. 2.12) in 1970, and Hacker, Pike, and Wilkins (Ref. 2.13) in 1971. An applied two-dimensional model fully describing transport phenomena in a shallow estuary was first reported by Leendertse (Ref. 2.12) also in 1970. Other studies in which hydrodynamics is applied with energy and species models are TRACOR (Ref. 2.14) and Masch (Ref. 2.15), both in 1971.

Two-Dimensional Estuarine Systems Models

The study of existing two-dimensional estuarine models can be divided into three parts. The first part is the work done on hydrodynamic models, or the long wave equations. The second part consists of the work done on modeling of the energy and mass transport phenomena that occurs in shallow estuaries. The third and last part discusses the numerical techniques applied to the model equations in order to obtain a solution.

Hydrodynamic Models

Up to 1968, all of the modeling done on shallow estuaries were studies on the transport of momentum. All these hydrodynamic models were based on a derivation done by Hansen (Ref. 2.4). The latest and most sophisticated of the hydrodynamic models was presented by Leendertse (Ref. 2.9) in 1967. The advantage of this model is due to the numerical technique used for solution, an advanced alternating direction implicit (ADI) technique. This technique is superior to the explicit techniques used on all the other hydrodynamic models that have the same equations as a basis. The long wave equations were obtained by Hansen by vertically integrating the general equations of motion and continuity. These vertically integrated equations are:

$$\frac{\partial U}{\partial t} + U\frac{\partial U}{\partial x} + V\frac{\partial U}{\partial y} - FV + g\frac{\partial L}{\partial x} = \frac{1}{\rho}(\tau_x^s - \tau_x^b) \qquad (2.1)$$

$$\frac{\partial V}{\partial t} + U\frac{\partial U}{\partial y} + V\frac{\partial V}{\partial y} + FU + g\frac{\partial L}{\partial y} = \frac{1}{\rho}(\tau_y^s - \tau_y^b) \qquad (2.2)$$

$$\frac{\partial L}{\partial t} + \frac{\partial (DU)}{\partial x} + \frac{\partial (DV)}{\partial y} = (R-Ev) \qquad (2.3)$$

Leendertse used the above equations, as summarized in Tables 2.1 and 2.2, to produce his hydrodynamic model that was later on used in conjunction with a species transport model in order to predict water quality in Jamaica Bay, New York.

Reid and Bodine (Ref. 2.10) in 1968 simplified the long wave equations to produce a model of Galveston Bay used to predict storm surges. This model used empirical correlations to correct for flow conditions due to submerged barriers, weirs and tidal inputs. The equations used are summarized in Tables 2.1 and 2.2. When compared to Leendertse's Model, this one ignores Coriolis forces, advection of momentum, and uses a quadratic bed resistance based on the Manning's coefficient as opposed to Leendertse's Chezy's coefficient. Also it uses an explicit "leap frog" technique to obtain a numerical solution. Even though this numerical technique is not

TABLE 2.1

HYDRODYNAMIC MODELS

Equation of Continuity[1]

Investigator	$\frac{\partial L}{\partial t} + \frac{\partial (DU)}{\partial x} + \frac{\partial (DV)}{\partial y} = R - Ev$				
Leendertse (Ref. 2.9)	X	X	X		
Reid and Bodine (Ref. 2.10)	X	X	X	X	
Masch, et al (Ref. 2.17)	X	X	X	X	X
Miyazaki, Ueno and Unoki (Ref. 2.18)	X	X	X		
Unoki and Isozaki (Ref. 2.7)	X	X	X		
Miyazaki (Ref. 2.6)	X	X	X		
Platzman (Ref. 2.5)	X	X	X		
Hansen (Ref. 2.4)	X	X	X		

[1] The equations used in the works referenced are formed by adding the terms that have been checked.

TABLE 2.2

HYDRODYNAMIC MODEL

Equation of Motion
(X-Component)

Investigator	$\frac{\partial U}{\partial t}$	$+ U \frac{\partial U}{\partial x}$	$+ V \frac{\partial U}{\partial y}$	$- FV$	$+ g \frac{\partial L}{\partial x} =$	$\frac{\tau_x{}^s}{\rho}$	$- \frac{\tau_x{}^b}{\rho}$
Leendertse (Ref. 2.9 and 2.12)	X	X	X	X	X	$KW \cos\theta^{(+)}$	$gU \frac{(U^2 + V^2)^{\frac{1}{2}}}{C^2}$
Reid and Bodine (Ref. 10)	X				X	$KW^2 \cos\theta^{(+)}$	$fU \frac{(U^2 + V^2)^{\frac{1}{2}}}{D^2}$
Masch, et al (Ref. 2.17)	X			X	X	$KW^2 \cos\theta^{(+)}$	$fU \frac{(U^2 + V^2)^{\frac{1}{2}}}{D^2}$
Miyazaki, Ueno and Unoki (Ref. 2.18)	X			X	X	$p_a Y^2 W\|W\|^{(*)}$	$\alpha V\|V\| - \beta(\tau^s/\rho)^{(**)}$
Unoki and Isozaki (Ref. 2.7)	X			X	X	$p_a Y^2 W\|W\|^{(*)}$	$-\frac{\tau^s/\rho}{2} + \frac{3\mu(U^2+V^2)^{\frac{1}{2}}}{D^2}{}^{(***)}$
Miyazaki (Ref. 2.6)	X			X	X	$p_a Y^2 W\|W\|^{(*)}$	$\alpha V\|V\| - \beta(\tau^s/\rho)^{(**)}$

TABLE 2.2

(continuation)

Investigator	$\frac{\partial U}{\partial t} + U\frac{\partial U}{\partial x} + V\frac{\partial U}{\partial y} - FV + g\frac{\partial L}{\partial x} = \tau_x^s/\rho - \tau_x^b/\rho$						
Platzman (Ref. 2.5)	X				X	$K^* \rho \int D^{-1} \overline{R} \cdot \overline{M}^{(o)} dx$	
Hansen (Ref. 2.4)	X	X	X	X	X	$\eta \cdot W\|W\|^{(oo)}$	$r \cdot U\|U\|^{(ooo)}$

(+) $K=K_1$ $W \leq W_c$ - critical wind speed = 14 knots

$K=K_1 + K_2(1 - \frac{W_c}{W})^2$ $W \geq W_c$ $K_1 = 1.1*10^{-6}$ $K_2 = 2.5*10^{-6}$

(*) $\gamma^2 = 2.6*10^{-3}$

(**) $\alpha = 2.6*10^{-3}$ $\beta = 0.25 \sim 0.50$

(***) μ = coefficient of eddy viscosity (numerical value not reported)

(o) $K^* > 1$, $\overline{M} \equiv \int v dz$, $\overline{R} \equiv T(h)/\rho$, $T(h)$ = surface stress by wind (not reported)

(oo) $\eta = 3.2*10^{-6}$

(ooo) $r = 2.6*10^{-3}$

as advantageous as ADI, Reid and Bodine's Model compares well with Leendertse's Method. This conclusion was obtained by Sobey (Ref. 2.16) when several numerical methods to solve the long wave equations were compared by him in 1970.

Masch, et. al., (Ref. 2.17) presents a hydrodynamic model identical to the Galveston Bay Model by Reid and Bodine except that he includes the Coriolis force terms. Masch uses this model as a basis for a salinity model of the San Antonio and Matagorda Bays in Texas (Ref. 2.15).

Miyazaki, Ueno, and Unoki (Ref. 2.18), in 1962, developed a hydrodynamic model based on the long wave equations in which advection of momentum was ignored. This model was used to investigate typhoon surges along the Japanese coast. In this study, special care was given to analyze wind generated currents. Using this work as a base, Unoki and Isozaki (Ref. 2.7) in 1963 studied the effects of storm surges caused by typhoons on a dike with openings in Tokyo Bay. In this work, empirical equations to calculate the flow through the opening of a dike were developed. It was later on that Reid and Bodine used this work to arrive at a series of empirical equations for flow uses in their Galveston Bay Model. Miyazaki (Ref. 2.6) also used the same equations to produce a model to study the effects of Hurricane Carla 1961 in the Gulf of Mexico. The equations used by the past three works mentioned are summarized on Tables 2.1 and 2.2. The numerical technique these works use is the "leap frog" explicit.

Platzman (Ref. 2.5) in 1958, developed a model to study the surge of June 26, 1954 on Lake Michigan. The main forcing function on this model was a drastic change in atmospheric pressure due to an intense and fast-moving squall line. This model describes the surge generated by this pressure gradient and is the only one found in the literature that uses atmospheric pressure gradients as a forcing function. All of the other hydrodynamic models have tidal variation as a forcing function, and most ignore atmospheric pressure effects. It was in this work that Platzman developed the explicit "leap frog" numerical technique used by most of the recent investigators. The equations used by Platzman in his model are summarized in Tables 2.1 and 2.2.

Hansen (Ref. 2.4) in 1956 crystallized the idea he first presented in 1938 (Ref. 2.3) of vertically integrating the equations of motion and continuity to produce a two-dimensional hydrodynamic model, or the long-wave equations. He used his model, in conjunction with a rudimentary explicit numerical scheme, to predict hydrodynamic behavior in open shallow seas. Coriolis forces and advection of momentum were considered in this model. The equations used are summarized in Tables 2.1 and 2.2.

The following part of this chapter will deal with the equations used in conjunction with the hydrodynamic model in order to produce energy and mass transfer models for shallow estuaries.

Energy and Species Transport Models

The idea of using hydrodynamic models of shallow estuaries in conjunction with models of the energy and mass transport was first reported and developed by TRACOR (Ref. 2.11) in 1968. Even though it was logical to derive the energy and species transport two-dimensional model from the general equations of energy and species continuity just as Hansen derived his hydrodynamic model from the general equations of change, this was not done until Leendertse (Ref. 2.12) presents a mathematical derivation in 1970. This model by Leendertse is used for water quality prediction in Jamaica Bay, New York, and is the best of the existing models for species

transport phenomena. Leendertse derives only the species transport equation as his water quality model is not concerned with energy transport. Using his previous (Ref. 2.9) hydrodynamic model which uses an alternating direction implicit (ADI) numerical scheme, Leendertse developed his water quality model using the same advanced numerical technique. This combination gives the best species transport model reported in the literature. The vertically averaged species continuity equation is:

$$\frac{\partial(DS)}{\partial t} + \frac{\partial(DUS)}{\partial x} + \frac{\partial(DVS)}{\partial y} = \frac{\partial}{\partial x}\left(D\mathfrak{D}_{sx}\frac{\partial S}{\partial x}\right) + \frac{\partial}{\partial y}\left(D\mathfrak{D}_{sy}\frac{\partial S}{\partial y}\right) + SS \qquad (2.4)$$

Leendertse's vertically averages species continuity equation is also summarized in Table 2.3. The first mathematical derivation of the vertically averaged energy equation was given by Hacker, Pike and Wilkins (Ref. 2.13) in 1971. This equation is, logically, analogous to the vertically averaged species continuity equation and can be written as:

$$\rho C_p\left[\frac{\partial(DT)}{\partial t} + \frac{\partial(DUT)}{\partial x} + \frac{\partial(DVT)}{\partial y}\right] = \frac{\partial}{\partial x}\left(Dk_x\frac{\partial T}{\partial x}\right) + \frac{\partial}{\partial y}\left(Dk_y\frac{\partial T}{\partial y}\right) + SS \qquad (2.5)$$

and is shown in Table 2.4.

TRACOR (Ref. 2.14) in 1971 presented a model for energy and mass transfer for shallow estuaries. This work, combined with their hydrodynamic model (Ref. 2.11), produced a combined transport model. In this combined model, the species continuity equation was solved by using a simplistic explicit technique and the energy transport equation was also solved by neglecting convective terms reducing the problem to zero dimension. The equations used by TRACOR in this work are summarized in Tables 2.3 and2.4.

Masch (Ref. 2.15) presented a hydrodynamic and salinity model for San Antonio and Matagorda Bays, Texas in 1971. The hydrodynamic model is solved similarly to the one presented by TRACOR (Ref. 2.14). The salinity model is solved by the alternating direction implicit scheme, similarly to Leendertse (Ref. 2.12), The advantages of solving the salinity model with the implicit scheme are lost due to the fact that the input velocities used were generated by an explicit technique and thus the salinity model is limited to the conditions set for the hydrodynamic model. The energy equation was not solved in this work. The equation used is summarized in Table 2.3.

Numerical Techniques

Numerical techniques used for the solution of vertically averaged two-dimensional models for momentum, energy and mass transfer can be broadly classified in two groups; explicit schemes and implicit schemes. Until 1967, only explicit schemes were used to solve the

TABLE 2.3

SPECIES TRANSPORT MODEL

Investigator	$\frac{\partial(DS_A)}{\partial t} + \frac{\partial(UDS_A)}{\partial x} + \frac{\partial(VDS_A)}{\partial y} - \frac{\partial}{\partial y}(D\mathcal{D}_{A_x}\frac{\partial S_A}{\partial x}) - \frac{\partial}{\partial y}(D\mathcal{D}_{A_y}\frac{\partial S_A}{\partial y}) - DSS_A = 0$					
Leendestse (Ref. 2.9)	X	X	X	X	X	X
Tracor (Ref. 2.11)	X	X	X	X	X	X
Masch (Ref. 2.14)	X	X	X	X	X	X

TABLE 2.4

ENERGY TRANSPORT MODEL

Investigator	$\rho C_p \frac{\partial(\bar{T}D)}{\partial t} + \frac{\partial(UD\bar{T})}{\partial x} + \frac{\partial(VD\bar{T})}{\partial y} - \frac{\partial}{\partial x}(Dk_x \frac{\partial \bar{T}}{\partial x}) - \frac{\partial}{\partial y}(Dk_y \frac{\partial \bar{T}}{\partial y}) - DSS_E = 0$					
Tracor (Ref. 2.11)	X	X	X	X	X	X
Hacker, et. al. (Ref. 2.13)	X	X	X	X	X	X

long-wave equations. While some differences exist among the techniques used by the different investigators, the explicit schemes used were basically the same. The explicit numerical technique used with the hydrodynamic models is best exemplarized by the work of Reid and Bodine(Ref. 2.10). The area under study is placed under a square grid system with a rough approximation of the irregular boundaries, as shown in Fig. 2.1. The partial differential equations that form the hydrodynamical model are transformed into difference equations with the substitution of difference approximations for the partial derivative terms. The difference approximation used, due to their "leap-frog" pattern, is the central difference approximation. Reid and Bodine did this, and the resulting algebraic equations were arranged so that the unknowns are the velocities and water levels of the subsequent time step. These equations are:

$$U_{i+1,j} = \frac{1}{G_{1i,j}} \left[U_{i+1,j} + \frac{g\Delta t}{2\Delta x} (D_{i+1,j} + D_{ij})(L_{i,j} - L_{i+1,j}) + x_{i+1,j}\ \Delta t \right] \tag{2.6}$$

$$V_{i,j+1} = \frac{1}{G_{zi,j}} \left[V_{i,j+1} + \frac{g\Delta t}{2\Delta y} (D_{i,j+1} + D_{i,j})(L_{i,j} - L_{i,j+1}) + y_{i,j+1}\ \Delta t \right] \tag{2.7}$$

where:

$$D_{i,j} = h_{i,j} + L_{i,j} \tag{2.8}$$

$$G_{1i,j} = 1+f\Delta t\left\{\left[4U_{i+1,j}\right]^2+ \left[V_{i,j} + V_{i+1,j} + V_{i+1,j+1} + V_{i,j+1}\right]^2\right\}^{\frac{1}{2}} * (D_{i,j} + D_{i+1,j})^{-2} \tag{2.9}$$

$$G_{2i,j} = 1+f\Delta t\left\{\left[4V_{i,j+1}\right]^2+ \left[V_{i,j} + V_{i+1,j} + V_{i,j+1} + V_{i+1,j+1}\right]^2\right\}^{\frac{1}{2}} *(D_{i,j} + D_{i,j+1})^{-2} \tag{2.10}$$

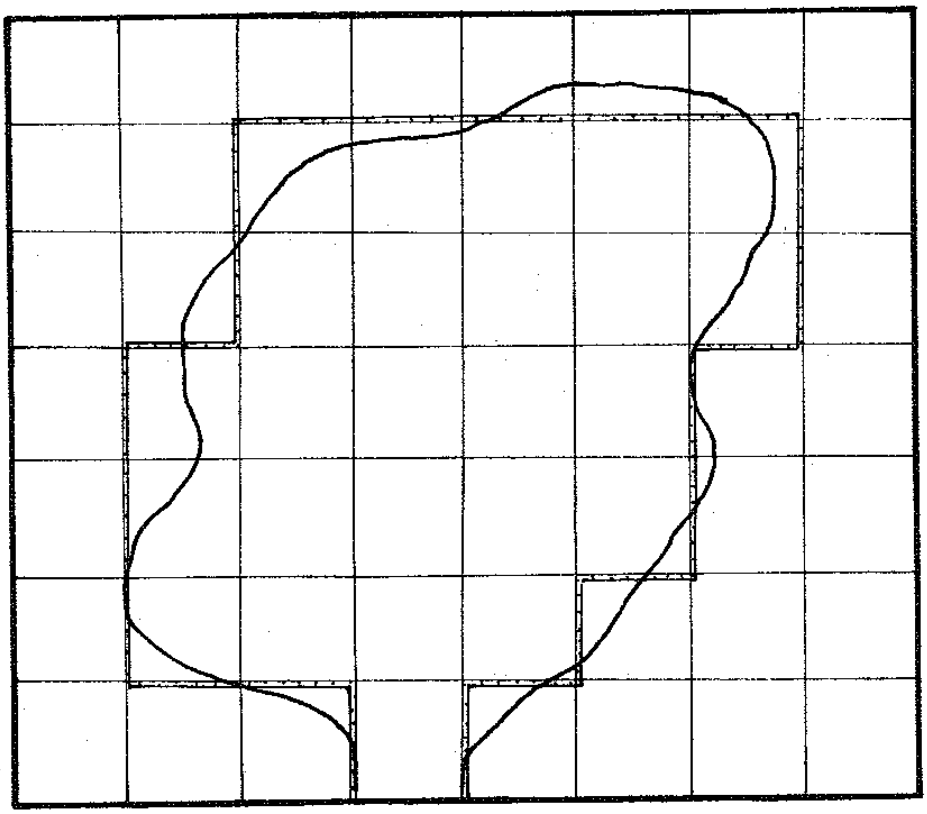

Figure 2.1. Square Grid Over Irregularly Shaped Bay.

The values used are stored as shown in Fig. 2.2 and the solution advances as shown in Fig. 2.3. Care had to be taken when special barriers appear. The numerical equations are appropriately modified for islands, submerged barriers, open sea connections, etc. For further explanation, see Ref. 2.10.

Explicit schemes suffer from the disadvantage that they are conditionally stable. Platzman (Ref. 215) classified the long-wave equations as of the hyperbolic type. While this system of three partial differential equations cannot be mathematically classified, Platzman assumed that the two-dimensional long-wave equations behave as the one-dimensional system. With this assumption, the long-wave equations can be classified as of the hyperbolic type. This proof is shown in Appendix A. Subsequent researchers seemed to go along with this assumption. With this, the stability criterion for the above scheme can be obtained, and it is

$$\Delta t < \frac{\Delta S}{\sqrt{2gD_{max}}} \quad ; \quad \Delta S = \Delta x = \Delta y \qquad (2.11)$$

This condition puts a severe cost on long, real-time solutions as computer time is extensive. All hydrodynamic models used similar explicit techniques with the exception of Leendertse (Ref.2.9). All energy and species models presented also use numerical techniques similar to the one presented above with the exception of Leendertse (Ref. 2.12) and Masch (Ref. 12.15).

Implicit schemes for vertically averaged equations of change are difficult to obtain. It was not until 1967 that Leendertse presented an implicit scheme for solving the long-wave equations. The advantage of this technique over the explicit one is its inherent stability and rapid convergence. Leendertse (Ref. 2.9) proved the stability and convergence of his alternating direction implicit scheme. This numerical technique is presented in Chapter IV. An identical scheme was used by Leendertse to solve the species continuity two-dimensional model for Jamaica Bay, New York (Ref. 2.12). The vertically averaged species continuity and energy equations are of the parabolic type and alternating direction implicit schemes are ideally suitable for their solution. Masch also used this technique for modeling salinity in the San Antonio and Matagorda Bays, Texas (Ref. 2,15). This numerical technique is shown for the vertically averaged species continuity equation in Chapter IV.

The combination of the hydrodynamic model and the energy and species transport models with the appropriate numerical technique results in a numerical transport model of the area under study. The validity of these models has been established in the literature (Refs. 2.5, 2.8, 2.9, 2.10, 2.12, 2.14). Naturally, certain specific conditions change from area to area and appropriate parameters have to be specified for a given area to be studied.

There are studies in which the two dimensions under study form a vertical instead of a horizontal plane. These studies refer to vertically stratified estuaries and are an extension of one-dimensional models. These have been reviewed by Harleman and Ippen (Ref. 2.22) and are not pertinent to this study.

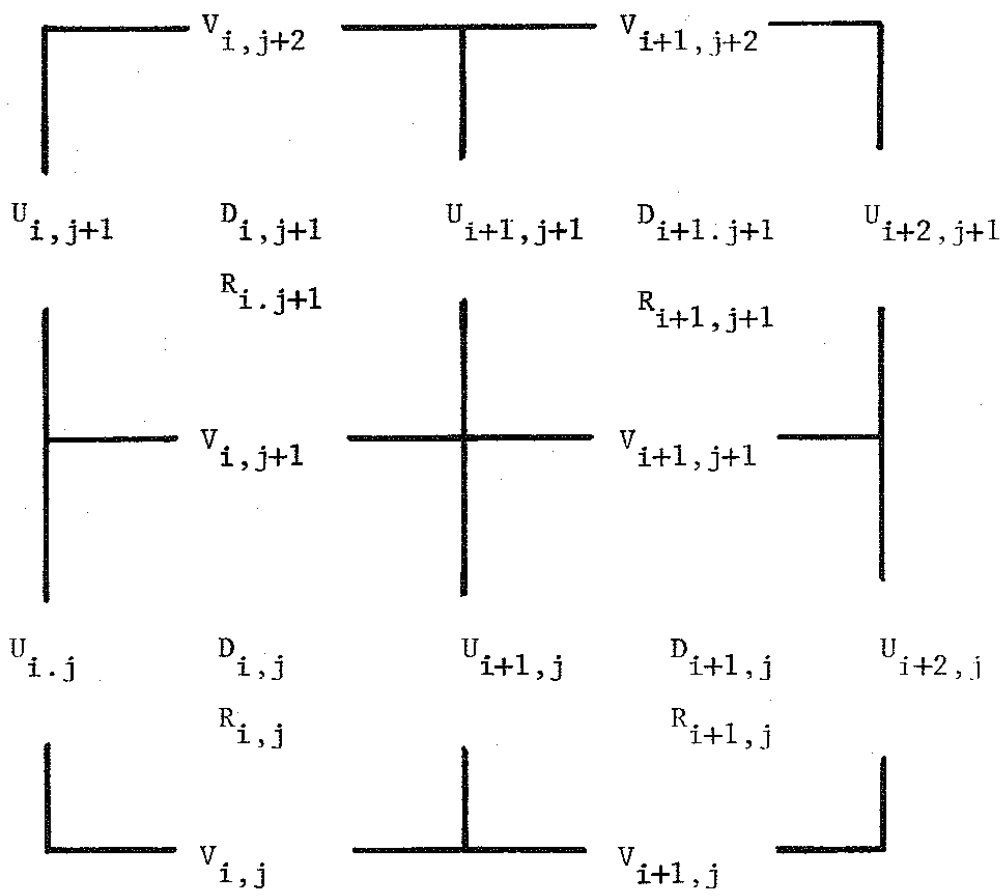

Figure 2.2. Schematic Showing Variable Grid Point Location.

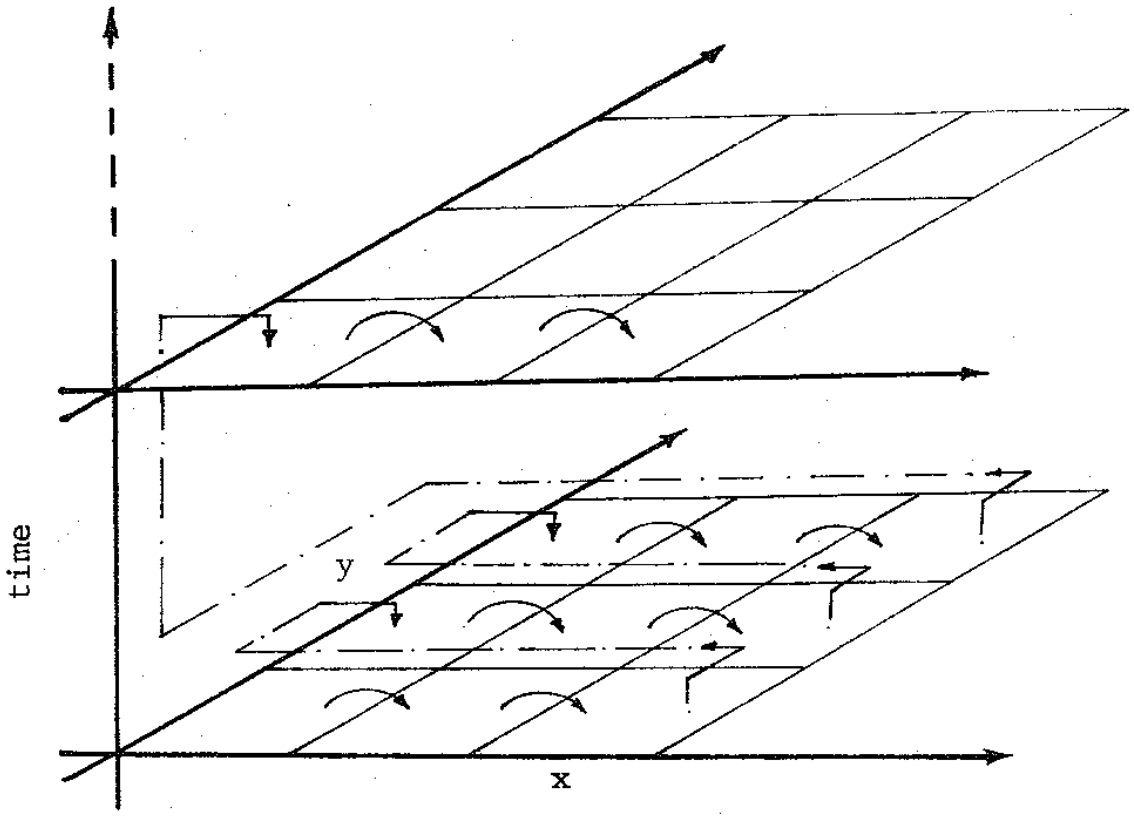

Figure 2.3. Explicit "Leap-frog" Solution March.

One-Dimensional Estuarine Systems Models

With the exception that both are used to model estuaries, there is very little in common between one-dimensional and two-dimensional estuarine models. One-dimensional models reported have not been derived by mathematical modifications of the general equations of change, and they are simply obtained from basic principles by ignoring the depth and width variations. Thus, they have only variations in the one dimension of length along the estuary or river. This simplification makes analytical solution possible in some cases. Most of the concern in one-dimensional estuarine studies is the modeling of mass transfer in long and narrow estuaries especi¬ ally for dissolved oxygen, BOD etc. The wide, shallow estuaries cannot be accurately modeled with one-dimensional equations. One-dimensional modeling is represented by the works of Pritchard (Refs. 2.2, 2.20, 2.21, 2.22), Harleman (Refs. 2.23, 2.23, 2.25, 2.26), Ippen (Refs. 2.27, 2.28, 2.29) and Holley (Refs. 2.30, 2.31).

Future Estuarine Modeling

Three-dimensional models (Ref. 2.32) will come into being with faster and larger memory computers. However, the increased accuracy obtained by three-dimensional models could be considered a luxury in many cases. Modeling of estuaries is usually done either to predict water quality or as a part of an overall system analysis (See Fig. 1.1). Solutions for long time periods are of more importance than increased resolution in the spacial dimensions. Estuarine models today give results that have not been bettered by experimental measurements. The need to model long term variations is great. The natural scientist is interested in seasonal and yearly variations, and to obtain these results with today's models is excessively time-consuming. The obvious answer is to produce a time-averaged model that can take large time steps. However, the difficulties of this procedure have not yet been resolved (See Appendix C). A seasonal estuarine model is the future step in shallow coastal waters systems analysis.

Contributions

In order to produce better two-dimensional estuarine models, a deeper understanding of the equations involved is needed. Nowhere in the literature, with the exception of Ref. 2,13, are the equations for the vertically average models adequately derived. Also, all the models presented are concerned with either storm surges or water quality existing in given bays. There are extensive estuaries especially in the Gulf Coast, and these marshes are flushed regularly with the tides. This process has been treated in. the literature as flooding of tidal flats. It is of interest to the biologist to know the flow patterns and species transport in these areas, as it is here that the high primary productivity that is characteristic of the estuary takes place. Barataria Bay, the estuary this work is concerned with, is a complex and vast body of water. This area is being studied, and the main thrust of this work is to develop vertically averaged transport models that will become part of the system analysis. To summary this work will:

1. Rigorously derive the vertically averaged equations that describe the momentum, energy and mass transfer in a shallow estuary.

2. Develop and verify a transport model, using the above mentioned equations that describe water level variations, velocity profiles, temperature and salinity distributions in Barataria Bay.

3. Include in the above mentioned model, the marshes that surround the main body of water of Barataria Bay.

4. Present results of the above mentioned model for typical and atypical conditions on the Barataria Bay estuary.

REFERENCES

2.1 Bird, R.B., W.E Stewart, and E.N. Lightfoot, Transport Phenomena, Wiley and Sons, Inc., New York, N.Y. (1960), pp. 75, 84, 318 and 559.

2.2 Pritchard, D.W., "Dispersion and Flushing of Pollutants in Estuaries," Journal of Hydraulics Division of the ASCE, 95: NY7, Proc. Paper 6334 (Jan. 1969), pp. 115-124.

2.3 Hansen, W., "Amplitudenverhaltnis und Phasenunterschied der Harmonischen Koxistanten in der Nordsee," Ann, d. Hydr. u Marit. Met., 66 (9), (1938), pp. 429-443.

2.4 Hansen, W., "Theorie zur Errechnung des Wasserstandes und der Stromungen in Randmeeren nebst Anwedungen," Tellus, Vol. 8, No. 3, (1956), pp. 287-300.

2.5 Platzman, G.W., "A Numerical Computation of the Surge of 26 June 1954 on Lake Michigan," Geophysics, Vol. 6, (1958), pp.407-438.

2.6 Miyazaki, M., "A Numerical Computation of the Storm Surge of Hurricane Carla 1961 in the Gulf of Mexico," Technical Report No. 10, Dept. of Geophysical Sciences, University of Chicago, Chicago, 111.

2.7 Unoki, S. and I. Isozaki, "On the Effect of a Dike with Openings on the Storm Surge Caused by a Typhoon," Coastal Engineering in Japan, Tokyo, Vol. 6, (1963), pp. 57-65.

2.8 Hansen, W. , "The Reproduction of the Motion in the Sea by Means of Hydrodynamical-Numerical Methods," Mitteil. Inst. Meeresk., Vol. 5, (1966), p. 57.

2.9 Leendertse, J.J., "Aspects of a Computational Model for Long-Period Water-Wave Propagation," Memo. RM-5294-PR, the RAND Corporation, Santa Monica, Calif. (1967).

2.10 Reid, R.O. and B.R. Bodine, "Numerical Model for Storm Surges in Galveston Bay," Proceedings ASCE, Journal of the Waterways and Harbors Division, Vol. 94, No. WW1, (February, 1968), pp. 33-57.

2.11 "Galveston Bay Study: Phase I," Technical Report T.D. No. 68-588-U, TRACOR, Austin, Texas (1968).

2.12 Leendertse, J.J., "A Water Quality Simulation for Well Mixed Estuaries and Coastal Seas; Volume I, Principles of Computation," RM-6230-RC, The RAND Corporation, Santa Monica, Calif. (1970).

2.13 Hacker, S. , R.W, Pike and B. Wilkins, Jr., "Analysis of the Energy Species, and Momentum Transfer in the Louisiana Coastal Marsh Region," Coastal Studies Bulletin No. b, Louisiana State University, Baton Rouge, La., (1971), pp. 109-153.

2.14 "Galveston Bay Project '- Water Quality Modeling and Data Management: Phase II Technical Progress Report," Document Number T70-AU-7636-U, TRACOR, Austin, Texas (1971).

2.15 Masch, F.D., "Tidal Hydrodynamic and Salinity Models for San Antonio and Matagorda Bays, Texas," A Report to Texas Water Development Board, F.D. Masch and Assoc, Austin, Texas (1971).

2.16 Sobey, R.J., "Finite Difference Schemes Compared for Wave-Deformation Characteristics in Mathematical Modeling of Two-Dimensional Long-Wave Propagation," Technical Memo, No. 32, U.S. Army, Corps of Engineers, Coastal Engineering Research Center, Washington D.C., (1970).

2.17 Masch, F.D., et al, "A Numerical Model for the Simulation of Tidal Hydrodynamics in Shallow Irregular Estuaries," Technical Report HYD 12-6901, Hydraulic Engineering Laboratory, The University of Texas at Austin, Texas, (1969).

2.18 Miyazaki, M., T. Ueno, and S. Unoki, "Theoretical Investigations of Typhoon Surges along the Japanese Coast (II),n The Oceanographical Magazine» Vol. 13, No. 2, (1962), pp. 103-117.

2.19 Pritchard, D.W., Estuarine Hydrography, Advances in Geophysics, Academic Press, New York, N.Y., (1952).

2.20 Pritchard, D.W., "The Equations of Mass Continuity and Salt Continuity in Estuaries," Journal of Marine Research, Vol. 17, (1958), pp. 412-423.

2.21 Pritchard, D.W., "Computation of the Longitudinal Salinity Distribution in the Delaware Estuary for Various Degrees of River Inflow Regulation," Technical Report XVIII, Chesapeake Bay Institute, The Johns Hopkins University, (1959).

2.22 Harleman, D.R.F. and A.T. Ippen, "Two-Dimensional Aspects of Salinity Intrusion in Estuaries: Analysis of Salinity and Velocity Distributions," Technical Bulletin No. 13, Committee on Tidal Hydraulics, U.S. Army Corps of Engineers, (1967).

2.23 Harleman, D.R.F. and G. Abraham, "One-Dimensional Analysis of Salinity Intrusion in the Rotterdam Waterway," Publication No. 44, Delft Hydraulics Laboratory, (1966).

2.24 Harleman, D.R.F,, et al, "Numerical Studies of Unsteady Dispersion in Estuaries," Journal of the Sanitary Engineering Division of the ASCE, Vol. 94, No. SA5, Proceedings Paper 6160, (October, 1968), pp. 879-911.

2.25 Harleman, D.R.F., and C.H. Lee, "The Computation of Tides and Currents in Estuaries and Canals," Technical Bulletin No. 16, Committee on Tidal Hydraulics, U.S. Army Corps of Engineers, (1969).

2.26 Harleman, D.R.F., et al, "An Analysis of One-Dimensional Convective Diffusion Phenomena in an Idealized Estuary," Technical Report No. 42, Hydrodynamics Laboratory, Department of Civil Engineering, M.I.T., (1961).

2.27 Ippen, A.T., et al, "Turbulent Diffusion and Gravitational Convection in an Idealized Estuary," Technical Report No. 38, Hydrodynamics Laboratory, Department of Civil Engineering, M.I.T., (1960).

2.28 Ippen, A.T. and D.R.F. Harleman, "One-Dimensional Analysis of Salinity Intrusion in Estuaries," T.B. No. 5, Committee on Tidal Hydraulics, U.S. Army Corps of Engineers, (1961).

2.29 Ippen, A.T., "Salt-Water Fresh-Water Relationships in Tidal Canals," Proceedings of the Second Annual American Water Resources Conference, Chicago, Illinois, (1966).

2.30 Holley, E.R. and D.R.F. Harleman, "Dispersion of Pollutants in Estuary Type Flow," Report No. 74, Hydrodynamics Laboratory, Department of Civil Engineering, M.I.T., (1965).

2.31 Holley, E.R., et al, "Dispersion in Homogeneous Estuary Flow," Journal of the Hydraulics Division of the ASCE, Vol 98, No. HY8, Proceedings Paper 7488, (August, 1970), pp. 1691-1709.

2.32 Pritchard, D.W., "Three Dimensional Models," Estuarine Modeling An Assessment, Project No. 160700ZV, TRACOR, Austin, Texas, (1971), pp. 5-21.

CHAPTER III

DERIVATION OF EQUATIONS FOR THE TRANSPORT PHENOMENA OF SHALLOW ESTUARINE BAY SYSTEMS

Introduction

The purpose of this chapter is to rigorously derive the vertically averaged equations that describe the momentum, energy and mass transfer processes in a shallow, vertically mixed estuarine bay. The vertical integration of the general equations of continuity and motion results in the Hydrodynamical Model. The same mathematical procedure, when applied to the general equations of energy and species continuity, produces the Energy Transport and Mass Transport Models respectively.

The first part of this chapter will consist of the derivation of the Hydrodynamical Model. The two subsequent parts will be the derivation of the Energy Transport Model and the Mass Transport Model. Special care will be given to the terms arising due to diffusion and convection at the surface and bottom of the body of water.

Hydrodynamic Mode1

The Hydrodynamic model is obtained by transforming the equations of continuity and motion. In order to transform these equations, a certain number of approximations have to be made. These approximations apply to all the equations derived in this chapter. Table 3.1 summarizes these approximations.

Equation of Continuity

The general equation of continuity is given by Dronkers (Ref. 3.1) for a turbulent incompressible fluid, as:

$$\frac{\partial u}{\partial x} + \frac{\partial v}{\partial y} + \frac{\partial w}{\partial z} = 0 \qquad (3.1)$$

The most important effects are two dimensional and are in the horizontal plane. Thus, the general equation can be transformed into two dimensions by vertical integration. In other words, the average values of the variables in the vertical direction can be obtained so as to produce a two-dimensional model to describe the physical system.

Integrating Eq. (3.1) in the z-direction, from the bottom, h, to the surface, L, we obtain:

$$\int_h^L \frac{\partial u}{\partial x} dz + \int_h^L \frac{\partial v}{\partial y} dz + w(x,y,L,t) - w(x,y,h,t) = 0 \qquad (3.2)$$

If $F_n(x,y,t) = 0$ is defined as the equation representing a surface, e.g., the bay air-water surface or water-bottom surface, then at every point on either surface the substantial derivative of F_n can be written as:

TABLE 3.1

APPROXIMATIONS USED IN THE DERIVATION OF
TRANSPORT PHENOMENA EQUATIONS FOR SHALLOW ESTUARIES

Approximation	Terms Neglected
Incompressible Flow: Constant density is assumed due to negligible changes in density from temperature and salinity variations.	$\nabla \cdot \rho$
Two-Dimensional Effects: The important effects occur in the horizontal plane.	Inertia and stress terms in the z-direction
No Underground Seepage: Flow of water through the bottom is negligible.	$w(x,y,h,t)$
No Gravity Effects: Flow is in the horizontal plane.	$g_x \; ; \; \sum_{i=1}^{n} g_i j_i$
No Diffusive Transport of Momentum: Due to the low velocities found in the system.	$2\left(-\left[\mu^{\text{laminar}} + \mu^{\text{eddy}}\right] \frac{\partial^2 u}{\partial x^2}\right)$ $\left[\left(\mu^{\text{laminar}} + \mu^{\text{eddy}}\right)\left(\frac{\partial^2 u}{\partial y^2} + \frac{\partial^2 v}{\partial x \partial y}\right)\right]$ $\overline{\overline{\tau}} : \vec{\nabla}\vec{v}$
No Bottom Slip: The velocities at the bottom are zero.	$u(h)$ $v(h)$
No Momentum due to Rain: Momentum by rainfall is negligible.	$wu(L)$ $wv(L)$
Uniform Velocity Profiles in the Vertical Direction: A uniform velocity is assumed. Experimental measurements are shown in Chapter IV.	$u(z)$ $v(z)$

TABLE 3.1

(Continued)

Approximation	Terms Neglected
No Bottom Variation with Time: The bottom profile does not change with time.	$\frac{\partial h}{\partial t}$
No PV Work: Due to the fluid being incompressible	$\left(\frac{\partial \ln Vol}{\partial \ln T}\right)_{p,n_i} \frac{Dp}{Dt}$
No Heats of Mixing: Heat of mixing of the species considered is negligible.	$\tilde{H}_i \vec{\nabla}.\vec{J}_i$
Binary Diffusion: Due to low concentrations, species diffuse independently from each other.	$\mathcal{D}^*_{A,\text{multicomponent}} = \mathcal{D}^*_{A,\text{binary}}$

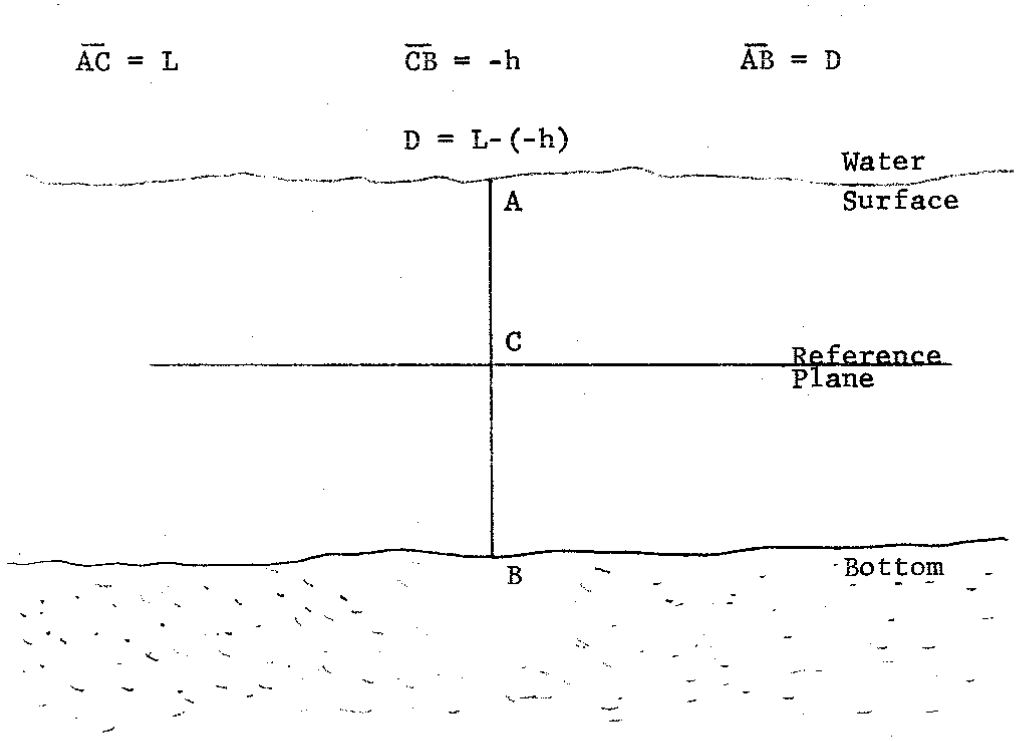

Figure 3.1. Definition of Variables for Shallow Estuarine Body of Water.

$$\frac{DF_n}{Dt} = \frac{\partial F_n}{\partial t} + u\frac{\partial F_n}{\partial x} + v\frac{\partial F_n}{\partial y} = 0 \qquad (3.3)$$

In Figure (3.1), h is the distance from the bottom to the given reference plane (mean water level of the estuary) and L is the corresponding distance to the water surface from the reference plane. At the bottom $F_{nb} = h(x,y)$. Substituting into Eq. (3.3):

$$\frac{DF_{nb}}{Dt} = u\frac{\partial h}{\partial x} + v\frac{\partial h}{\partial y} = 0 \qquad (3.4)$$

At the surface of the estuary $F_{ns} = L(x,y,t)$. Substituting into Eq. (3.3):

$$\frac{DF_{ns}}{Dt} = \frac{\partial L}{\partial t} + u\frac{\partial L}{\partial x} + v\frac{\partial L}{\partial y} = 0 \qquad (3.5)$$

If the Leibnitz integral rule is applied to the first terms of Eq. (3.2), this expression becomes:

$$\frac{\partial}{\partial x}\int_h^L u\,dz - u(x,y,L,t)\frac{\partial L}{\partial x} + u(x,y,h,t)\frac{\partial h}{\partial x} +$$

$$\frac{\partial}{\partial y}\int_h^L v\,dz - v(x,y,L,t)\frac{\partial L}{\partial y} + v(x,y,h,t)\frac{\partial h}{\partial y} + w(x,y,L,t) - w(x,y,h,t) = 0 \qquad (3.6)$$

Grouping:

$$\frac{\partial}{\partial x}\int_h^L u\,dz + \frac{\partial}{\partial y}\int_h^L v\,dz - \left[u\frac{\partial L}{\partial x} + v\frac{\partial L}{\partial y}\right] + \left[u\frac{\partial h}{\partial x} + v\frac{\partial h}{\partial y}\right] +$$

$$w(x,y,L,t) - w(x,y,h,t) = 0 \qquad (3.7)$$

Note that the terms included in the first bracket on the left hand side of Eq. (3.7) are equal to by Eq. (3.5). Also note that the sum of terms in the second bracket is equal to zero by Eq. (3.4). Then Eq. (3.7) reduces

$$\frac{\partial}{\partial x}\int_h^L u\,dz + \frac{\partial}{\partial y}\int_h^L v\,dz + \frac{\partial L}{\partial t} + w(x,y,L,t) - w(x,y,h,t) = 0 \qquad (3.8)$$

Defining:

$$U = \frac{1}{D}\int_h^L u\,dz \qquad (3.9)$$

$$V = \frac{1}{D}\int_h^L v\,dz \qquad (3.10)$$

Then, Eq. (3.8) becomes:

$$\frac{\partial(DU)}{\partial x} + \frac{\partial(DV)}{\partial y} + \frac{\partial L}{\partial t} + w(x,y,L,t) - w(x,y,h,t) = 0 \qquad (3.11)$$

Assuming no underground seepage,

$$w(x,y,h,t) = 0 \qquad (3.12)$$

The w velocity at the surface is the net of the rainfall rate and the evaporation:

$$w(x,y,L,t) = R\text{-}Ev \qquad (3.13)$$

The minus sign for the term w(L) in Eq. (3.11) is eliminated due to the fact that the direction of the rain is in the minus z-direction. Thus, Eq. (3.11) can be written as:

$$\frac{\partial(DU)}{\partial x} + \frac{\partial(DV)}{\partial y} + \frac{\partial L}{\partial t} = R\text{-}Ev \qquad (3.14)$$

Eq. (3.14) is the vertically integrated continuity equation, and it forms part of the Hydrodynamic Model. The other parts of the Hydrodynamic Model consists of the components of the vertically integrated equation of motion. In Eq. (3.14) the terms DU and DV can be thought as average discharge rates,

$$DU = Q_x \qquad (3.15)$$

$$DV = Q_y \qquad (3.16)$$

Using the above definitions, Eq. (3.14) can be written as:

$$\frac{\partial Q_x}{\partial x} + \frac{\partial Q_y}{\partial y} + \frac{\partial L}{\partial t} = R\text{-}Ev \qquad (3.17)$$

Equations of Motion

The general time-averaged turbulent equation of motion for a fluid is given as (Ref. 2.1):

$$\rho\frac{\vec{Dv}}{Dt} = -\vec{\nabla}\rho - \vec{\nabla}\vec{\vec{\tau}} + \rho\vec{g} \qquad (3.18)$$

In the above equation, the term r represents the sum of the laminar and turbulent stresses as shown in Eq. (3.19)

$$\overline{\overline{\tau}} = \overline{\overline{\tau}}^{\text{laminar}} + \overline{\overline{\tau}}^{\text{turbulent}} \tag{3.19}$$

Eq. (3.18) can be expanded in a rectangular coordinate system. When the x-y plane of this coordinate system is on the surface of the earth, as it is in this case, the system is moving with the velocity of the surface of the earth as it rotates around its axis. Due to this motion of the coordinate system, a new term appears in Eq. (3.18). This term is the Coriolis force. Expanding Eq. (3.18) in this fashion for the x-component, results in:

$$\frac{\partial u}{\partial t} + u\frac{\partial u}{\partial x} + v\frac{\partial u}{\partial y} + w\frac{\partial u}{\partial z} - Fv = -\frac{1}{\rho}\frac{\partial p}{\partial x} \tag{3.20}$$

$$\frac{1}{\rho}\left[\frac{\partial \tau_{xx}}{\partial x} + \frac{\partial \tau_{xy}}{\partial y} + \frac{\partial \tau_{xz}}{\partial z}\right] + g_x$$

The x-y plane is oriented in such a fashion as to be parallel to the horizontal plane, consequently the effect of gravity is eliminated. Therefore, the x-component equation of motion reduces to:

$$\frac{\partial u}{\partial t} + u\frac{\partial u}{\partial x} + v\frac{\partial u}{\partial y} + w\frac{\partial u}{\partial z} - Fv = -\frac{1}{\rho}\frac{\partial p}{\partial x} - \frac{1}{\rho}\left[\frac{\partial \tau_{xx}}{\partial x} + \frac{\partial \tau_{xy}}{\partial y} + \frac{\partial \tau_{xz}}{\partial z}\right] \tag{3.21}$$

Integrating in the vertical direction, from the bottom to the surface, gives:

$$\int_h^L \left[\frac{\partial u}{\partial t} + u\frac{\partial u}{\partial x} + v\frac{\partial u}{\partial y} + w\frac{\partial u}{\partial z}\right]dz - \int_h^L Fv\,dz = -\frac{1}{\rho}\int_h^L \frac{\partial p}{\partial x}\,dz \tag{3.22}$$

$$-\frac{1}{\rho}\int_h^L \left[\frac{\partial \tau_{xx}}{\partial x} + \frac{\partial \tau_{xy}}{\partial y} + \frac{\partial \tau_{xz}}{\partial z}\right]dz$$

The expressions for the shear and normal stresses, as given by Bird (Ref. 3.2), in terms of the viscosity and velocity gradients are now substituted into Eq. (3.22) and the result is the following equation:

$$\int_h^L \left[\frac{\partial u}{\partial t} + u\frac{\partial u}{\partial x} + v\frac{\partial u}{\partial y} + w\frac{\partial u}{\partial z}\right]dz - \int_h^L Fv\,dz = -\frac{1}{\rho}\int_h^L \frac{\partial p}{\partial x}\,dz$$

$$-\frac{1}{\rho}\int_h^L \left[2\left(\left(\mu^{\text{laminar}} + \mu^{\text{eddy}}\right)\frac{\partial^2 u}{\partial x^2}\right) - \left(\mu^{\text{laminar}} + \mu^{\text{eddy}}\right)\left(\frac{\partial^2 u}{\partial y^2} + \frac{\partial^2 v}{\partial x \partial y}\right) + \right.$$

$$\left.\frac{\partial \tau_{zx}}{\partial z}\right]dz \tag{3.23}$$

To continue the derivation it must be assumed that the velocity is uniform in the vertical direction in order to evaluate the inertial terms in the equation. Due to the shallowness of the bay under study, this approximation is reasonable. Some experimental measurements confirming the above approximation are shown in Appendix B.

Using Leibnitz's rule, Eq. (3.23) transforms to:

$$\frac{\partial}{\partial t}\int_h^L u\,dz - u(x,y,L,t)\frac{\partial L}{\partial t} + u(x,y,h,t)\frac{\partial h}{\partial t} +$$

$$U\left[\frac{\partial}{\partial x}\int_h^L u\,dz - u(x,y,L,t)\frac{\partial L}{\partial x} + u(x,y,h,t)\frac{\partial h}{\partial x}\right] +$$

$$V\left[\frac{\partial}{\partial y}\int_h^L u\,dz - u(x,y,L,t)\frac{\partial L}{\partial y} + u(x,y,h,t)\frac{\partial h}{\partial y}\right] + \qquad (3.24)$$

$$w\left[\int_h^L \frac{\partial u}{\partial z}dz\right] - F\int_h^L v\,dz = -\frac{1}{\rho}\frac{\partial p}{\partial x}\int_h^L dz -$$

$$\frac{1}{\rho}\int_h^L\left[2\left(-\left(\mu^{laminar}+\mu^{eddy}\right)\frac{\partial^2 u}{\partial x^2}\right)-\left(\mu^{laminar}+\mu^{eddy}\right)\left(\frac{\partial^2 u}{\partial y^2}+\frac{\partial^2 v}{\partial x\partial y}\right)\right]dz - \frac{1}{\rho}\int_h^L\frac{\partial \tau_{xz}}{\partial z}dz$$

As a result of the low velocities existing in the system, the diffusive transport of momentum plays a negligible role. Consequently, if the terms in brackets in the right hand side of Eq. (3.24) are neglected, Eq. (3.24) reduces to:

$$\frac{\partial}{\partial t}\int_h^L u\,dz + U\frac{\partial}{\partial x}\int_h^L u\,dz + V\frac{\partial}{\partial y}\int_h^L u\,dz + \left[wu(L) - wu(h)\right] -$$

$$u(x,y,L,t)\left[\frac{\partial L}{\partial t} + u\frac{\partial L}{\partial x} + v\frac{\partial L}{\partial y}\right] + u(x,y,h,t)\left[\frac{\partial h}{\partial t} + u\frac{\partial h}{\partial x} + v\frac{\partial h}{\partial y}\right] - \qquad (3.25)$$

$$F\int_h^L v\,dz = -\frac{1}{\rho}\frac{\partial p}{\partial x}\int_h^L dz - \frac{1}{\rho}\int_h^L\frac{\partial \tau_{xz}}{\partial z}dz$$

The terms in the second bracket are equal to zero by Eq. (3.5).The bottom plane h(x,y) does not vary with time, thus, the terms in the third bracket are also equal to zero by Eq. (3.4). Also, is zero

because u(h) is zero (no bottom slip) and u(L) is the rainfall rate which is negligible as far as momentum added to the system is concerned.

Therefore, Eq. (3.25) transforms to:

$$\frac{\partial}{\partial t}\int_h^L u\,dz + U\frac{\partial}{\partial x}\int_h^L u\,dz + V\frac{\partial}{\partial y}\int_h^L u\,dz - F\int_h^L v\,dz = - \frac{1}{\rho}\frac{\partial p}{\partial x}\int_h^L dz - \frac{1}{\rho}\int_h^L \frac{\partial \tau_{xz}}{\partial z}\,dz \tag{3.26}$$

Vertically averaged velocities were defined by Eqs. (3.9) and (3.10); using these definitions and the approximation of uniform vertical profiles it can be stated that:

$$\frac{1}{D}\int_h^L u\,dz = U \tag{3.27}$$

$$\frac{1}{D}\int_h^L v\,dz = V \tag{3.28}$$

where

$$D = h + L \tag{3.29}$$

Using these definitions, Eq. (3.26) can be written as:

$$\frac{\partial (UD)}{\partial t} + U\frac{\partial (UD)}{\partial x} + V\frac{\partial (UD)}{\partial y} - FVD = - \frac{D}{\rho}\frac{\partial p}{\partial x} - \frac{1}{\rho}\left[\tau_{xz}(L) - \tau_{xz}(h)\right] \tag{3.30}$$

If the derivative terms in the left-hand side of Eq. (3.30) are expanded and Eqs. (3.4) and (3.5) are used, Eq. (3.30) can be written as:

$$D\frac{\partial U}{\partial t} + DU\frac{\partial U}{\partial x} + DV\frac{\partial U}{\partial y} - FVD = - \frac{D}{\rho}\frac{\partial p}{\partial x} - \frac{1}{\rho}\left[\tau_{xz}(L) - \tau_{xz}(h)\right] \tag{3.31}$$

or:

$$\frac{\partial U}{\partial t} + U\frac{\partial U}{\partial x} + V\frac{\partial U}{\partial y} - FV = -\frac{1}{\rho}\frac{\partial p}{\partial x} - \frac{1}{D\rho}\left[\tau_{xz}(L) - \tau_{xz}(h)\right] \tag{3.32}$$

Using Eqs. (3.27) and (3.28), Eq. (3.32) reduces to:

$$\frac{\partial U}{\partial t} + U\frac{\partial U}{\partial x} + V\frac{\partial U}{\partial y} - FV = -\frac{1}{\rho}\frac{\partial p}{\partial x} - \frac{1}{D\rho}\left[\tau_{xz}(L) - \tau_{xz}(h)\right] \tag{3.33}$$

To obtain the expression to evaluate the pressure gradient term in the above equation, the z-component of the equation of motion can be simplified by the previously stated assumptions to give:

$$-\frac{\partial p}{\partial z} - \rho g = 0 \tag{3.34}$$

This equation can be vertically integrated to yield

$$p = p_a + \rho g(L-h) \tag{3.35}$$

Taking the derivative of the above equation with respect to x at a constant value of z gives:

$$\frac{\partial p}{\partial x} = \rho g \frac{\partial L}{\partial x} \tag{3.36}$$

Substituting Eq. (3.36) into Eq. (3.33) results in

$$\frac{\partial U}{\partial t} + U\frac{\partial U}{\partial x} + V\frac{\partial U}{\partial y} - FV = -g\frac{\partial L}{\partial x} - \frac{1}{D\rho}\left[\tau_{xz}(L) - \tau_{xz}(h)\right] \tag{3.37}$$

The above equation is the vertically integrated x-component of the equation of motion. The v-component of the equation of motion can be derived in the same fashion. The assumptions used to derive these equations were listed in Table 3.1. These assumptions are used throughout the rest of the derivations. To be able to solve this equation, the stress terms must be evaluated. The next two sections will be devoted to this evaluation.

Empirical Relationships for the Bottom Stresses

In Figure 3.2, a description of liquid flow in the x-direction is given. After Masch (Ref. 2.15) the energy slope Se is defined as:

$$-Se = \frac{\phi}{\rho} = \frac{\tau_{xz}(h)}{D\rho} \qquad (3.38)$$

Letting describe the bottom friction force, then:

$$-Se = \frac{\phi}{\rho} = \frac{\text{Friction Force/Area/Length}}{\text{Weight Force/Volume}} = \frac{\text{Friction Force}}{\text{Weight Force}}$$

and:

$$-SeD = \tau_{xz}(h)/\rho \qquad (3.39)$$

Even though the energy slope is negative in the direction of flow, as shown in Fig. 3.2, the negative sign accounts for the friction force acting in a direction opposite to the flow. The energy slope can be evaluated in terms of the velocity by using either the Chezy or Manning equations. Both of these equations are empirical fits of experimental data.

By the Chezy equation:

$$U = C(R_h Se)^{1/2} \qquad (3.40)$$

In wide channels R_h, the hydraulic radius, is essentially equal to the depth of flow, D. If C is defined as:

$$C = \frac{A}{(f_1)^{1/2}} \qquad (3.41)$$

and then combining Eqs. (3.40) and (3.41) gives the following:

$$Se = f_1 |U| UD^{-1} \qquad (3.42)$$

The absolute value is needed to preserve the sign of the energy slope as the velocity changes direction in a tidal system.

By the Manning equation:

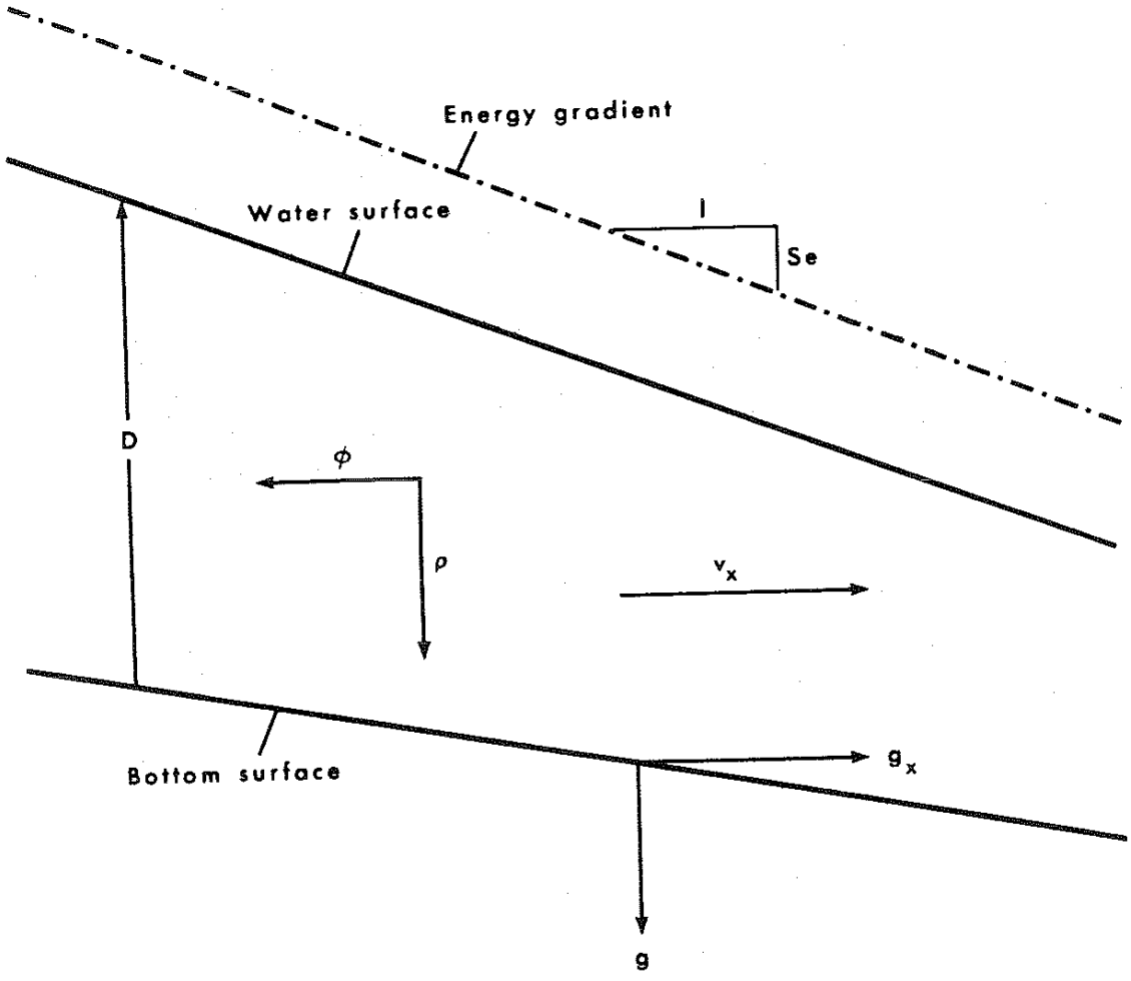

Figure 3.2. Definition of Energy Gradient.

$$U = \frac{1.486\ R_h^{2/3} S_e^{1/2}}{h} \tag{3.43}$$

so:

$$U^2 = \frac{2.208}{h^2} R_h^{4/3} S_e \tag{3.44}$$

then:

$$S_e = \frac{h^2}{2.208} \left(\frac{U^2}{R_h^{4/3}} \right) \tag{3.45}$$

Using $R_h = D$ for a wide channel:

$$S_e = \left[\frac{h^2}{2.208 D^{4/3}} \right] U^2 = f_2 |U| U D^{-1} \tag{3.46}$$

where

$$f_2 = \left[\frac{h^2}{2.208\ D^{1/3}} \right] \tag{3.47}$$

If Eq. (3.46) is multiplied by D:

$$S_e D = f_2 |U| U \tag{3.48}$$

or

$$-S_e D = f_2 |U| DUD/D^2 = f_2 |Q| Q_x D^{-2} \tag{3.49}$$

If the friction factor for Eqs, (3.46) and (3.42) is defined as:

$$f = gD/C^2 \tag{3.50}$$

And from Eq. (3.39)

$$\tau_{xz}(h) = - S_e D \rho \tag{3.51}$$

then, substituting Eq. (3.49) in the above relationship and using Eq (3.50) results in:

$$\tau_{xz}(h) = \rho g \frac{|Q|Q_x D^{-1}}{C^2} \tag{3.52}$$

or,

$$\tau_{xz}(h) = \rho g \frac{|Q|Q_x}{DC^2} = \rho g \frac{|Q|U}{C^2} \tag{3.53}$$

thus,

$$\tau_{xz}(h) = \rho g \frac{(U^2+V^2)^{1/2}U}{C^2} \tag{3.54}$$

This last relationship is the one used in this work. The Chezy coefficient is calculated as (Ref. 2.12):

$$C = \frac{1.49}{n} D^{1/6} \tag{3.55}$$

The bottom roughness coefficient, n, is given in the literature (Ref 21.2), and its most common value given is 0.026.

Empirical Relationships for the Surface Stresses

To obtain an empirical relationship for the surface stresses, the kinematic form for the wind stress is taken as (Ref. 3.2).

$$X = \frac{\tau_{xz}(L)}{D\rho} = K_1 W^2 \cos\theta \tag{3.56}$$

$$Y = \frac{\tau_{yz}(L)}{D\rho} = K_1 W^2 \sin\theta \tag{3.57}$$

$$K_1 = 0.0026 * \rho_a \tag{3.58}$$

The above relationship has been used by many previous studies (Refs. 2.10, 2.11, 2.14) successfully and will be used in the present work.

Hydrodynamic Model Equations

Substituting Eq. (3.56) and (3.54) in Eq. (3.37) will result in the vertically integrated x-component of the equation of motion for the Hydrodynamic Model, as given by Eq. (3.59). A similar derivation to the one shown will result in the equation for the y-component, as shown in Eq. (3.60). Thus, the Hydrodynamic Model equations are:

$$\frac{\partial(DU)}{\partial x} + \frac{\partial(DV)}{\partial y} + \frac{\partial L}{\partial t} = R\text{-}Ev \tag{3.14}$$

$$\frac{\partial U}{\partial t} + U\frac{\partial U}{\partial x} + V\frac{\partial U}{\partial y} - FV + g\frac{\partial L}{\partial x} = X - g\frac{U(U^2+V^2)^{1/2}}{DC^2} \tag{3.59}$$

$$\frac{\partial V}{\partial t} + U\frac{\partial V}{\partial x} + V\frac{\partial V}{\partial y} + FU + g\frac{\partial L}{\partial y} = Y - g\frac{V(U^2+V^2)^{1/2}}{DC^2} \tag{3.60}$$

Energy Transport Model

The general, time-averaged, turbulent energy transport equation is given by Bird, Stewart and Lightfoot (Ref. 2.1) as:

$$\rho\frac{D\hat{E}}{Dt} = -\vec{\nabla}.\left(\vec{q}^{\,\text{laminar}} + \vec{q}^{\,\text{turb}}\right) - \pi:\vec{\nabla}\vec{v} + \sum_i j_i g_i \tag{3.61}$$

Defining enthalpy per unit mass,

$$\hat{H} = \hat{E} + p/\rho \tag{3.62}$$

Taking the substantial derivative gives:

$$\frac{D\hat{H}}{Dt} = \frac{D\hat{E}}{Dt} + \frac{1}{\rho}\frac{Dp}{Dt} - \frac{p}{\rho^2}\frac{D\rho}{Dt} \tag{3.63}$$

Defining the pressure tensor, $\overline{\overline{\pi}}$:

$$\overline{\overline{\pi}} = \overline{\overline{\tau}} + p\overline{\overline{\delta}} \tag{3.64}$$

$$\overline{\overline{\pi}}:\vec{\nabla}\vec{v} = \left(\overline{\overline{\tau}} + p\overline{\overline{\delta}}\right):\vec{\nabla}\vec{v} = \overline{\overline{\tau}}:\vec{\nabla}\vec{v} + p\overline{\overline{\delta}}:\vec{\nabla}\vec{v} \tag{3.65}$$

$$\overline{\overline{\pi}}:\vec{\nabla}\vec{v} = \overline{\overline{\tau}}:\vec{\nabla}\vec{v} + p\vec{\nabla}.\vec{v} \tag{3.66}$$

Substituting Eqs. (3.66) and (3.63) into Eq. (3.61):

$$\rho \frac{D\hat{H}}{Dt} = -\vec{\nabla}.\vec{q} - \overline{\overline{\tau}}:\vec{\nabla}\vec{v} - p\left(\vec{\nabla}.\vec{v} + \frac{1}{\rho}\frac{D\rho}{Dt}\right) + \frac{Dp}{Dt} + \sum_i \vec{j}_i g_i \qquad (3.67)$$

Noting that the continuity equation is:

$$\left(\vec{\nabla}.\vec{v} + \frac{1}{\rho}\frac{D\rho}{Dt}\right) = 0 \qquad (3.68)$$

then, Eq.(3.67) becomes:

$$\rho \frac{D\hat{H}}{Dt} = -\vec{\nabla}.\left(\vec{q}^{\,laminar} + \vec{q}^{\,turb}\right) - \overline{\overline{\tau}}:\vec{\nabla}\vec{v} + \frac{Dp}{Dt} + \sum_i \vec{j}_i g_i \qquad (3.69)$$

Enthalpy per unit mass, $\hat{H}$, is a function of temperature, pressure and composition; thus:

$$\hat{H} = \hat{H}(T,P,h_i) \qquad (3.70)$$

so:

$$\frac{DH}{Dt} = \left(\frac{\partial\hat{H}}{\partial T}\right)_{p,n_i}\frac{DT}{Dt} + \left(\frac{\partial\hat{H}}{\partial p}\right)_{T,n_i}\frac{Dp}{Dt} + \sum_{i=1}^{m}\left(\frac{\partial\hat{H}}{\partial n_i}\right)_{T,p,n_{j\neq i}}\frac{Dn_i}{Dt} \qquad (3.71)$$

By definition:

$$\left(\frac{\partial\hat{H}}{\partial T}\right)_{p_i n_i} \equiv C_p \qquad (3.72)$$

$$\left(\frac{\partial\hat{H}}{\partial n_i}\right)_{T,p,n_{j\neq i}} \equiv \tilde{H}_i \qquad (3.73)$$

Using basic thermodynamic relationships,

$$\left(\frac{\partial\hat{H}}{\partial P}\right)_{T,n_i} = \left[Vol - T\left(\frac{\partial Vol}{\partial T}\right)_{p,n_i}\right] \qquad (3.74)$$

$$Vol\left[1 - \frac{T}{Vol}\left(\frac{\partial Vol}{\partial T}\right)_{p,n_i}\right] = \frac{1}{\rho}\left[1 - \left(\frac{\partial \ln Vol}{\partial \ln T}\right)_{p,n_j}\right] \qquad (3.75)$$

A form of the species continuity equation is (Ref. 2.1):

$$\rho \frac{Dw_i}{Dt} = \vec{\nabla}.\vec{j}_i + r_i \tag{3.76}$$

or:

$$\frac{Dw_i}{Dt} = \left[-\vec{\nabla}.J_i + R_i\right] \frac{M_i}{\rho} \tag{3.77}$$

but

$$\frac{Dni}{Dt} = \frac{1}{M_i} \frac{Dw_i}{Dt} \tag{3.78}$$

then:

$$\frac{Dni}{Dt} = \frac{1}{\rho} \left[-\vec{\nabla}.\vec{J}_i + R_i\right] \tag{3.79}$$

Substituting Eqs. (3.79), (3.75), (3.73) and (3.72) into Eq. (3.71) and multiplying through by the density we obtain:

$$\rho \frac{D\hat{H}}{Dt} = \rho C_p \frac{DT}{Dt} + \left[1 - \left(\frac{\partial \ln Vol}{\partial \ln T}\right)_{p,n_i}\right] \frac{DP}{Dt} \tag{3.80}$$

Substituting Eq. (3.80) into Eq. (3.69) leads to:

$$\rho C_p \frac{DT}{Dt} = -\vec{\nabla}.\left(\vec{q}^{\,laminar} + \vec{q}^{\,turb}\right) - \overline{\overline{\tau}}:\vec{\nabla}\vec{v} + \sum_{i=1}^{m} j_i g_i - \left(\frac{\partial \ln Vol}{\partial \ln T}\right)_{p,n_i} \frac{Dp}{Dt} + \sum_{i=1}^{m} \tilde{H}_i \left[\vec{\nabla}.J_i - R_i\right] \tag{3.81}$$

Using the assumptions stated in Table 3.1, Eq. (3.81) becomes:

$$\rho C_p \frac{DT}{Dt} = \vec{\nabla}.\left(\vec{q}^{\,laminar} + \vec{q}^{\,turb}\right) - \sum_{i=1}^{m} \tilde{H}_i R_i \tag{3.82}$$

or the above can be written as the following using the continuity equation

$$\rho C_p \frac{\partial T}{\partial t} + \rho C_p \vec{\nabla}.T\vec{v} = - \vec{\nabla}.\vec{q}^{turb} - \sum_{i=1}^{m} \tilde{H}_i R_i \tag{3.83}$$

Expanding in rectangular coordinates gives (and letting turb = t)

$$\rho C_p\left[\frac{\partial T}{\partial t} + \frac{\partial (uT)}{\partial x} + \frac{\partial (vT)}{\partial y} + \frac{\partial (wT)}{\partial z}\right] =$$

$$-\left[\frac{\partial q_x^t}{\partial x} + \frac{\partial q_y^t}{\partial y} + \frac{\partial q_z^t}{\partial z}\right] - \sum_{i=1}^{m} \tilde{H}_i R_i \tag{3.84}$$

Eq. (3.84) is the general energy transport equation as applied to a shallow estuarine bay. To obtain the vertically averaged energy equation, Eq. (3.84) is integrated in the vertical direction, as shown below.

$$\rho C_p \int_h^L \left[\frac{\partial T}{\partial t} + \frac{\partial (uT)}{\partial x} + \frac{\partial (vT)}{\partial y} + \frac{\partial (wT)}{\partial z}\right] dz =$$

$$- \int_h^L \left[\frac{\partial q_x^t}{\partial x} + \frac{\partial q_y^t}{\partial y} + \frac{\partial q_z^t}{\partial z}\right] dz - \int_h^L \sum_{i=1}^{m} \tilde{H}_i R_i dz \tag{3.85}$$

Using an average vertical velocity, it is possible to apply Leibnitz's integration rule to Eq. (3.85). Taking each term individually gives:

$$\int_h^L \frac{\partial T}{\partial t} dz = \frac{\partial}{\partial t} \int_h^L T dz - T(x,y,L,t) \frac{\partial L}{\partial t} + T(x,y,h,t) \frac{\partial h}{\partial t} \tag{3.86}$$

$$\int_h^L \frac{\partial (uT)}{\partial x} dz = \frac{\partial}{\partial x} U \int_h^L T dz - uT(x,y,L,t) \frac{\partial L}{\partial x} + uT(x,y,h,t) \frac{\partial h}{\partial x} \tag{3.87}$$

$$\int_h^L \frac{\partial (vT)}{\partial y} dz = \frac{\partial}{\partial y} V \int_h^L T dz - vT(x,y,L,t) \frac{\partial L}{\partial y} + vT(x,y,h,t) \frac{\partial h}{\partial y} \tag{3.88}$$

$$\int_h^L \frac{\partial (wT)}{\partial z} dz = wT(L) - wT(h) \tag{3.89}$$

$$\int_h^L \frac{\partial q_x^t}{\partial x}\,dz = \frac{\partial}{\partial x}\int_h^L q_x dz - q^t(x,y,L,t)\,\frac{\partial L}{\partial x} + q^t(x,y,h,t)\,\frac{\partial h}{\partial x} \tag{3.90}$$

$$\int_h^L \frac{\partial q_y^t}{\partial y}\,dz = \frac{\partial}{\partial y}\int_h^L q_y dz - q^t(x,y,L,t)\,\frac{\partial L}{\partial y} + q^t(x,y,h,t)\,\frac{\partial h}{\partial y} \tag{3.91}$$

$$\int_h^L \frac{\partial q_z^t}{\partial z}\,dz = q(L) - q(h) \tag{3.92}$$

$$\int_h^L \sum_{i=1}^{m} \tilde{H}_i R_i\,dz = D \sum_{i=1}^{m} \tilde{H}_i \bar{R}_i \tag{3.93}$$

Substituting Eqs. (3.86) through (3.93) into Eq. (3.85) results in:

$$\rho C_p\Bigg[\frac{\partial}{\partial t}\int_h^L T dz + \frac{\partial}{\partial x}\,U\int_h^L T dz + \frac{\partial}{\partial y}\,V\int_h^L T dz -$$

$$T(x,y,L,t)\left(\frac{\partial L}{\partial t} + U\,\frac{\partial L}{\partial x} + V\,\frac{\partial L}{\partial y}\right) + T(x,y,h,t)\left(\frac{\partial h}{\partial t} +$$

$$U\,\frac{\partial h}{\partial x} + V\,\frac{\partial h}{\partial y}\right) + wT(L) - wT(h)\Bigg] = - \tag{3.94}$$

$$\Bigg[\frac{\partial}{\partial x}\int_h^L q_x^t dz + \frac{\partial}{\partial y}\int_h^L q_y^t dz - q^t(x,y,L,t)\left(\frac{\partial L}{\partial x} + \frac{\partial L}{\partial y}\right) +$$

$$q^t(x,y,h,t)\left(\frac{\partial h}{\partial x} + \frac{\partial h}{\partial y}\right) + q(L) - q(h)\Bigg] - D\sum_{i=1}^{m} \tilde{H}_i \bar{R}_i$$

Using Fourier's Law and integrating, the following definitions result:

$$\bar{T} \equiv \frac{1}{D}\int_h^L T dz \tag{3.95}$$

$$\bar{q}_x \equiv \frac{1}{D}\int_h^L q_x^t dz = -k_x \frac{\partial \bar{T}}{\partial x} \tag{3.96}$$

$$\bar{q}_y \equiv \frac{1}{D}\int_h^L q_y^t dz = -k_y \frac{\partial \bar{T}}{\partial y} \tag{3.97}$$

Substituting the last three equations into Eq. (3.94) and using Eqs. (3.4) and (3.5) gives:

$$\rho C_p \left[\frac{\partial \bar{T}D}{\partial t} + \frac{\partial(\bar{T}DU)}{\partial x} + \frac{\partial(\bar{T}DV)}{\partial y}\right] - \frac{\partial}{\partial x}\left(Dk_x \frac{\partial \bar{T}}{\partial x}\right)$$

$$- \frac{\partial}{\partial y}\left(Dk_y \frac{\partial \bar{T}}{\partial y}\right) - \left[\rho C_p wT(L) - \rho C_p wT(h) + q(L) - q(h) - D\sum_{i=1}^{m} \tilde{H}_i \bar{R}_i\right] = 0 \tag{3.98}$$

In the above equation, the terms in the second bracket represent the sinks and sources (SS_E) of energy in the following form:

$\rho C_p wT(L)$	-	Heat flow due to water leaving (evaporation) or entering (rainfall) through the surface
$\rho C_p wT(h)$	-	Heat flow due to water leaving or entering through the bottom (seepage)
$q(L)$	-	Heat flux at the surface (convection, radiation)
$q(h)$	-	Heat flux at the bottom (convection, radiation)
$D\sum_{i=1}^{m} \tilde{H}_i \bar{R}_i$	-	Heat flux due to reaction

Eq. (3.98) can be written as:

$$\rho C_p \left[\frac{\partial(\bar{T}\bar{D})}{\partial t} + \frac{\partial(\bar{T}\bar{D}\bar{U})}{\partial x} + \frac{\partial(\bar{T}\bar{D}\bar{V})}{\partial y}\right] - \frac{\partial}{\partial x}\left(Dk_x \frac{\partial \bar{T}}{\partial x}\right) - \\ - \frac{\partial}{\partial y}\left(Dk_y \frac{\partial \bar{T}}{\partial y}\right) - SS_E = 0 \qquad (3.99)$$

Note that the thermal conductivity can be different for the x- and y-directions. This formulation allows the medium to be anisotropic, however this is not necessarily so in estuarine flows. In modeling, the estuary values of the thermal conductivity and also the diffusivity are used. These are larger than the values of the molecular properties. These values take into account the turbulent transfer of mass momentum and energy, and they are usually called dispersion coefficients. These coefficients are a function of the turbulent properties of the flow and there are no rigorous methods for calculating them a priori. Dispersion coefficients are usually obtained by adjusting the values of the dispersion coefficients such that the model gives a reasonable fit of data taken in estuary.

Equation (3.99) is the vertically averaged energy transport equation. It is a second order, parabolic, partial differential equation, and it constitutes the Energy Transport Model.

Sinks and Sources for the Energy Transport Model

To obtain the sinks and sources terms for the Energy Transport Model, surface balances can be performed at the water surface and at the bottom of the bay. An energy balance at the surface can be obtained by integrating the energy equation, Eq. (3.61), across the surface from z^- (in the water) to z^+ (in the air). The final result is obtained by taking the limit as goes to zero. Simplifying Eq. (3.69) on the basis of restrictions given earlier for a shallow estuarine bay gives:

$$\rho\left[\frac{\partial \hat{H}}{\partial t} + u\frac{\partial \hat{H}}{\partial x} - v\frac{\partial \hat{H}}{\partial y} + w\frac{\partial \hat{H}}{\partial z}\right] = -\left[\frac{\partial q_x^{1+t}}{\partial x} + \frac{\partial q_y^{1+t}}{\partial y} + \frac{\partial q_z^{1+t}}{\partial z}\right] \qquad (3.100)$$

Performing the integration gives:

$$\rho\int_{z^-}^{z^+}\left[\frac{\partial \hat{H}}{\partial t} + u\frac{\partial \hat{H}}{\partial x} + v\frac{\partial \hat{H}}{\partial y}\right]dz + \rho\int_{z^-}^{z^+} W\frac{\partial \hat{H}}{\partial z}\,dz = \\ -\int_{z^-}^{z^+}\left[\frac{\partial q_x^{1+t}}{\partial x} + \frac{\partial q_y^{1+t}}{\partial y}\right]dz - \int_{z^-}^{z^+}\frac{\partial q_z^{1+t}}{\partial z}\,dz \qquad (3.101)$$

The above can be written in terms of average values, using the mean value theorem, as:

$$\rho\left[\frac{\partial \hat{H}}{\partial t} + u\frac{\partial \hat{H}}{\partial x} + v\frac{\partial \hat{H}}{\partial y}\right]\int_{z^-}^{z^+} dz + \rho w\int_{z^-}^{z^+}\frac{\partial \hat{H}}{\partial z}\,dz = -\left[\frac{\partial q_x^{1+t}}{\partial x} + \frac{\partial q_y^{1+t}}{\partial y}\right]\int_{z^-}^{z^+} dz - \int_{z^-}^{z^+}\frac{\partial q_z^{1+t}}{\partial z}\,dz \qquad (3.102)$$

Performing the integration, taking the limit as Az goes to zero, and rearranging gives:

$$\rho w(\hat{H}^+ - \hat{H}^-) + q^+ = q^- \qquad (3.103)$$

The terms on the left-hand side represent the net energy arriving at the interface on the air side, and the term on the right-hand side represents the net energy leaving at the interface from the liquid side. Each of these terms will now be discussed in detail.

The first term on the left-hand side of the above equation represents the net convective and evaporative energy transfer to the surface. It can be written as:

$$\rho w(\hat{H}^+ - \hat{H}^-) = [R-Ev](\hat{H}^+ - \hat{H}^-)\rho \qquad (3.104)$$

where $^{\rho R(\hat{H}^+ - \hat{H}^-)}$ represents the convective energy transfer to the interface associated with the rainfall and is the convective and evaporative energy associated with water being vaporized at the surface, i.e.,

$$\rho R(\hat{H}^+ - \hat{H}^-) = \rho C_p(T_s - T_{Rain})R \qquad (3.105)$$

$$\rho Ev(\hat{H}^+ - \hat{H}^-) = [\lambda + C_p(T_s - T_{air})]\rho Ev = q_{ev} \qquad (3.106)$$

Where TS is the temperature of the interface. The rainfall rate, R, is a specified input, known from records or statistically simulated. The evaporation rate, Ev, is evaluated empirically (Callaway, et al., (Ref. 3.4):

$$Ev = Nw(e_s - e_a) \qquad (3.107)$$

Where N is an empirical evaporation coefficient, and e is the partial pressure of water vapor. A value of $5*10^{-7}$ ft^2/lb_m, reported by Calloway (3.4), will be used in this study. The vapor pressure terms are computed using the Clasius-Glapeyron equation. Callaway, et. al, (Ref. 3.4) reports the following equations which were used in this study.

$$e_s = 2.1718*10^8 \exp(-4157.0/(T_s-34.07)) \quad (3.108)$$

$$e_a = 2.1718*10^8 \exp(-4157.0/(T_s - 34.07)) - P_a(T_a - T_{wB})(6.6 * 10^{-4} + 7.59 * 10^{-7}(T_{wB} - 273.16)) \quad (3.109)$$

The second term on the left-hand side of Eq. (3.103) represents net energy transfer to the interface by convection and radiation. It can be written as:

$$q^+ = q_c + q_{\text{net radiation to the surface}} \quad (3.110)$$

The heat transferred by convection, q_c, can be calculated from the heat transfer by evaporation using the Bowen ratio (Ref. 3.4):

$$q_c = \lambda E v \rho B \quad (3.111)$$

The Bowen ratio is defined as the ratio of the heat transfer by convec¬ tion to that by evaporation and is given by:

$$B = 6.1 * 10^{-4} p_a \left[\frac{T_a - T_s}{e_s - e_a}\right] \quad (3.112)$$

The net radiative heat transfer to the surface is best visualized by examining Fig. 3.3. It is the algebraic sum of the solar radiation, q(solar radiation); the reflected radiation, q(ref.); the radiation reflected back from clouds, etc., q (back radiation); and surface radiation, q_w.

$$q_{\substack{\text{net radiative} \\ \text{transfer to surface}}} = q_{\substack{\text{solar} \\ \text{radiation}}} + q_{\substack{\text{back} \\ \text{radiation}}} - q_w - q_{ref} \quad (3.113)$$

The solar radiation is an experimentally determined variable for the area under study. For the reflected radiation, it is necessary either to determine this value experimentally or to estimate it. This is also the case for the back radiation, which depends on the cloud cover. The surface radiation can be computed if the emissivity, 6, of the surface is known by the use of the Stefan-Boltzmann law, which is:

$$q_w = \epsilon \sigma T_s^4 \quad (3.114)$$

A typical value of the emissivity is 0.97 as reported by Callaway, et al (Ref. 3.4).

Measurement of the total solar radiation, which is the sum of q(solar radiation) and q(back radiation), is usually performed with a pyrometer (Adams, combined with Eq. (1970). This sum is called q(rad). Eq. (3.110 can be combined with Eq. (3.113) to give:

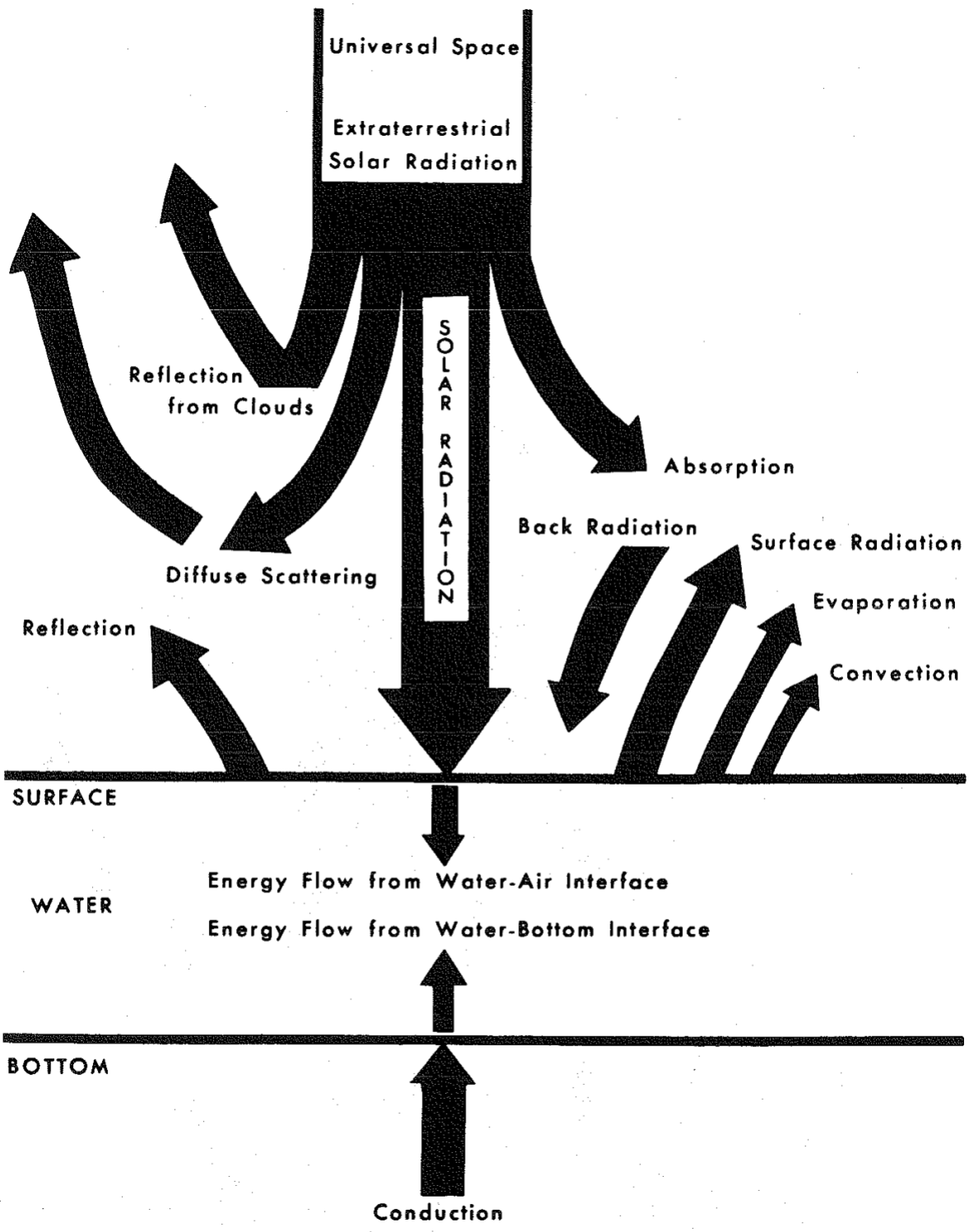

Figure 3.3. Interface Energy Flows. (after Geiger, Ref. 3.4)

$$q^{+} = q_c + q_{rad} - q_{ref} - q_w \qquad (3.115)$$

The term q^- of Eq. (3.103) is the same as the term q(L) of Eq. (3.98). Thus, combining Eq. (3.103) with Eqs. (3.105), (3.106), (3.111), (3.114), and (3.115) the equation for the surface energy balance is obtained.

$$q(L) = \rho C_p (T-T_{Rain}) R + [\lambda + C_p (T-T_{air})]\, Ev\rho + \lambda\, Ev\, \rho\, B + q_{rad} - q_{ref} - \epsilon\sigma T_s^4 \qquad (3.116)$$

The above equation represents the boundary condition that couples the energy transfer at the air-water interface to the differential equation that describes the energy transfer in the estuarine body of water, Eq. (3.98). A similar analysis can be conducted to describe the energy transfer at the water-bottom interface.

If a similar analysis is performed by integrating the energy equation across the water-bottom interface, it can be shown that the following equation will be obtained:

$$q(h) = - k_b \left(\frac{dT}{dz}\right)_b \qquad (3.117)$$

i.e. there is only conduction of energy into the ground from the water. Experimental values taken show that the conduction of heat at the bottom of the bay is negligible. These experimental values are shown in Appendix B.

Species Transport Model

The materials transport model is obtained by vertical integration of the species continuity equation. Given the special environment of a shallow estuarine bay, a binary system type equation can be used. The reason for this is that due to the relatively low concentrations of most of the species found in estuarine water, each species diffuses independently from others. Consequently, a binary diffusion coefficient can be used, where water is one component and the species in question is the other.

Bird, Stewart, and Lightfoot (Ref. 2.1) gives as the general time-averaged turbulent species continuity equation in a binary system:

$$\frac{\partial \rho_A}{\partial t} + (\vec{\nabla} . \rho_A \vec{v}) = (\vec{\nabla} . \rho \overset{*}{\mathcal{D}} \vec{\nabla} \omega_A) + r_A \qquad (3.118)$$

where $\overset{*}{\mathcal{D}}_A = \overset{*}{\mathcal{D}}_A^{\,laminar} + \overset{*}{\mathcal{D}}_A^{\,turb}$

Assuming that constant density applies, Eq. (3.117) transforms to:

$$\frac{\partial \rho_A}{\partial t} + (\vec{\nabla} . \rho_A \vec{v}) = \vec{\nabla} \cdot \overset{*}{\mathbb{D}}_A \vec{\nabla} \rho_A + r_A \qquad (3.119)$$

Expanding:

$$\frac{\partial \rho_A}{\partial t} + \frac{\partial}{\partial x}(\rho_A u) + \frac{\partial}{\partial y}(\rho_A v) + \frac{\partial}{\partial z}(\rho_A w) =$$

$$\frac{\partial}{\partial x}\left(\overset{*}{\mathbb{D}}_{A_X} \frac{\partial \rho_A}{\partial x}\right) + \frac{\partial}{\partial y}\left(\overset{*}{\mathbb{D}}_{A_Y} \frac{\partial \rho_A}{\partial y}\right) + \frac{\partial}{\partial z}\left(\overset{*}{\mathbb{D}}_{A_Z} \frac{\partial \rho_A}{\partial z}\right) + r_A \qquad (3.120)$$

Eq. (3.120) is the general species continuity equation and can be applied to a shallow estuarine bay. Integrating this equation in the vertical direction, in order to obtain a two-dimensional equation, results in:

$$\int_h^L \left[\frac{\partial \rho_A}{\partial t} + \frac{\partial}{\partial x}(\rho_A u) + \frac{\partial}{\partial y}(\rho_A v) + \frac{\partial}{\partial z}(\rho_A w)\right] dz =$$

$$\int_h^L \left[\frac{\partial}{\partial x}\left(\overset{*}{\mathbb{D}}_{A_X} \frac{\partial \rho_A}{\partial x}\right) + \frac{\partial}{\partial y}\left(\overset{*}{\mathbb{D}}_{A_Y} \frac{\partial \rho_A}{\partial y}\right) + \frac{\partial}{\partial z}\left(\overset{*}{\mathbb{D}}_{A_Z} \frac{\partial \rho_A}{\partial z}\right)\right] dz + \int_h^L r_A dz \qquad (3.121)$$

Assuming a vertically uniform velocity profile, as was done with the energy equation, and applying Leibnitz's rule to each term in Eq. (3.121) gives:

$$\int_h^L \frac{\partial \rho_A}{\partial t} dz = \frac{\partial}{\partial t} \int_h^L \rho_A dz - \rho_A(x,y,L,t) \frac{\partial L}{\partial t} + \rho_A(x,y,h,t) \frac{\partial h}{\partial t} \qquad (3.122)$$

$$\int_h^L \frac{\partial}{\partial x}(\rho_A u) dz = \frac{\partial}{\partial x} U \int_h^L \rho_A dz - u\rho_A(x,y,L,t)\frac{\partial L}{\partial x} + u\rho_A(x,y,h,t) \frac{\partial h}{\partial x} \qquad (3.123)$$

$$\int_h^L \frac{\partial}{\partial y}(\rho_A v)dz = \frac{\partial}{\partial y} V \int_h^L \rho_A dz - V\rho_A(x,y,L,t)\frac{\partial L}{\partial y} + V\rho_A(x,y,h,t)\frac{\partial h}{\partial y} \quad (3.124)$$

$$\int_h^L \frac{\partial}{\partial z}(\rho_A w)dz = \rho_A w(L) - \rho_A w(h) \quad (3.125)$$

$$\int_h^L \frac{\partial}{\partial x}\left(\overset{*}{\mathcal{D}}_{A_X}\frac{\partial \rho_A}{\partial x}\right)dz = \frac{\partial}{\partial x}\int_h^L \overset{*}{\mathcal{D}}_{A_X}\frac{\partial \rho_A}{\partial x}\,dz - \overset{*}{\mathcal{D}}_{A_X}\frac{\partial \rho_A}{\partial x}(x,y,L,t)\frac{\partial L}{\partial x} + \overset{*}{\mathcal{D}}_{A_X}\frac{\partial \rho_A}{\partial x}(x,y,h,t)\frac{\partial h}{\partial x} \quad (3.126)$$

Developing the first term on the right hand side of Eq. (3.126) by Leibnitz's rule:

$$\int_h^L \overset{*}{\mathcal{D}}_{A_X}\frac{\partial \rho_A}{\partial x}dz = \frac{\partial}{\partial x}\int_h^L \overset{*}{\mathcal{D}}_{A_X}\rho_A dz - \overset{*}{\mathcal{D}}_{A_X}\rho_A(x,y,L,t)\frac{\partial L}{\partial x} + \overset{*}{\mathcal{D}}_{A_X}\rho_A(x,y,h,t)\frac{\partial h}{\partial x} \quad (3.127)$$

$$\int_h^L \frac{\partial}{\partial y}\left(\overset{*}{\mathcal{D}}_{A_Y}\frac{\partial \rho_A}{\partial y}\right)dz = \frac{\partial}{\partial y}\int_h^L \overset{*}{\mathcal{D}}_{A_Y}\frac{\partial \rho_A}{\partial y}\,dz - \mathcal{D}_{A_Y}\rho_A(x,y,L,t)\frac{\partial L}{\partial y} + \overset{*}{\mathcal{D}}_{A_Y}\frac{\partial \rho_A}{\partial y}(x,y,h,t)\frac{\partial h}{\partial y} \quad (3.128)$$

Developing the first term on the right hand side of Eq. (3.128) by Leibnitz's rule:

$$\int_h^L \overset{*}{\mathcal{D}}_{A_Y}\frac{\partial \rho_A}{\partial y}dz = \frac{\partial}{\partial y}\int_h^L \overset{*}{\mathcal{D}}_{A_Y}\rho_A dz - \overset{*}{\mathcal{D}}_{A_Y}\rho_A(x,y,L,t)\frac{\partial L}{\partial y} + \overset{*}{\mathcal{D}}_{A_Y}\rho_A(x,y,h,t)\frac{\partial h}{\partial y} \quad (3.129)$$

$$\int_h^L \frac{\partial}{\partial z}\left(\overset{*}{\mathcal{D}}_{A_Z}\frac{\partial \rho_A}{\partial z}\right)dz = \overset{*}{\mathcal{D}}_{A_Z}\frac{\partial \rho_A}{\partial z}(L) - \overset{*}{\mathcal{D}}_{A_Z}\frac{\partial \rho_A}{\partial z}(h) \tag{3.130}$$

$$\int_h^L r_A dz = \bar{r}_A D \tag{3.131}$$

It can be noted here that when the diffusion coefficient is taken to be independent of depth, it becomes a dispersion coefficient by definition. Substituting Eqs. (3.122) through (3.131) into Eq. (3.121) results in:

$$\frac{\partial}{\partial t}\int_h^L \rho_A dz + \frac{\partial}{\partial x} U \int_h^L \rho_A dz + \frac{\partial}{\partial y} V \int_h^L \rho_A dz -$$

$$\rho_A(x,y,L,t)\left[\frac{\partial L}{\partial t} + u\frac{\partial L}{\partial x} + v\frac{\partial L}{\partial y}\right] + \rho_A(x,y,h,t)\left[\frac{\partial h}{\partial t} + u\frac{\partial h}{\partial x} + v\frac{\partial h}{\partial y}\right] +$$

$$\rho_A w(L) - \rho_A w(h) = \frac{\partial}{\partial x}\left(\mathcal{D}_{A_X}\frac{\partial}{\partial x}\int_h^L \rho_A dz - \overset{*}{\mathcal{D}}_{A_X}\rho_A(x,y,L,t)\frac{\partial L}{\partial x} +\right.$$

$$\left.\overset{*}{\mathcal{D}}_{A_X}\rho_A(x,y,h,t)\frac{\partial h}{\partial x}\right) - \overset{*}{\mathcal{D}}_{A_X}\frac{\partial \rho_A}{\partial x}(x,y,L,t)\frac{\partial L}{\partial x} + \overset{*}{\mathcal{D}}_{A_X}\frac{\partial \rho_A}{\partial x}(x,y,h,t)\frac{\partial h}{\partial x} + \tag{3.132}$$

$$\frac{\partial}{\partial y}\left(\mathcal{D}_{A_Y}\frac{\partial}{\partial y}\int_h^L \rho_A dz - \overset{*}{\mathcal{D}}_{A_Y}\rho_A(x,y,L,t)\frac{\partial L}{\partial y} + \overset{*}{\mathcal{D}}_{A_Y}\rho_A(x,y,h,t)\frac{\partial h}{\partial y}\right) -$$

$$\overset{*}{\mathcal{D}}_{A_Y}\frac{\partial \rho_A}{\partial y}(x,y,L,t)\frac{\partial L}{\partial y} + \overset{*}{\mathcal{D}}_{A_Y}\frac{\partial \rho_A}{\partial y}(x,y,h,t)\frac{\partial h}{\partial y} + \overset{*}{\mathcal{D}}_{A_Z}\frac{\partial \rho_A}{\partial z}(L) -$$

$$\overset{*}{\mathcal{D}}_{A_Z}\frac{\partial \rho_A}{\partial z}(h) + \bar{r}_A D$$

Defining a vertically averaged concentration

$$S_A = \frac{1}{D}\int_h^L \rho_A dz \tag{3.133}$$

and rearranging, Eq. (3.132) becomes:

$$\frac{\partial}{\partial t}(DS_A) + \frac{\partial}{\partial x}(UDS_A) + \frac{\partial}{\partial y}(VDS_A) - \rho_A(x,y,L,t)\left[\frac{\partial L}{\partial t} + u\frac{\partial L}{\partial x} + v\frac{\partial L}{\partial y}\right]$$

$$+ \rho_A(x,y,h,t)\left[\frac{\partial h}{\partial t} + u\frac{\partial h}{\partial x} + v\frac{\partial h}{\partial y}\right] + \rho_A w(L) - \rho_A w(h) =$$

$$\frac{\partial}{\partial x}\left(\text{Þ}_{A_X}\frac{\partial(DS_A)}{\partial x}\right) + \frac{\partial}{\partial y}\left(\text{Þ}_{A_Y}\frac{\partial(DS_A)}{\partial y}\right) - \frac{\partial}{\partial x}\left(\overset{*}{\text{Þ}}_{A_X}\rho_A(x,y,L,t)\frac{\partial L}{\partial x}\right) +$$

(3.134)

$$\frac{\partial}{\partial x}\left(\overset{*}{\text{Þ}}_{A_X}\rho_A(x,y,h,t)\frac{\partial h}{\partial x}\right) - \overset{*}{\text{Þ}}_{A_X}\frac{\partial \rho_A}{\partial x}(x,y,L,t)\frac{\partial L}{\partial x} + \overset{*}{\text{Þ}}_{A_X}\frac{\partial \rho_A}{\partial x}(x,y,h,t)\frac{\partial h}{\partial x} -$$

$$\frac{\partial}{\partial y}\left(\overset{*}{\text{Þ}}_{A_Y}\rho_A(x,y,L,t)\frac{\partial L}{\partial y}\right) + \frac{\partial}{\partial y}\left(\overset{*}{\text{Þ}}_{A_Y}\rho_A(s,y,h,t)\frac{\partial h}{\partial y}\right) - \overset{*}{\text{Þ}}_{A_Y}\frac{\partial \rho_A}{\rho y}(x,y,L,t)\frac{\partial L}{\partial y} +$$

$$\overset{*}{\text{Þ}}_{A_Y}\frac{\partial \rho_A}{\partial y}(x,y,h,t)\frac{\partial h}{\partial y} + \overset{*}{\text{Þ}}_{A_Z}\frac{\partial \rho_A}{\partial z}(L) - \overset{*}{\text{Þ}}_{A_Z}\frac{\partial \rho_A}{\partial z}(h) + \overline{r}_A D$$

Substituting Eqs. (3.4) and (3.5) into Eq. (3.134) and neglecting the higher order diffusive terms gives:

$$\frac{\partial(DS_A)}{\partial t} + \frac{\partial(UDS_A)}{\partial x} + \frac{\partial(VDS_A)}{\partial y} = \frac{\partial}{\partial x}\left(D\text{Þ}_{A_X}\frac{\partial S_A}{\partial x}\right) + \frac{\partial}{\partial y}\left(D\text{Þ}_{A_Y}\frac{\partial S_A}{\partial y}\right) +$$

(3.135)

$$\left[\text{Þ}_{A_Z}\frac{\partial \rho_A}{\partial z}(L) - \text{Þ}_{A_Z}\frac{\partial \rho_A}{\partial z}(h) - \rho_A w(L) + \rho_A w(h) + \overline{r}_A D\right]$$

The terms in brackets in the previous equation represent the sinks and sources of species A. These sinks and sources take into account convection and diffusion through the air and bottom surfaces, and chemical reactions. Eq. (3.135) can be written as:

$$\frac{\partial(DS_A)}{\partial t} + \frac{\partial(UDS_A)}{\partial x} + \frac{\partial(VDS_A)}{\partial y} = \frac{\partial}{\partial x}\left(D\text{Þ}_{A_X}\frac{\partial S_A}{\partial x}\right) + \frac{\partial}{\partial y}\left(D\text{Þ}_{A_Y}\frac{\partial S_A}{\partial y}\right) + SS_A$$

(3.136)

Eq. (3.136) is the vertically averaged species transport equation. Note the similarity to the energy equation Eq. (3.99), Eq. (3.136) shows diffusivity can be different for the x and y directions.

As stated before, these terms are often referred to as the dispersion coefficients. Appropriate dispersion coefficients are usually obtained by adjusting the model to match experimental data for a specific location.

Sinks and Sources for the Mass Transport Model

A species balance at the surface can be obtained by integrating the general species equation, Eq. (3.118), across the surface from z^- (in the water) to z^+ (in the air). The final result is obtained by taking the limit as goes to zero. The species equation for a shallow estuarine bay is given by Eq. (3.120). Integrating Eq. (3.120) as stated gives:

$$\int_{z^-}^{z^+} \left[\frac{\partial \rho_A}{\partial t} + \frac{\partial}{\partial x}(\rho_A u) + \frac{\partial}{\partial y}(\rho_A v)\right] dz + \int_{z^-}^{z^+} \frac{\partial}{\partial z}(w\rho_A) dz =$$

$$\int_{z^-}^{z^+} \left[\frac{\partial}{\partial x} \mathcal{D}_{A_X} \frac{\partial \rho_A}{\partial x} + \frac{\partial}{\partial y} \mathcal{D}_{A_Y} \frac{\partial \rho_A}{\partial y}\right] dz + \int_{z^-}^{z^+} \left(\frac{\partial}{\partial z} \mathcal{D}_{A_Z} \frac{\partial \rho_A}{\partial z}\right) dz + \bar{r}_A D \qquad (3.137)$$

The above can be written in terms of average values using the mean value theorem as:

$$\overline{\left[\frac{\partial \rho_A}{\partial t} + \frac{\partial}{\partial x}(\rho_A u) + \frac{\partial}{\partial y}(\rho_A v)\right]} \int_{z^-}^{z^+} dz + \int_{z^-}^{z^+} \frac{\partial}{\partial z}(w\rho_A) dz =$$

$$\overline{\left[\frac{\partial}{\partial x} \mathcal{D}_{A_X} \frac{\partial \rho_A}{\partial x} + \frac{\partial}{\partial y} \mathcal{D}_{A_Y} \frac{\partial \rho_A}{\partial y}\right]} \int_{z^-}^{z^+} dz + \int_{z^-}^{z^+} \left(\frac{\partial}{\partial x} \mathcal{D}_{A_Z} \frac{\partial \rho_A}{\partial z}\right) dz + \bar{r}_A D \qquad (3.138)$$

Assuming diffusivity is not a function of depth, performing the integration, taking the limit as Δz goes to zero, and rearranging gives:

$$w\rho_A^+ - \mathcal{D}_{A_Z} \frac{\partial \rho_A^+}{\partial z} = w\rho_A^- - \mathcal{D}_{A_Z} \frac{\partial \rho_A^-}{\partial z} \qquad (3.139)$$

The first term on the left-hand side of Eq (3.139) represents the convective species flux from the air to the surface. The convective flow in this case is due to rainfall and evaporation; so this term can be written as:

$$w\rho_A^+ = w\rho\omega_A^+ = \rho[R-Ev]\omega_A^+ = \rho R\omega_A^+ - \rho Ev\omega_A^+ \qquad (3.140)$$

For the equation representing the balance of water, the mass fraction, ω_A, is equal to one; for other cases, it is less than or equal to one. However, it is possible to take in account the carbon dioxide and oxygen dissolved in the rain water.

The second term on the left-hand side represents the diffusive species flux from the air to the surface. This term can be written in terms of a mass transfer coefficient K_A as:

$$\mathcal{D}_{A_Z} \frac{\partial \rho_A}{\partial z}^{+} = K_A (C_A^{*} - C_{A,\ surface}) = J_A \qquad (3.141)$$

The terms on the right-hand side of Eq. (3.139) are terms found in the Mass Transport Model. The first term on the right-hand side of Eq. (3.139), ${}^{w\rho_A}{}^{-}$ is equivalent to the term ${}^{\rho_A w(L)}$ in Eq. (3.135), and the second term, ${}^{\mathcal{D}_{A_Z}{}^{*}\ (\partial \rho_A/\partial z)}{}^{-}$, is equivalent to ${}^{\mathcal{D}_{A_Z}(\partial \rho_A(L)/\partial z)}$ in Eq. (3.135). Eqs. (3.140) and (3.141) represent the source and sink terms that couple the mass transfer at the air-water interface to the differential equation that describes the mass transfer in the estuarine bay, Eq. (3.136).

If a similar analysis is performed by integrating the species continuity equation across the water bottom interface, it can be shown that the following equation will be obtained:

$$\mathcal{D}_{A_Z} \frac{\partial \rho_A}{\partial z}^{+} = \mathcal{D}_{A_Z} \frac{\partial \rho_A}{\partial z}^{-} + r_{A,\ bottom} \qquad (3.142)$$

The mass transfer occurring at the bottom is due to diffusion and bottom chemical reaction. Due to the existing conditions at the bottom of the estuarine body of water, the evaluation of this diffusive and reactive term is conveniently evaluated with a mass transfer coefficient as used in the surface balance. The bottom reaction phenomenon is the net production of species associated with microbial activity on the bottom of the estuarine body of water. This reaction phenomenon is described by empirical rate equations. These empirical relationships for the bottom mass transfer, the bottom reaction phenomenon, and also the surface mass transfer are discussed in the literature. (See Refs. 2.11, 3.4, 3.5, and 3.6).

Boundary and Initial Conditions

In order to obtain a solution to the equations derived, certain boundary and initial conditions are necessary. These conditions are summarized in Table 3.2.

Initial conditions are required and realistic ones can be generated by starting the bay "at rest" and march in time for several tidal cycles. For the bay "at rest", all velocities are zero and all tidal levels, temperatures, and species concentrations have a constant value. The model can then be operated until all disturbances due to the unrealistic initial conditions disappear. Now, the calculated bay conditions can be used as an initial condition for another run.

The boundary conditions apply to the open and closed boundaries of the bay under study. At the closed boundaries all transfer of momentum, energy and mass is set to zero. At the entrance to the bay, the sea tidal level, temperature and salinity are specified as a function of time. Thus influx of water, temperature and species concentration are determined or can be calculated.

TABLE 3.2

BOUNDARY AND INITIAL CONDITIONS

INITIAL CONDITIONS	U, V, L are equal to zero T's have a constant set value P's have a constant set value
BOUNDARY CONDITIONS	velocities perpendicular to the boundaries are zero
	$\frac{\partial L}{\partial x} = 0$ at the boundary
	$\frac{\partial L}{\partial y} = 0$ at the boundary
	$\frac{\partial U}{\partial x} = 0$ at the boundary
	$\frac{\partial V}{\partial y} = 0$ at the boundary
	$\frac{\partial T}{\partial x} = 0$ at the boundary
	$\frac{\partial T}{\partial y} = 0$ at the boundary
	$\frac{\partial P}{\partial x} = 0$ at the boundary
	$\frac{\partial P}{\partial y} = 0$ at the boundary
	T = TSEA at the entrances
	P = PSEA at the entrances
	L = LSEA at the entrances

The Hydrodynamic Model, the Energy Transport Model, and the Mass Transport Model equations are summarized in Table 3.3. The sinks and sources terms for the energy equation are summarized in Table 3.4. No sources and sinks terms are needed for the modeling of salinity. The next chapter will discuss the numerical solution of these equations.

TABLE 3.3

EQUATIONS FOR THE OVERALL MODEL

HYDRODYNAMIC MODEL	$\frac{\partial(DU)}{\partial x} + \frac{\partial(DV)}{\partial y} + \frac{\partial L}{\partial t} = R - Ev$	(3.14)
	$\frac{\partial U}{\partial t} + U\frac{\partial U}{\partial x} + V\frac{\partial U}{\partial y} - FV + g\frac{\partial L}{\partial x} = X - g\frac{U(U^2+V^2)^{1/2}}{DC^2}$	(3.59)
	$\frac{\partial V}{\partial t} + U\frac{\partial V}{\partial x} + V\frac{\partial V}{\partial y} + FU + g\frac{\partial L}{\partial y} = Y - g\frac{V(U^2+V^2)^{1/2}}{DC^2}$	(3.60)
ENERGY TRANSPORT MODEL	$\rho Cp\left[\frac{\partial(\overline{T}D)}{\partial t} + \frac{\partial(UD\overline{T})}{\partial x} + \frac{\partial(VD\overline{T})}{\partial y}\right] - \frac{\partial}{\partial x}\left(Dky\frac{\partial\overline{T}}{\partial x}\right) - \frac{\partial}{\partial y}\left(Dky\frac{\partial\overline{T}}{\partial y}\right) - SS_E = 0$	(3.98)
MASS TRANSPORT MODEL	$\frac{\partial(DS_A)}{\partial t} + \frac{\partial(UDS_A)}{\partial x} + \frac{\partial(VDS_A)}{\partial y} - \frac{\partial}{\partial x}\left(DQ_{AX}\frac{\partial S_A}{\partial x}\right) - \frac{\partial}{\partial y}\left(DQ_{AY}\frac{\partial S_A}{\partial y}\right) - SS_A = 0$	(3.135)

TABLE 3.4

ENERGY SOURCE AND SINK TERMS

Sky Radiation	Water Surface Radiation	Evaporation	Surface Convection	Bottom Conduction
Evaluated Experimentally Approximate value = 0.333 kcal/m^2*sec	$q_w = \epsilon\sigma T_s^4$ (3.114)	$q_{ev} = [\lambda + C_p(T_s - T_a)]Ev\rho$ (3.106) $E_v = NW(e_s - e_a)$ (3.107)	$q_c = \lambda\, Ev\rho\, B$ (3.111) $B = 6.1*10^{-4}*$ (3.112) $P_a\left[\frac{T_a - T_s}{e_s - e_a}\right]$	$q_b = -k_b\left(\frac{\partial T}{\partial z}\right)_b$ (3.117)

REFERENCES

3.1 Dronkers, J. J., Tidal Computations in Rivers and Coastal Waters, John Wiley and Sons, Inc. New York, N.Y. (1964)

3.2 Bird, R. B. , W. E. Stewart, and E. N. Lightfoot, Transport Phenomena, John Wiley and Sons, Inc., New York, N.Y. (1960), pp. 79, 80.

3.3 Van Dorn, W., "Wind Stresses on an Artificial Pond," J. Marine Res, Vol. 12, No. 3, (1953), pp. 249-276.

3.4 Geiger, R. The Climate Near the Ground, Harvard University Press, Cambridge, Mass., (1968) p.7.

3.5 Callaway, R. J., et al, "Mathematical Modeling of the Columbia River from the Pacific Ocean to the Bonneville Dam, Part I," U. S. Department of the Interior, IVPCA, Corvalis, Oregon, (1969), pp. 49-53

3.6 Churchill, F., et al, "The Prediction of Stream Reaeration Rate," Proceedings ASCE, Journal of the Sanitary Engineering Division, Vol, 88, No. 1, (1962), pp. 1-46.

3.7 O'Connor, D. J. and W. E. Dobbins, "Mechanisms of Reareation in Natural Streams," ASCE Trans., N.Y., Vol. 123, (1958).

CHAPTER IV

NUMERICAL IMPLEMENTATION OF THE TRANSPORT PHENOMENA EQUATIONS OF SHALLOW ESTUARINE BAY SYSTEMS

Introduction

In order to solve the equations derived in the previous chapter, the Alternating Directions Implicit Technique (Refs. 4.1 and 4.2) is used because it is considered the most suitable. The use of this technique in transport phenomena equations for shallow estuarine bay systems was first reported by Leendertse (Ref. 2.9) for a hydrodynamic model of Jamaica Bay, New York. This scheme was later extended to include a pollution dispersion model in the same area. The numerical technique presented in this chapter is derived from the scheme used by Leendertse in his Jamaica Bay Model.

The first part of this chapter will present the numerical implementation of the Hydrodynamic Model. The second part will present the numerical implementation of the Energy Transport Model and the Mass Transport Model. These latter two models are in identical mathematical form; therefore, the same algorithm applies to both of them. The last part deals with numerical operations to describe special conditions inside the calculation grid.

Finite Difference Approximation of the Hydrodynamic Model

In order to use a finite difference approximation on the Hydrodynamic Model, the variables are placed on a space staggered grid, as shown in Fig. 4.1. This space staggered grid was first used by Platzman (Ref. 2.5)

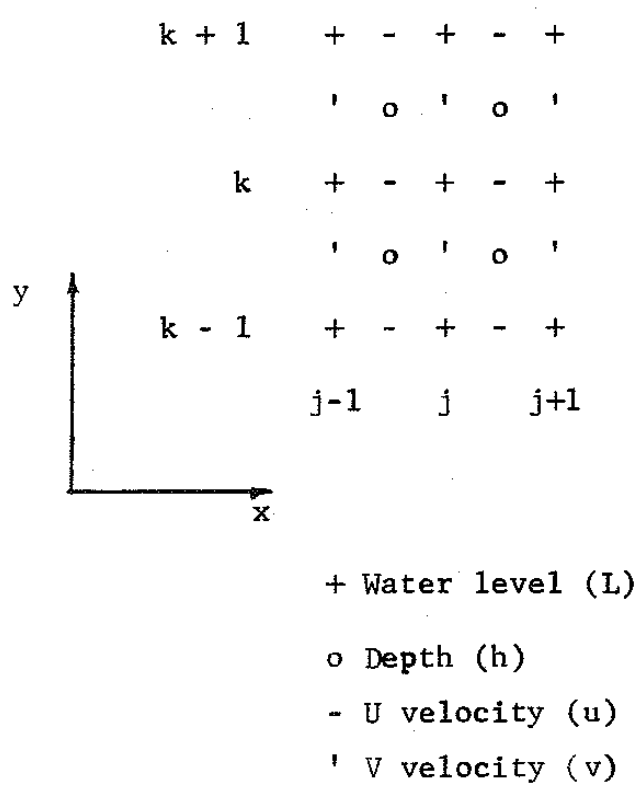

Fig. 4.1. Space-staggered scheme.

This grid is advantageous as it allows the numerical problem to be placed in a tridiagonal matrix form. The water levels, L, are located at integer values of j and k, the depths, h, are stored at half integer values of j and k. The U velocities are located at half integer values of j and integer values of k, and the V velocities are located at integer values of j and half integer values of k.

The Alternating Direction Implicit Technique works over the grid in the following fashion: the x-component of the equation of motion and the continuity equation are applied on a given row and the resulting equations are solved implicitly for the U velocities and the water L, in the given row. The same procedure is followed in the next row, and so on, until the whole field under the grid is covered. With the implicitly calculated values of U and L, the V velocities can be explicitly calculated by using the continuity equation. The field then has been covered in one direction. The next step alternates direction. Thus, the y-component of the equation of motion and the continuity equation are applied on a given column and the resulting equations are solved implicitly for the V velocities and the water levels, L, in the given column. The same procedure is followed in the next column, and so on, until the whole field under the grid is covered. With the implicitly calculated values of V and L, the U velocities of this second step can be explicitly calculated by using the continuity equation. When the two operations mentioned above are combined, it is found that all the unknowns (U velocities, V velocities and water levels, L) have been calculated implicitly. These two operations combine to form a time step. The solution for the next time step is found by repeating this procedure.

In order to make the derivation of the finite difference equations more manageable, the following "short hand" notation is used:

$$F_n \equiv F_n(j\Delta x, k\Delta y, n\Delta t) \tag{4.1}$$

$$\bar{F}_n^x \equiv 1/2\{F_n[(j+1/2)\Delta x, k\Delta y, n\Delta t] + F_n[(j-1/2)\Delta x, k\Delta y, n\Delta t]\} \tag{4.2}$$

$$\delta_x F_n \equiv \frac{1}{\Delta x}\{F_n[(j+1/2)\Delta x, k\Delta y, n\Delta t] - F_n[(j-1/2)\Delta x, k\Delta y, n\Delta t]\} \tag{4.3}$$

$$F_n^+ \equiv 1/4\{F_n[(j+1/2)\Delta x, (k+1/2)\Delta y, n\Delta t] + F_n[(j+1/2)\Delta x, (k-1/2)\Delta y, n\Delta t] + F_n[(j-1/2)\Delta t, (k+1/2)\Delta y, n\Delta t] + F_n[(j-1/2)\Delta x, (k-1/2) * \Delta y, n\Delta t]\} \tag{4.4}$$

$$\Delta_{t/2} F_n \equiv \frac{2}{\Delta t}\{F_n[j\Delta x, k\Delta y, (n+1/2)\Delta t] - F_n[j\Delta t, k\Delta y, n\Delta t]\} \tag{4.5}$$

$$F_{n+} \equiv F_n\,[j\Delta x, k\Delta y, (n+1/2)\,\Delta t] \tag{4.6}$$

$$F_{n\_} \equiv F_n\,[j\Delta x, k\Delta y, (n-1/2)\Delta t] \tag{4.7}$$

$$\bar{F}_n^{t/2} \equiv 1/2\,[F_{n+} + F_n] \tag{4.8}$$

Eqs. (4.2) and (4,3) are shown for x. Similar equations can be written for y and t.

First Half-time Step

As it was previously mentioned, the first half-time step is used to calculate the U velocities and the water levels. The x-component of the equation of motion of the Hydrodynamic Model,

$$\frac{\partial U}{\partial t} + U\frac{\partial U}{\partial x} + V\frac{\partial U}{\partial y} - FV + g\frac{\partial L}{\partial x} + g\frac{U(U^2+V^2)^{1/2}}{D\,C^2} - X = 0 \tag{4.9}$$

and the continuity equation,

$$\frac{\partial L}{\partial t} + \frac{\partial (DU)}{\partial x} + \frac{\partial (DV)}{\partial y} = R\text{-}Ev \tag{4.10}$$

can be written in finite difference form. The finite difference form of the x-component of the equation of motion is:

$$\delta_t U - F\overset{+}{V} + U_+ \overline{\delta x}^x U_- + \overset{+}{V} \overline{\delta y U_-}^y + g\,\overline{\delta x L}^t +$$

$$g\,\frac{\overline{U}^{t/2}\left[(U_-)^2 + (\overset{+}{V})^2\right]^{1/2}}{(\overline{h}^y + \overline{L}^x)(\overline{C}^x)^2} - \frac{\tau_x^s}{\rho(\overline{h}^y + \overline{L}^x)} = 0 \quad \text{at } j+1/2,k,n \tag{4.11}$$

the finite difference form of the continuity equation is:

$$\Delta_{t/2} L + \delta x[(\overline{h}^y + \overline{L}^x)\,U_+] + \delta y[(\overline{h}^x + \overline{L}^y)V] = 0 \quad \text{at } j,k,n \tag{4.12}$$

The rainfall rate, R, and evaporation, Ev, are not included at this time but they are an integral part of the numerical technique. The effects of rainfall and evaporation are included at the end of every half-time step by changing the water levels appropriately. Expanding the above equation results in:

$$\begin{aligned}
&\frac{2}{\Delta t}(L_{j,k}^{n+1/2} - L_{j,k}^n) + [(h_{j+1/2,k+1/2} + h_{j+1/2,k-1/2} + L_{j+1,k}^n \\
&\quad + L_{j,k}^n)\,U_{j+1/2,k}^{n+1/2} - (h_{j-1/2} + h_{j-1/2,k-1/2} + L_{j-1,k}^n \\
&\quad + L_{j,k}^n)\,U_{j-1/2,k}^{n+1/2}]\,\frac{1}{2\Delta x} + [(h_{j+1/2,k+1/2} + h_{j-1/2,\,k+1/2} \\
&\quad + L_{j,k+1}^n + L_{j,k}^n)\,V_{j,k+1/2}^n - (h_{j+1/2,k-1/2} + h_{j-1/2,k-1/2} \\
&\quad + L_{j,k}^n + L_{j,k-1}^n)\,V_{j,k-1/2}^n]\,\frac{1}{2\Delta y} = 0
\end{aligned} \tag{4.13}$$

Eq. (4.13) can be rewritten as:

$$-r_{j-1/2}\,U_{j-1/2,k}^{n+1/2} + L_{j,k}^{n+1/2} + r_{j+1/2}\,U_{j+1/2,k}^{n+1/2} = A_j^n \tag{4.14}$$

in which:

$$\Delta x = \Delta y \tag{4.15}$$

$$r_{j-1/2} = (h_{j-1/2,k+1/2} + h_{j-1/2,k-1/2} + L^n_{j-1,k} + L^n_{j,k}) \frac{\Delta t}{4\Delta x} \tag{4.16}$$

$$r_{j+1/2} = (h_{j+1/2,k+1/2} + h_{j+1/2,k-1/2} + L^n_{j+1,k} + L^n_{j,k}) \frac{\Delta t}{4\Delta x} \tag{4.17}$$

$$A^n_j = L^n_{j,k} + (h_{j+1/2,k-1/2} + h_{j-1/2,k-1/2} + L^n_{j,k} + L^n_{j,k-1}) V^n_{j,k-1/2} (\frac{\Delta t}{4\Delta x}) - (h_{j+1/2,k+1/2} + h_{j-1/2,k+1/2} + L^n_{j,k+1} + L^n_{j,k}) V^n_{j,k+1/2} (\frac{\Delta t}{4\Delta x}) \tag{4.18}$$

The x-component of the equation of motion, Eq. (4.11) can be expanded as:

$$\frac{1}{\Delta t}(U^{n+1/2}_{j+1/2,k} - U^{n-1/2}_{j+1/2,k}) - F\overset{+}{V} + (U^{n-1/2}_{j+3/2,k} - U^{n-1/2}_{j-1/2k}) * U^{n+1/2}_{j+1/2,k} \frac{1}{2\Delta x} + (U^{n-1/2}_{j+1/2,k+1} - U^{n-1/2}_{j+1/2,k-1}) \frac{\overset{+}{V}}{2\Delta x} + (L^{n+1/2}_{j\ 1,k} - L^{n+1/2}_{j,k} + L^{n-1/2}_{j+1,k} - L^{n-1/2}_{j,k}) \frac{g}{2\Delta x} + (\frac{g}{2})(U^{n+1/2}_{j+1/2,k} + U^{n-1/2}_{j+1/2,k}) * \frac{[(U^{n-1/2}_{j+1/2,k})^2 + (\overset{+}{V})^2]^{1/2}}{(\bar{h}^y + \bar{L}^x)(\bar{C}^x)^2} - \frac{\tau^s_x}{\rho(\bar{h}^y + \bar{L}^x)} = 0 \text{ at } j+1/2,k,n \tag{4.19}$$

Eq. (4.19) can be rewritten as:

$$-r_j L^{n+1/2}_{j,k} + r'_{j+1/2} U^{n+1/2}_{j+1/2,k} + r_{j+1} L^{n+1/2}_{j+1,k} = B^n_{j+1/2,k} \tag{4.20}$$

in which:

$$r_j = r_{j+1} = \frac{g\Delta t}{2\Delta x} \tag{4.21}$$

$$r'_{j+1/2} = 1 + \frac{\Delta t}{2\Delta x}(U^{n-1/2}_{j+3/2,k} - U^{n-1/2}_{j-1/2,k}) + \frac{\frac{g\Delta t}{2}\left[(U^{n-1/2}_{j+1/2,k})^2 + (\overline{\overline{V}})^2\right]^{1/2}}{(\overline{h}^y + \overline{L}^x)(\overline{C}^x)^2} \tag{4.22}$$

$$B^n_{j+1/2,k} = U^{n-1/2}_{j+1/2,k} + \left[F\Delta t - \frac{\Delta t}{2\Delta x}(U^{n-1/2}_{j+1/2,k+1} - U^{n-1/2}_{j+1/2,k-1})\right]\overline{\overline{V}} - g\frac{\Delta t}{2\Delta t}(L^{n-1/2}_{j+1,k} - L^{n-1/2}_{j,k}) + \frac{\tau^s_x\,\Delta t}{\rho(\overline{h}^y + \overline{L}^x)} - \frac{\frac{g\Delta t}{2}\,U^{n-1/2}_{j+1/2,k}\left[(U^{n-1/2}_{j+1/2,k})^2 + (\overline{\overline{V}})^2\right]^{1/2}}{(\overline{h}^y + \overline{L}^x)(\overline{C}^x)^2} \tag{4.23}$$

Eqs. (4.14) and (4.20) can now be solved for the unknown values of the U velocities and water levels on the kth. row if boundary conditions are specified at both ends of the row. These boundary conditions can be: the U velocities at both ends, the U velocity at one end and the water level at the other end or the water levels at both ends. If there are U grid points in the given row (j = 1,2,3,... .N), Eqs. (4.14) and (4.20) can be placed in matrix form in which the matrix will be tridiagonal and the unknown vector will have (2N-2) elements. For example, let the known boundary conditions be $L_{l,k}$ and $U_{n+1/2,k}$; the system of equations that result can be written in matrix form as:

$$\begin{bmatrix} r'_{1+1/2} & r_2 & & & & \\ -r_{1+1/2} & 1 & r_{2+1/2} & & & \\ & -r_2 & r_{2+1/2} & r_3 & & \\ & & -r_{2+1/2} & 1 & r_{3+1/2} & \\ & & & & & \\ & & & & -r_{n-1}r'_{n-1/2} & r_n \\ & & & & & -r_{n-1/2} \quad 1 \end{bmatrix} \begin{bmatrix} U_{1+1/2,k} \\ L_{2,k} \\ U_{2+1/a,k} \\ L_{3,k} \\ \\ U_{n-1/2,k} \\ L_{n,k} \end{bmatrix} = \begin{bmatrix} B_{1+1/2}+r_1 L_{1,k} \\ A_2 \\ B_{2+1/2} \\ A_3 \\ \\ B_{n-1/2} \\ A_n - r_{n+1/2} U_{n+1/2,k} \end{bmatrix} \quad (4.24)$$

If the boundary conditions are $U_{1+1/2,k}$ and $U_{n+1/2,k}$, then the resulting matrix system is:

$$\begin{bmatrix} -r_1 & r_2 & & & & \\ 0 & 1 & r_{2+1/2} & & & \\ & -r_2 & r'_{2+1/2} & r_3 & & \\ & & -r_{2+1/2} & 1 & r_{3+1/2} & \\ & & & & & \\ & & & & -r_{n-1}r'_{n-1/2} & r_n \\ & & & & & -r_{n-1/2} \quad 1 \end{bmatrix} \begin{bmatrix} L_{1,k} \\ L_{2,k} \\ U_{2+1/2,k} \\ L_{3,k} \\ \\ U_{n-1/2,k} \\ L_{n,k} \end{bmatrix} = \begin{bmatrix} B_{1+1/2} - r'_{1+1/2} U_{1+1/2,k} \\ A_2 + r_{1+1/2} U_{1+1/2,k} \\ B_{2+1/2} \\ A_3 \\ \\ B_{n-1/2} \\ A_n - r_{n+1/2} U_{n+1/2,k} \end{bmatrix} \quad (4.25)$$

Thus, by knowing the values of water levels at the time level n, the V velocities at time level n, the U velocities at time level n-1/2 and the boundary conditions at time level n + 1/2, the values of water levels and U velocities for the n + 1/2 level can be calculated by applying the Thomas Algorithm to the tridiagonal matrix. The values are obtained for the whole grid as the above calculation is repeated for all the rows.

Once all the rows have been swept, the first half-time step for the hydrodynamics has been completed. The second half-time step follows.

Second Half-time Step

In the second half-time step, (n + l/2)t to (n + l)t, the V velocities and the water levels are calculated. The y-component of the equation of motion of the Hydrodynamic Model,

$$\frac{\partial V}{\partial t} + U\frac{\partial V}{\partial x} + V\frac{\partial V}{\partial y} + FU + g\frac{\partial L}{\partial y} + g\frac{V(U^2+V^2)^{1/2}}{DC^2} - Y = 0 \qquad (4.26)$$

and the continuity equation,

$$\frac{\partial L}{\partial t} + \frac{\partial (DU)}{\partial x} + \frac{\partial (DV)}{\partial y} = R - E_v \qquad (4.10)$$

can be written in finite difference form. The finite difference form of the y-direction equation of motion is

$$\delta_t V + F\overline{U}^{+} + \overline{U\delta_x V}^{x}_{-} + V_{+}\overline{\delta V}^{y}_{-} + g\,\overline{\delta y L}^{t} + g\frac{\overline{V}^{t}[(\overline{U}^{+})^2 + (V_{-})^2]^{1/2}}{(\overline{h}^{x} + \overline{L}^{y})(\overline{C}^{v})^2} - \frac{\tau_y^s}{\rho(\overline{h}^{x} + \overline{L}^{y})} = 0 \text{ at } j,k+1/2,n+1/2 \qquad (4.27)$$

The above equation can be expanded as:

$$\frac{1}{\Delta t}(V^{n+1}_{j,k+1/2} - V^{n}_{j,k+1/2}) + F\overline{U}^{+} + (V^{n}_{j+1,k+1/2} - V^{n}_{j-1,k+1/2})\frac{\overline{U}^{+}}{2\Delta x} + (F^{n}_{j,k+3/2} - V^{n}_{j,k-1/2})\,V^{n+1}_{j,k+1/2}\,\frac{1}{2\Delta x} + (L^{n+1}_{j,k+1} - L^{n+1}_{j,k} + L^{n}_{j,k+1} - L^{n}_{j,k})\frac{g}{2\Delta x} + \frac{(\frac{g}{2})(V^{n+1}_{j,k+1/2}+V^{n}_{j,k+1/2})[(\overline{U}^{+})^2 + (V^{n}_{j,k+1/2})^2]^{1/2}}{(\overline{h}^{x} + \overline{L}^{y})(\overline{C}^{y})^2} - \frac{\tau_y^s}{\rho(\overline{h}^{x} + \overline{L}^{y})} = 0 \text{ at } j,k+1/2,n+1/2 \qquad (4.28)$$

Eq. (4.28) can be rewritten as:

$$-r_k L^{n+1}_{j,k} + r'_{k+1/2} V^{n+1}_{j,k+1/2} + r_{k+1} L^{n+1}_{j,k+1} = B^{n+1/2}_{j,k+1/2} \qquad (4.29)$$

in which:

$$r_k = r_{k+1} = \frac{g\Delta t}{2\Delta x} \tag{4.30}$$

$$r'_{k+1/2} = 1 + \frac{\Delta t}{2\Delta x}(V^n_{j,k-3/2} - V^n_{j,k-1/2}) + \frac{\frac{g\Delta t}{2}\left[(\overline{U}^{\pm})^2 + (V^n_{j,k+1/2})^2\right]^{1/2}}{(\overline{h}^x + \overline{L}^y)(\overline{C}^y)^2} \tag{4.31}$$

$$B^{n+1/2}_{j,k+1/2} = V^n_{j,k+1/2} + \left[-F\Delta t - \frac{\Delta t}{2\Delta t}(V^n_{j+1,k+1/2} - V^n_{j-1,k+1/2})\right]\overline{U}^{\pm} - g\frac{\Delta t}{2\Delta x}(L^n_{j,k+1} - L^n_{j,k}) + \frac{\tau^s_y\,\Delta t}{\rho(\overline{h}^x + \overline{L}^y)} - \frac{\frac{g\Delta t}{2}\,V^n_{j,k+1/2}\left[(\overline{U}^{\pm})^2 + (V^n_{j,k+1/2})^2\right]^{1/2}}{(\overline{h}^x + \overline{L}^y)(\overline{C}^y)^2} \tag{4.32}$$

The finite difference form of the continuity equation for the second half-time step is:

$$\Delta_{t/2}L + \delta_x[(\overline{h}^y + \overline{L}^x)U] + \delta_y[(\overline{h}^x + \overline{L}^y)V_+] = 0 \text{ at } j,k,n+1/2 \tag{4.33}$$

As it was done in the previous half-time step, the rainfall and evaporation changes are included at the end of the calculations by changing the water levels appropriately. Expansion of Eq. (4.33) results in

$$\begin{aligned}\frac{2}{\Delta t}(L^{n+1}_{j,k} - L^{n+1/2}_{j,k}) + \big[&(h_{j+1/2,k+1/2} + h_{j+1/2,k-1/2} + L^{n+1/2}_{j+1,k} + L^{n+1/2}_{j,k})\,U^{n+1/2}_{j+1/2,k} \\ &- (h_{j-1/2,k+1/2} + h_{j-1/2,k+1/2} + L^{n+1/2}_{j,k+1} + L^{n+1/2}_{j,k})\,U^{n+1/2}_{j-1/2,k}\big]\frac{1}{2\Delta x} \\ + \big[&(h_{j+1/2,k+1/2} + h_{j-1/2,k+1/2} + L^{n+1/2}_{j,k+1} + L^{n+1/2}_{j,k})\,V^{n+1}_{j,k+1/2} - (h_{j+1/2,k-1/2} \\ &+ h_{j-1/2,k-1/2} + L^{n+1/2}_{j,k} + L^{n+1/2}_{j,k-1})V^{n+1}_{j,k-1/2}\big]\frac{1}{2\Delta x} = 0\end{aligned} \tag{4.34}$$

The above equation can be also written as:

$$-r_{k-1/2}V^{n+1}_{j,k-1/2} + L^{n+1}_{j,k} + r_{k+1/2}V^{n+1}_{j,k+1/2} = A^{n+1/2}_{k} \qquad (4.35)$$

in which:

$$r_{k-1/2} = (h_{j-1/2,k+1/2} + h_{j-1/2,k-1/2} + L^{n+1/2}_{j,k-1} + L^{n+1/2}_{j,k})\frac{\Delta t}{4\Delta x} \qquad (4.36)$$

$$r_{k+1/2} = (h_{j+1/2,k+1/2} + h_{j-1/2,k+1/2} + L^{n+1/2}_{j,k+1} + L^{n+1/2}_{j,k})\frac{\Delta t}{4\Delta x} \qquad (4.37)$$

$$A^{n+1/2}_{k} = L^{n+1/2}_{j,k} + (h_{j+1/2,k+1/2} + h_{j-1/2,k-1/2} + L^{n+1/2}_{j,k} + L^{n+1/2}_{j-1,k})\, U^{n+1/2}_{j-1/2,k}(\frac{\Delta t}{4\Delta x}) - (h_{j+1/2,k+1/2} + h_{j+1/2.k-1/2} + L^{n+1/2}_{j+1,k} + L^{n+1/2}_{j,k})\, U^{n+1/2}_{j+1/2,k}\,(\frac{\Delta t}{4\Delta x}) \qquad (4.38)$$

Eqs. (4.29) and (4.35) can now be solved for the unknown values of the V velocities and water levels on the jth column if boundary conditions are specified at both ends of the column. Similar to the first-half step, these boundary conditions can be the V velocities at both ends, the water level at one end and the V velocity at the other end, or the water levels at both ends. Again, the resulting system of equations can be put in matrix form. For example: in a column with N grid points and boundary conditions of $L_{j,1}$ and $V_{j,n+1/2}$ the matrix is:

$$
\begin{bmatrix}
r'_{1+1/2} & r_2 & & & & \\
-r_{1+1/2} & 1 & r_{2+1/2} & & & \\
 & -r_2 & r'_{2+1/2} & r_3 & & \\
 & & -r_{2+1/2} & 1 & r_{3+1/2} & \\
 & & & & & \\
 & & & & -r_{n-1} & r'_{n-1/2} \; r_n \\
 & & & & & -r_{n-1/2} \; 1
\end{bmatrix}
\begin{bmatrix}
V_{j,1+1/2} \\ L_{j,2} \\ V_{j,2+1/2} \\ L_{j,3} \\ \\ V_{j,n-1/2} \\ L_{j,n}
\end{bmatrix}
=
\begin{bmatrix}
B_{1+1/2}+r_1 L_{j,1} \\ A_2 \\ B_{2+1/2} \\ A_3 \\ \\ B_{n-1/2} \\ A_n - r_{n+1/2} V_{j,n+1/2}
\end{bmatrix}
\qquad (4.39)
$$

Thus, by knowing the values of water levels at the time level n+1/2, the U velocities at time level n+1/2, the V velocities at time level n and the appropriate boundary conditions at time level n+1, the values of water and V velocities for the n+1 level can be calculated by applying the Thomas Algorithm to the tridiagonal matrix. The values are obtained for the whole grid as the above calculation is repeated for all the columns.

The combination of the first half-time step and the second halftime step result in the implicit calculation of the velocities and water levels in a whole time step. The calculation proceeds as the above mentioned steps are repeated.

Open End Boundary Conditions

The field of computation has tidal entrances as boundaries. The values of the water levels in these tidal entrances are known as a function of time. However, as the open sea is beyond this field of computation, the horizontal velocities of the incoming waters is not known. In order to circumvent this problem, it is assumed that the advective terms are zero at the boundaries. Thus, if the entrance is in a row in the field of computation, the x-component of the equation of motion, Eq. (4.11), reduces to:

$$
\delta_t U - F\overset{+}{V} + \overset{+}{V}\,\overline{\delta_y U}^{y} + g\,\overline{\delta_x L}^{t} + g\,\overline{U}^{t}\,\frac{[(U\_)^2+(\overset{+}{V})^2]^{1/2}}{(\overline{h}^{y}+\overline{L}^{x})(\overline{C}^{x})^2} -
$$

$$
\frac{\tau_x^s}{\rho(\overline{h}^{y}+\overline{L}^{x})} = 0 \quad \text{at } j+1/2,k,n \qquad (4.40)
$$

This equation applies to the grid points representing a tidal entrance in the x-direction. The same reasoning applies to tidal entrances in the y-direction; with the y-component of the equation of motion, eq. (4.27), reducing to:

$$\delta_t V + F\overline{U} + \overline{U}\,\overline{\delta_x V}^{x} + g\,\frac{\overline{\delta_y L}^{t} + G\,\overline{V}^{t}\left[(\overline{U})^2+(V\_)^2\right]^{1/2}}{(\overline{h}^{x}+\overline{L}^{y})(\overline{C}^{y})^2} - \frac{\tau_y^s}{\rho(\overline{h}^{x}+\overline{L}^{y})} = 0 \quad \text{at } j,k+1/2,n+1/2 \tag{4.41}$$

Eq. (4.40) along with the continuity equation is placed in the system of equations in which one of the known boundary conditions is the tidal level. Such system is exemplarized by the matrix (4.24), Only one change is necessary in the matrix and that is a change in the coefficient for the equation in question. The appropriate value of $r'_{j+1/2}$ becomes:

$$r'_{j+1/2} = 1 + \frac{g\Delta t\left[(U^{n-1/2}_{j+1/2,k})^2+(\overline{V})^2\right]^{1/2}}{2(\overline{h}^{y}+\overline{L}^{x})(\overline{C}^{x})^2} \tag{4.42}$$

The same procedure applies to tidal entrances in the y-direction. Eq (4.41) along with the continuity equation is placed in the system of equations in which one of the known boundary conditions is the tidal level. Such system is exemplarized by the matrix coefficient $r'_{k+1/2}$ is modified and becomes:

$$r'_{k+1/2} = 1 + \frac{g\Delta t\left[(\overline{U})^2+(V^{n}_{j,k+1/2})^2\right]^{1/2}}{2(\overline{h}^{x}+\overline{L}^{y})(\overline{C}^{y})^2} \tag{4.43}$$

Finite Difference Approximation of the Energy Transport and Mass Transport Models

The space staggered grid shown in Fig. 4.1 is also used for the finite difference approximation of the Energy Transport and Mass Transport Models. Species concentration and temperature are stored at half integer values of j and k, the dispersion coefficients in the x- direction are stored at half integer values of j and integer values of k, and the dispersion coefficients in the y-direction are stored at integer values of j and half integer values of k. The Alternating Directions Implicit scheme used in the Hydrodynamic Model is also used for these two models. The Mass Transport and Energy Transport Models are solved simultaneously with the Hydrodynamic Model. These models are operated upon as follows: after the first half-time step for the Hydrodynamic Model has been carried out, the first half-time steps for the Energy and Mass Transport Models are executed. As it was stated before, the mathematical operations of the Energy and Mass

Transport Models are identical. They can be referred to as the Species Transport Model or STM. Thus, in the first half-time step, STM is solved in the x-direction for each species under consideration. Next, the second half-time step of the Hydrodynamic Model is executed and following this, the second half-time step of STM is executed ii the y-direction for each species under consideration.

First Half-time Step

The first half-time step is used to calculate the species concentration (or temperature) implicitly in the x-direction. The Energy Transport Model or the Mass Transport Model, Eqs. (3.98) and (3.135) can be written as:

$$\frac{\partial(PD)}{\partial t} + \frac{\partial(DUP)}{\partial x} + \frac{\partial(DVP)}{\partial y} - \frac{\partial}{\partial x}\left(D\mathcal{B}_{px}\frac{\partial P}{\partial x}\right) -$$

$$\frac{\partial}{\partial y}\left(D\mathcal{B}_{py}\frac{\partial P}{\partial y}\right) - SS_p = 0 \qquad (4.44)$$

in which D_{Px} is equal to k/pCp for the Energy Transport Model and equal to B_{Ax} for the Mass Transport Model, P can be either salinity, temperature or any other species: while B_{px} and B_{py} are the dispersion coefficients for salt, energy, or other species under consideration. The finite difference form for the Species Transport Model for the first half-time step can be written as:

$$\Delta_{t/2}[P(\overset{+}{h} + L)] + \delta_x[(\overline{h}^y + \overline{L}^x)U_+\overline{P}^x_+] + \delta_y[(\overline{h}^x + \overline{L}^y)V\overline{P}^y] -$$

$$\delta_x[(\overline{h}^y + \overline{L}^x_+)D_{px+}\delta_x P_x] - \delta_y[(\overline{h}^x + \overline{L}^y)D_{py}\delta_y P] + (\overset{+}{h}+L)SS_p = 0 \text{ at } j,k,n \qquad (4.45)$$

Eq. (4.45) can be expanded to:

$$[P^{n+1/2}_{j,k}(\overset{+}{h} + L^{n+1/2}_{j,k}) - P^{n}_{j,k}(\overset{+}{h} + L^{n}_{j,k})]\frac{1}{2\Delta t} - [(L^{n}_{j-1,k}+L^{n}_{j,k}$$

$$+ h_{j-1/2,k-1/2}+ h_{j-1/2,k+1/2}) U^{n+1/2}_{j-1/2,k} (P^{n+1/2}_{j-1,k} + P^{n+1/2}_{j,k}) -$$

$$(L^{n}_{j,k}+ L^{n}_{j+1,k} + h_{n+1/2,k-1/2}+ h_{j+1/2,k+1/2}) U^{n+1/2}_{j+1/2,k}$$

$$* (P^{n+1/2}_{j,k}+ P^{n+1/2}_{j+1,k})]\frac{1}{4\Delta x} - [(L^{n}_{j,k-1}+ L^{n}_{j,k} + h_{j-1/2,k-1/2}$$

$$+ h_{j+1/2,k-1/2})V^{n}_{j,k-1/2}(P^{n}_{j,k-1}+ P^{n}_{j,k}) - (L^{n}_{j,k+1}+ L^{n}_{j,k}$$

$$+ h_{j-1/2,k+1/2}+ h_{j+1/2,k+1/2})V^{n}_{j,k+1/2}(P^{n}_{j,k+1}+ P^{n}_{j,k})]\frac{1}{4\Delta x} +$$

$$[(L^{n+1/2}_{j-1,k} + L^{n+1/2}_{j,k} + h_{j-1/2,k-1/2}+ h_{j-1/2,k+1/2})D^{n+1/2}_{pxj-1/2,k}$$

$$* (P^{n+1/2}_{j,k}- P^{n+1/2}_{j-1,k}) - (L^{n+1/2}_{j,k}+ L^{n+1/2}_{j+1,k} + h_{j+1/2,k-1/2}+ h_{j+1/2,k+1/2}$$

$$* D^{n+1/2}_{pxj+1/2,k} (P^{n+1/2}_{j+1,k} - P^{n+1/2}_{j,k})][\frac{1}{2(\Delta x)}2] + [(L^{n}_{j,k-1} + L^{n}_{j,k} +$$

$$h_{j-1/2,k-1/2} + h_{j+1/2,k-1/2}) D^{n}_{pyj,k-1/2}(P^{n}_{j,k}- P^{n}_{j,k-1}) - (L^{n}_{j,k}$$

$$+ L^{n}_{j,k+1}+ h_{j-1/2,k+1/2}+ h_{j+1/2,k+1/2})D^{n}_{pyj,k+1/2}(P^{n}_{j,k+1}$$

$$- P^{n}_{j,k})][\frac{1}{2(\Delta x)}2] + (\overset{+}{h} + L^{n}_{j,k}) SS^{n}_{pj,k} = 0 \qquad (4.46)$$

eq. (4.46) has only three unknowns: $P^{n+1/2}_{j,k}$, $P^{n+1/2}_{j-1,k}$, and $P^{n+1/2}_{j+1,k}$. Therefore, the equations for a given row can be put in a tridiagonal form. Multiplying through by $\Delta t/2$, Eq. (4.46) can be written as:

$$a_j P^{n+1/2}_{j-1,k} + b_j P^{n+1/2}_{j,k} + c_j P^{n+1/2}_{j+1,k} = d_j \qquad (4.47)$$

in which:

$$a_j = -\left(L^n_{j-1,k} + L^n_{j,k} + h_{j\ 1/2,k-1/2} + h_{j-1/2,k+1/2}\right)U^{n+1/2}_{j-1/2,k}$$

$$*\left(\frac{\Delta t}{8\Delta x}\right) - \left(L^{n+1/2}_{j-1,k} + L^{n+1/2}_{j,k} + h_{-1/2,k-1/2} + h_{j-1/2,k+1/2}\right)$$

$$* D^{n+1/2}_{pxj-1/2,k}\left[\frac{\Delta t}{4(\Delta x)^2}\right] \qquad (4.48)$$

$$b_j = \left(\overset{+}{h} + L^{n+1/2}_{j,k}\right) - \left(L^n_{j-1,k} + L^n_{j,k} + h_{j-1/2,k-1/2} + h_{j-1/2,k+1/2}\right)$$

$$* U^{n+1/2}_{j-1/2,k}\left(\frac{\Delta t}{8\Delta t}\right) + \left(L^n_{j,k} + L^n_{j+1,k} + h_{j+1/2,k-1/2} + h_{j+1/2,k+1/2}\right)$$

$$* U^{n+1/2}_{j+1/2,k}\left(\frac{\Delta t}{8\Delta x}\right) + \left(L^{n+1/2}_{j-1,k} + L^{n+1/2}_{j,k} + h_{j-1/2,k-1/2} + h_{j-1/2,k+1/2}\right)$$

$$* D^{n+1/2}_{pxj-1/2,k}\left[\frac{\Delta t}{4(\Delta x)^2}\right] + \left(L^{n+1/2}_{j,k} + L^{n+1/2}_{j+1,k} + h_{j+1/2,k-1/2} + h_{j+1/2,k+1/2}\right)$$

$$* D^{n+1/2}_{pxj+1/2,k}\left[\frac{\Delta t}{4(\Delta x)^2}\right] \qquad (4.49)$$

$$c_j = \left(L^n_{j,k} + L^n_{j+1,k} + h_{j+1/2,k-1/2} + h_{j+1/2,k+1/2}\right)U^{n+1/2}_{j+1/2,k}\left(\frac{\Delta t}{8\Delta x}\right)$$

$$- \left(L^{n+1/2}_{j,k} + L^n_{j+1,k} + h_{j+1/2,k-1/2} + h_{j+1/2,k+1/2}\right)D^{n+1/2}_{pxj+1/2,k}$$

$$\left[\frac{\Delta t}{4(\Delta x)^2}\right] \qquad (4.50)$$

$$d_j = P^n_{j,k}\left[\overset{+}{h} + L^n_{j,k}\right] - \left[\overset{+}{h} + L^n_{j,k}\right]SS^n_{pj,k}\frac{\Delta t}{2} + \left[\left(L^n_{j,k-1} + L^n_{j,k} +\right.\right.$$

$$\left.h_{j-1/2,k-1/2} + h_{j+1/2,k-1/2}\right)V^n_{j,k-1/2}\left(P^n_{j,k-1} + P^n_{j,k}\right) - \left(L^n_{j,k} +\right.$$

$$\left.\left.L^n_{j,k+1} + h_{j-1/2,k+1/2} + h_{j+1/2,k+1/2}\right)V^n_{j,k+1/2}\left(P^n_{j,k+1} + P^n_{j,k}\right)\right]$$

$$* \left(\frac{\Delta t}{8\Delta x}\right) - \left[\left(L^n_{j,k-1} + L^n_{j,k} + h_{j-1/2,k-1/2} + h_{j+1/2,k-1/2}\right) D^n_{pyj,k-1/2}\right.$$

$$* \left(P^n_{j,k} - P^n_{j,k-1}\right) - \left(L^n_{j,k} + L^n_{j,k+1} + h_{j-1/2,k+1/2} + h_{j+1/2.k+1/2}\right)$$

$$\left.* D^n_{pyj,k+1/2}\left(P^n_{j,k+1} - P^n_{j,k}\right)\right]\left[\frac{\Delta t}{4(\Delta x)^2}\right] \qquad (4.51)$$

Eq. (4.47) can now be solved for the unknown values of species P of the kth row if boundary conditions are specified at both ends of the row. The boundary conditions consist of the appropriate values for the species under consideration. Equations for the grid points in a row can be put in a tridiagonal matrix; and if there are N grid points, there will be N-2 unknowns. Thus, for the first half-time step, the matrix for the kth row is;

$$\begin{bmatrix} b_2 & c_2 & & & & \\ a_3 & b_3 & c_3 & & & \\ & a_4 & b_4 & c_4 & & \\ & & & & & \\ & & & a_{n-2} & b_{n-2} & c_{n-2} \\ & & & & a_{n-1} & b_{n-1} \end{bmatrix} \begin{bmatrix} P_{2,k} \\ P_{3,k} \\ P_{4,k} \\ \\ P_{n-2,k} \\ P_{n-1,k} \end{bmatrix} = \begin{bmatrix} d_2 - a_2 P_{1,k} \\ d_3 \\ d_4 \\ \\ d_{n-2} \\ d_{n-1} - c_{n-1} P_{n,k} \end{bmatrix} \qquad (4.52)$$

Thus, by knowing the values of the V velocities, the source term, the water levels and the species concentration at the nth time level, the U velocities, the water levels, and the boundary conditions at the time level n+1/2; the values of the species concentration at the time level n+1/2 can be calculated using the Thomas Algorithm. The values are obtained for the whole grid as the above calculation is repeated for all the rows. After implicitly calculating the species concentration in the x-direction, they are implicitly calculated in the y-direction in the second half-time step.

Second Half-time Step

In the second half-time step, the species concentration is calculated implicitly in the y-direction. The finite difference form of the Species Transport Model, Eq. (4.44), for this step can be written as:

$$\Delta_{t/2}[P(P\overset{+}{h} + L)] + \delta x[(\overline{h}^{y} + \overline{L}^{x})\, U\overline{P}^{x}] + \delta y[(\overline{h}^{x} + \overline{L}^{y})V_{+}\overline{P}^{y}_{+}] -$$

$$\delta x[(\overline{h}^{y} + \overline{L}^{x})D_{px}\delta xP] - \delta y[(\overline{h}^{x} + \overline{L}^{y}_{+})D_{px} + \delta yP_{+}]$$

$$+ (\overset{+}{h} + L)\, SS_{p} = 0 \quad \text{at } j,k,n+1/2 \qquad (4.53)$$

Eq. (4.53) can be expanded to:

$$[P^{n+1}_{j,k}(\overset{+}{h} + L^{n+1}_{j,k}) - P^{n+1/2}_{j,k}(\overset{+}{h} + L^{n+1/2}_{j,k})]\frac{1}{2\Delta t} - [(L^{n+1/2}_{j-1,k} + L^{n+1/2}_{j,k} +$$

$$h_{j-1/2,k-1/2} + h_{j-1/2,k+1/2})U^{n+1/2}_{j-1/2,k}(P^{n+1/2}_{j-1,k} + P^{n+1/2}_{j,k}) - (L^{n+1/2}_{j,k}$$

$$+ L^{n+1/2}_{j+1,k} + h_{j+1/2,k-1/2} + h_{j+1/2,k+1/2})U^{n+1/2}_{j+1/2,k}(P^{n+1/2}_{j,k} + P^{n+1/2}_{j+1,k})]$$

$$* \frac{1}{4\Delta x} - [(L^{n+1/2}_{j,k-1} + L^{n+1/2}_{j,k} + h_{j-1/2,k-1/2} + h_{j+1/2,k-1/2})V^{n+1}_{j,k-1/2}$$

$$* (P^{n+1}_{j,k-1} + P^{n+1}_{j,k}) - (L^{n+1/2}_{j,k} + L^{n+1/2}_{j,k+1} + h_{j-1/2,k+1/2} + h_{j+1/2,k+1/2})$$

$$* V^{n+1}_{j,k+1/2}(P^{n+1}_{j,k+1} + P^{n+1}_{j,k})]\frac{1}{4\Delta x} + [(L^{n+1/2}_{j-1,k} + L^{n+1/2}_{j,k} + h_{j-1/2,k-1/2}$$

$$+ h_{j-1/2,k+1/2})D^{n+1/2}_{pxj-1/2,k}(P^{n+1/2}_{j,k} - P^{n+1/2}_{j-1,k}) - (L^{n+1/2}_{j,k} + L^{n+1/2}_{j+1,k}$$

$$h_{j+1/2,k-1/2} + h_{j+1/2,k+1/2})D^{n+1/2}_{pxj+1/2,k}(P^{n+1/2}_{j+1,k} - P^{n,1/2}_{j,k})]$$

$$[\frac{1}{2(\Delta x)}] + [(L^{n+1}_{j,k-1} + L^{n+1}_{j,k} + h_{j-1/2,k-1/2} + h_{j+1/2,k-1/2})$$

$$* D^{n+1}_{pyj,k-1/2}(P^{n+1}_{j,k} - P^{n+1}_{j,k-1}) - (L^{n+1}_{j,k} + L^{n+1}_{j,k+1} + h_{j-1/2,k+1/2}$$

$$+ h_{j+1/2,k+1/2})D^{n+1}_{pyj,k+1/2}(P^{n+1}_{j,k+1} - P^{n+1}_{j,k})][\frac{1}{2(\Delta x)}] +$$

$$(\overset{+}{h} + L^{n+1/2}_{j,k})\, SS^{n+1/2}_{p} = 0 \qquad (4.54)$$

Eq. (4.54) has only three unknowns: $P^{n+1}_{j,k-1}$, $P^{n+1}_{j,k}$, and $P^{n+1}_{j,k+1}$. Therefore, the equations for a given column can be put in a tridiagonal form. Multiplying by $\Delta t/2$, Eq. (4.54) can be written as:

$$a_k P^{n+1}_{j,k-1} + b_k P^{n+1}_{j,k} + c_k P^{n+1}_{j,k+1} = d_k \qquad (4.55)$$

in which:

$$a_k = -\left(L^{n+1/2}_{j,k-1} + L^{n+1/2}_{j,k} + h_{j-1/2,k-1/2} + h_{j+1/2,k-1/2}\right)V^{n+1}_{j,k-1/2}$$

$$* \left(\frac{\Delta t}{8\Delta x}\right) - \left(L^{n+1}_{j,k-1} + L^{n+1}_{j,k} + h_{j-1/2,k-1/2} + h_{j+1/2,k-1/2}\right)D^{n+1}_{pyj,k-1/2}$$

$$* \left[\frac{\Delta t}{4(\Delta x)^2}\right] \qquad (4.56)$$

$$b_k = \left(\overset{+}{h} + L^{n+1}_{j,k}\right) - \left(L^{h+1/2}_{j,k-1} + L^{n+1/2}_{j,k} + h_{j+1/2,k-1/2} + h_{j-1/2,k-1/2}\right)$$

$$* V^{n+1}_{j,k-1/2}\left(\frac{\Delta t}{8\Delta x}\right) + \left(L^{n+1/2}_{j,k} + L^{n+1/2}_{j,k+1} + h_{j-1/2,k+1/2} + h_{j+1/2,k+1/2}\right)$$

$$* V^{n+1}_{j,k+1/2}\left(\frac{\Delta t}{8\Delta x}\right) + \left(L^{n+1}_{j,k-1} + L^{n+1}_{j,k} + h_{j-1/2,k-1/2} + h_{n+1/2,k-1/2}\right)$$

$$* D^{n+1}_{pyj,k-1/2}\left[\frac{\Delta t}{4(\Delta x)^2}\right] + \left(L^{n+1}_{j,k} + L^{n+1}_{j,k+1} + h_{j-1/2,k+1/2} + h_{j+1/2,k+1/2}\right)$$

$$* D^{n+1}_{pyj,k+1/2}\left[\frac{\Delta t}{4(\Delta x)^2}\right] \qquad (4.57)$$

$$c_k = \left(L^{n+1/2}_{j,k} + L^{n+1/2}_{j,k+1} + h_{j-1/2,k+1/2} + h_{j+1/2,k+1/2}\right)V^{n+1}_{j,k+1/2}$$

$$* \left(\frac{\Delta t}{8\Delta x}\right) + \left(L^{n+1}_{j,k} + L^{n+1}_{j,k+1} + h_{j+1/2,k+1/2} + h_{j+1/2,k+1/2}\right)$$

$$* D^{n+1}_{pyj,k+1/2}\left[\frac{\Delta t}{4(\Delta x)^2}\right] \qquad (4.58)$$

$$d_k = P^{n+1/2}_{j,k}\left[\overset{+}{h} + L^{n+1/2}_{j,k}\right] - \left[\overset{+}{h} + L^{n+1/2}_{j,k}\right]SS^{n+1/2}_{p\,j,k}\,\frac{\Delta t}{2} + \left[\left(L^{n+1/2}_{j,k-1}\right.\right.$$

$$\left. + L^{n+1/2}_{j,k} + h_{j-1/2,k-1/2} + h_{j-1/2,k+1/2}\right)U^{n+1/2}_{j-1/2,k}\left(P^{n+1/2}_{j-1,k} + P^{n+1/2}_{j,k}\right) -$$

$$\left(L^{n+1/2}_{j,k} + L^{n+1/2}_{j+1,k} + h_{j+1/2,k-1/2} + h_{j+1/2,k+1/2}\right)U^{n+1/2}_{j+1/2,k}\left(P^{n+1/2}_{j,k}\right.$$

$$\left. + P^{n+1/2}_{j+1,k}\right)\left]\left[\frac{\Delta t}{8\Delta x}\right] - \left[\left(L^{n+1/2}_{j-1,k} + L^{n+1/2}_{j,k} + h_{j-1/2,k-1/2} + h_{j-1/2,k+1/2}\right)\right.$$

$$* D^{n+1/2}_{pxj-1/2,k}\left(P^{n+1/2}_{j,k} - P^{n+1/2}_{j-1,k}\right) - \left(L^{n+1/2}_{j,k} + L^{n+1/2}_{j+1,k} + h_{j+1/2,k-1/2}\right.$$

$$\left. + h_{j+1/2,k+1/2}\right)D^{n+1/2}_{pxj+1/2,k}\left(P^{n+1/2}_{j+1,k} - P^{n+1/2}_{j,k}\right]\left[\frac{\Delta t}{4(\Delta x)^2}\right] \qquad (4.59)$$

Eq, (4.55) can now be solved for the unknown values of species P or the jth column if boundary conditions are specified at both ends of the column. Equations for the grid points in a column can be put in a tridiagonal matrix and if there are N grid points, there will be N-2 unknowns. Thus, for the second half-time step, the matrix for the jth column is:

$$\begin{bmatrix} b_2 & c_2 & & & & \\ a_3 & b_3 & c_3 & & & \\ & a_4 & b_4 & c_4 & & \\ & & & & a_{n-2}b_{n-2}c_{n-2} & \\ & & & & a_{n-1}b_{n-1} & \end{bmatrix} \begin{bmatrix} P_{j,2} \\ P_{j,3} \\ P_{j,4} \\ \\ P_{j,n-2} \\ P_{j,n-1} \end{bmatrix} = \begin{bmatrix} d_2 - a_2P_{j,1} \\ d_3 \\ d_4 \\ \\ d_{n-2} \\ d_{n-1} - c_{n-1}P_{j,n} \end{bmatrix} \quad (4.60)$$

Thus by knowing the values of the U velocities, the source term, the water levels and the species concentration at the (nth + 1/2) time level, the V velocities, the water levels and the boundary conditions at the (nth + 1) time level; the values of the species concentration at the (nth + 1) level can be calculated by using the Thomas Algorithm, The values for the whole grid are implicitly calculated as the above operation is repeated for all the columns.

Open End Boundary Conditions

The concentrations of the species under study must be described as a function of time at the open end locations. During outflow conditions, the boundary concentrations are obtained by extrapolating linearly from the values calculated within the computational field. The concentrations at the boundaries are calculated by applying the species equation, Eq. (4.44), to the point in question and putting the equation in a numerical form:

$$P_{1,k}^{n+1/2} = P_{1,k}^{n} - U_{1+1/2,k}^{n+1/2}(P_{2,k}^{n} - P_{1,k}^{n})\frac{\Delta t}{2\Delta x} - \theta_{px1+1/2,k}^{n+1/2}[P_{3,k}^{n} - 2P_{2,k}^{n} + P_{1,k}^{n}]\frac{\Delta t}{2(\Delta x)^2} \quad (4.61)$$

and

$$P_{j,1}^{n+1/2} = P_{j,1}^{n} - V_{j,1+1/2}^{n+1/2}(P_{j,2}^{n} - P_{j,1}^{n})\frac{\Delta t}{2\Delta x} - \theta_{pyj,1+1/2}^{n+1/2}[P_{j,3}^{n} - 2P_{j,2}^{n} + P_{j,1}^{n}]\frac{\Delta t}{2(\Delta x)^2} \quad (4.62)$$

When the tidal inflow is such that the flow is into the field of computation, the boundary values are not calculated. These values of input concentration vary between the last value calculated during tidal outflow and the open sea value of the concentration of the species under consideration. For the Barataria Bay case, this variation was measured and it is shown in Fig. B-21. The functional relationship shown, which is essentially a step function, will be used in calculations for Barataria Bay.

Numerical Operations for Special Conditions

In order to properly simulate bay conditions, the geometry of the bay has to be included. Internal barriers such as islands create changes in the transport phenomena. Therefore, special numerical operations have to be performed to account for these conditions. In this section, the special numerical operations will be discussed for momentum, energy, and mass transfer.

Hydrodynamical Model

The numerical operations needed to account for internal barriers in the Hydrodynamic Model are. in the form of modifications to the matrix set for calculations. For a barrier against flow in the x-direction, such as the one shown in Fig. 4.2, the U velocity is known to be zero along the j = m +1/2 line. Therefore, the matrix for the kth, row is:

$$\begin{bmatrix} r'_{1+1/2} r_2 & & & & & & \\ -r_{1+1/2} l & r_{2+1/2} & & & & & \\ & \ddots & \ddots & & & & \\ & & r_{m+1/2} & & & & \\ & & -r_m r_{m+1/2} & r_{m+1} & & & \\ & & & -r_{m+1/2} & \ddots & & \\ & & & & -r_{n-1} r'_{n-1/2} & r_n & \\ & & & & & -r_{n-1/2} l & \end{bmatrix} \begin{bmatrix} U_{1+1/2,k} \\ L_{2,k} \\ \vdots \\ U_{m+1/2,k} \\ \vdots \\ U_{n-1/2,k} \\ L_{n,k} \end{bmatrix} = \begin{bmatrix} B_{1+1/2} + r_1 L_{1,k} \\ A_2 \\ \vdots \\ A_m \\ B_{m+1/2} \\ A_{m+1} \\ \vdots \\ B_{n-1/2} \\ A_n - r_{n+1/2} U_{n+1/2,k} \end{bmatrix} \quad (4.63)$$

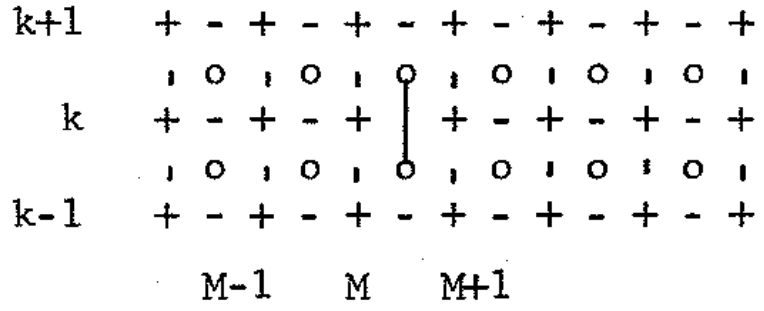

$$U_{M+1/2,k} = 0$$

\- V velocities

¦ U velocities

o Water depth (h)

\+ Water level (L)

Figure 4.2. Barrier Against Flow in the x-direction.

The equation set Eq. (4.63) is changed to the following form since U(m) is known to be zero along the barrier:

$$\begin{bmatrix} r'_{1+1/2} & r_2 & & & & \\ -r_{1+1/2} & 1 & r_{2+1/2} & & & \\ & \vdots & \vdots & & & \\ & & 0 & & & \\ & & -r_m & 0 & r_{m+1} & \\ & & & 0 & \vdots & \\ & & & & & -r_{n-1/2} \quad 1 \end{bmatrix} \begin{bmatrix} U_{1+1/2,k} \\ L_{2,k} \\ \vdots \\ U_{m+1/2,k} \\ \vdots \\ L_{n,k} \end{bmatrix} = \begin{bmatrix} B_{1+1/2} + r, L_{1,k} \\ A_2 \\ \vdots \\ A_m - r_{m+1/2} U_{m+1/2,k} \\ B_{m+1/2} - r'_{m+1/2} U_{m+1/2,k} \\ A_{m+1} + r_{m+1/2} U_{m+1/2,k} \\ \vdots \\ A_n - r_{n+1/2} U_{n,k} \end{bmatrix} \quad (4.64)$$

Now the system has become singular but it is still solvable by a modified Thomas Algorithm. To do this, whenever the values of the column are zero the results obtained for the unknown that are multiplied by the zero column are set to zero, and the solution is allowed to proceed. The same procedure is followed for barriers against the flow in the y-direction. This procedure is also applied when islands are included in the field of calculation, in which case the water level is set to zero by the modified Thomas Algorithm if the conditions are appropriate.

Another operation needed is the one to allow for flooding of the "dry" grid points. After each sweep, the "dry11 points are checked for flooding. If the average water level around the "dry" point is such that the "dry1' point is under water, then the water level at the ndryH point is set by the following equation:

$$L^{n+1/2}_{j,k} = 1/4(L^{n+1/2}_{j-1,k-1} + L^{n+1/2}_{j-1,k+1} + L^{n+1/2}_{j+1,k-1} + L^{n+1/2}_{j+1,k+1}) \quad (4.65)$$

To insure conservation of mass, the water added to the previously "dry" point is substracted from three adjacent grid points:

$$L^{n+1/2}_{j-1,k-1} = L^{n+1/2}_{j-1,k-1} - L^{n+1/2}_{j,k} /3 \quad (4.66)$$

$$L^{n+1/2}_{j+1,k-1} = L^{n+1/2}_{j+1,k-1} - L^{n+1/2}_{j,k} /3 \quad (4.67)$$

$$L^{n+1/2}_{j-1,k+1} = L^{n+1/2}_{j-1,k+1} - L^{n+1/2}_{j-1,k} /3 \quad (4.68)$$

The same procedure is followed for calculations in the y-direction.

Energy Transport and Mass Transport Models

Just as with the Hydrodynamic Model, the Energy Transport and Mass Transport Models use numerical operations in the form of matrix modifications in order to account for internal barriers. The internal boundaries in this case are the closed boundaries. Closed boundaries are those grid points in which both the convective and dispersive transport of constituents is zero. For example, the situation shown in Fig. 4.3 shows a right closed boundary for a step marching by columns. Thus, the transport through cross sections between j=N and j=N+l is zero and Eq. (4.55) reduces to:

$$a_k P_{j,k-1} + b_k P_{j,k} = d_k \qquad (4.69)$$

as

$$c_k = 0 \qquad (4.70)$$

Similarly, as in Fig. 4.4, if there is a left closed boundary, Eq. (4.55) reduces to:

$$b_k P_{j,k} + c\ P_{j,k+1} = d_k \qquad (4.71)$$

as

$$a_k = 0 \qquad (4.72)$$

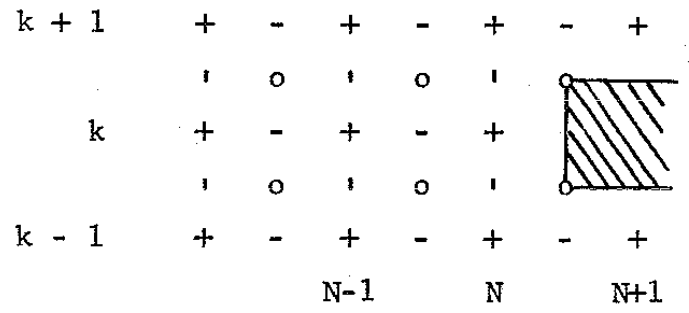

Fig. 4.3. Right Closed Boundary.

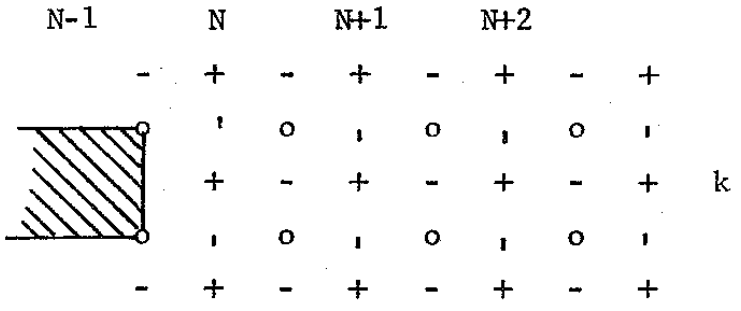

Fig. 4.4. Left Closed Boundary .

Explicit Scheme For the Energy Transport Model and the Mass Transport Model.

The same space staggered scheme used for the implicit scheme is used for the explicit scheme. The results obtained from the Hydrodynamic Model are used for inputs for the explicit solution of the Mass and Energy Transport Models. The Hydrodynamic Model is carried out for two half-time steps and then the Mass and Energy Transport Models are executed at every time step. As it was the case in the implicit scheme, the numerical operations of the explicit solutions of the Energy and Mass Transport Models are identical.

Expanding Eq, (4.44), the Energy or Mass Transport Model can bewritten as:

$$\frac{\partial(PD)}{\partial t} + \frac{\partial(DUP)}{\partial x} + \frac{\partial(DVP)}{\partial y} - \left(\frac{\partial(D\Theta_{px})}{\partial x}\frac{\partial P}{\partial x} + D\Theta_{px}\frac{\partial^2 P}{\partial x^2} \right)$$

$$- \left(\frac{\partial(D\Theta_{py})}{\partial y}\frac{\partial P}{\partial y} + D\Theta_{py}\frac{\partial^2 P}{\partial y 2} \right) - SS_p = 0 \qquad (4.73)$$

The above equation can be put in a finite difference form using theforward difference approximation. The resulting equation is:

$$\frac{P^{n+1}_{j,k}D^{n+1}_{j,k} - P^{n}_{j,k}D^{n}_{j,k}}{\Delta t} + \frac{(D^{n+1}_{j+1,k}U^{n+1/2}_{j+1,k}P^{n}_{j+1,k} - D^{n+1}_{j,k}U^{n+1/2}_{j,k}P^{n}_{j,k})}{\Delta x}$$

$$+ \frac{(D^{n+1}_{j,k+1}V^{n+1}_{j,k+1}P^{n}_{j,k+1} - D^{n+1}_{j,k}V^{n+1}_{j,k}P^{n}_{j,k})}{\Delta y}$$

$$- \frac{(D^{n+1}_{j+1,k}\Theta^{n+1}_{pxj+1,k} - D^{n+1}_{j,k}\Theta^{n+1}_{pxj,k})}{\Delta x}\frac{(P^{n}_{j+1,k} - P^{n}_{j,k})}{\Delta x}$$

$$- D^{n+1}_{j,k}\Theta^{n+1}_{pxj,k}\frac{(P^{n}_{j+1,k} - 2P^{n}_{j,k} + P^{n}_{j-1,k})}{(\Delta x)^2}$$

$$- \frac{(D^{n+1}_{j,k+1}\Theta^{n+1}_{pyj,k} - D^{n+1}_{j,k}\Theta^{n+1}_{pyj,k})}{\Delta x}\frac{(P^{n}_{j,k+1} - P^{n}_{j,k})}{\Delta x}$$

$$- D^{n+1}_{j,k}\Theta^{n+1}_{pyj,k}\frac{(P^{n}_{j,k+1} - 2P^{n}_{j,k} + P^{n}_{j,k-1})}{(\Delta y)^2} - SS^{n+1}_{pj,k} = 0 \qquad (4.74)$$

Rearranging and solving for $P^{n+1}_{j,k}$ at the latest time interval results in:

$$P^{n+1}_{j,k} = \frac{P^{n}_{j,k} D^{n}_{j,k}}{D^{n+1}_{j,k}} - \frac{\Delta t}{D^{n+1}_{j,k}} \left[\frac{(D^{n+1}_{j+1,k} U^{n+1/2}_{j+1,k} P^{n}_{j+1,k} - D^{n+1}_{j,k} U^{n+1/2}_{j,k} P^{n}_{j,k})}{\Delta x} \right.$$

$$+ \frac{(D^{n+1}_{j,k+1} V^{n+1}_{j,k+1} P^{n}_{j,k+1} - D^{n+1}_{j,k} V^{n+1}_{j,k} P^{n}_{j,k})}{\Delta y} - \frac{(D^{n+1}_{j+1,k} \Theta^{n+1}_{pxj+1,k} - D^{n+1}_{j,k} \Theta^{n+1}_{pxj,k})}{\Delta x}$$

$$* \frac{(P^{n}_{j+1,k} - P^{n}_{j,k})}{\Delta x} - D^{n+1}_{j,k} \Theta^{n+1}_{px,j,k} \frac{(P^{n}_{j+1,k} - 2P^{n}_{j,k} + P^{n}_{j-1,k})}{(\Delta x)^2}$$

$$- \frac{(D^{n+1}_{j,k+1} \Theta^{n+1}_{pyj,k} - D^{n+1}_{j,k} \Theta^{n+1}_{py,j,k})}{\Delta x} \frac{(P^{n}_{j,k+1} - P^{n}_{j,k})}{\Delta x}$$

$$\left. - D^{n+1}_{j,k} \Theta^{n+1}_{pyj,k} \frac{(P^{n}_{j,k+1} - 2P^{n}_{j,k} + P^{n}_{j,k-1})}{(\Delta y)^2} - SS^{n+1}_{pj,k} \right] \qquad (4.75)$$

The explicit solution of Eq. (4.72) is limited by the following stability criterion reported by TRACOR (Ref. 4.3); the size step is limited by:

$$\Delta x = \Delta y \leq \min \left[\frac{8\Theta min}{|Umax|}, \frac{8\Theta min}{|Vmax|} \right] \qquad (4.76)$$

and the time step is limited by:

$$\Delta t \leq \min \left[\frac{\Delta x}{2|Umax|}, \frac{\Delta x}{2|Vmax|} \right] \qquad (4.77)$$

And

$$\Delta t \leq \frac{(\Delta x)^2}{4\ \Theta max} \qquad (4.78)$$

The computer procedures used for the Barataria Bay Model are shown in Appendix D.

Summary

In this chapter the Hydrodynamic Model, Energy Transport Model, and Mass Transport Model were put in numerical form: an implicit technique was developed for the Hydrodynamic Model, and implicit and explicit techniques were developed for the Energy and Mass Transport Models. The next chapter discusses the results obtained with the numerical techniques presented here.

REFERENCES

4,1 Ames, William F., Numerical Methods for Partial Differential Equations, Barns and Noble, Inc. New York, N.Y. (1969), pp. 148-157.

4.2 Von Rosenberg, Dale U., Methods for the Numerical Solution of Partial Differential Equations, American Elsevier Publishing Company, Inc., New York, N.Y. (1969), pp. 87-89.

4.3 "Mathematical Modeling of Thermal Discharges into Shallow Estuaries," Technical Report T70-AU-7425-U, TRACOR, Austin, Texas, (1968), pp. 4.1-32,33,

CHAPTER V

RESULTS OF THE HYDRODYNAMIC ENERGY TRANSPORT AND SPECIES TRANSPORT MODELS OF BARATARIA BAY

Introduction

Solutions of the transport phenomena equations of shallow estuarine bay systems were obtained for the Barataria Bay estuary. The purpose of this chapter is to present the results of these solutions. The first part of this chapter will present a description of the simulation and specific data used for Barataria Bay. The second part will present the results of the cases that were run: typical conditions, high fresh water runoff, drop in gulf salinity due to Mississippi river water, cold front passage, and tidal wave generated by a hurricane. The third part consists of comparisons of results obtained with field data and results from other investigators. The fourth part is a short discussion of results for the time-averaged equation of motion. The last part consists of a discussion of numerical considerations in the computer solution.

Simulation of Barataria Bay

To simulate an estuary the following types of information are needed: tidal heights history of the passes, fresh water runoff, atmospheric conditions, sea conditions, dispersion coefficients or energy and mass, bottom friction coefficients and bathymetric data. Tidal height history at the passes was obtained for Barataria Pass from the Louisiana Wild Life and Fisheries Comission (Ref 5.1). Fresh water runoff data was obtained for Barataria Bay from Gagliano, et. a1. (Ref.5.2). Atmospheric conditions were from the L.S.U. Sea Grant Program (Ref. 5.3) Sea conditions for the Gulf were obtained from the Louisiana Wild Life and Fisheries Commission (Ref. 5.1). Dispersion coefficients were obtaine from a Galveston Bay study by

Tracor (Ref. 5.4). Bottom friction coefficients were obtained from a Jamaica Bay simulation by Leendertse (Ref. 5.5). The bathymetric data for Barataria Bay was taken from the U.S. Coastal and Goedetic Service Map No. 1273.

The salinity dispersion coefficients used for the Barataria Bay estuary were obtained from a similar study of Galveston Bay. The bathymetry, hydrologic and geographical locations of Barataria Bay and Galveston Bay are very similar. The selection of salinity dispersion coefficients was based on locations reported in Galveston Bay that were similar in depth and velocities to Barataria Bay locations. The value of the salinity dispersion coefficients selected was 6,000 ft/sec for the bay system. These values, representing turbulent dispersion, are much higher than molecular diffusion values for salt in water. Molecular diffusion for sodium chloride in water is reported as 162 ft^2/sec by the Handbook of Chemistry and Physics (Ref. 5.6).

Temperature dispersion coefficients are not reported in the literature for conditions comparable to the ones found in Barataria Bay. Thus, as there is no method for determining dispersion coefficients a priori, it was assumed that the temperature dispersion coefficients are equal to salinity dispersion coefficients.

Bottom friction coefficients for the conditions found in Barataria Bay have been reported by a number of investigators (Reg. 2.10, 2.12). The value used in this case was a Manning friction factor of 0.026 (Ref. 5.5). This value was used in the Tracor study (Reg. 2.14) on Galveston Bay and also used by Leendertse (Ref. 2.9).

Tidal variation at the passes was modeled by fitting a sinusoidal curve to the tidal range. This was done because of a lack of data for the shape of the tidal curve at the passes. Tidal fluctuations generally follow a sinusoidal variation; therefore this procedure represents a good approximation of this variation within the accuracy of the computations. Tidal ranges at the different passes into Barataria Bay are the same but the times of high and low tide at Barataria pass is ahead of the other three passes.

Barataria Pass was taken as reference, Caminada Pass lags by 1.358 hours, and Quatre Bayou and Pass Abel are found to lag 0.875 hours as reported in the Tide Tables (Ref. 5.7). These lags were included in the tidal simulation.

The grid system was placed on the area of interest in a fashion that insured that all tidal passes were lined up with the bottom row of the grid system. The limits of the system modeled were chosen by a study of the area. Data was taken on the areas surrounding the bay to determine regions in which flows into or out of the bay are small enough to be neglected. These measurements are shown in Appendix B, Table B-2. Grid size was chosen to best represent the widths of the passes. However, a smaller grid size than the one used would be desirable. With the grid size chosen, only one grid point was assigned for each pass. A smaller grid size would provide a more accurate representation. However, a smaller grid size would require more computer storage than was available.

The Barataria Bay estuary was modeled using two finite difference networks: a 1300 yards square grid, shown in Figure 5.1; and an 1800 yards square grid, shown in Figure 5.2. The data used was stored in a computational grid like the one shown in Figure 5.3. The purpose of using two different grid sizes was to establish convergence of the solutions.

With the numerical solution the models predict a local average of the velocity, temperature and salinity through the marsh grass and channels of the marsh and open waters of the bay. It was found that if constant (except for tidal variations at the passes) boundary conditions were maintained. The solution for Barataria Bay reached quasi-steady state conditions. When the bay is in a quasi-steady state, the solution is repeated and conditions corresponding to the same time in subsequent tidal cycles are equal. Quasi-steady state was obtained after about three tidal cycles.

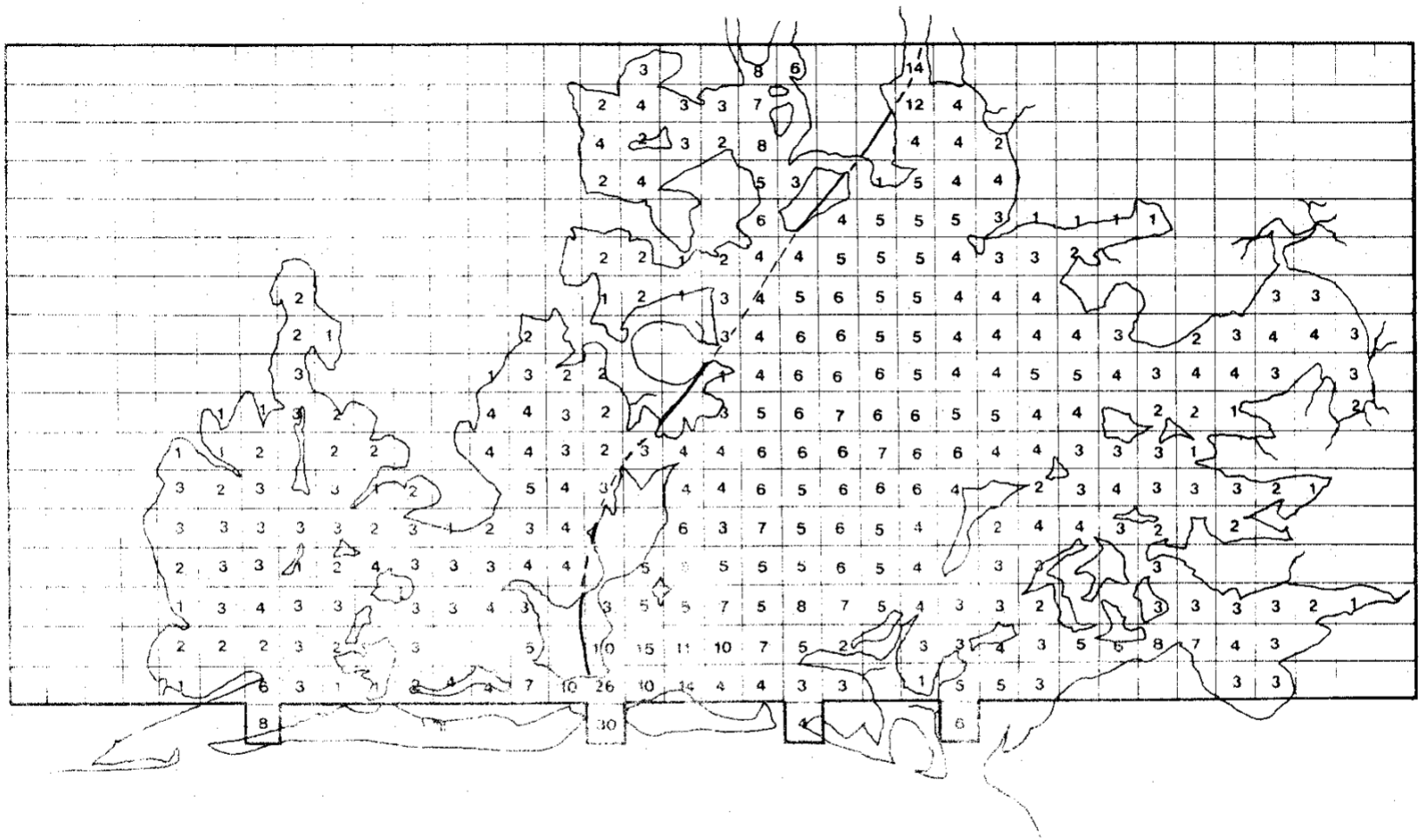

Figure 5.1. Finite Difference Grid (1300 yards square) on Barataria Bay (depth shown in feet).

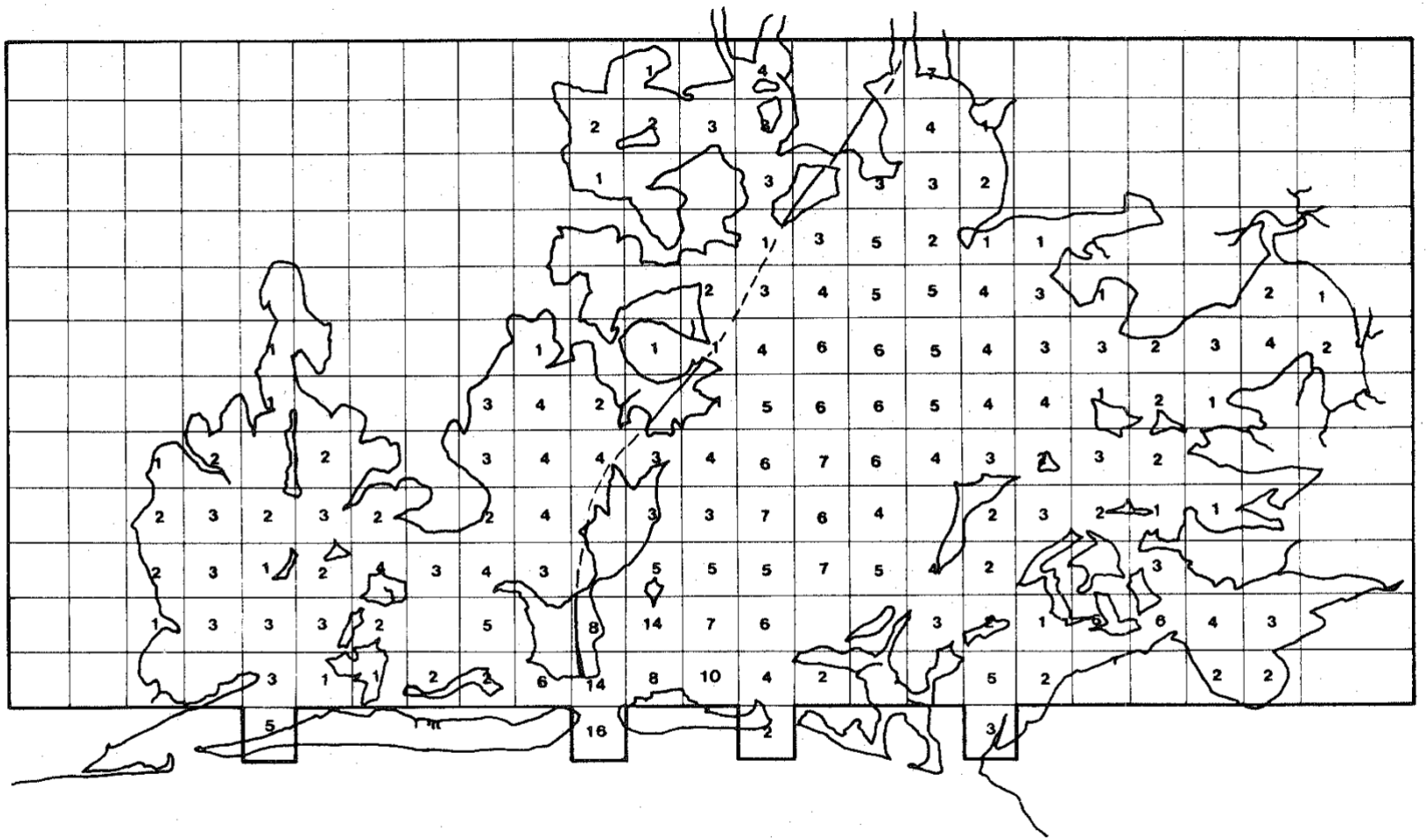

Figure 5.2. Finite Difference Grid (1800 yards square) on Barataria Bay (depth shown in feet).

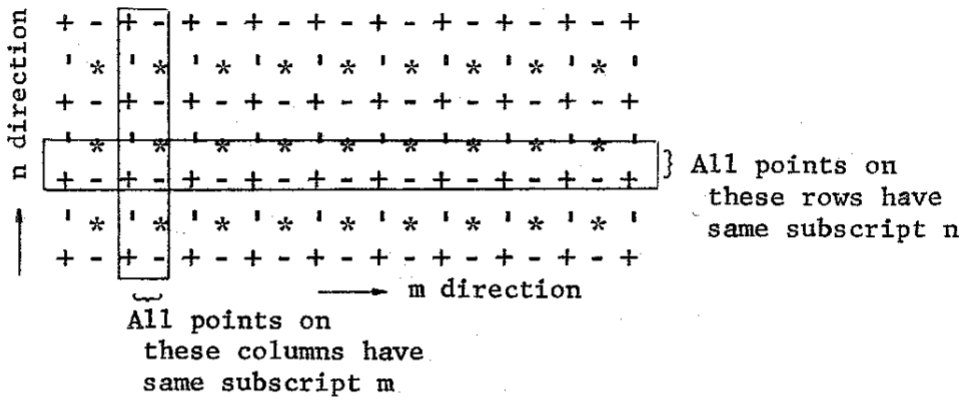

Figure 5.3. Computational Grid.

This same phenomena has been reported in the literature for the case of model start-up. It is reported that solutions reach quasi-steady conditions in two or three tidal cycles (Refs. 5.4 and 5.5) beginning with a bay with zero velocity and uniform temperature and concentration. In this work it was found that the bay would move from one quasi-steady state to another in three to five tidal cycles after a change in boundary conditions had been imposed. As a result of this phenomena, the model can be used to obtain daily averages which are representative of the quasi-steady state condition. These daily averages can be used as an accurate representation of monthly averages for periods in which the boundary conditions for the bay show small changes, e.g., the fresh water run-off into the bay is essentially constant and the tidal range stays essentially the same for the period under examination.

Results of the Barataria Bay Simulation

A solution of the transport equations was obtained for a number of important conditions which occur in Barataria Bay. These include: a typical period in May which is important to the shrimping season (It is in this period that the shrimp are exhibiting a rapid growth rate.) A high fresh water runoff flow through the system which simulates conditions that are encountered in a "wet year", a decrease in the Gulf salinity due to Mississippi River water meandering in front of the bay, a cold front passage which would simulate conditions that would adversely affect the marine species in the bay, and a tidal wave generated by a hurricane.

Typical Conditions

The first week of May, 1970 was selected because it is typical of the conditions that have been encountered in Barataria Bay for a number of years in the past. It does not fall into the category of a "wet year" or a "dry year" or a "cold spring", etc. Also this time of the year is very important to the growth rate of the commercially important species in the bay, especially shrimp. During this period the shrimp population is experiencing a rapid growth rate. The values of the environmental parameters used in the simulation are given in Table 5.1.

Velocity profiles for these conditions are shown in Figures 5.4 to 5.9. The first three figures show effects associated with outgoing tide, and the second three figures show effects associated with incoming tide. These figures were produced by assigning appropriate arrow lengths to velocity ranges as given in Table 5.2. This was necessary to produce a diagram that gives a satisfactory visual representation of the magnitude and direction of the water velocity. Referring to Figure 5.4, the velocity profiles are shown for the bay three hours after high tide at Barataria Pass. The water is flowing out of the bay at Barataria Pass; however, water is entering the bay at Caminada and Abel Passes and is shifting (near slack water conditions) at Quatre Bayou Pass. A definite circulation pattern is formed in which the flow is from incoming to outgoing waters. A point should be made clear at this time. The water flow does not stop at low or high tide. Waters have momentum that keep them moving after the level of the water has shifted. Slack tide, the period at which no water flows at the passes, occurs after low tide or high

TABLE 5.1

TYPICAL VALUES* OF THE CONDITIONS
FOUND IN THE BARATARIA BAY ESTUARY

VARIABLES	TYPICAL VALUES
Wind Speed	5,0 (ft/sec)
Wind Angle with Respect To Grand Isle Line **	1.0 (Radians)
Gulf Temperature	60.0 (°F)
Gulf Salinity	28.0 (%)
Air Wet Bulb Temperature	20.1 (°C)
Air Temperature	20.0 (°C)
Pressure	1000.0 (Millibars)
Range of Low Tide	1.1 (ft)
Range of High Tide	1.1 (ft)
Frequency	One tidal cycle per 20 hour
Fresh Water Runoff Rate	1000.0 (ft^3/sec)
Fresh Water Salinity	8.0 (%)
Fresh Water Temperature	Equal to the bay temperature at a corresponding depth
Water Density	62.4 (lbs/ft^3)
Noon Solar Radiation	0.3334 ($Kcal/m^2 sec$)

* First week in May, 1970

** 45° with respect to the East-West line

TABLE 5.2

ARROW LENGTHS OF DIFFERENT
VELOCITY RANGES

Velocity Range (ft/sec)	Arrow Length (inches)
0.5 - over	1/4
0.1 - 0.5	1/8
0.005 - 0.1	1/16
0 - 0.005	0

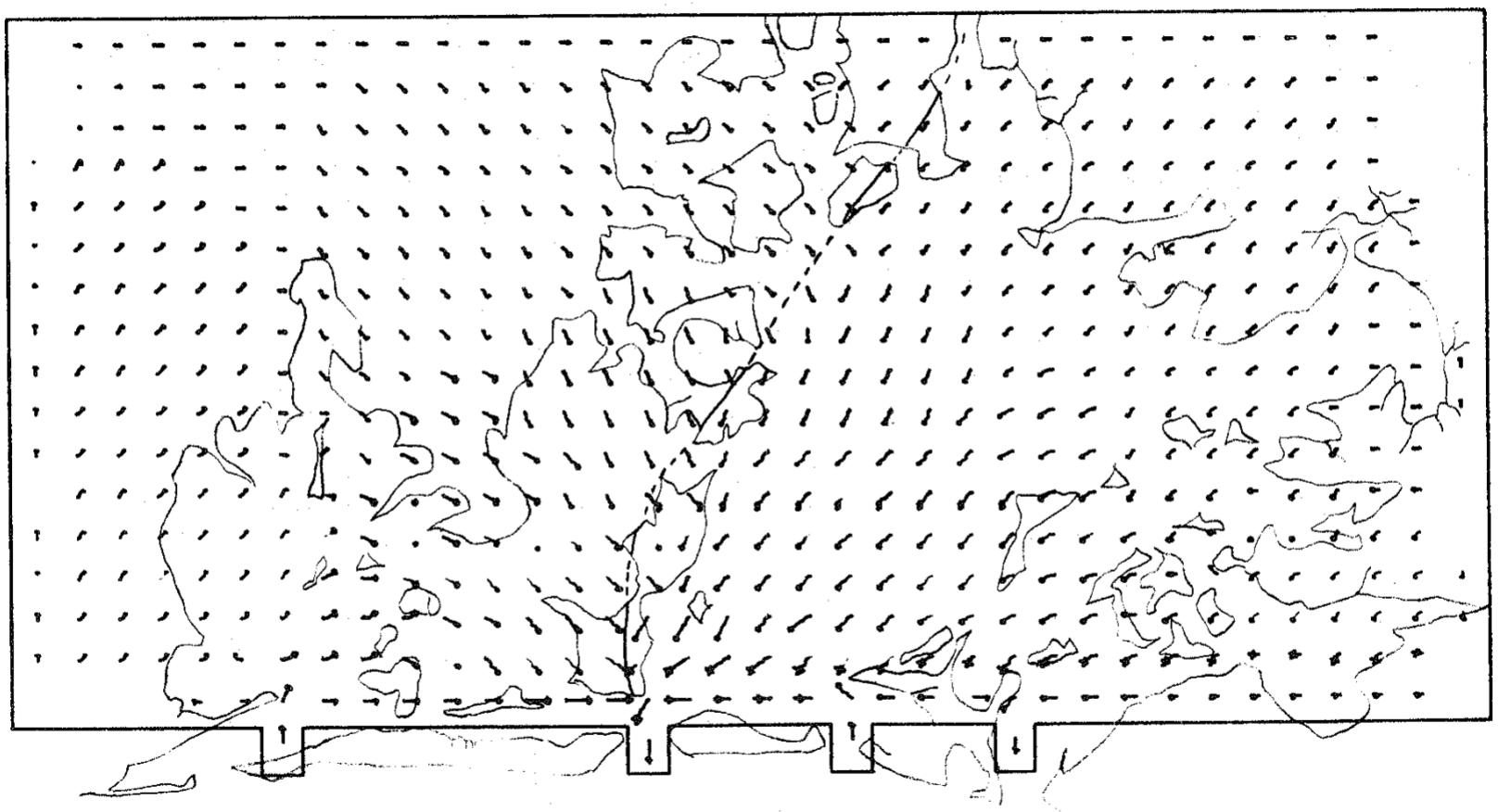

Figure 5.4. Typical Conditions Velocity Profiles. May 1st, 1970, 3 hours after high tide, 9:00 A.M.

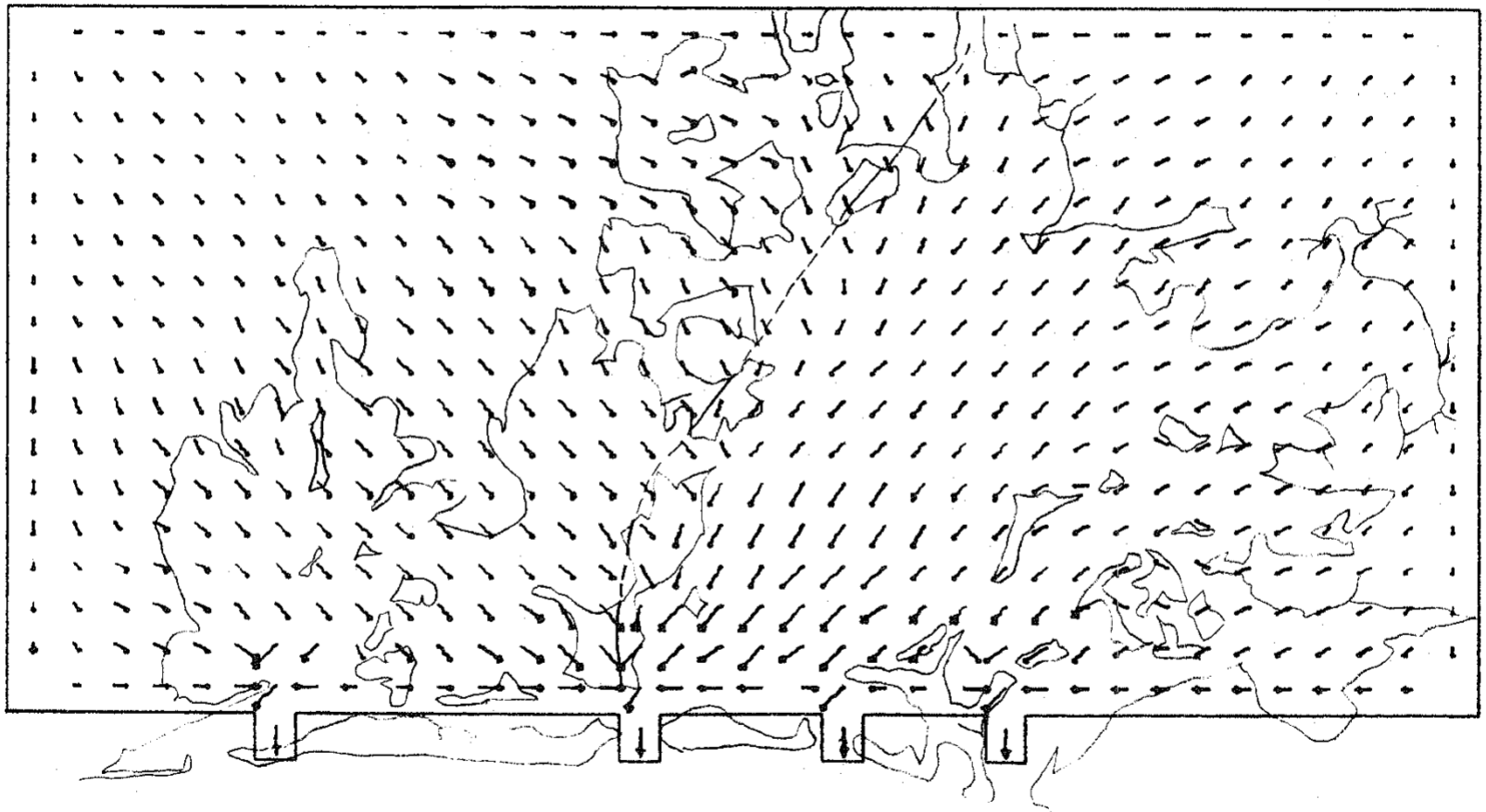

Figure 5.5. Typical Conditions Velocity Profiles. May 1st, 1970, 6 hours after high tide, 12:00 noon.

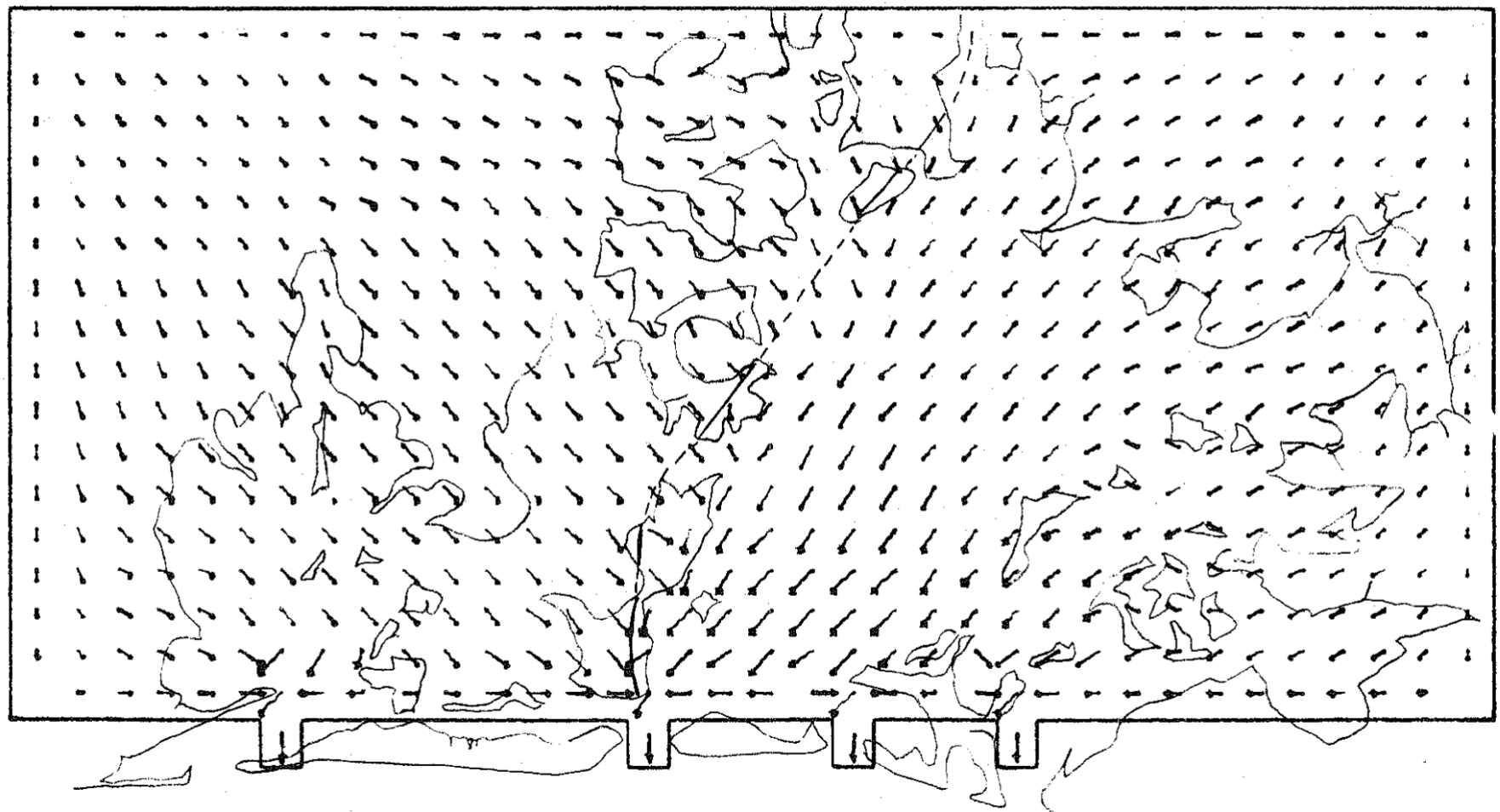

Figure 5.6. Typical Conditions Velocity Profiles. May 1st, 1970, 9 hours after high tide, 3:00 P.M.

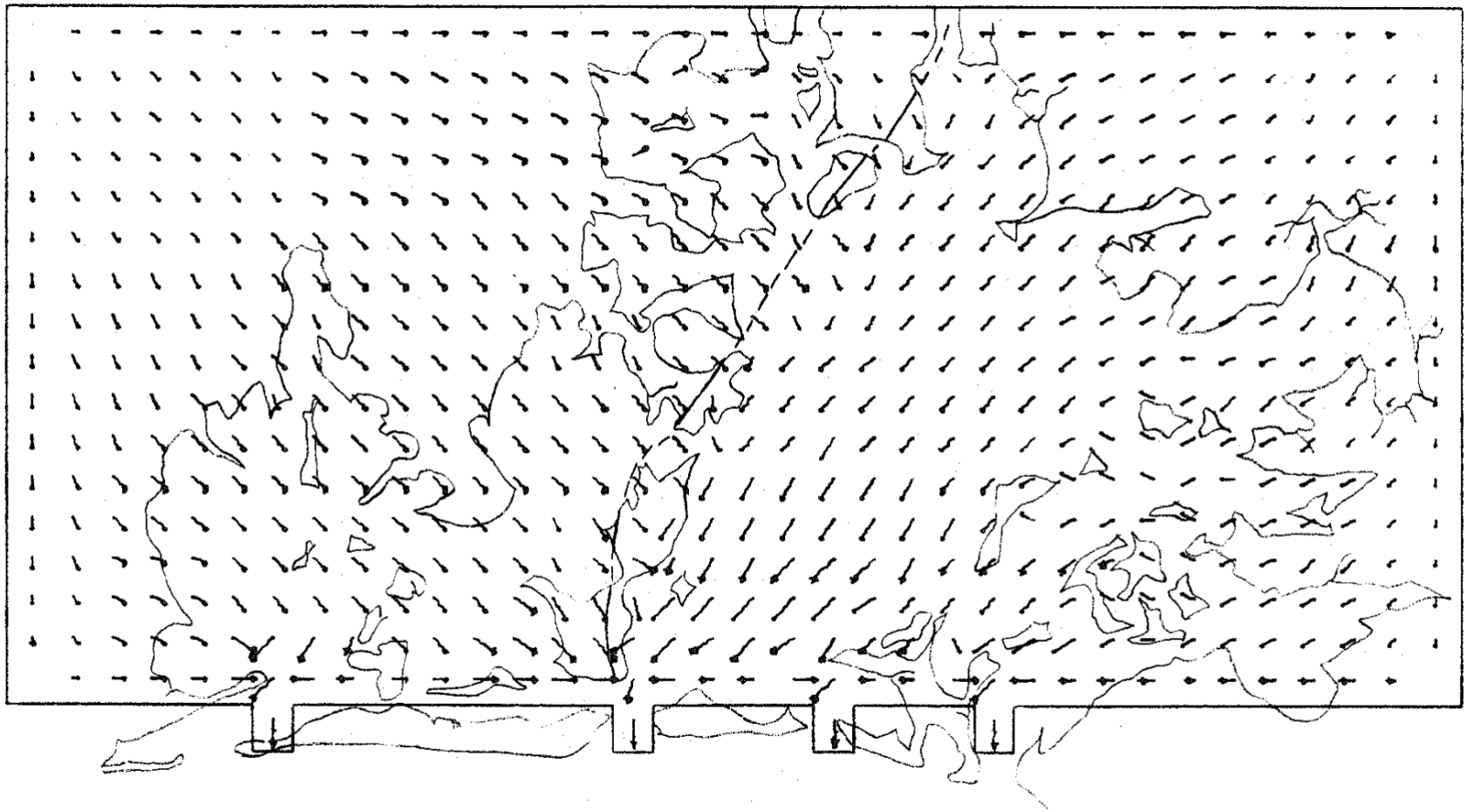

Figure 5.7. Typical Conditions Velocity Profiles. May 1st, 1970, 3 hours after low tide, 7:00 P.M.

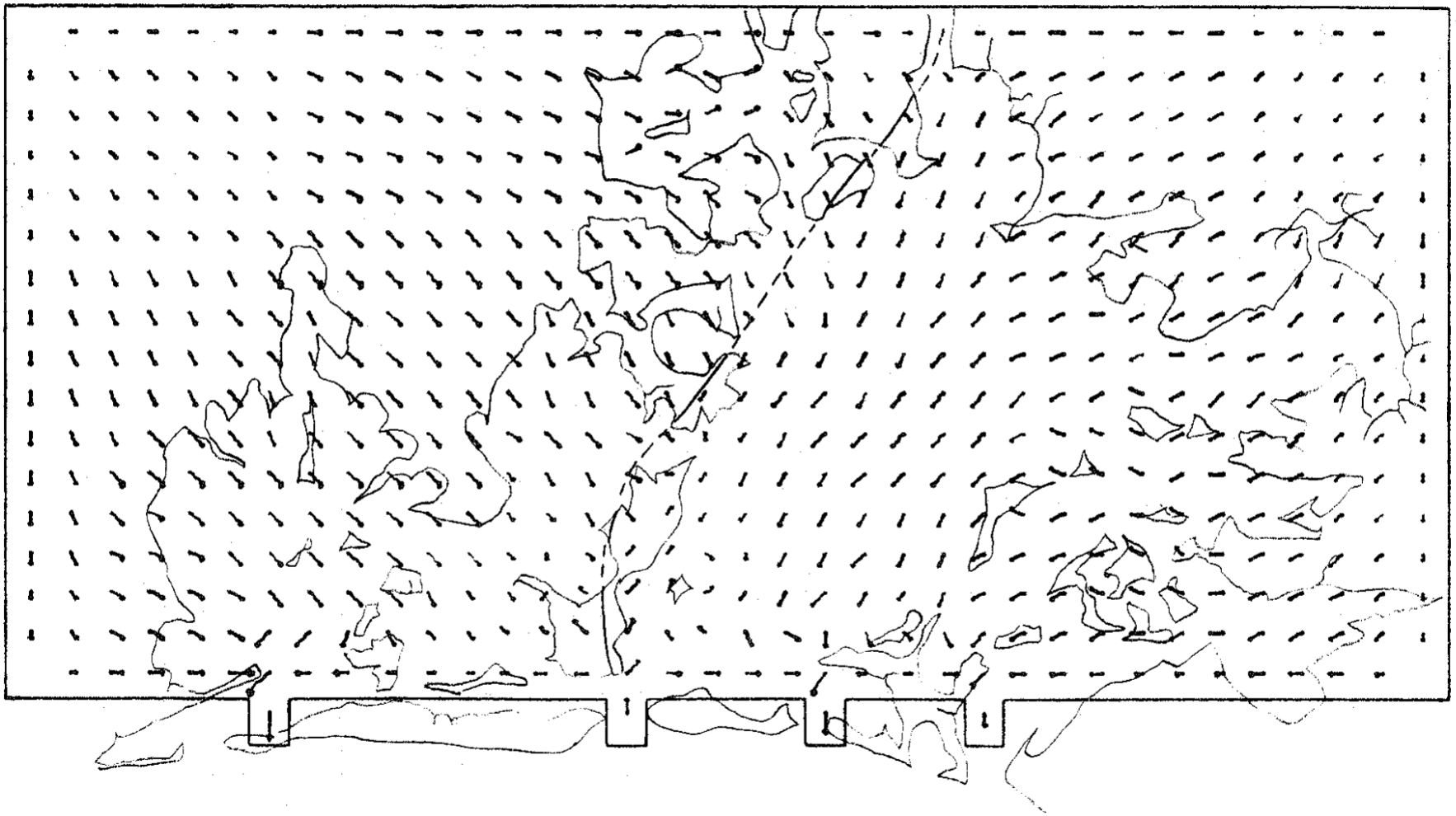

Figure 5.8. Typical Conditions Velocity Profiles, May 1st, 1970, 6 hours after low tide, 10:00 P.M.

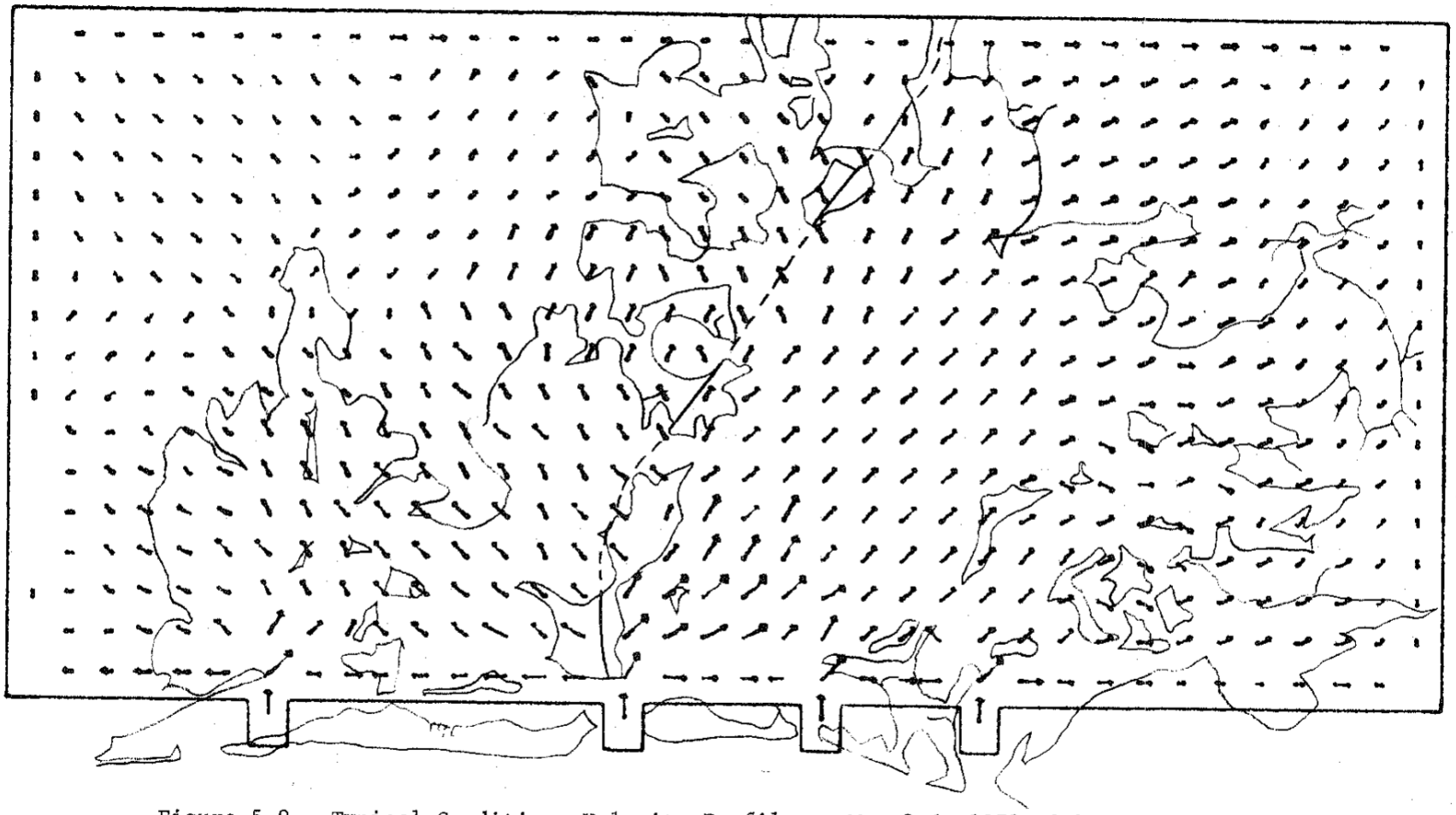

Figure 5.9. Typical Conditions Velocity Profiles. May 2nd, 1970, 9 hours after low tide, 1:00 A.M.

tide time. In Figure 5.5, the velocity profiles are shown in the bay at six hours after high tide at Barataria Pass. At this time the flow is out of all of the passes. It can be seen from the figure that Barataria Pass is the predominant water outlet for the Barataria Bay system.

In Figure 5.6 the velocity profiles are shown for the bay nine hours after high tide at Barataria Pass. This figure is similar to the previous one but the velocities shown are larger due to acceleration effects.

In Figure 5.7 circulation patterns can be distinguished three hours after low tide of Barataria Pass. The waters are still going out of the system due to the momentum of waters inside the bay.

In Figure 5.8 velocity profiles are shown six hours after low tide at Barataria Pass. Flow has reversed in Barataria Pass, and water is entering the system at this point. However, the water at the other passes is still flowing out. It can be noted that the speed of the waters leaving the bay has decreased since the previous time shown.

In Figure 5.9 velocity profiles are shown nine hours after low tide occurred at Barataria Pass. All passes have incoming waters. The largest velocities are originated by Barataria Pass, as was the case for the outgoing tide.

The salinity distribution patterns that correspond to these velocity profiles are shown in Figures 5.10 to 5.16. Figure 5.10 shows isohalines for the bay one hour after high tide. At this time, the deepest penetration of isohalines into the bay occurs. Conditions are close to slack water and water is about to stop entering the bay.

In Figure 5.11 isohalines are shown for the bay three hours after high tide. Isohalines start to recede towards the Gulf.

In Figure 5.12 isohalines are shown for the bay six hours after high tide. The 20o/oo isohaline has moved into the Gulf at Caminada Pass and Quatre Bayou Pass. The 15o/oo isohaline is closer to the Gulf as is the 10o/oo isohaline.

In Figure 5.13 isohalines are shown for the bay nine hours after high tide. The 20o/oo isohaline remains only around Barataria Pass. The 15o/oo isohaline is closer to the Gulf but with one exception. This exception is at a point between Caminada Pass and Barataria Pass. At this point the 15o/oo isohaline is further away from the Gulf than it was three hours previously. The reason for this phenomena is that in this region velocities are small at this particular period and dispersion becomes important. Therefore; the salinity at this point instead of rushing out to the Gulf disperses in the low velocity area. In Figure 5.14 isohalines are shown for the bay three hours after low tide. At this time, the isohalines are moving away from the Gulf. The waters have stopped going out and are about to reverse. The 15o/oo isohaline remains only around Barataria Pass.

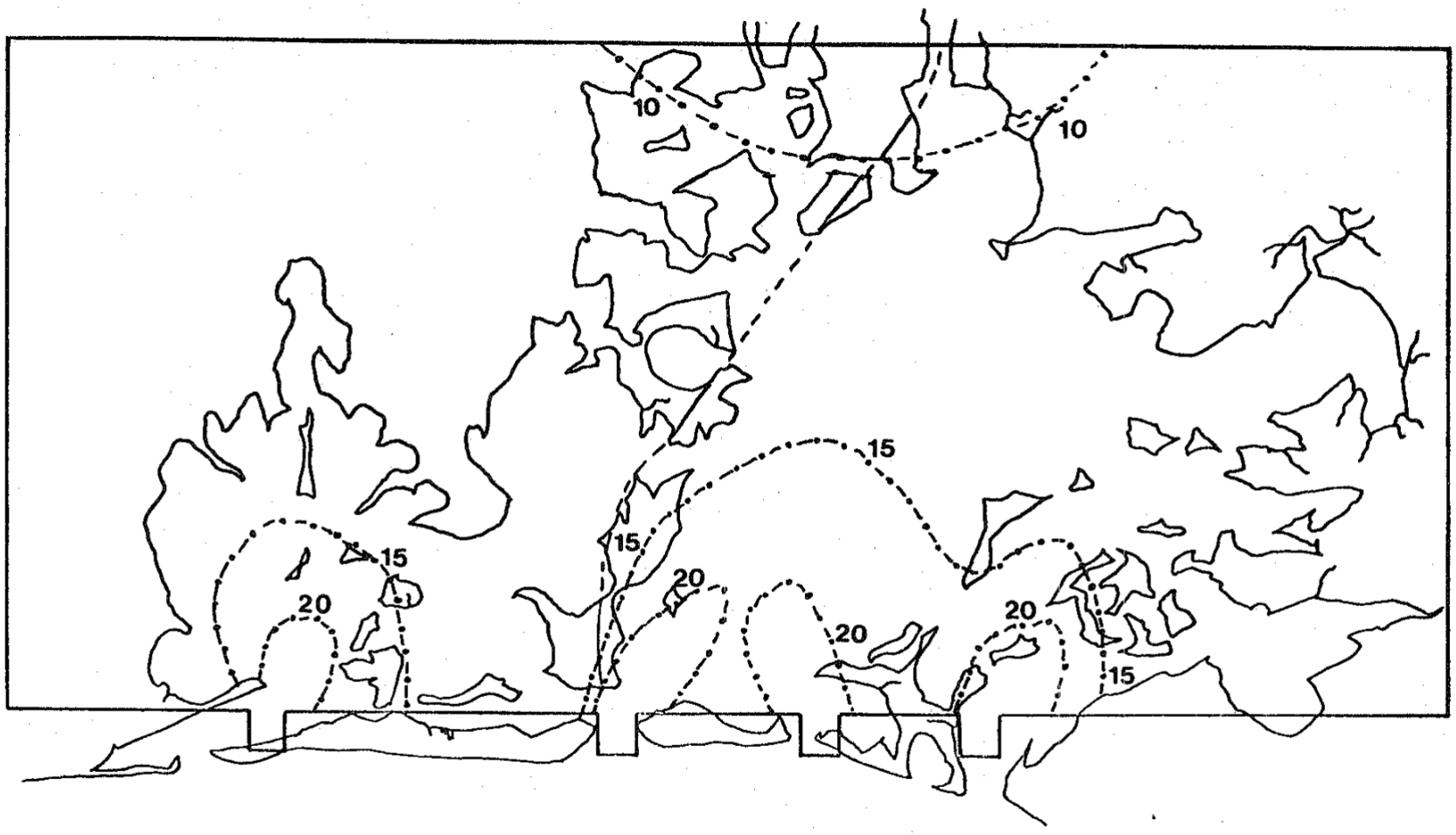

Figure 5.10. Typical Conditions Isohalines. May 1st, 1970, 1 hour after high tide, 7:00 A.M. (Salinity is in 0/00.)

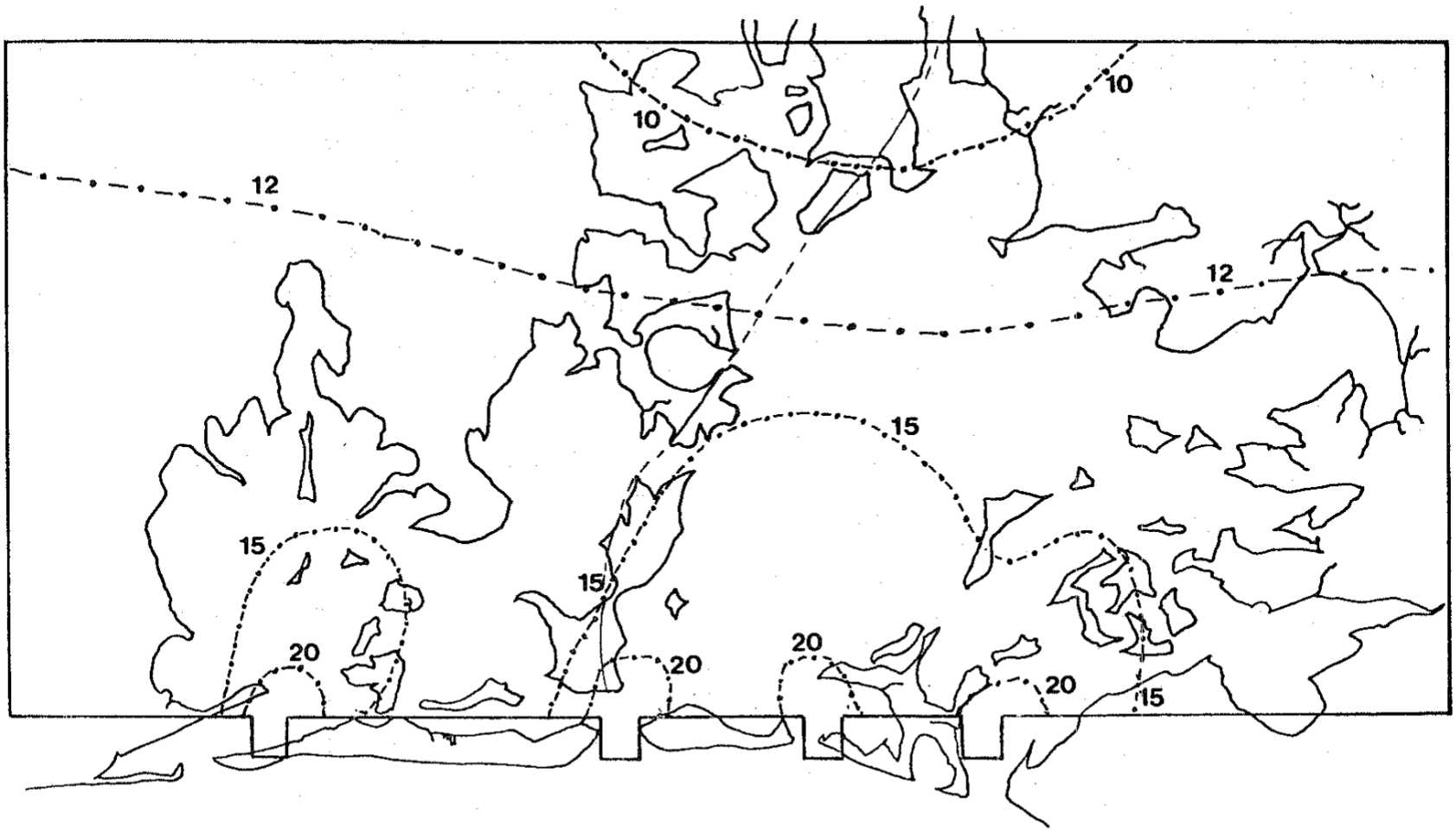

Figure 5.11. Typical Conditions Isohalines. May 1st, 1970, 3 hours after high tide, 9:00 A.M. (Salinity is in 0/00.)

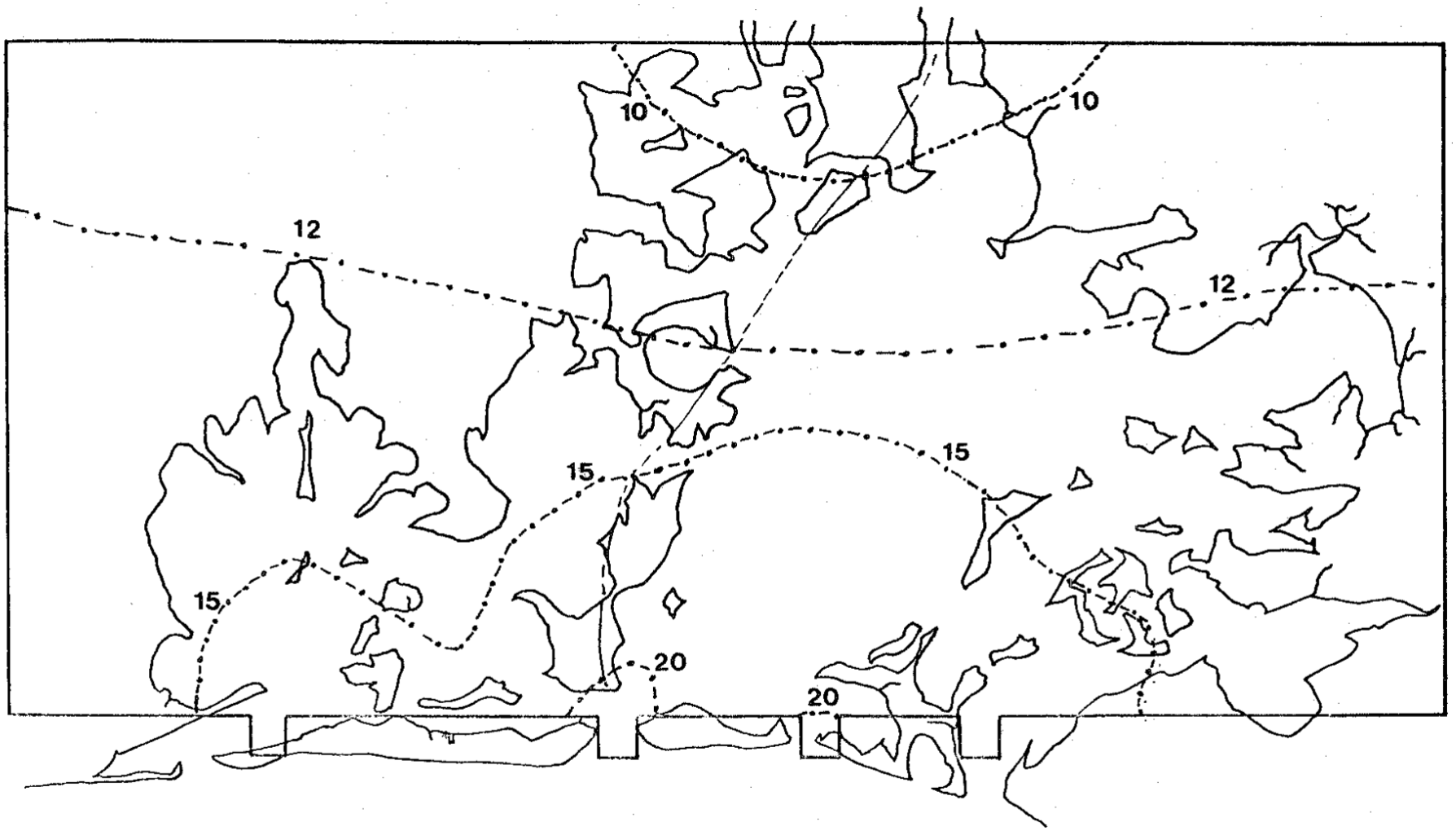

Figure 5.12. Typical Conditions Isohalines. May 1st, 1970, 6 hours after high tide, 12:00 noon. (Salinity is in 0/00.)

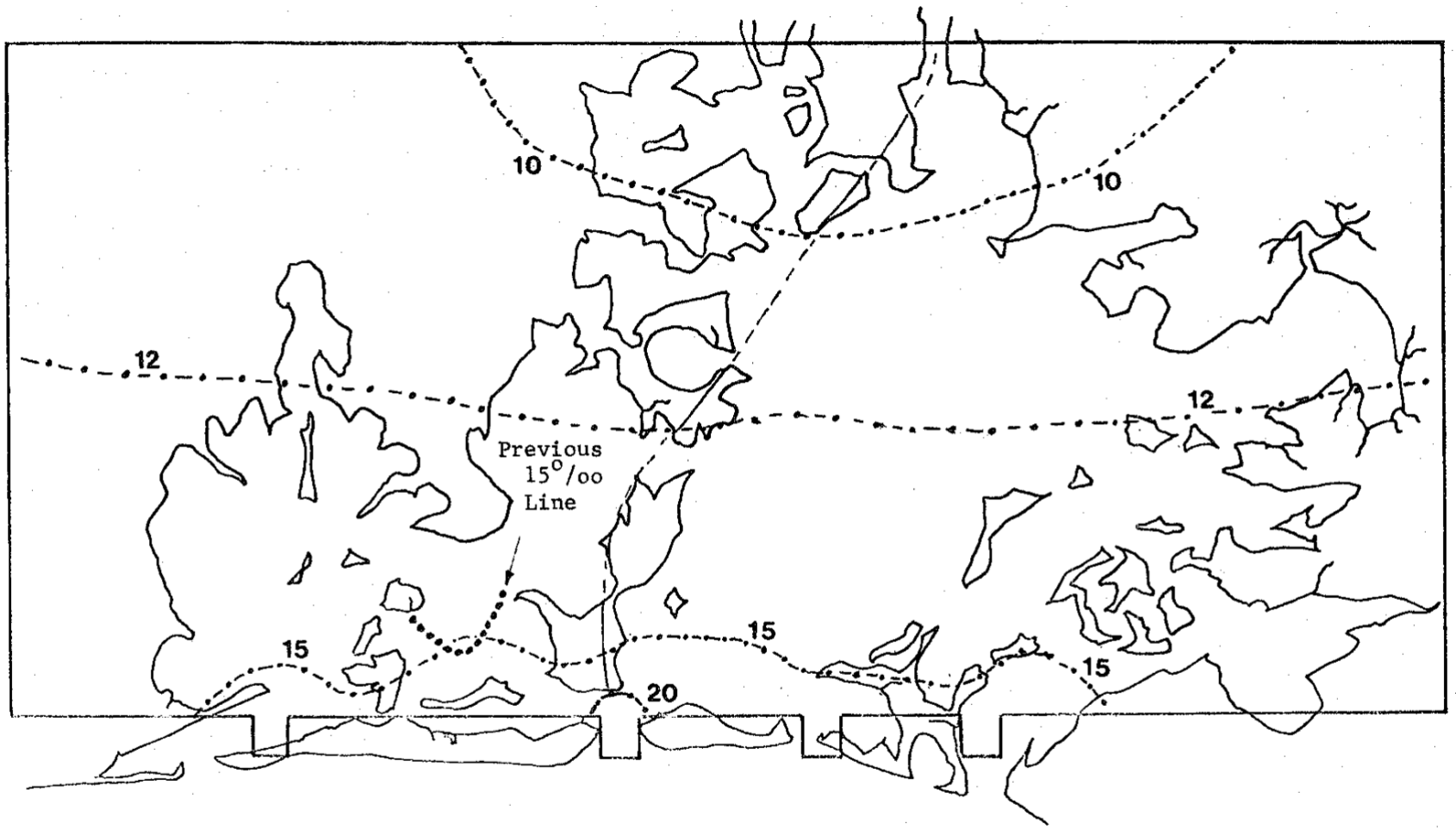

Figure 5.13. Typical Conditions Isohalines. May 1st, 1970, 9 hours after high tide, 3:00 P.M. (Salinity is in 0/00.)

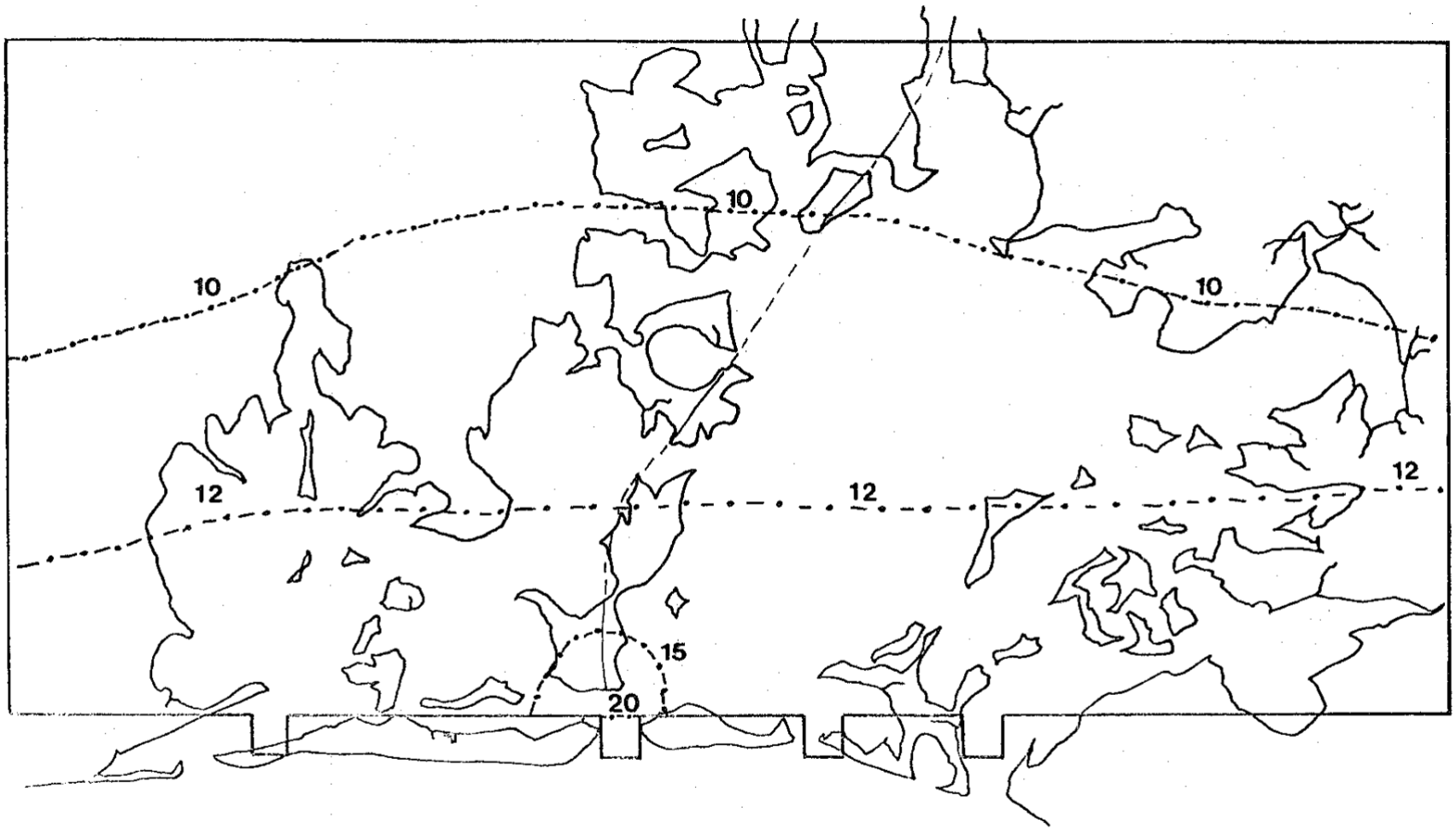

Figure 5.14. Typical Conditions Isohalines. May 1st, 1970, 3 hours after low tide, 7:00 P.M. (Salinity is in 0/00.)

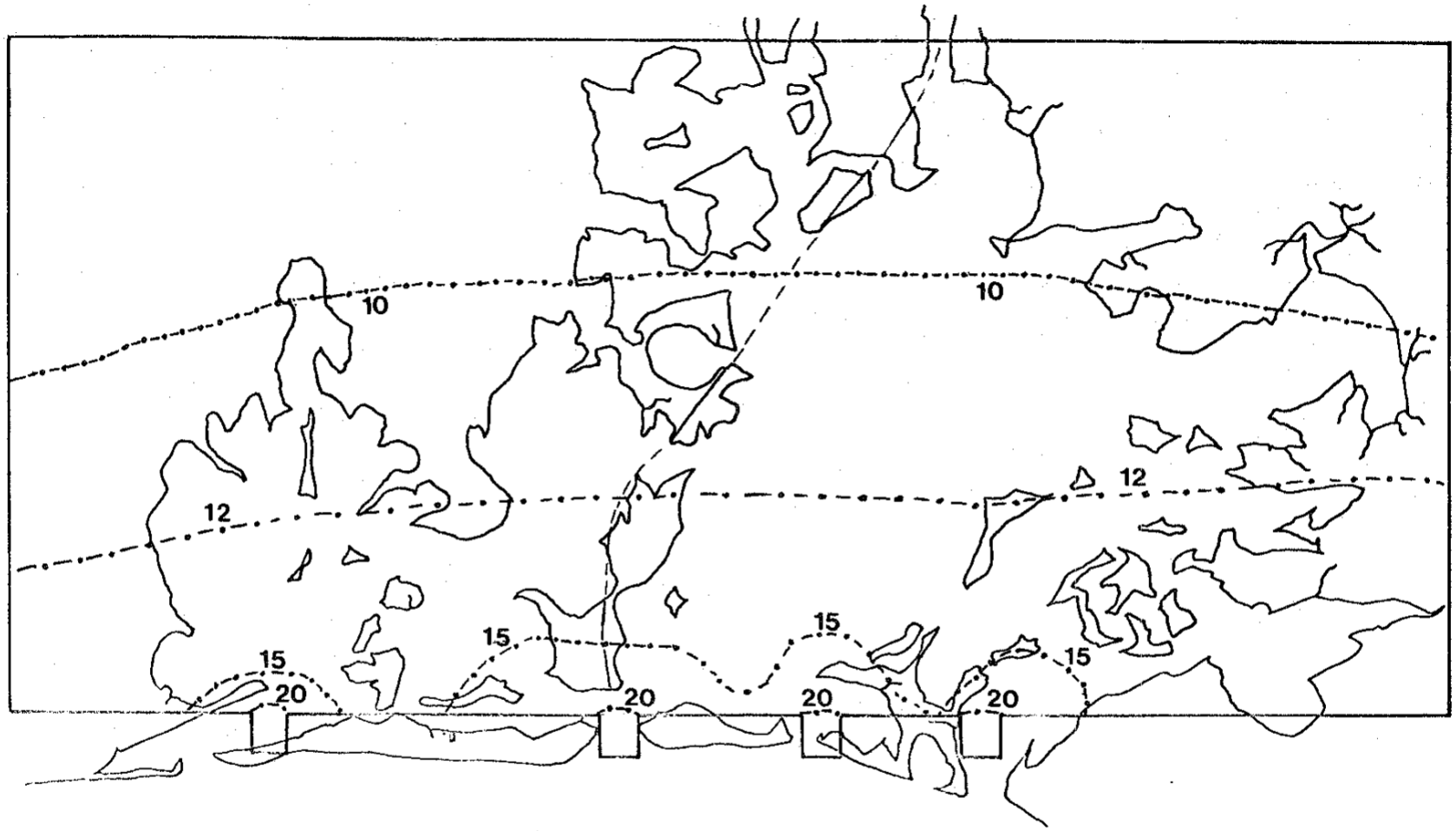

Figure 5.15. Typical Conditions Isohalines. May 1st, 1970, 6 hours after low tide, 10:00 P.M. (Salinity is in 0/00.)

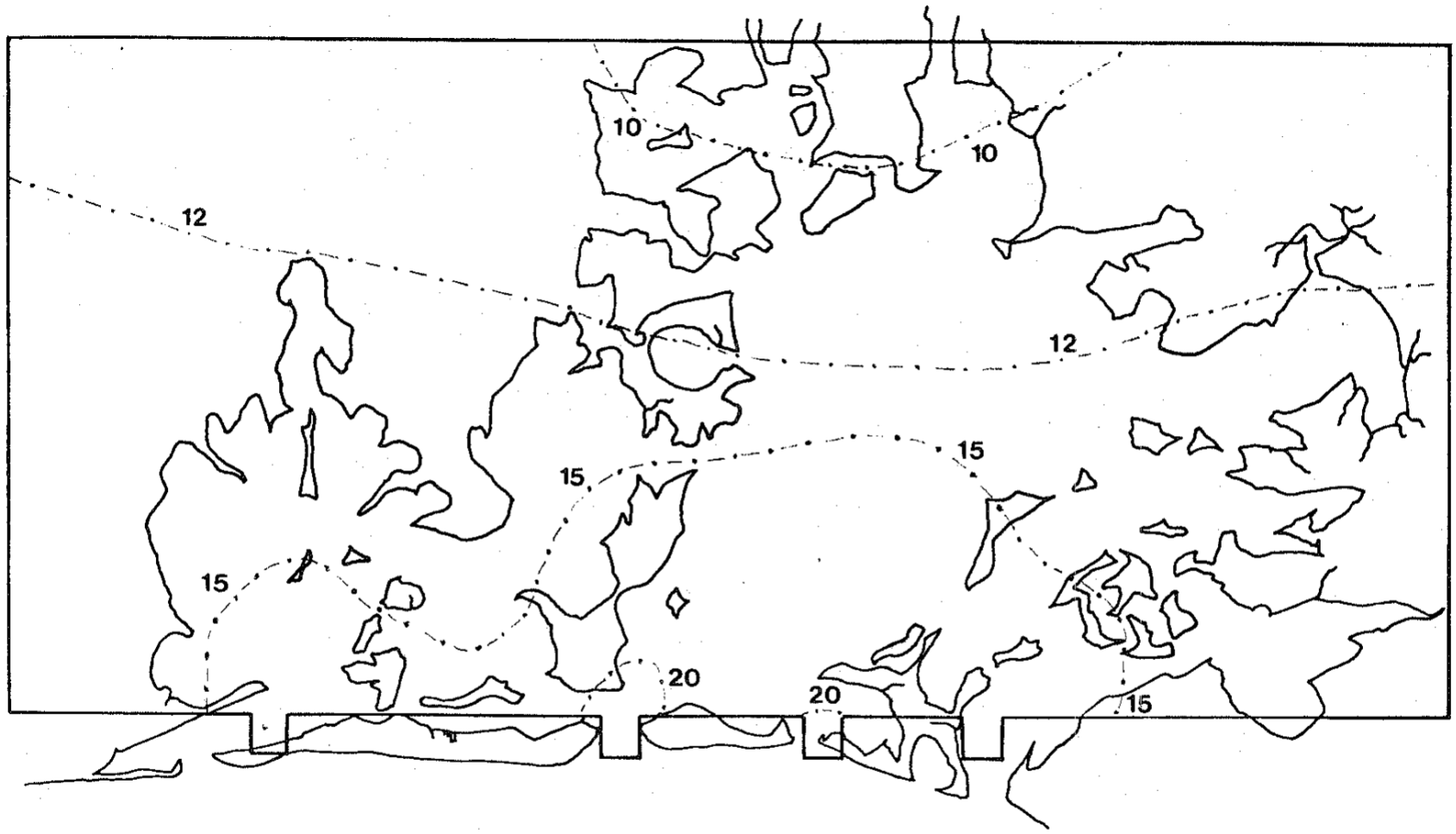

Figure 5.16. Typical Conditions Isohalines. May 2nd, 1970, 9 hours after low tide, 1:00 A.M. (Salinity is in 0/00.)

In Figure 5.15 isohalines are shown for the bay six hours after low tide. The waters are entering the bay from the Gulf. The 20o/oo and 15o/oo isohalines are again found in the bay and are proceeding inland. In Figure 5.16 isohalines are shown for the bay nine hours after low tide. As can be seen, the 15 and 20o/oo isohalines have reentered the bay, and a tidal cycle has been completed.

The temperatures of the bay that correspond with the above mentioned velocity profiles and salinity distributions were also obtained. It was found that temperatures in Barataria Bay are a weak function of velocities and depth and a strong function of solar radiation during the day and convection at night. In Figure 5.17 isotherms are shown for the bay six hours after low tide, at noon. As can be seen, the highest temperatures are in the shallow areas of the marsh and the upper reaches of the bay, away from the Gulf. Towards the Gulf, temperatures decrease since the Gulf is relatively cool. In Figure 5.18, isotherms are shown for the bay six hours after high tide, at midnight. The water is coming in from the Gulf, and the cool water forms the 61°F isotherms around the passes. Comparing this figure with the previous one, it is observed that the marshes have cooled down. The only waters with temperatures above 80°F are a small region in the upper reaches of the bay where the water is relatively deep (6 feet as compared with an average water depth of 2 feet in the marshes).

In Figure 5.19, the temperature variations are compared at a point of water depth of six feet located near St. Mary's Point with a point in the marsh where the water depth is an average of two feet. These locations are shown on Figure 5.18. The point which has a water depth of six feet is marked by a circle and the point which has a water depth of two feet is marked by a triangle. It was observed that in these typical conditions, the range of the diurnal variation was 14°F for a water depth of six feet. This range was somewhat higher (24°F) for a water depth of two feet in the marsh.

In Figure 5.20, the temperature variation is compared for a marsh location seven miles inland (shown by a circle in Figure 5.18) with the temperature variation for a marsh location two miles inland (close to the Gulf and shown by a square in Figure 5.18). As can be seen, the temperature variation of the point near the Gulf is dampened when compared to the temperature of the inland marsh point. The reason for this effect is that the Gulf water has moderating effects on the temperature of the points near the tidal passes.

It was found that for typical conditions, the effects of wind were small. For the typical conditions, wind affected water velocities in the bay by less than 0.001%. Leendertse (Ref. 5.5) reports that effects of a 20-knot wind on Jamaica Bay are "insignificant". However, winds do affect the bay. Winds blowing over the Gulf affect the heights of the tide at the passes, and this in turn affects the flow in the bay.

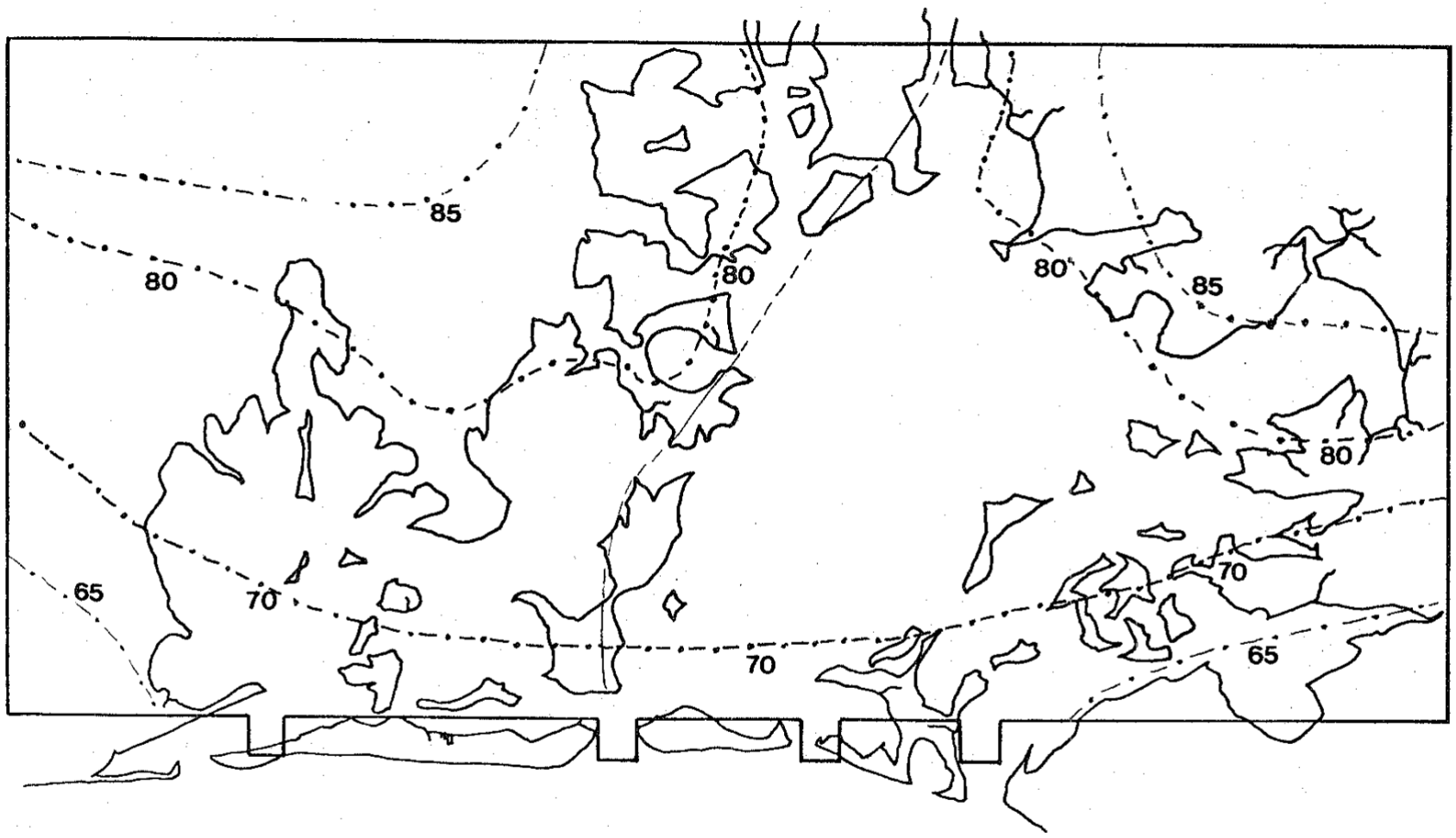

Figure 5.17. Typical Conditions Isotherms. May 1st, 1970, at 12:00 noon, 6 hours after high tide. (Temperature is in degrees F.)

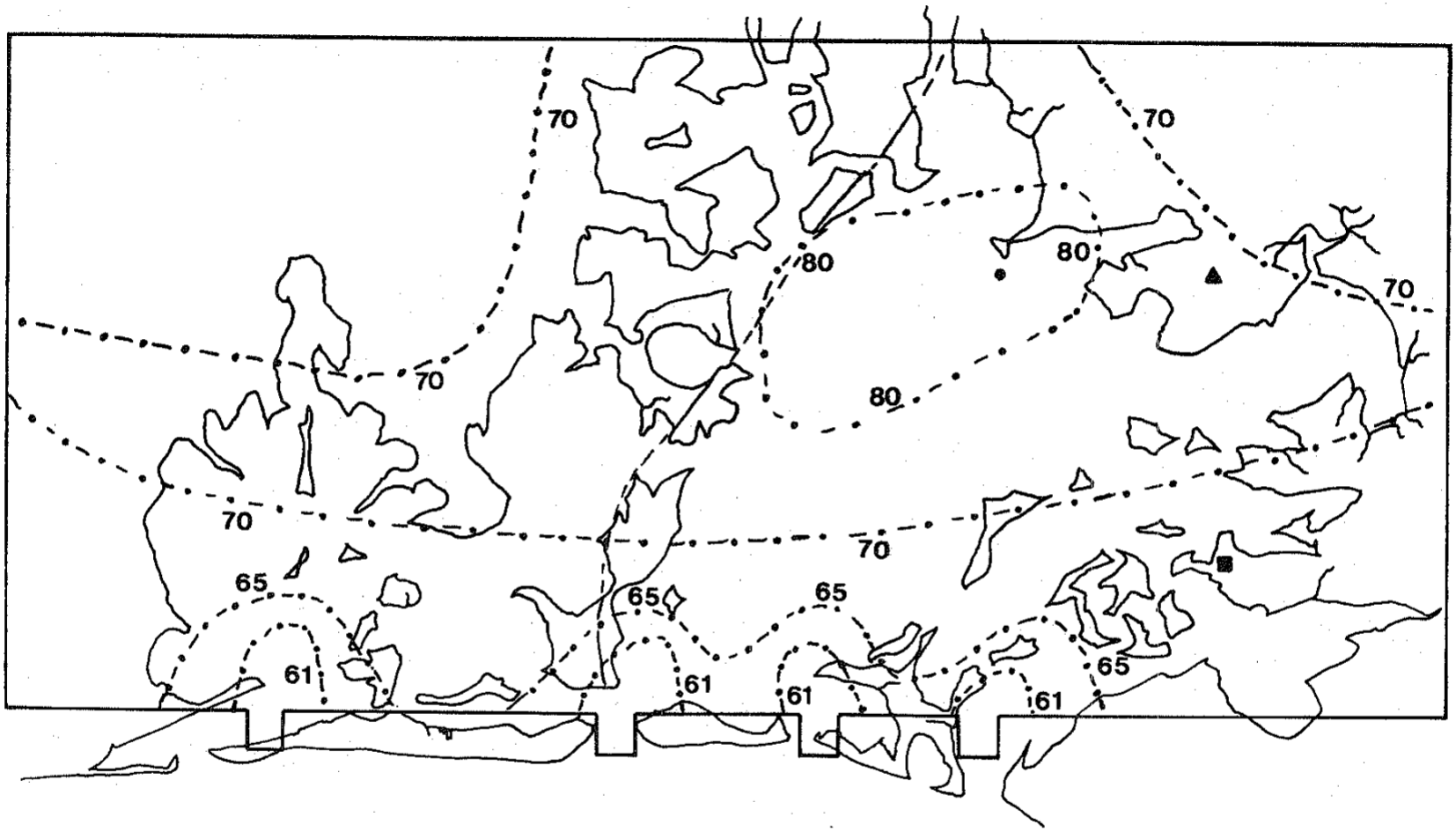

Figure 5.18. Typical Conditions Isotherms. May 1st, 1970, at 10:00 P.M., 6 hours after low tide. (Temperature is in degrees F.)

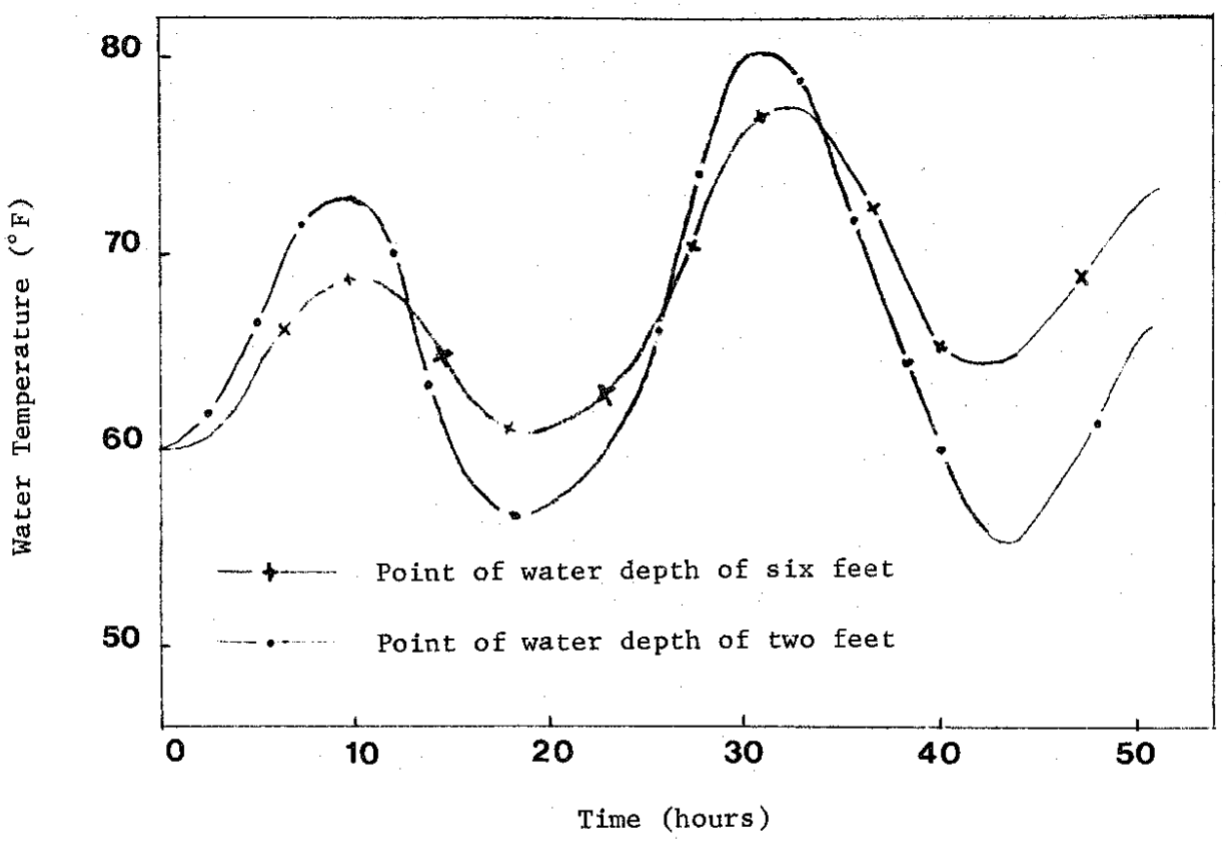

Figure 5.19. Typical Conditions Temperature Variation at Locations of Different Depths. May 1st and May 2nd, 1970 (Starting at May 1st, 6:00 A.M.). See Figure 5.18 for location of points.

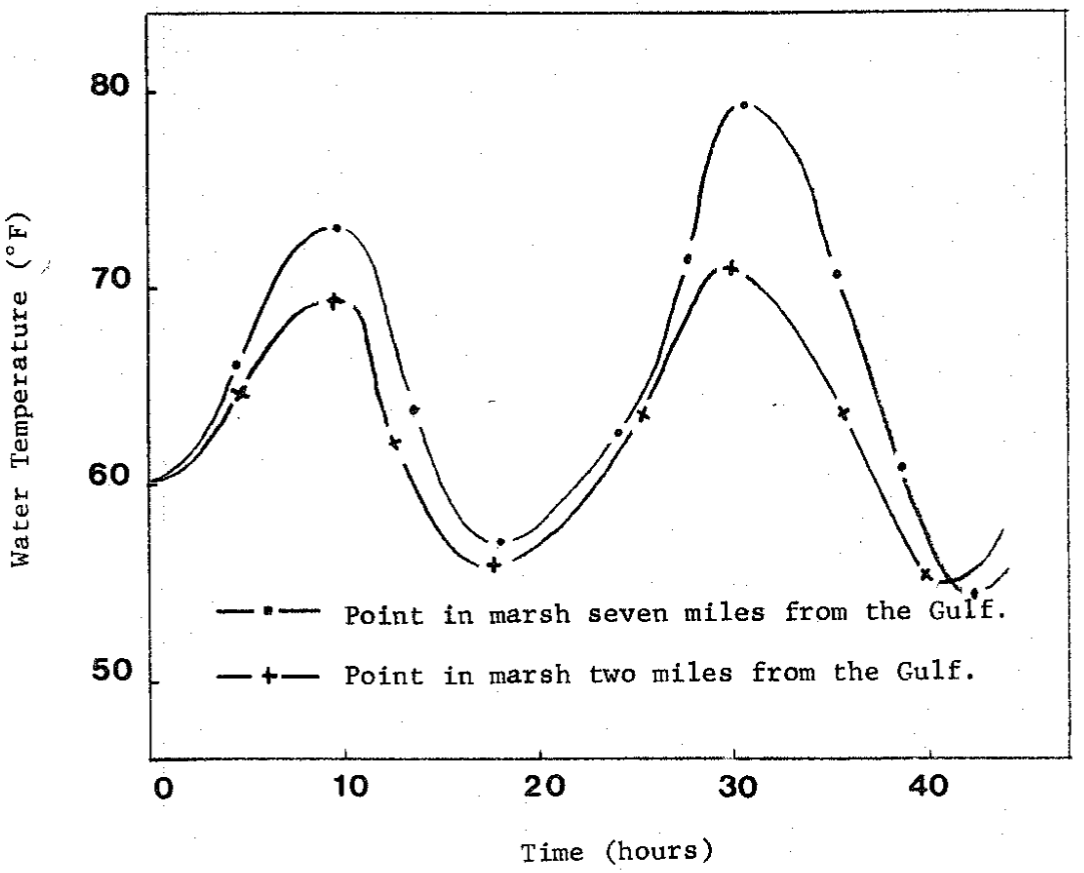

Figure 5.20. Typical Conditions Temperature Variation At Locations of Different Distance to the Gulf. May 1st and May 2nd, 1970 (Starting at May 1st, 6:00 P.M.). See Figure 5.18 for location of points.

High Fresh Water Runoff

Barataria Bay is part of a hydrological unit of large area bounded by the Mississippi River and Bayou Lafourche. All the runoff from rainfall that is collected by this area flows to the Gulf through Barataria Bay. The fresh water that enters Barataria Bay through its upper reaches when mixed with water from the Gulf, produces the salinity conditions necessary for the marine life than an estuary supports. Salinity effects are of primary importance to the commercially important species that exist in Barataria Bay. For example, oysters have an optimum range of salinity in which they thrive. If salinity is too high, the oyster drill can appear and essentially wipe out entire oyster reefs within several weeks time. Control of salinity in oyster producing areas is of great importance. A case of high fresh water runoff entering the bay was run in order to show the capability of the model to predict behavior of isohalines under different fresh water inflow conditions.

Data for fresh water runoff into Barataria Bay were obtained from Gagliano, et al (Ref. 5.2). Typical average daily runoff into Barataria Bay was found to be 1,000 ft^2/sec. For the case of high fresh water runoff a value of 3,000 ft^3 /sec was used. Gagliano (Ref. 5.2) reports conditions of fresh water runoff up to six times the average value. The figure of 3,000 ft^3 /sec is a realistic figure for a high fresh water runoff case.

Solutions were obtained for this high fresh water runoff case, and, as with the results for typical conditions, a quasi-steady state was reached in three tidal cycles. The results obtained are shown at interval corresponding with typical conditions (previously shown) in Figures 5.21 to 5.26. Referring to these figures the expected results are obtained of having the isohalines moved closer to the Gulf. In this particular case, tripling the fresh water runoff rate was found to move the 15o/oo isohaline one third to one half mile closer to the Gulf depending on the relative location to Barataria Pass. The information shown in these figures could be extrapolated or interpolated for other values of runnoff. However, extrapolation can be made only on the open bay region behind the passes. Non-linearities generated by islands and other barriers would require the program to be run for the specific case under study for an accurate prediction of the position of the isohalines. In Figure 5.26 the effect of these non-linearities are shown. The 15o/oo isohalines shown cross each other at a point close to islands located near Barataria Pass.

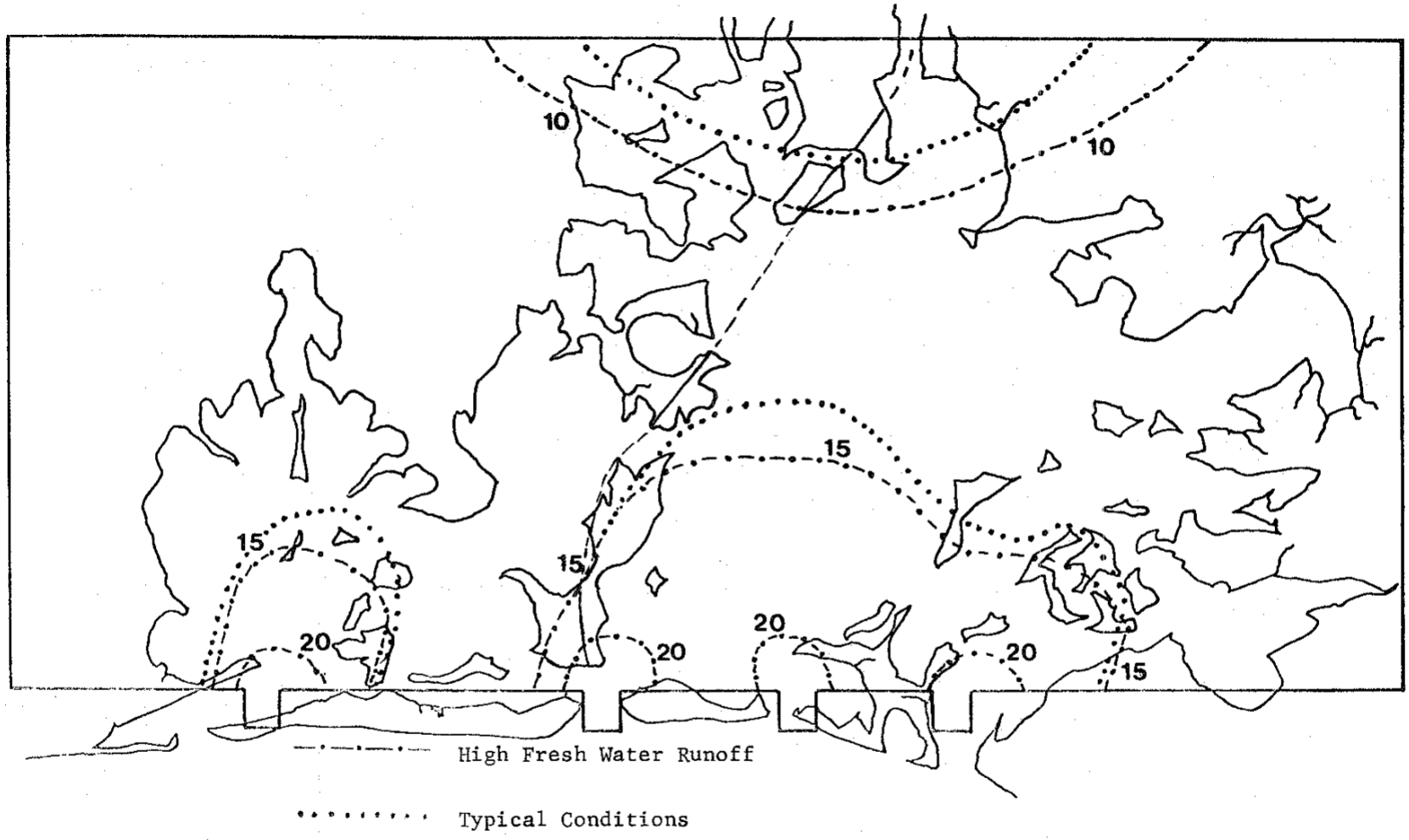

Figure 5.21. Comparison of High Fresh Water Runoff Isohalines with Typical Conditions Ischalines. Three hours after high tide. (Salinity is in 0/00.)

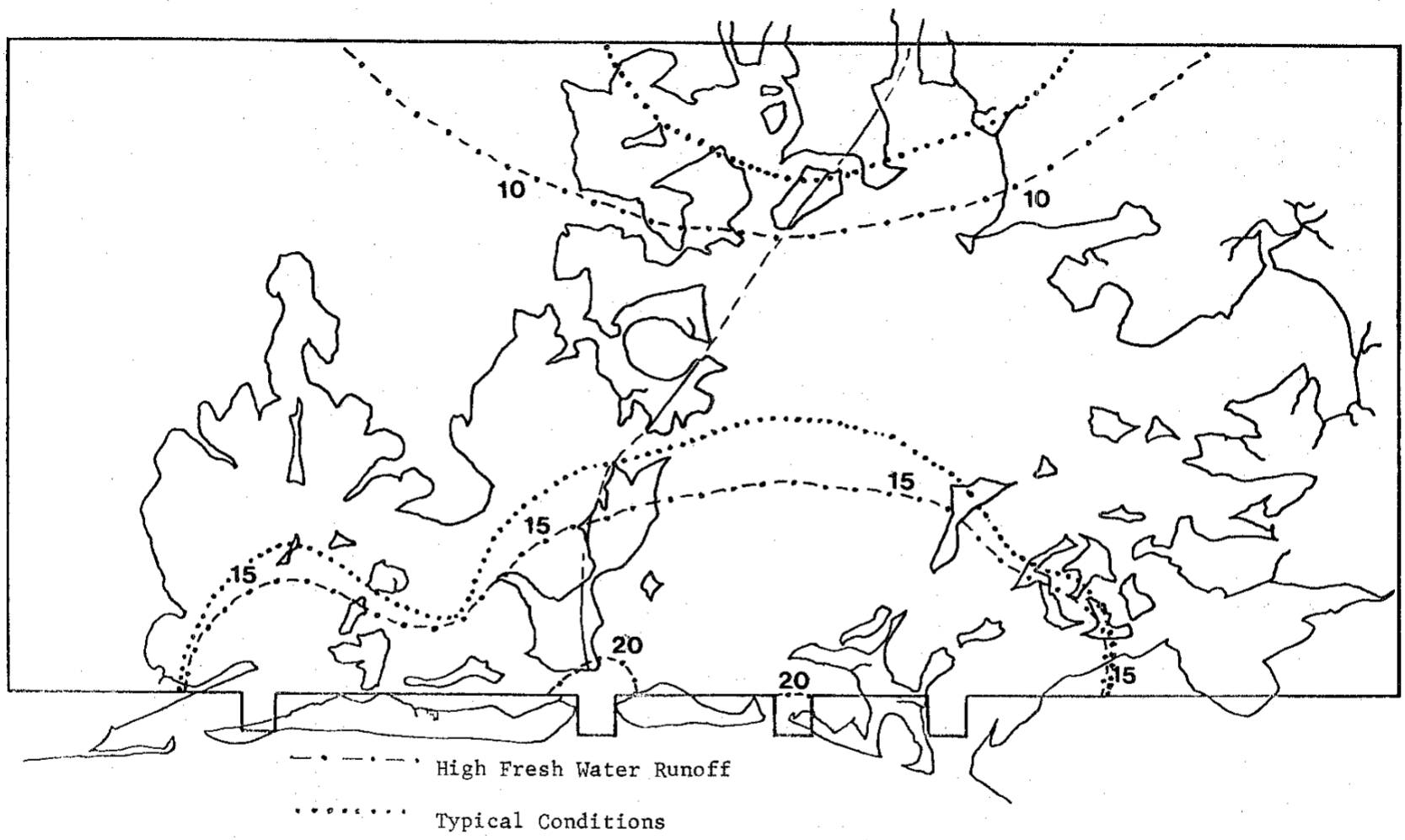

Figure 5.22. Comparison of High Fresh Water Runoff Isohalines with Typical Conditions Isohalines. Six hours after high tide. (Salinity is in 0/00.)

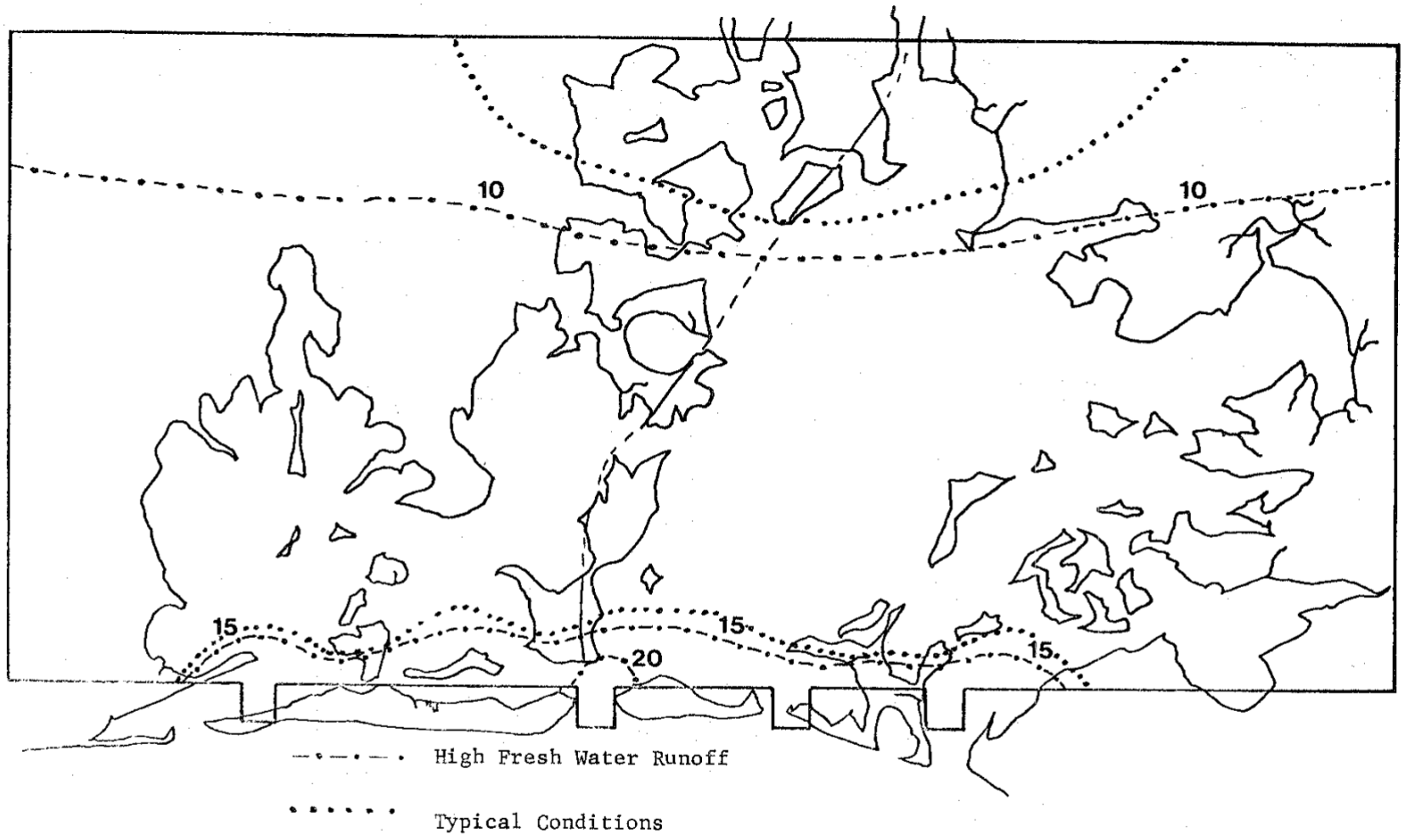

Figure 5.23. Comparison of High Fresh Water Runoff Isohalines with Typical Conditions Isohalines. Nine hours after high tide. (Salinity is in 0/00.)

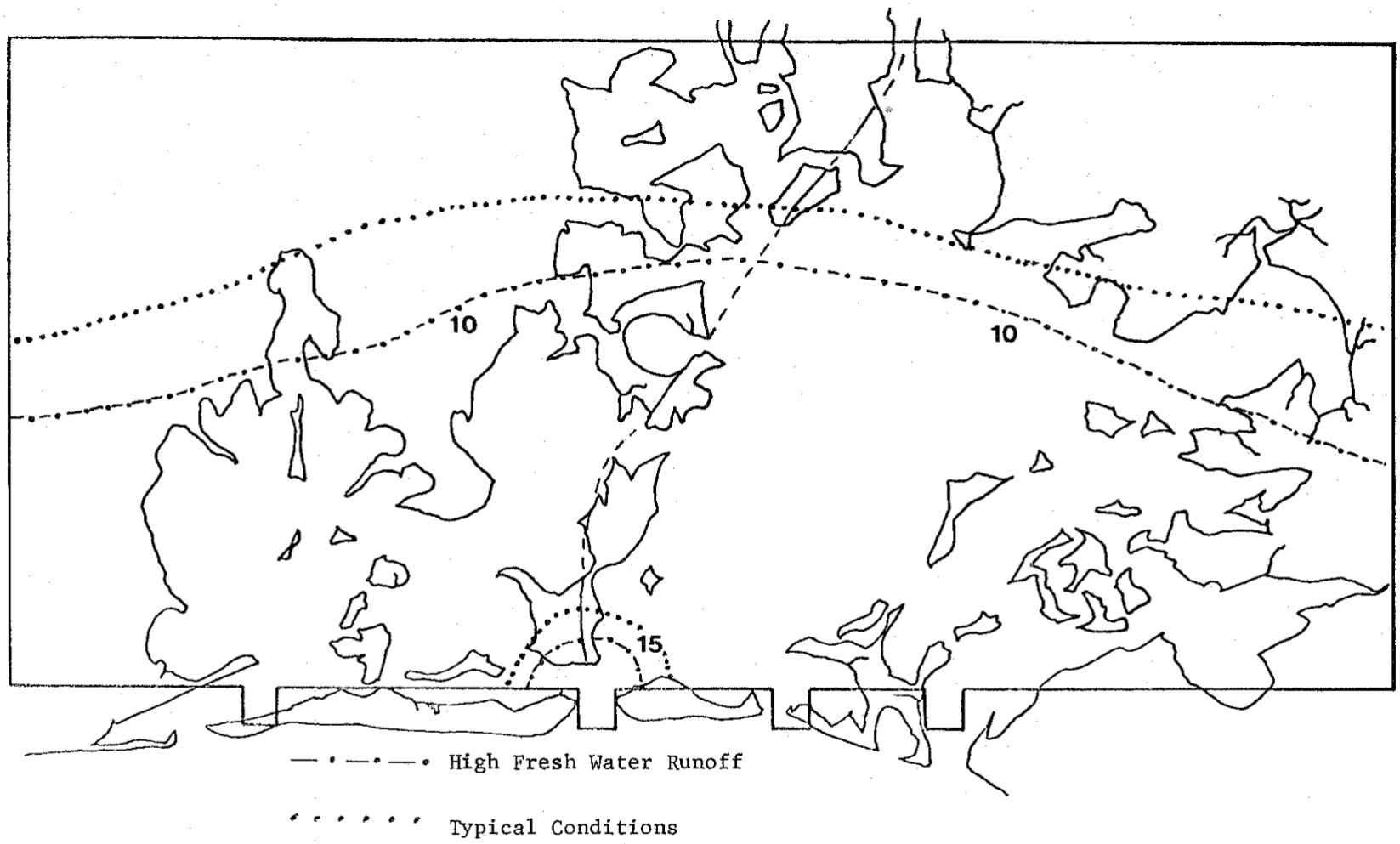

Figure 5.24. Comparison of High Fresh Water Runoff Isohalines with Typical Conditions Isohalines. Three hours after low tide. (Salinity is in 0/00.)

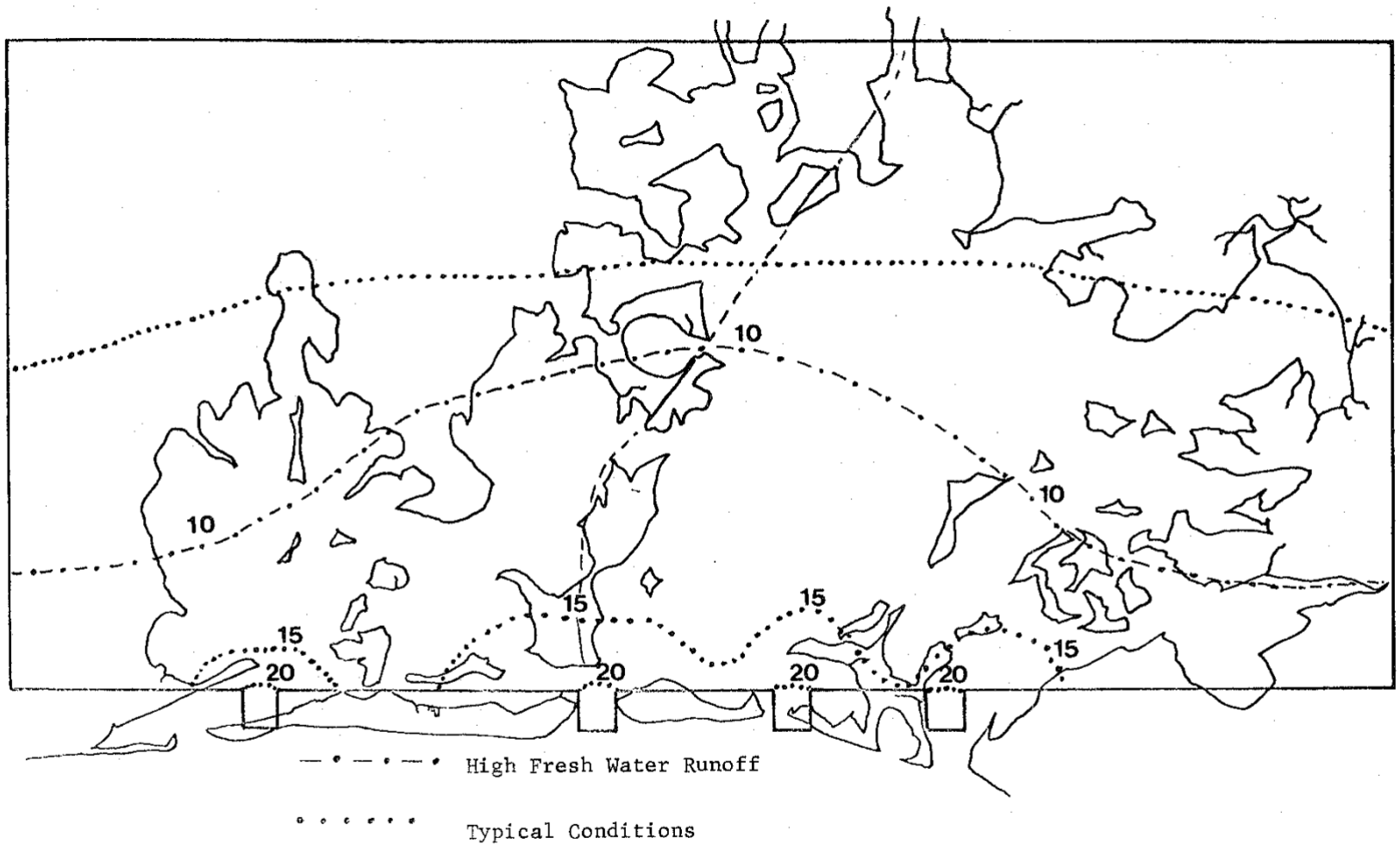

Figure 5.25. Comparison of High Fresh Water Runoff Isohalines with Typical Conditions Isohalines. Six hours after low tide. (Salinity is in 0/00.)

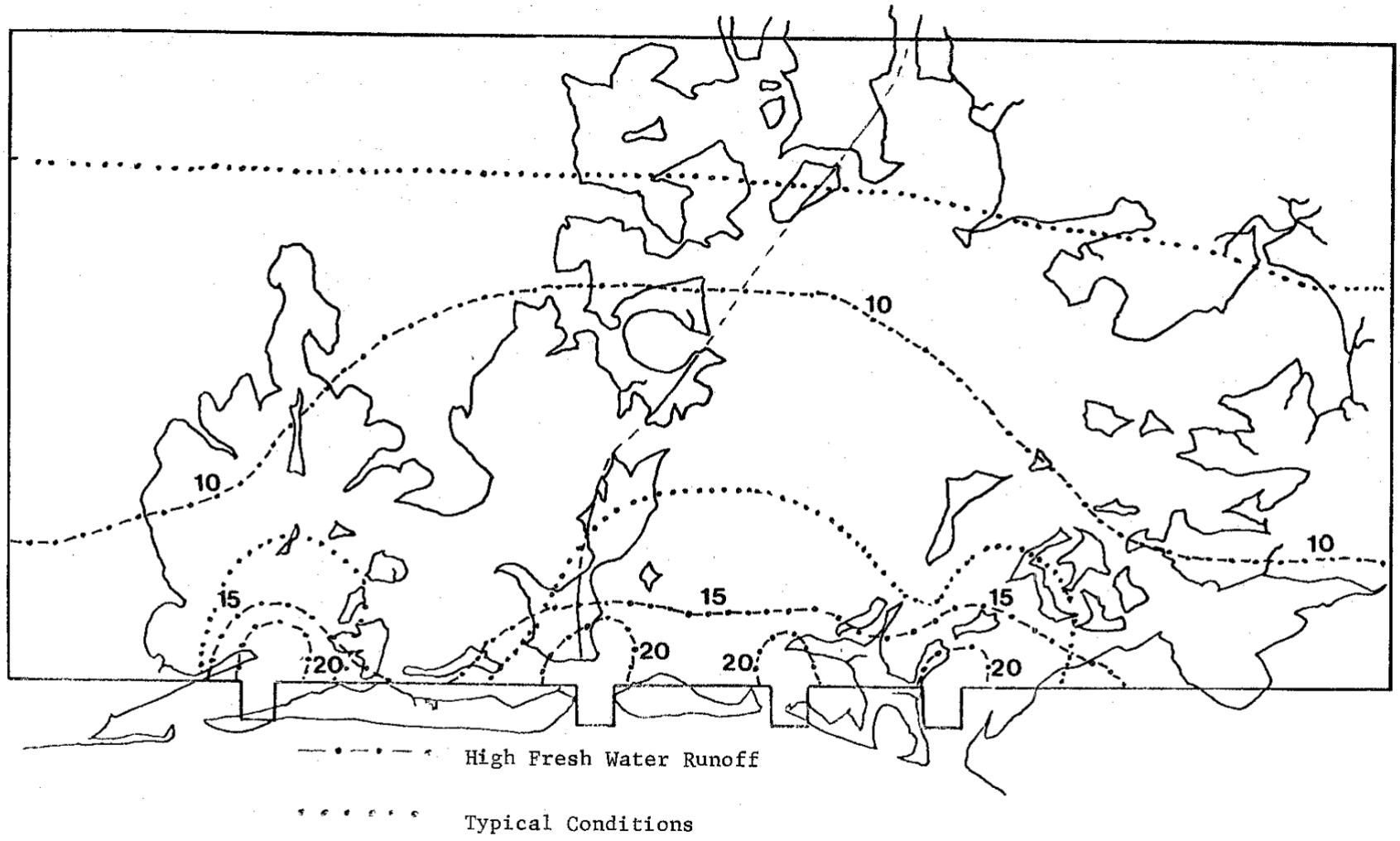

Figure 5.26. Comparison of High Fresh Water Runoff Isohalines with Typical Conditions Isohalines. Nine hours after low tide. (Salinity is in 0/00.)

Drop in Gulf Salinity Due to Mississippi River Water

Occasionally, the meandering waters of the Mississippi River sweep in front of Barataria Bay and cause the Gulf salinity to decrease markedly. A seemingly impossible condition appears in the bay; salinity is highest at a point inside the bay and decreases towards the Gulf. The case run was such that salinity was dropped to 10o/oo at high tide. Although this phenomena has been reported in the literature Gagliano, et al (Ref. 5-8), no data is available on the range of salinity drop due to this phenomena. This phenomena is rare, and it may appear once a year. However, it does not persist for more than about a two day period.

Results of this run are compared to the typical conditions at one hour after high tide in Figures 5.27 to 5.28., and then three hours after high tide in Figure 5.29. As can be seen in Figures 5,28 and 5.29, the sudden drop of Gulf salinity creates conditions that are unusual. Pockets of high salinity are created in front of the passes, a condition not encountered under any other circumstances. This same phenomena that was reported by Gagliana (Ref. 5.8) for a situation in which the Gulf salinity dropped from 28o/oo to 20o/oo. High salinity pockets, like the ones shown in Figure 5.28 and 5.29, were observed inside Barataria Bay.

Cold Front Passage

Cold fronts are typical weather phenomena in Barataria Bay in winter and early spring. The modeling of these conditions is of interest as the commercially important species, mainly shrimp, are highly susceptible to sudden temperature changes. A severe cold front at the time of juvenile shrimp migration into the estuary can have serious effects on the shrimping season (Ref. 5.9). A cold front passing through the Barataria Bay area was modeled by creating cloudy conditions followed by clear skies, a drop in ambient temperature of 20°F and a drop 8°F in the wet bulb temperature for a period of 12 hours. The front moved through the area at 10:00 A.M.

Results are shown for a shallow point (water depth of two feet), and a deep point (water depth of six feet) in Figure 5.30. Typical conditions over a two day period are compared to conditions for the cold front passage in Figure 5.30 for a shallow point and in Figure 5.31 for a deep point- The passage of the cold front has a much more pronounced effect in a shallow point than in a deep point. The temperature in a shallow point drops 10°F from typical conditions, the temperature at the deeper point drops only 3°F.

Tidal Wave Effects

The Barataria Bay area is subjected to hurricanes, and they can have devastating effects on the regions, especially the biology of the estuary. The ability to predict hurricane effects on Barataria Bay is of outmost Importance. The conditions simulated was the one originated by Hurricane Camille, August 17, 1969. For this hurricane tidal heights at the inlets of Barataria Bay were measured at twice the normal tidal range. Results were obtained for velocity profiles,

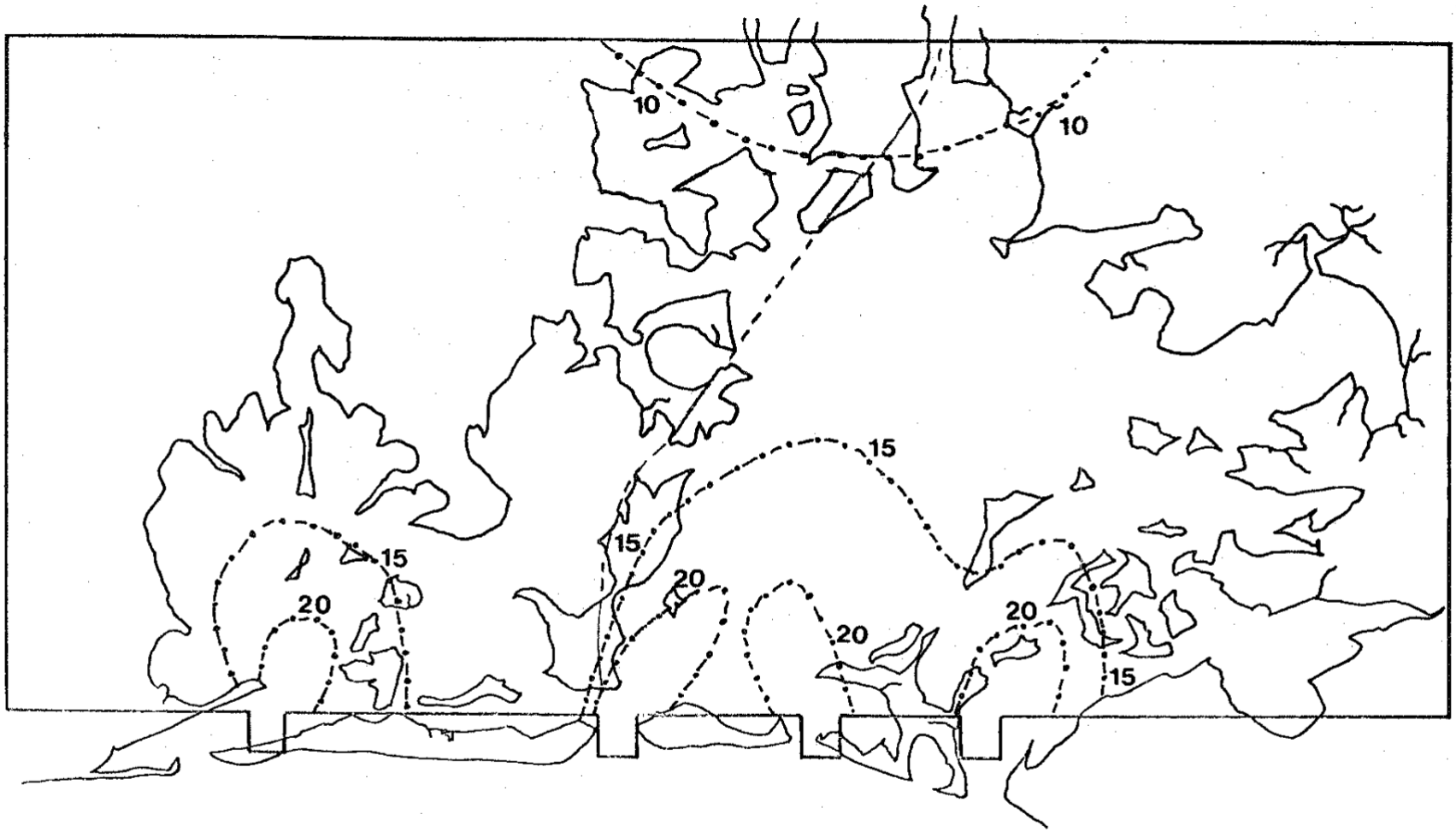

Figure 5.27. Isohalines at Typical Conditions. May 1st, 1970. One hour after high tide, 7:00 A.M. (Salinity is in 0/00.)

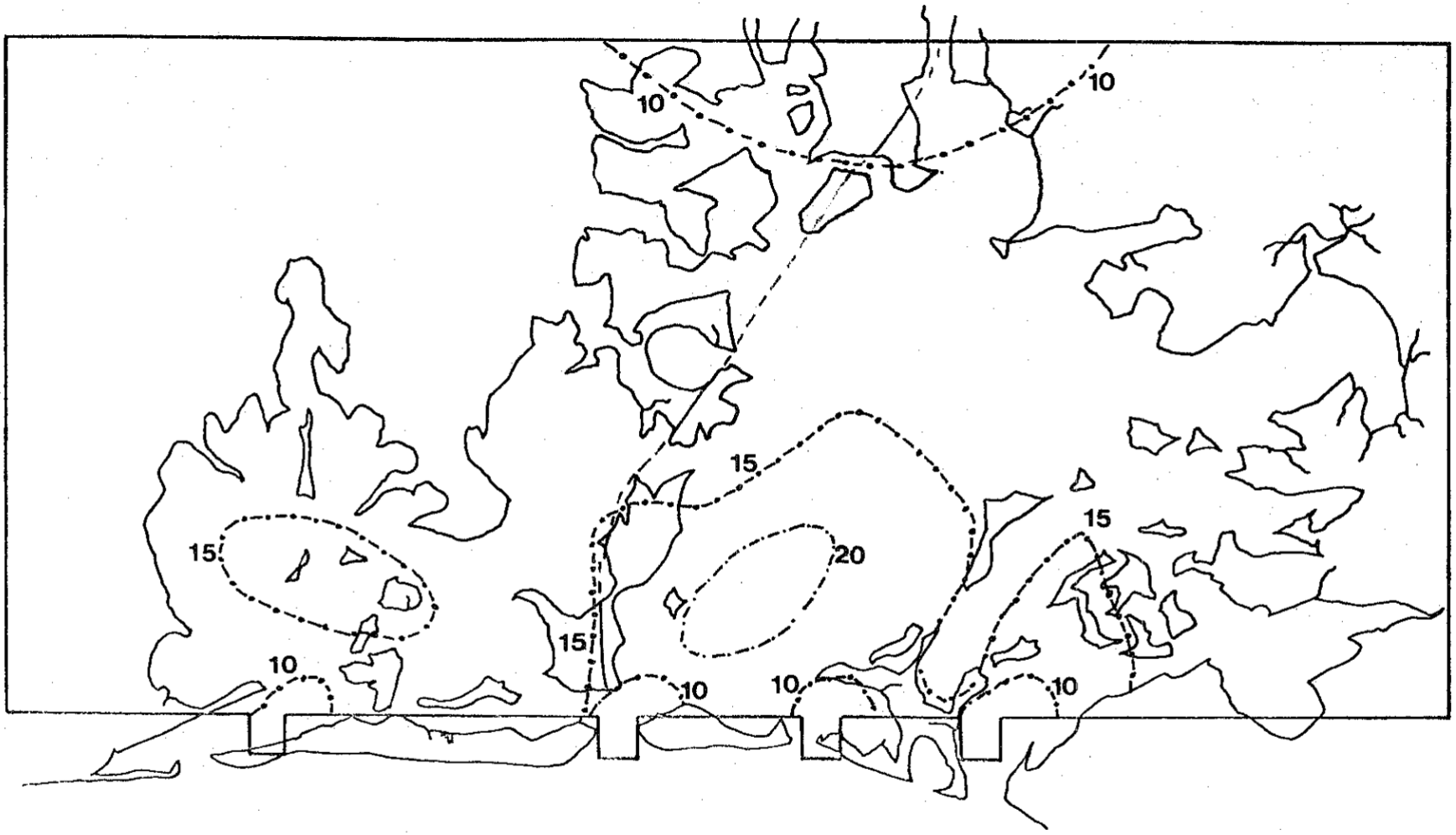

Figure 5.28. Isohalines at Dropping Gulf Salinity Due to Mississippi River Waters. One hour after high tide. (Salinity is is 0/00.)

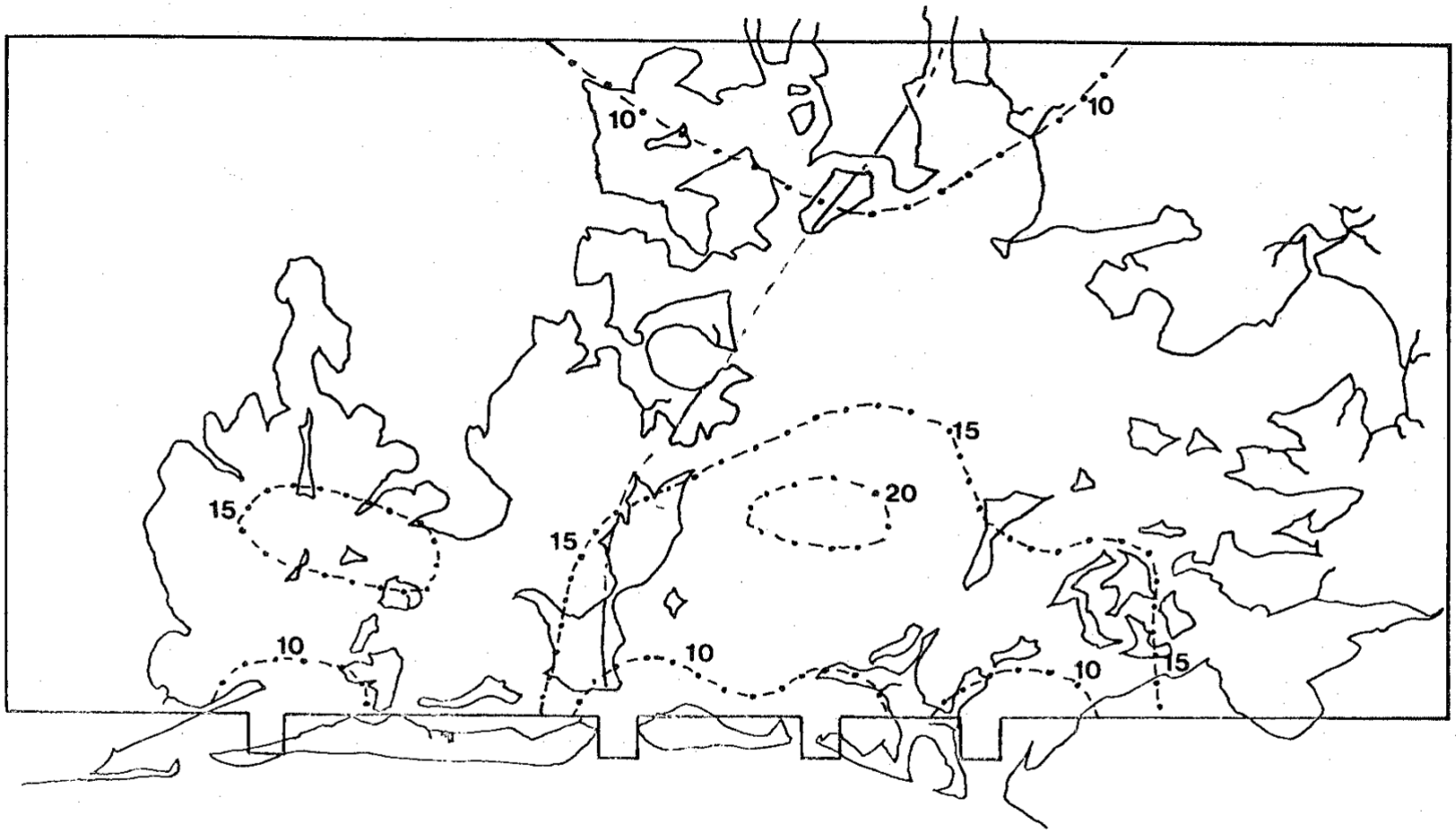

Figure 5.29. Isohalines at Dropping Gulf Salinity Due to Mississippi River Waters. Three hours after high tide. (Salinity is in 0/00.)

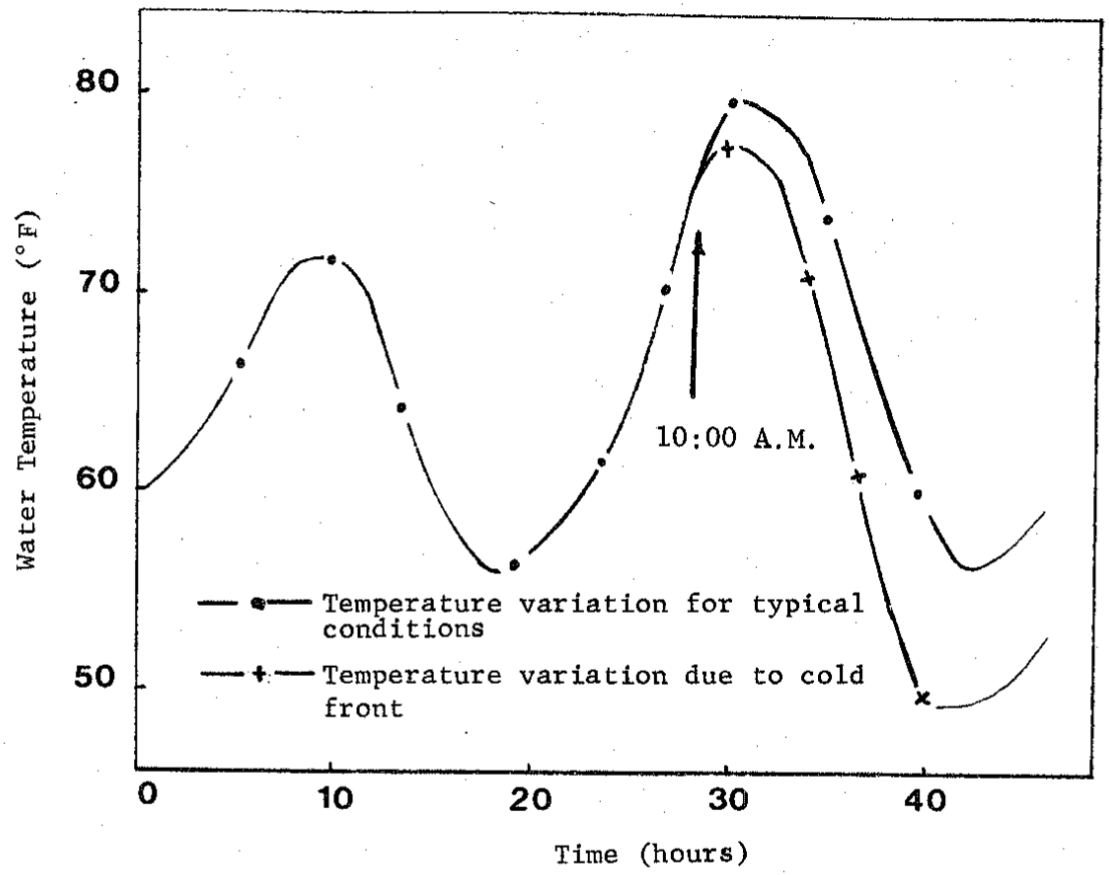

Figure 5.30. Temperature Variation at a Point of Water Depth of Two Feet in Barataria Bay Showing a Cold Front Passage at 30 hours, May 1st and 2nd, 1970. (Starting May 1st, 6:00 A.M.)

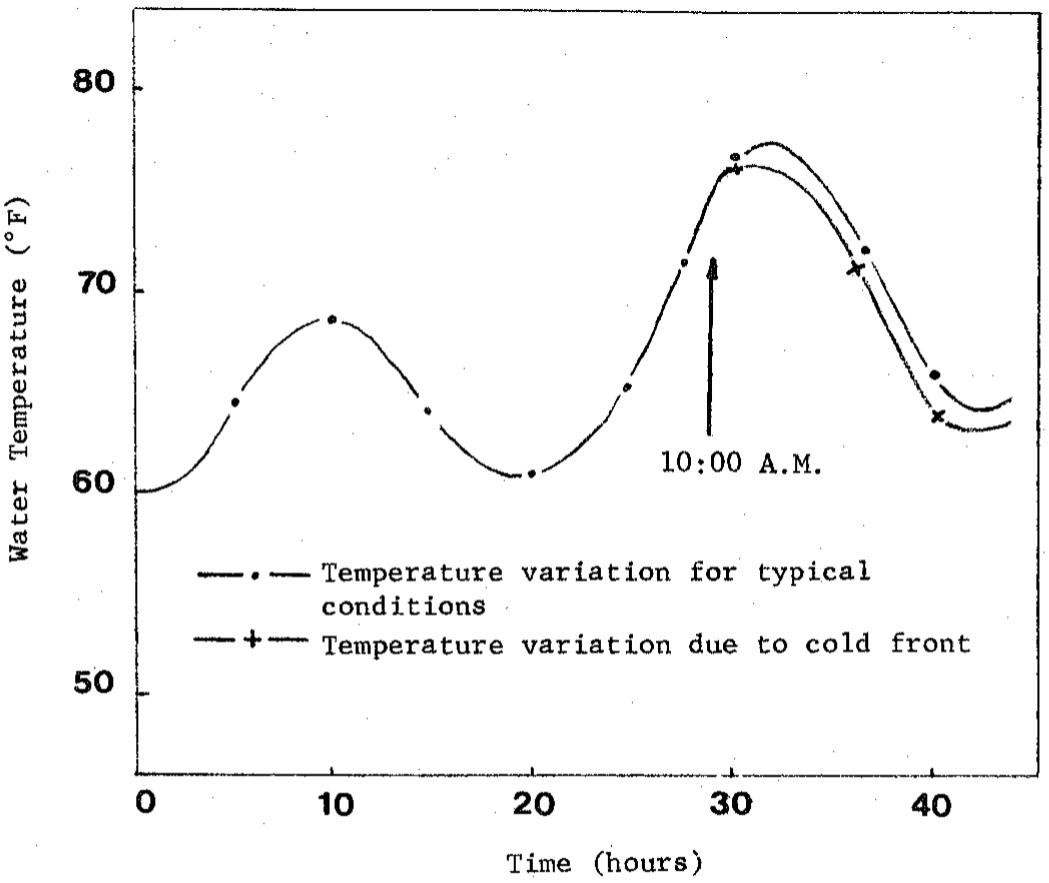

Figure 5.31. Temperature Variation at a Point of Water Depth of Six Feet in Barataria Bay Showing a Cold Front Passage at 30 hours, May 1st and 2nd, 1970. (Starting May 1st, 6:00 A.M.).

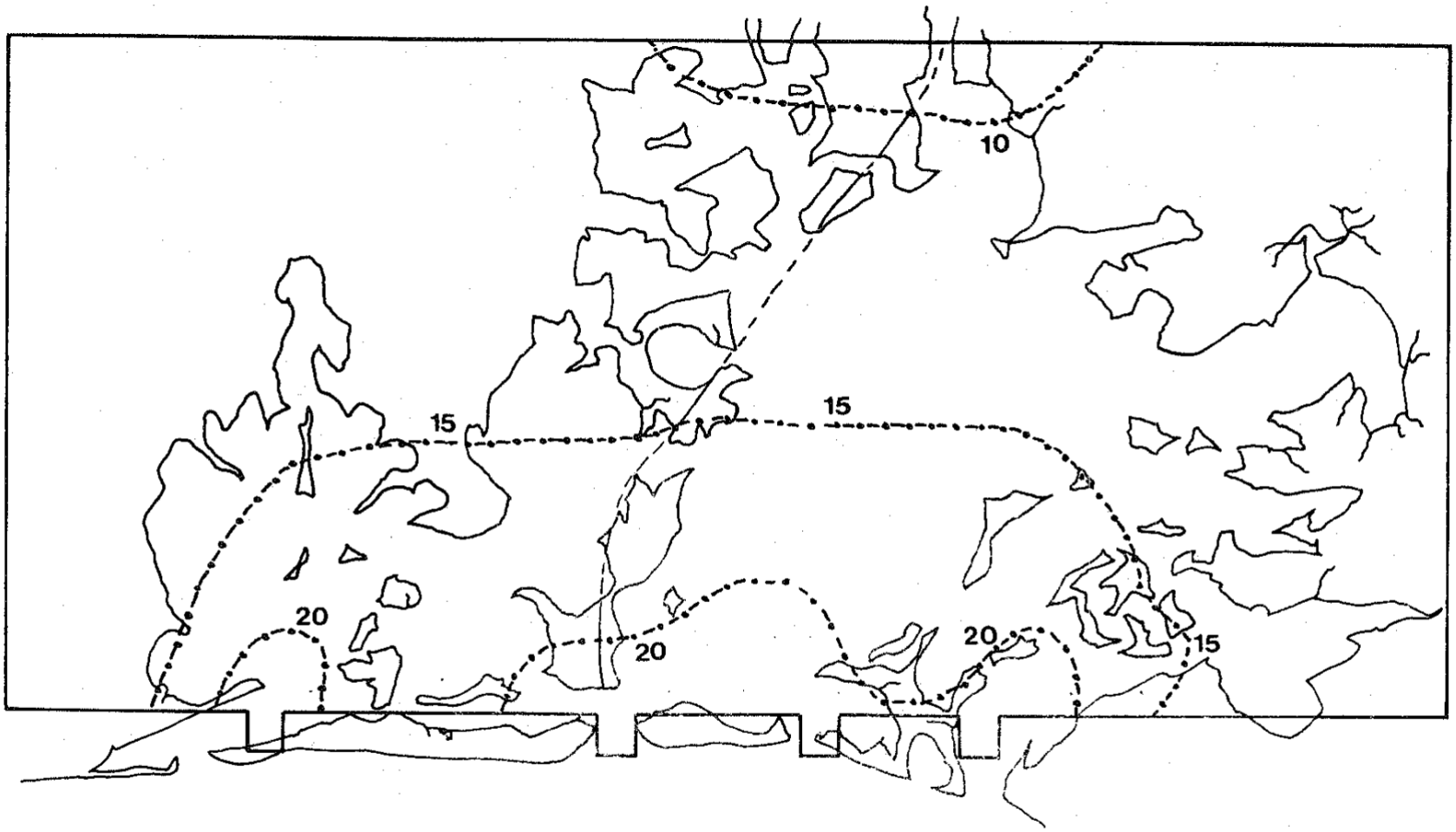

Figure 5.32. Tidal Wave Effects Isohalines. Two hours after low tide. (Salinity is in 0/00.)

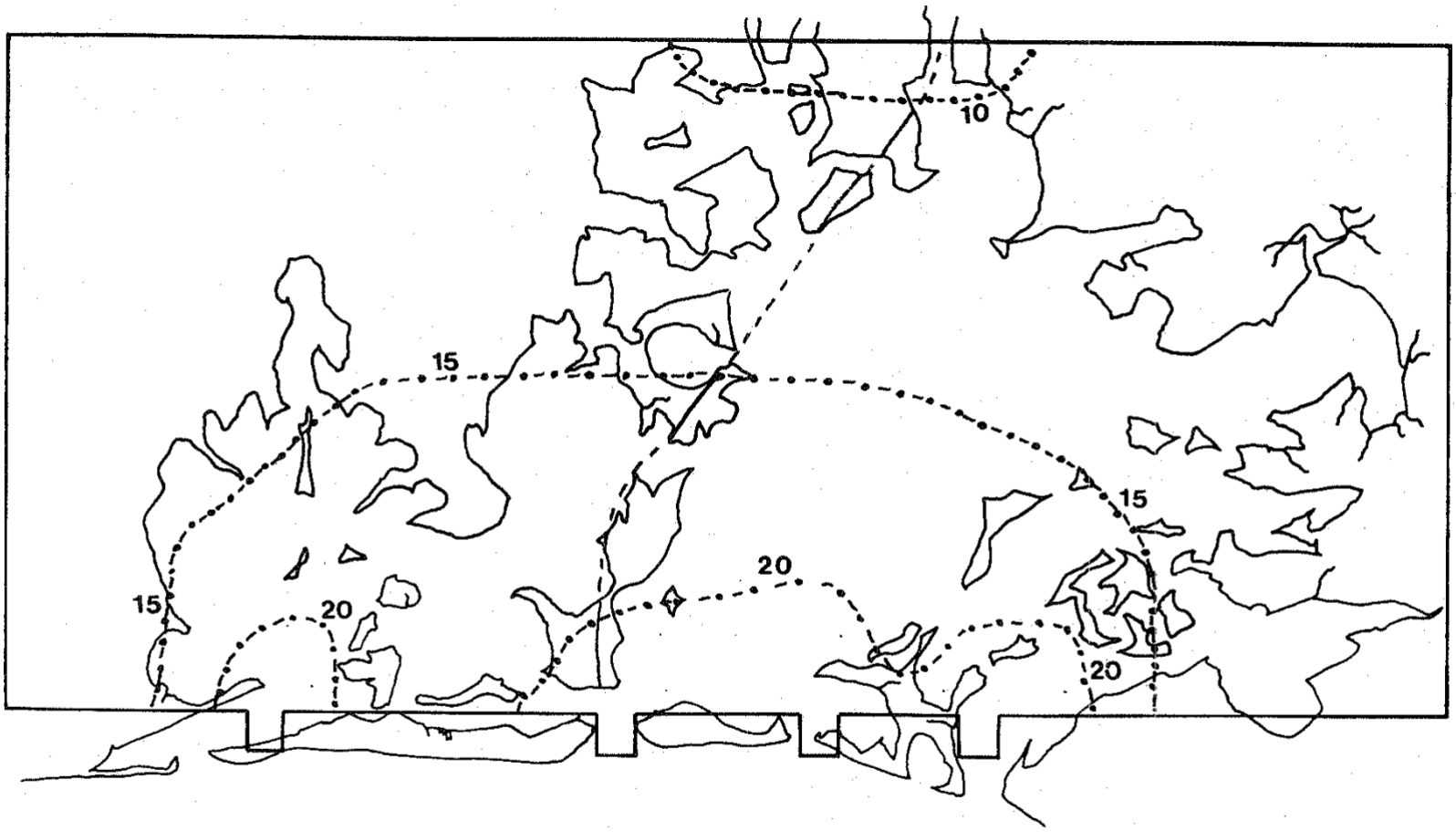

Figure 5.33. Tidal Wave Effects Isohalines. Four hours after low tide. (Salinity is in 0/00.)

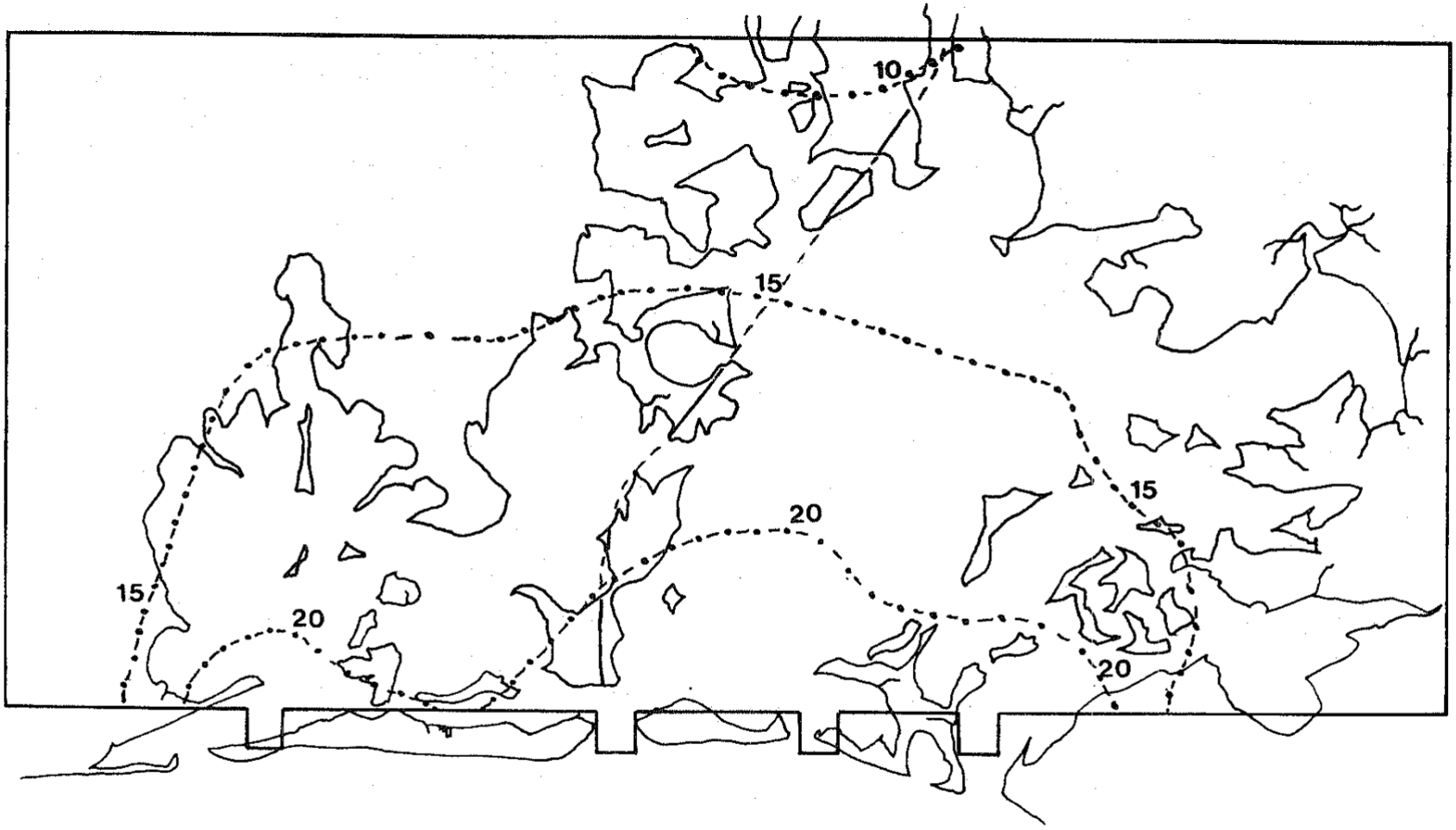

Figure 5.34. Tidal Wave Effects Isohalines. Six hours after low tide. (Salinity is in 0/00.)

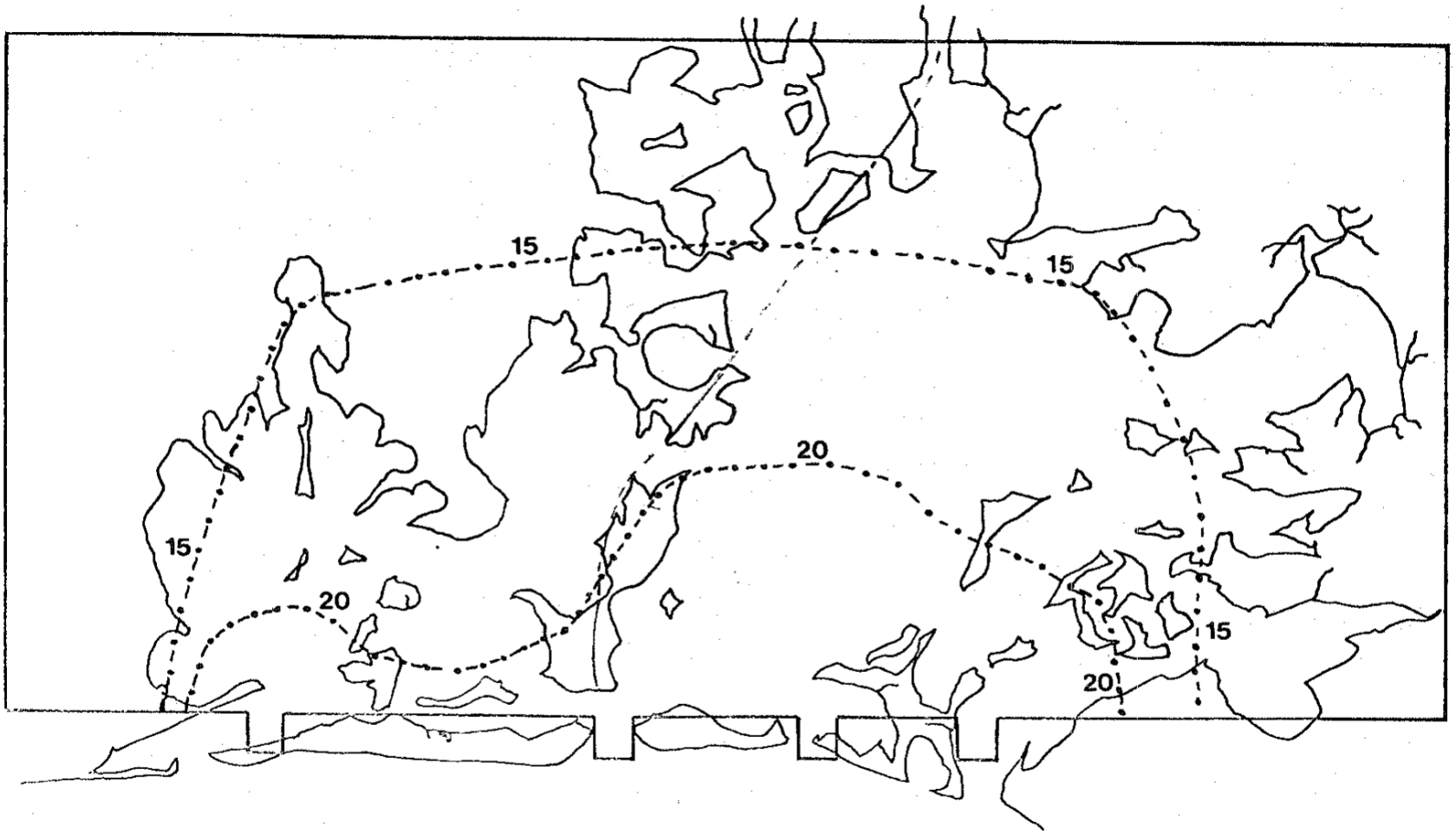

Figure 5.35. Tidal Wave Effects Isohalines. Eight hours after low tide. (Salinity is in 0/00.)

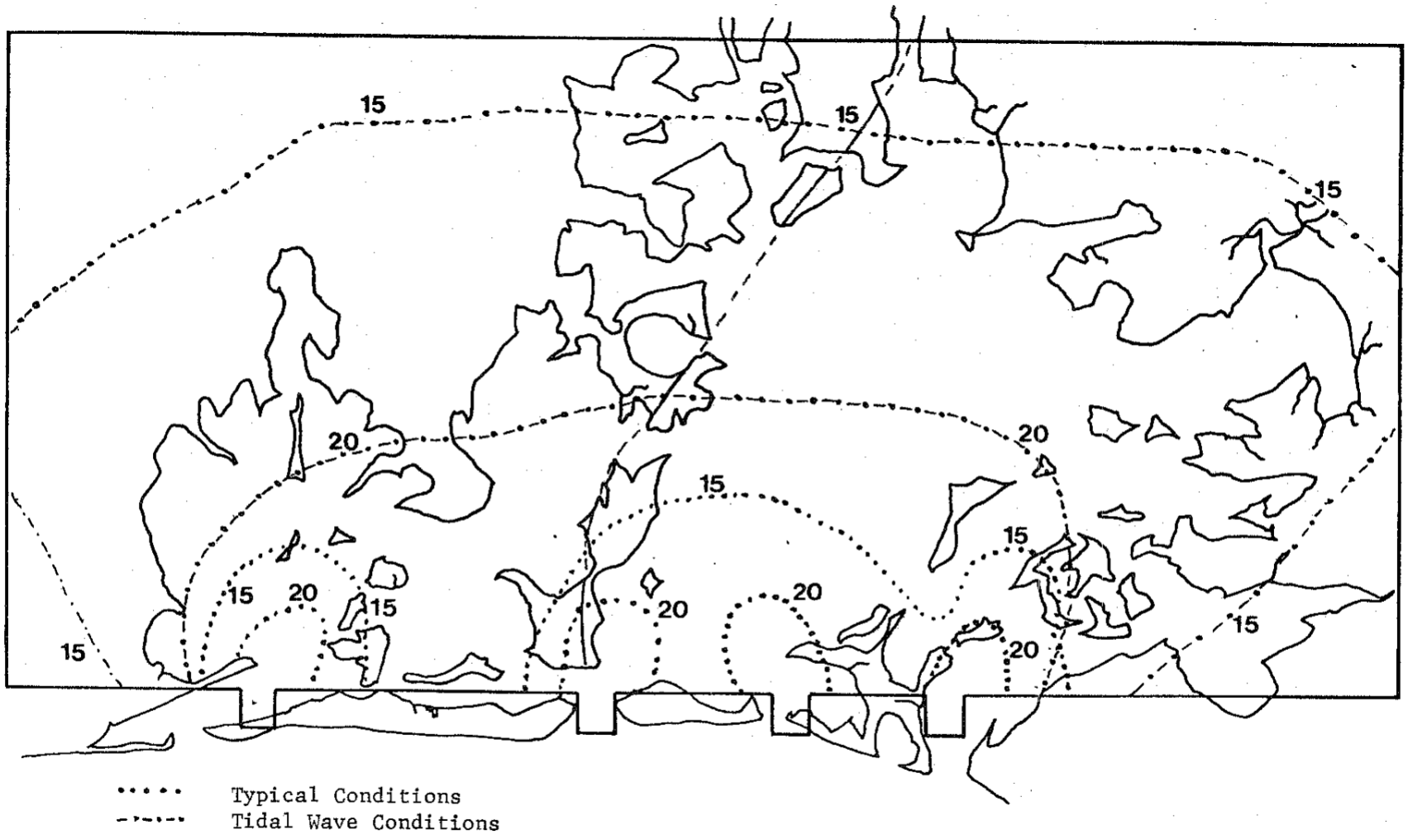

Figure 5.36. Tidal Wave Effects Isohalines. Compared to Typical Conditions Isohalines. Ten hours after low tide. (Salinity is in 0/00.)

salinity, and temperature distributions for the passage of the hurricane. Salinity effects are shown in Figures 5-32 to'5.36. The 15o/oo was pushed 8 miles inland, 6 miles more than in typical conditions. This can be seen in Figure 5-36. Temperatures in the bay waters were not greatly changed since the Gulf temperature and bay temperature are not drastically different.

Circulation patterns were similar to the circulation patterns found in normal conditions. However, velocities were found to be twice the velocities of typical conditions. Similarly, tidal heights doubled the normal tidal variation. Following this tidal wave, normal conditions were used for two tidal cycles. From these runs it could be seen that the bay would return to standard conditions in five tidal cycles.

Results obtained for this simulation could not be compared to some data which was available at Airplane Lake because the other data which was on record was not sufficient to furnish all of the necessary initial and boundary conditions to the model Hurricane Camille.

Comparison of Results with Field Data and Other Investigators Comparison with Field Data

In the validation of hydrodynamic models of this type, comparisons are usually made with tidal gauges located throughout the estuary. With this type of data, it is not necessary to measure the corresponding velocities since they are related to the tidal heights by the continuity equation. The tidal height field data suitable for comparison with the Barataria Bay Model were tidal records at Airplane Lake kept by the LSU Sea Grant Program (Ref. 5.3). A comparison of model results and field data is shown in Figure 5.37 for January 20 and 21, 1970 at Airplane Lake. The simulation accurately predicted the field data, and the maximum deviation at any one time was 15%. The reason for the higher amplitude of the field data is due to canals that lead directly from the main body of the bay to the Airplane Lake location. Tidal variations at Barataria Pass from the records of the Louisiana Wildlife and Fisheries Commission (Ref. 5.1) were used as the boundary conditions for the Hydrodynamic Model to make these predictions at Airplane Lake.

The Airplane Lake location was the only one with data available for model verification. More points throughout the bay would have been highly desirable, but the cost for additional instruments was prohibitive. A complete field data gathering program, as the one used by Leendertse (Ref. 5.5) in Jamaica Bay, can cost upwards of one million dollars.

An important point to note is that the Airplane Lake gauge is located within the marsh and not in the open waters of the bay. Thus, it was possible to show that the Hydrodynamic Model can accurately predict tidal variations in marsh areas connected to the open bay. This is the first time that tidal variations and local average water velocities have been modeled in coastal marshes. The closest work to this was reported by Leendertse (Ref. 2.12) in the modeling of tidal flats in Jamaica Bay. It can be said that the Hydrodynamic Model accurately represents the flow in the marsh, and it also represents the flow in the open bay as well. This conclusion is

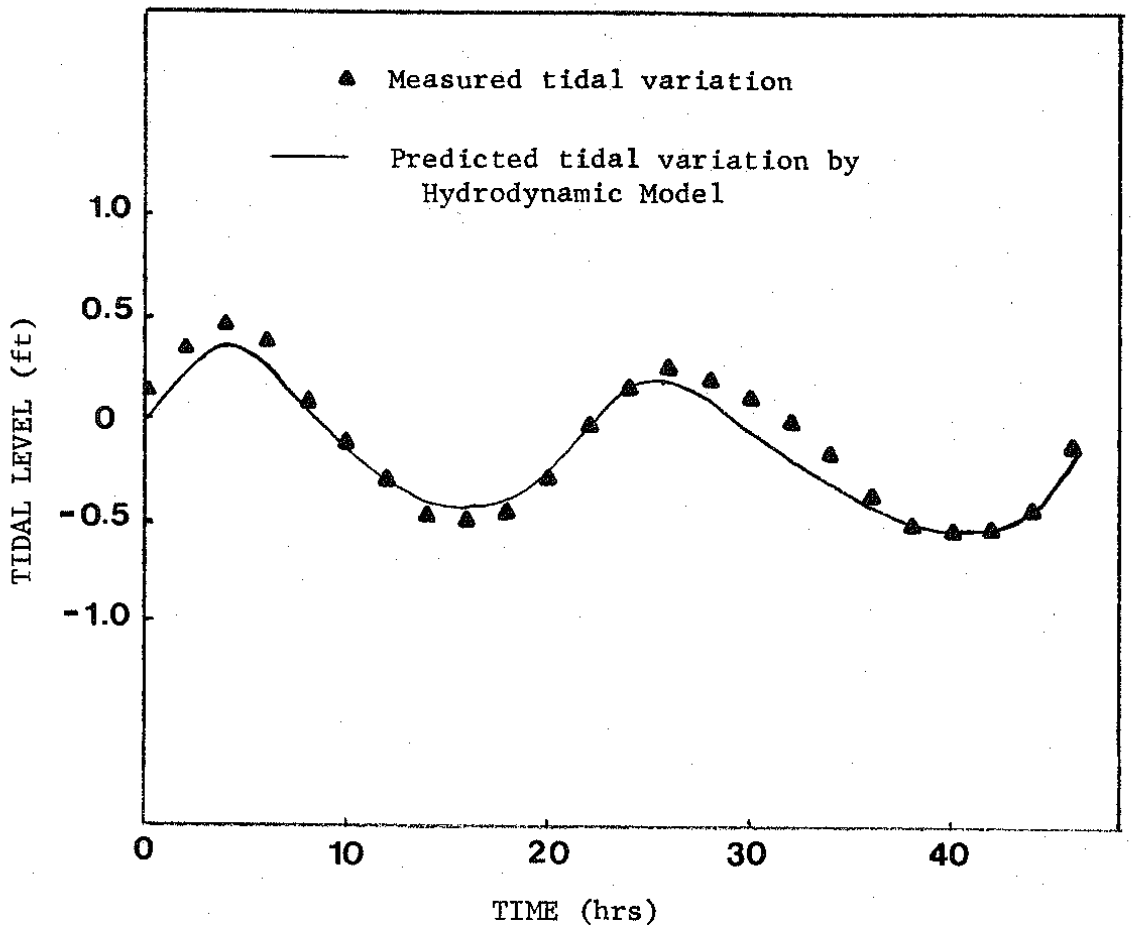

Figure 5.37. Computer Simulation of Tides of January 20 and 21, 1970, compared with Field Data.

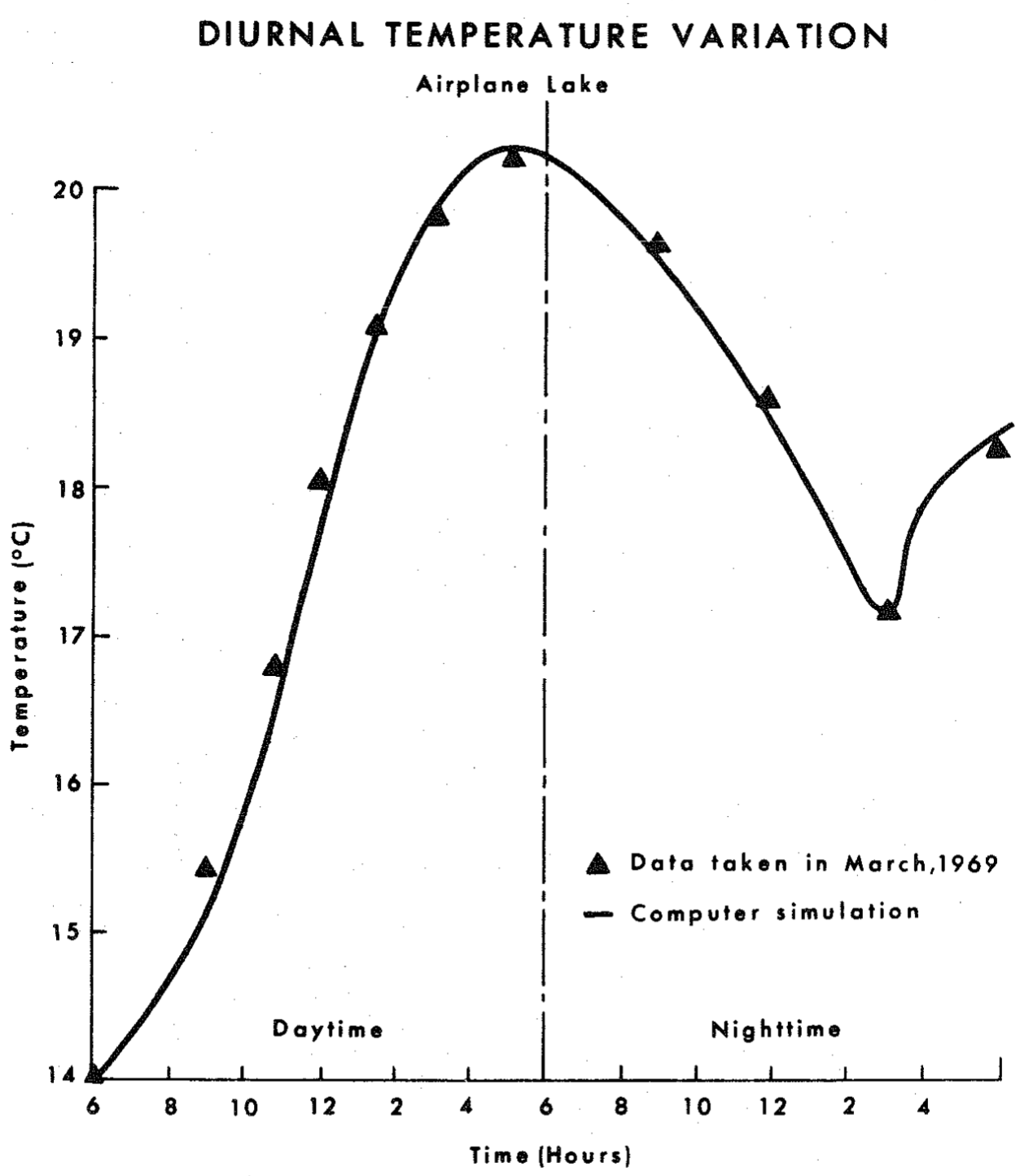

Figure 5.38. Computer Simulation of Temperature Variation at Airplane Lake, March 19, 1969. Comparison with Field Data.

based on the fact that the Hydrodynamic Model is the same model that was employed to model Jamaica Bay (Ref. 2.12) and Galveston Bay (Ref. 2.14).

In validation of energy transport models, comparisons are usually made between field temperature data and model results. Temperature variation data were taken by Smith (Ref.5.10) at the Airplane Lake location the day of March 19, 1969. A comparison of the model and this data is shown in Figure 5.38. Referring to the figure, the model described the data within the accuracy of the measurements.

In validation of salinity transport models, comparisons are usually made of isohalines measured in the field with model results. For Barataria Bay, the only available isohaline data are monthly average isohalines reported by Gagliano (Reg. 5.8). Using this data, a comparison was developed for March 1961. This data is compared to a computed daily average in Figures 5.39 and 5.40. Also shown in these figures are the high and low tide, l0o/oo isohaline lines for comparison. The disadvantages of the field data is that it only covers the open bay waters located directly behind Barataria Pass, and does not include the rest of the bay system.

In conclusion, the Hydrodynamic Model, the Energy Transport Model and the Materials Transport Model accurately predict tidal variations, velocity profiles, and temperature and salinity distributions in the marsh and in the open bay. This is based on comparisons with the limited available data for the system. Further substantiation is given in the next section.

Comparison with Other Investigators

Of the hydrodynamic models reported in the literature, there are two that represent bays that have hydrodynamic characteristics close to that of Barataria Bay. These two are the Galveston Bay model reported by Masch (Ref. 5.11) and the Jamaica Bay model reported by Leendertse (Ref. 5.5). Velocities calculated by these two models are compared to the Barataria Bay model results in Table 5.3. As can be seen, the velocity ranges are very close among the models presented. Although it was not justified to repeat the calculations for these bays, this comparison serves to show that essentially the same results would be obtained.

An energy transport model was presented by TRACOR for Galveston Bay (Ref. 5.12). Input data for a no convection case presented for Galveston Bay was used with the Barataria Bay model. The results of this simulation are shown in Figure 5.41. The results obtained with the Barataria Bay Model were identical to the graphical results shown by TRACOR.

No possible comparisons can be made for the salinity results obtained with the Barataria Bay model and models reported in the literature by Leendertse (Ref. 5.5) and Masch (Ref.5.11). Reasons for these are; differences in bathymetry and input conditions are so great that any comparison is not possible without actually simulating the bays themselves. However, it can be stated that results predicted by the models behaved the same in a qualitative fashion.

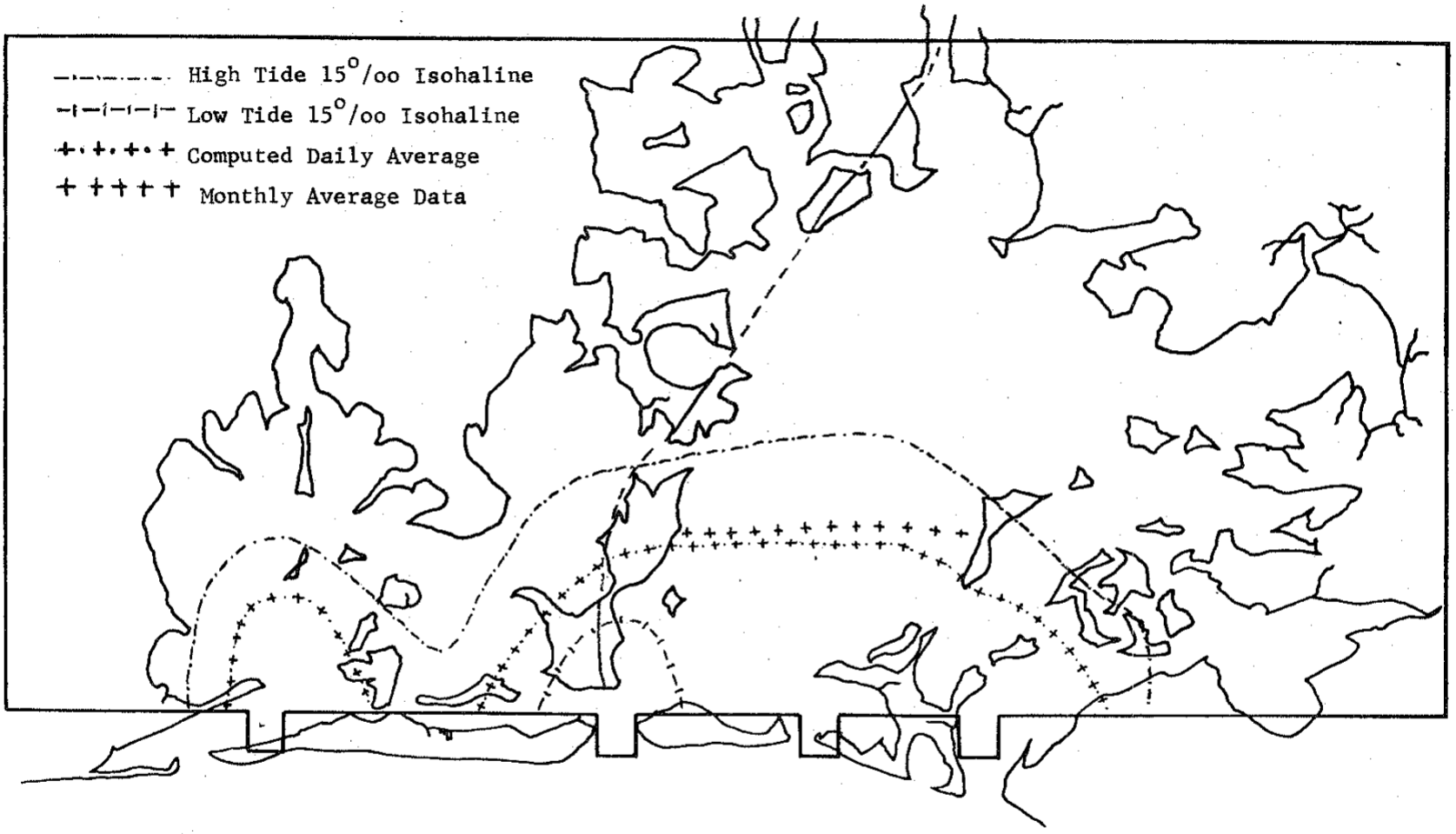

Figure 5.39. Comparison of Daily Computed Average and Monthly Average Data for the 15 °/oo Isohaline in Barataria Bay at Similar Conditions.

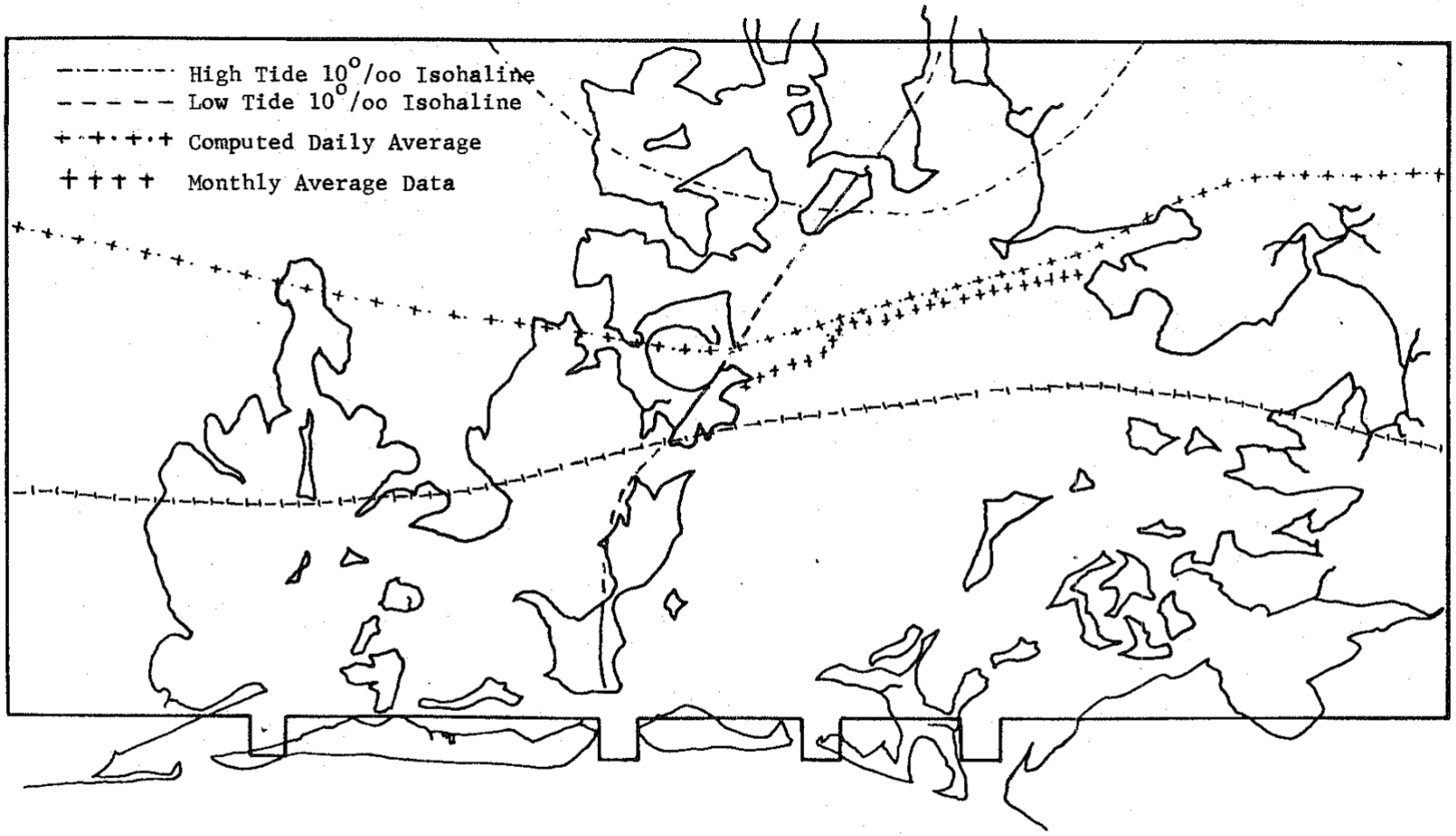

Figure 5.40. Comparison of Daily Computed Average and Monthly Average Data for the 10 °/oo Isohaline in Barataria Bay at Similar Conditions.

TABLE 5.3

RANGE OF VELOCITIES (FEET/SECOND) CALCULATED BY DIFFERENT MODELS IN SIMILAR ESTUARINE BAYS

Model	Region		
	Entrances	Middle Region	Boundaries
Jamaica Bay Model (Ref. 5.5)	1.0 - 3.0	0.5 - 1.0	0 - 0.5
Galveston Bay Model (Ref. 5.9)	1.0 - 4.0	0.4 - 1.0	0 - 0.4
Barataria Bay Model	1.0 - 4.0	0.3 - 0.8	0 - 0.3

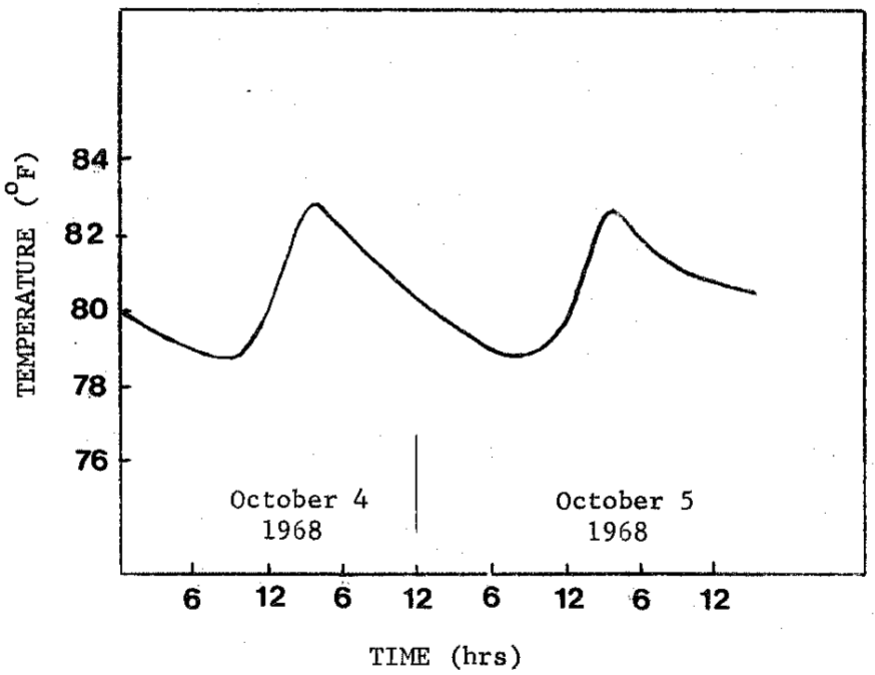

Figure 5.41. Galveston Bay Simulation for Temperature, October 4 and 5, 1968, Using Data Given by TRACOR (Ref. 5.11).

From the above considerations it can be stated that the Barataria Bay model is comparable in behavior to other similar models presented in the literature.

Some Results for the Time Averaged Equation of Motion

Time averaged equations are obtained by integrating the transport equations with respect to time over a tidal cycle. These time averaged equations are derived in Appendix C. In this form the equations could be integrated with time steps of a tidal cycle and permit computations of a length that are not feasible at the present. Time steps of a tidal cycle would allow modeling of long periods of time such as one year or longer. Time-averaging creates extra terms in the equations, and these terms must be modeled if they are of importance. To assess the importance of the terms generated by time-averaging, the terms of the time averaged x-component of the equation of motion,

$$\frac{\partial \bar{U}}{\partial t} + \bar{U}\frac{\partial \bar{U}}{\partial x} + \bar{V}\frac{\partial \bar{U}}{\partial y} - F\bar{V} + g\frac{\partial \bar{L}}{\partial x} + \bar{\tau}^{b}_{x} - \bar{\tau}^{s}_{x} = - \int_{o}^{t} \left[U' \frac{\partial U'}{\partial x} + V' \frac{\partial U'}{\partial y} \right] dt \qquad \text{(C-46)}$$

were evaluated over a tidal cycle. For convenience the results were calculated neglecting Coriolis force, which is known to be small, and the surface stress which corresponds to a no wind condition. As shown in Table 5.4, the integral term resulting from the time averaging is of the same order of magnitude as the largest term in the time averaged x-component of the equation of motion. This term is the slope of the water surface term. As expected, the convective forms are relatively small.

The modeling of the terms resulting from the time-averaging and the use of a time averaged model promises to be an area for fruitful research because of the savings in computational time for solutions which require long time periods.

Numerical Considerations in the Computer Solution

Of the numerical techniques used, the only ones that require that stability criteria be met are the explicit solutions of the energy and species transport models. These stability criteria are presented in the literature by TRACOR (Ref. 5.4) and Masch (Ref. 5.10)and were shown in Chapter IV as Equations 4.75, 4.76, and 4.77. These criteria were met for the results shown for Barataria Bay.

TABLE 5.4

MAGNITUDE OF THE TERMS IN THE TIME-AVERAGED
X-COMPONENT OF THE EQUATION OF MOTION OVER A TIDAL CYCLE
(ft/hr^2)

$\frac{\partial \bar{U}}{\partial t}$	+	$\bar{U}\frac{\partial \bar{U}}{\partial x}$	+	$\bar{V}\frac{\partial \bar{U}}{\partial y}$	+	$g\frac{\partial \bar{L}}{\partial x}$	+	$\bar{\tau}_x^b$	=	$\int_o^t U'\frac{\partial U'}{\partial x}dt - \int_o^t V'\frac{\partial U'}{\partial y}dt$
0	-	0.110	-	0.412	+	65.49	+	0.343	=	65.31

Leendertse (Ref. 2.9) presents a study of the hydrodynamic model used here. In this study, a great deal of effort was dedicated to the proof of stability and convergence of the numerical techniques used. The same technique used for the Hydrodynamic Model was used for the Species and Energy Transport Models. This technique is known as the Alternating Directions Implicit techniques (ADI) and it is referenced in the literature (Refs. 4.1 and 4.2) as being unconditionally stable. Also mentioned in the literature by Ames (Ref. 5.13) is the theorem that in a well posed problem, stability is the necessary and sufficient condition for convergence.

Two grid sizes were used to establish stability, convergence and accuracy. Results for tidal variation, temperature and salinity are compared for the two grids in Figures 5.42 to 5.44 for a representative point (located 7 miles inland from Quatre Bayou Pass). Results for both grid sizes used are close but not equal. This is explained by the fact that when using these two different grid sizes, (1300 yards and 1800 yards) in actuality two different systems were being modeled. This is because the bathymetry is not exactly the same in the two systems. The only way to exactly reproduce the bathymetry was to make the grid one half of the grid size in the numerical solutions. This was impossible to do due to computer storage limitations. In using the 1800 yards grid (smallest number of grid points over the system), more than one half of the computer's fast storage was used. If the grid size were to be halved, the computer storage requirements would have to be quadrupled, and this was impossible on the system available. Consequently, it was necessary to compromise, and the grid size of 1300 yards consumed 75% of the computers fast storage. Naturally, the smaller the grid size is, the larger is the number of grid points, and the better the resolution. However, large grid sizes have faster computational times. With the large grid size, a 24 hour tidal cycle could be computed with 18 minutes CPU time using a Fortran G compiler in the IBM 360/65. The smaller grid size used was found to take twice the time of the large grid size.

The main problem found during the computer solution was related to inaccuracies generated by the relatively large grid sizes used. These inaccuracies were most pronounced at the tidal passes. After several refinements it was found that implicit solution of the hydrodynamics and explicit solution of the energy and transport models worked best. This is to say, no instabilities were encountered. Use of the implicit scheme for the energy and transport models showed instabilities. Up to this time, the reason for these instabilities has not been found. The only place in the literature in which an implicit solution of the species equation has been reported is in the Jamaica Bay simulation by Leendertse (Ref. 5.5). Although results for this simulation are presented using his implicit scheme no details of the computer program were given for the species model. However, detailed explanation is given on the computer implementation of his hydrodynamic model (Ref. 2.9).

All the results reported in this chapter were obtained with the continuity and motion equations solved implicity and the energy and species equation solved explicitly using the 1800 yards grid size; with the exception of the velocity profiles shown, which were obtained with the 1300 yard grid size.

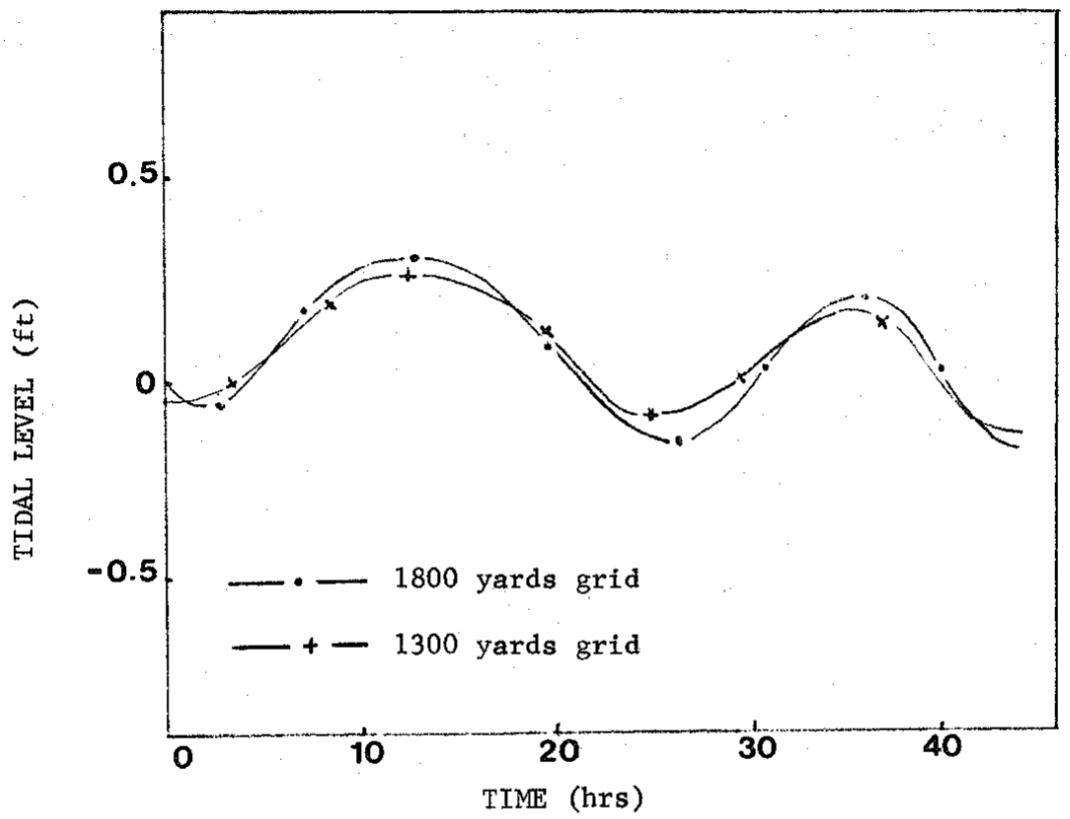

Figure 5.42. Comparison of Different Grid Sizes. Tidal Amplitude Variation. Point at Seven Miles Inland from Quatre Bayou Pass. May 1st and 2nd, 1970. (Starting May 1st, 6:00 A.M.).

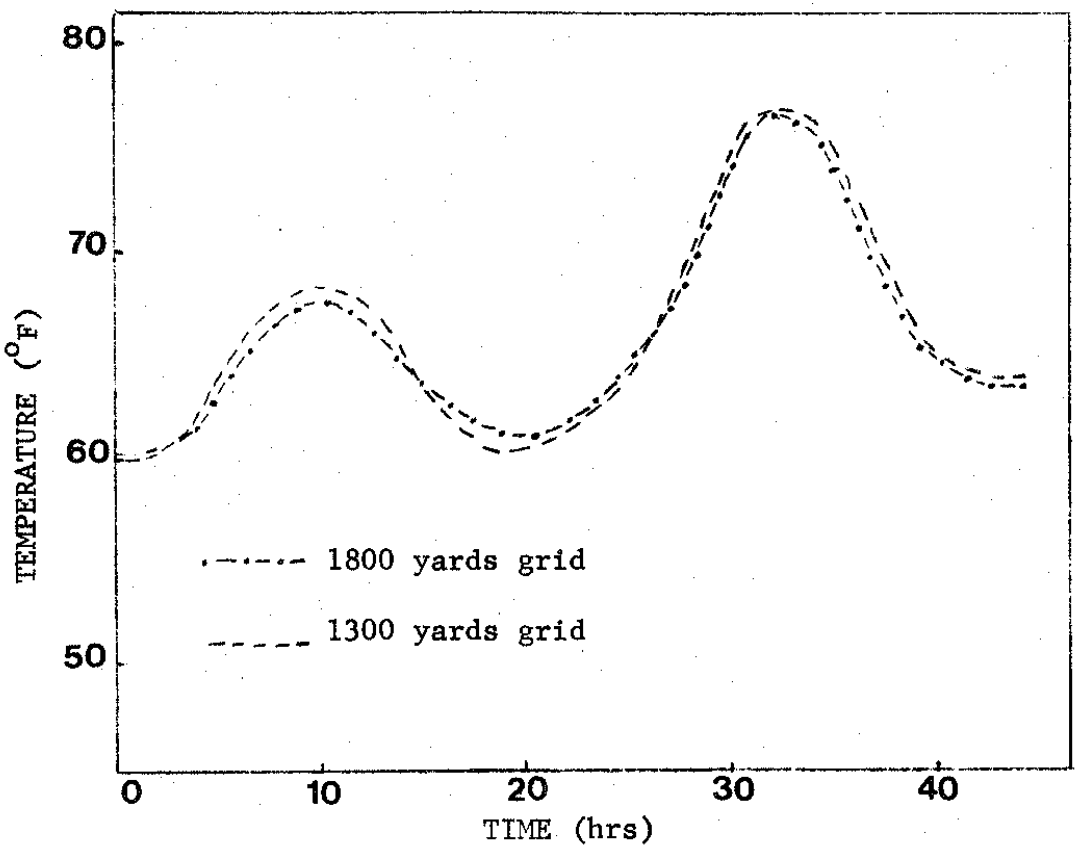

Figure 5.43. Comparison of Different Grid Sizes. Temperature Variation. Seven Miles Inland from Quatre Bayou Pass. May 1st. and 2nd, 1970. (Starting May 1st, 6:00 A.M.).

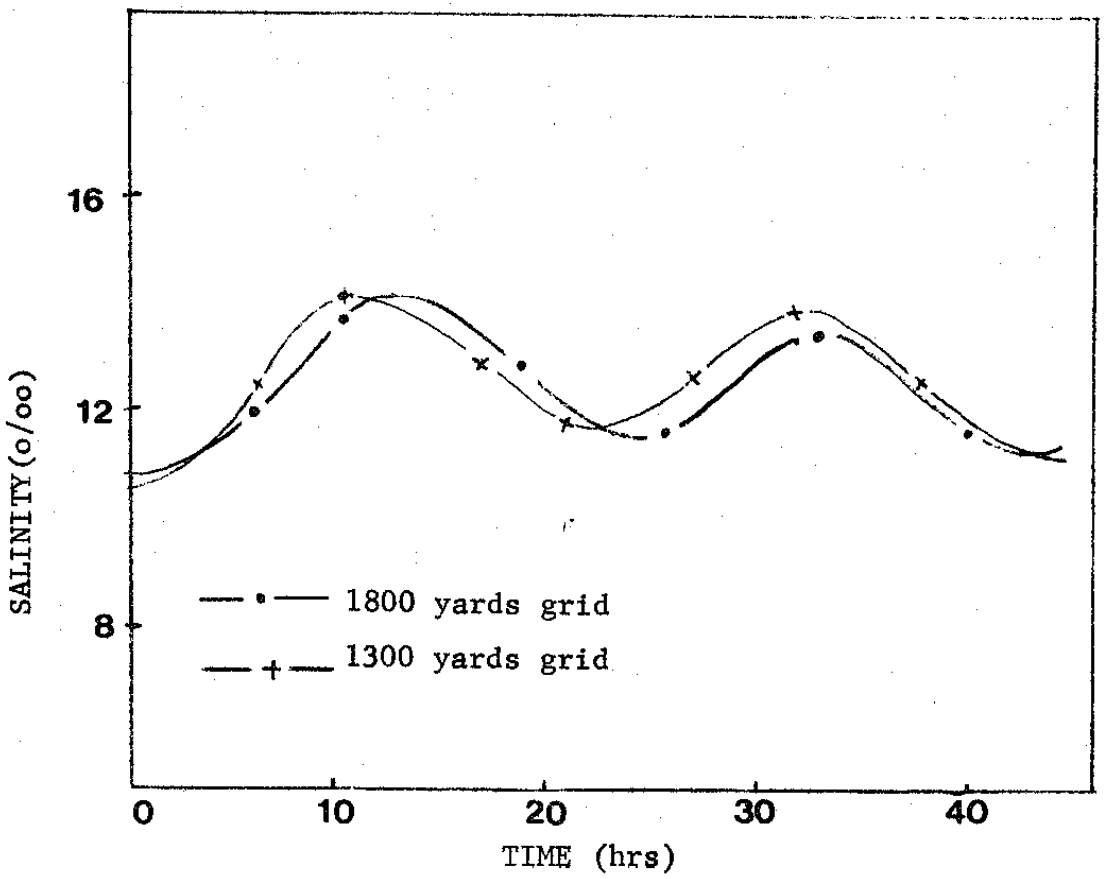

Figure 5.44. Comparison of Different Grid Sizes. Salinity Variation. Point at Seven Miles Inland from Quatre Bayou Pass. May 1st. and 2nd, 1970. (Starting May 1st, 6:00 A.M.)

REFERENCES

5.1 Barret, Barney, Louisiana Wildlife and Fisheries Comission Personal Communication (1970).

5.2 Gagliano, S. M., et al, "Hydrologic and Geologic Studies of Coastal Louisiana: Selected Environmental Parameters Coastal Louisiana, 1945, 1946, 1959-65". Report No. 10, Coastal Studies Institute, Louisiana State University, Baton Rouge, Louisiana (1970).

5.3 Data Management System, LSU Sea Grant Program, Baton Rouge, La.

5.4 Espey, W. H., et al, "Galveston Bay Study: Phase II", Technical Report T.D. 70-AU-1636-U, TRACOR, Austin, Texas, (1971), pp. 8-20 to 8-28.

5.5 Leendertse, J. J., and E. C. Gritton, "A Water- Quality Simulation Model for Well Mixed Estuaries and Coastal Seas: Vol. III, Jamaica Bay Simulation". R-709-NYC, The Rand Corporation, Santa Monica, California (1971) pp. 30-56.

5.6 Handbook of Chemistry and Physics, 49th Edition, The Chemical Rubber Co. (1968) p. F-4.7.

5.7 Tide Tables, High and Low Water Predictions, East Coast of North America and South America, U.S. Department of Commerce, 1970.

5.8 Gagliano, S.U., et al, "Hydrologic and Geologic Studies of Coastal Louisiana: Statistical Models of Salinity Distributions, Southeastern Louisiana Estuaries". Coastal Studies Institute, Louisiana State University, Baton Rouge, Louisiana (1971), p. 28. Barrett, Barney, Louisiana Wildlife and Fisheries Comission. Personal Communication (1970).

5.9 Ford, T. B. and L. S.,St Amant, l!Manageoent Guidelines for Predicting Brown Shrimp", Paneus Aztecus, Production in Louisiana", Proc. Gulf and Caribbean Fisheries Institute, 23 149-161 (197), p. 154.

5.10 Smith, W. G., Barataria Gazette, LSU Sea Grant Program, LSU, Baton Rouge, Louisiana (1969).

5.11 Masch, F. D., et al, "Influence of Tidal Inlets on Salinity and Related Phenomena in Estuaries". Technical Report HYD 16-7O01CRWR 49, Hydraulic Engineering Laboratory, the University of Texas at Austin, Texas, (1970), pp.97-100.

5.12 Espey, W.'H-, et al, "Galveston Bay Study: Phase II*, Technical Report TD 70-AU 163G-U, Tracor, Austin, Texas, (1971) pp. 9-45 to 9-50.

5.13 Ames, W. F., Numerical Methods for Partial Differential Equations, Barnes and Nobles, Inc. (1969) p. 62.

CHAPTER VI

CONCLUSIONS AND RECOMMENDATIONS

Conclusions

Based upon the results of this research the following conclusions are drawn:

1. The Hydrodynamic Model accurately predicted the dynamics of tidal variations and velocity profiles in the Barataria Bay system for marsh areas as well as open waters of the bay. Verification of the analysis was made by comparing with experimental data obtained in the bay and by comparing with results obtained by other investigators in similar bays.

2. The Energy Transport Model accurately predicted the time-varying temperature distributions in the Barataria Bay system for marsh areas as well as open waters of the bay. Verification of the analysis was made by comparing with experimental data obtained in the bay and by comparing with results obtained by other investigators in similar bays.

3. The Materials Transport Model accurately predicted the time-varying salinity distributions in the Barataria Bay system for marsh areas as well as open waters of the bay. Verification of the analysis was made using comparisons of computed daily-average salinity distributions with measured salinity distributions reported in the literature.

4. Results were reported for the dynamics of tidal variations, velocity profiles and temperature and salinity distributions for conditions encountered in May of a typical year (1970) to demonstrate the range of capability of the analyses and to provide a set of reference solutions.

5. Analysis of the effect of high fresh water runoff was studied with the model to simulate conditions encountered in a "wet year." Results were obtained that show the shift in salinity profiles due to the increased fresh-water flow into the bay system.

6. Analysis of the effect of a cold-front passage was studied with the models to simulate this type of environmental condition that is encountered in early spring and is detrimental to the commercially important species in the bay system. Results were reported that show the effect of the cold front on water temperature at typical water depths in the bay, and this can amount to a 10°F drop within several hours.

7. Analysis of the effect of a tidal surge as the results of a hurricane like Hurricane Camille was studied. Results were reported that show the shift in high salinity Gulf waters into the upper reaches of the bay and were compared with the typical salinity conditions.

8. For typical conditions the models reached a quasi-steady state in three to five tidal cycles. With this characteristic, results from daily cycles can be extrapolated for longer periods of time if the input conditions to the bay stay relatively constant.

9. The transport phenomena models were time averaged to obtain a set of equations that can be used to take time steps of one tidal cycle. Evaluating the terms of these time-averaged equations showed that the terms generated by time integration cannot be neglected. Therefore, these time-averaged terms have to be evaluated in some form if the time-averaged model is to be of use.

10. The computer programs of the models are in a form that can be readily used by engineers and scientists for studies of ecological design, e.g., salinity control for fisheries management. Users manuals are included with the program for ease in applying their application.

Recommendations

Based upon the above mentioned conclusions the following recommen¬ dations are made:

1. Research should continue in the area of time-averaged equations. The successful modeling of the terms generated by time-averaging will allow great savings in computational time for long term solutions.

2. Studies should be made of ways to reline the computations in the areas near the passes with care to keep the computer storage requirements to a minimum and permit the use of an implicit solution of the equations.

APPENDIX A

CLASSIFICATION OF THE ONE-DIMENSIONAL LONG WAVE EQUATIONS

A way to classify the one-dimensional long wave equations is to reduce them to a simple form by ignoring the advection of momentum, the Coriolis force, and the wind friction. Doing this, the one-dimensional long wave equations can be written as:

$$\frac{\partial L}{\partial t} + D \frac{\partial U}{\partial x} = R - Ev \qquad \text{(A-1)}$$

$$\frac{\partial U}{\partial t} + g \frac{\partial L}{\partial x} = -\tau_x^b / \rho \qquad \text{(A-2)}$$

According to Ames (Ref. A-l), a general first order system can be written as:

$$a_1 \frac{\partial U}{\partial x} + b_1 \frac{\partial U}{\partial y} + c_1 \frac{\partial V}{\partial x} + d_1 \frac{\partial V}{\partial y} = fn_1 \qquad \text{(A-3)}$$

$$a_2 \frac{\partial U}{\partial x} + b_2 \frac{\partial U}{\partial y} + c_2 \frac{\partial V}{\partial x} + d_2 \frac{\partial V}{\partial y} = fn_2 \qquad \text{(A-4)}$$

The discriminant of this system is:

$$\text{Discriminant} = (a_1 d_2 - a_2 d_1 + b_1 c_2 - b_2 c_1)^2 - 4(a_1 c_2 - a_2 c_1)(b_1 d_2 - b_2 d_1) \qquad \text{(A-5)}$$

and Eqs. (A-3) and (A-4) can be classified using the determinant of the system: if Eq. (A-5) is negative the system is classified as elliptic, if it is equal to zero, the system is parabolic, and if Eq. (A-5) is positive, the system is hyperbolic.

Eqs. (A-3) and (A-4) are identical to Eqs. (A-l) and (A-2) if:

$a_1 = D$ (A-6)

$b_1 = 0$ (A-7)

$c_1 = 0$ (A-8)

$d_1 = 1$ (A-9)

$fn_1 = R\text{-}Ev$ (A-10)

$a_2 = 0$ (A-11)

$b_2 = 1$ (A-12)

$c_2 = g$ (A-13)

$d_2 = 0$ (A-14)

$fn_2 = \frac{-\tau_x^b}{\rho}$ (A-15)

Substituting Eqs. (A-6) through (A-15) into Eq. (A-5) results in:

$$\text{Discriminant} = (D*0 - 0*1 - 0*g - 1*0)^2 - 4(D*g - 0*0)(0*0 - 1*1) \qquad \text{(A-16)}$$

or:

Discriminant = (0) - 4(D*g)(-l) (A-17)

Discriminant = 4Dg > 0 (A-18)

Therefore, the one-dimensional, long wave equations can be classified as hyperbolic.

REFERENCES

A-1 Ames, William F., Numerical Methods for Partial Differential Equations, Barns and Noble, Inc., New York, N.Y., (1969), pp. 5-7,

APPENDIX B

SOME EXPERIMENTAL MEASUREMENTS OF

TRANSPORT PHENOMENA IN THE BARATARIA BAY ESTUARY

Introduction

The purpose of this appendix is to present experimental measurements that were made in the Barataria Bay estuary. The objectives of these measurements were to establish special

functions and to verify the various assumptions and approximations that were made in the derivation and application of the model equations.

This appendix consists of three parts. The first part is concerned with hydrodynamic and bathymetric measurements, the second part deals with energy transport measurements, and the third part describes the salinity measurements.

Hydrodynamic and Bathymetric Measurements

The main objectives of these measurements were to evaluate the approximation of a uniform vertical velocity and to measure typical flow rates. These measurements were taken at several points in the Barataria Bay area, as shown in Fig, B-l. A number of measurements were taken at the passes, the connections of the bay with the ocean, and in the streams in the upper end of the bay where fresh water flows into the system.

Bathymetric data was needed for the passes. This data is shown in Figs. B-2, B-3, B-4, and B-5. Bathymetry data was taken with a Raytheon Depthfinder fathometer (See Table B-l). Experimental flow data are shown for Quatre Bayou Pass (Figs. B-6, B-7, B-8), Pass Abel (Figs. B-9, B-10, B-11), Barataria Pass (Figs. B-12, B-13, B-14), Caminada Pass (Figs. 13-15, B-16, B-17), and Airplane Lake (Fig. B-18). The data were taken at every location at three evenly spaced points with a B-10 Ducted Current Meter (See Table B-l). As can be seen from these figures, a uniform vertical velocity is a reasonable approximation for shallow estuarine bays. There is a thin boundary layer next to the bottom. A salt wedge appeared to distort the velocity profile in the channel in Quatre Bayou Pass. As a point of interest, horizontal velocity profiles for the entrance to Airplane Lake are shown in Fig. B-19. Some flow, temperature and salinity data was taken at the fresh water inlets of the bay. This data is shown in Table B-2.

Energy Transport Measurements:

The main objective of these experiments was to determine the magnitude of the heat loss at the bottom of the bay due to conduction. Temperature profiles in the bottom of a typical estuarine body of water, Airplane Lake, were measured with a thermocouple attached to a solid metal shaft and a tele-thermometer (See Table B-l). These results are shown in Fig, B-20. The conditions under which these data were taken were such that the value obtained for the temperature gradient, $dT(Z_b)/dz$, was near its maximum (a clear, hot summer day at noon). This value obtained for the temperature gradient at the water-bottom interface was approximately

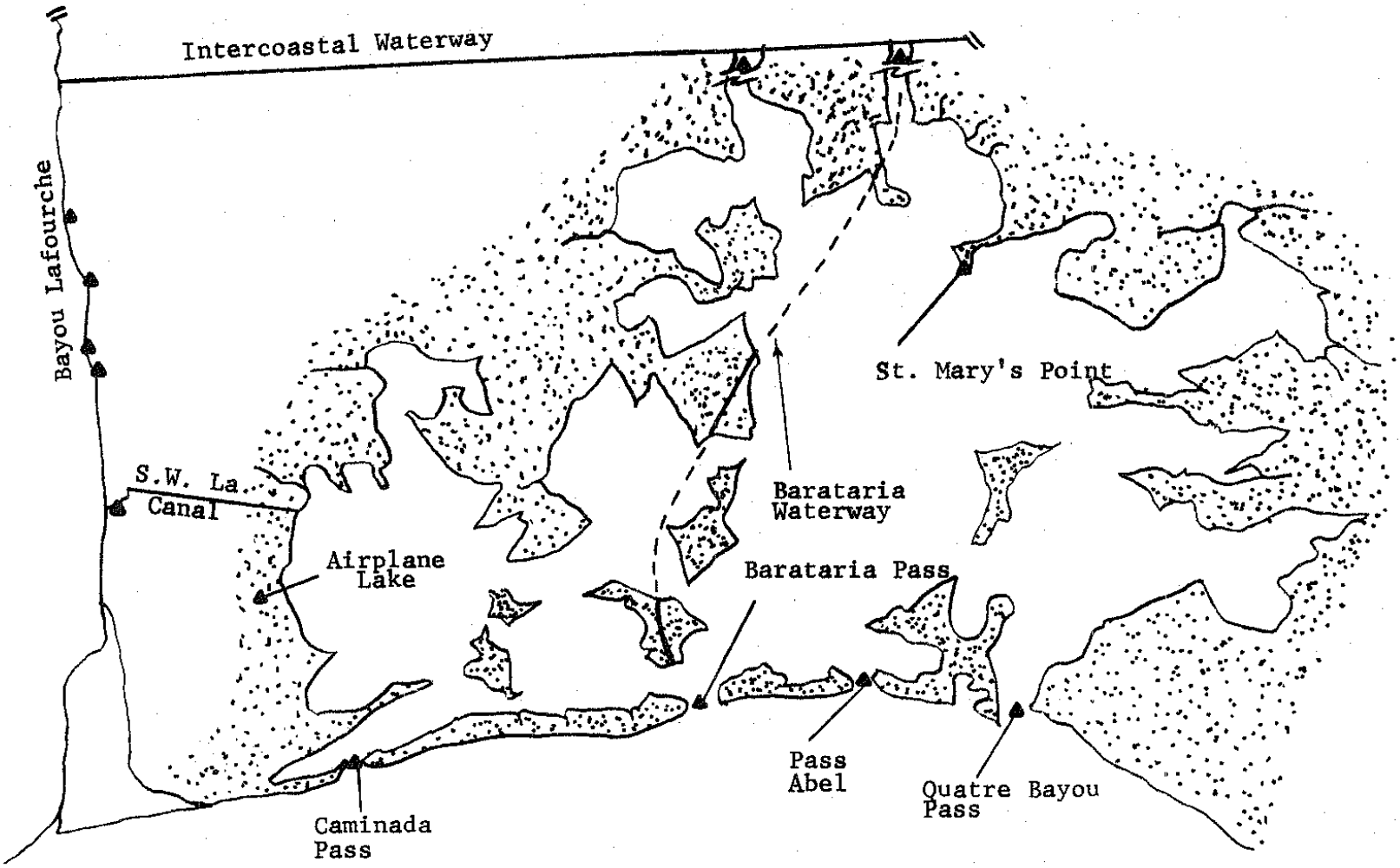

Figure B-1. Barataria Bay Sampling Points (▲ Sampling Points)

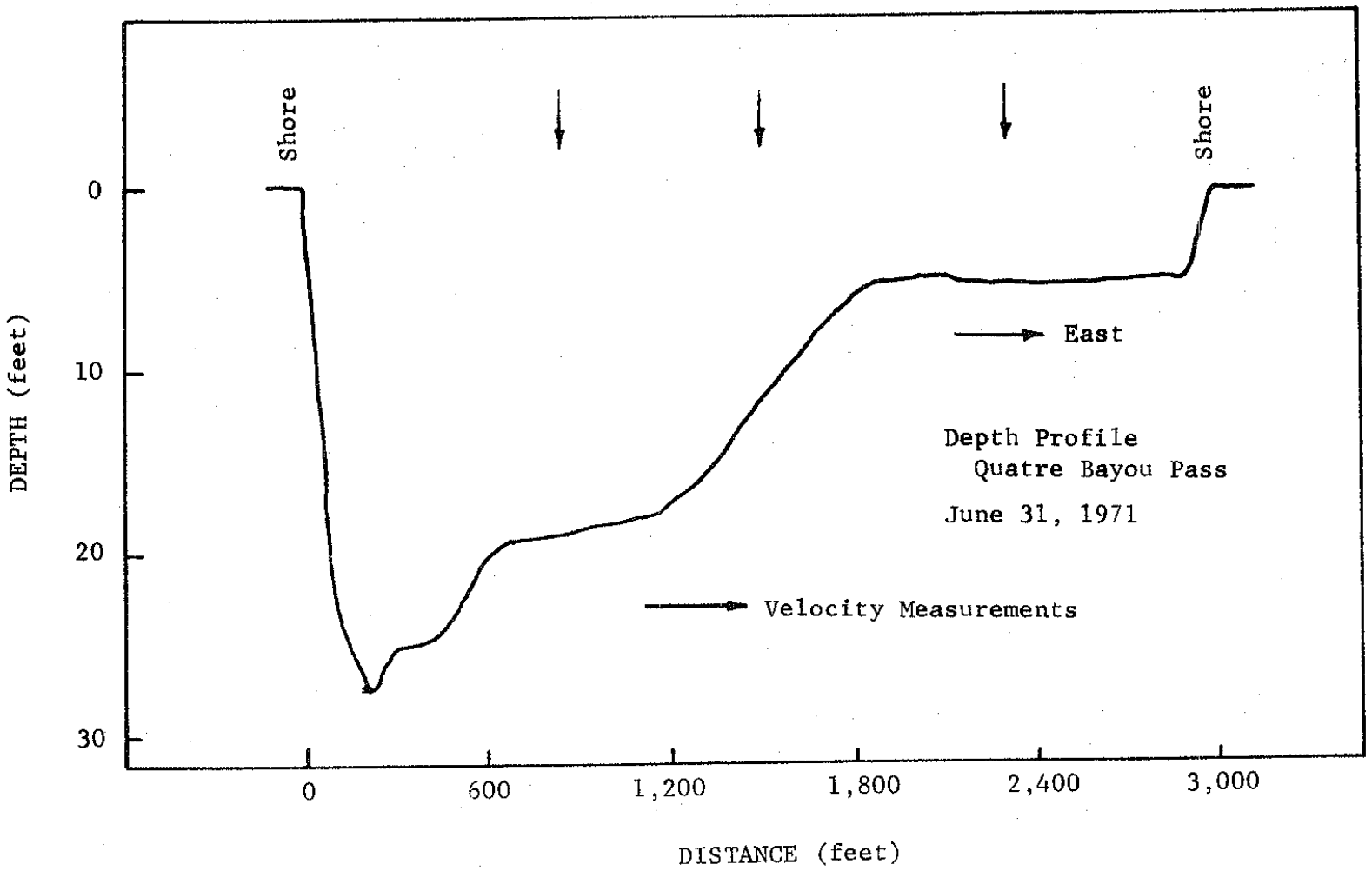

Figure B-2. Depth Profile of Quatre Bayou Pass

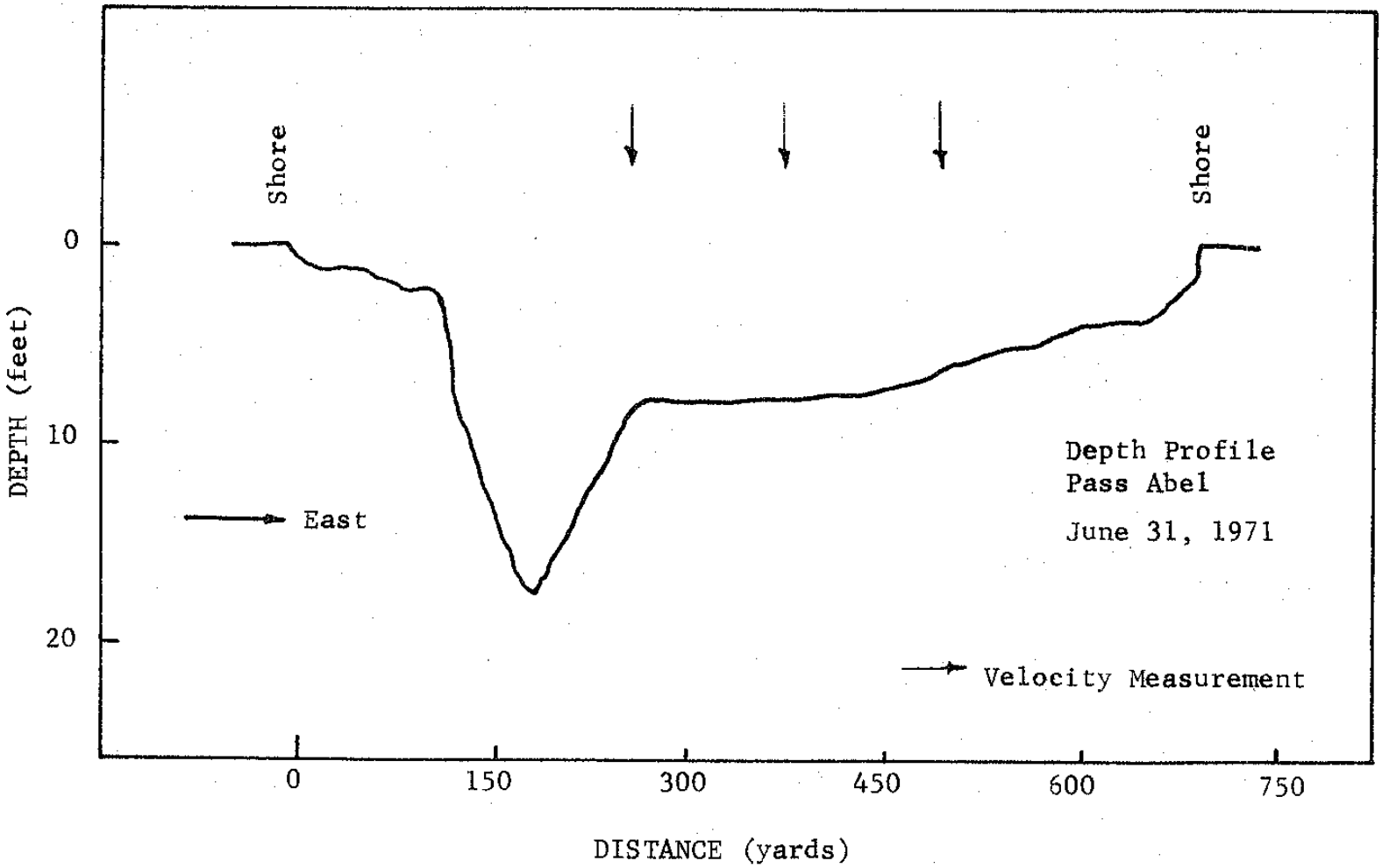

Figure B-3. Depth Profile of Pass Abel

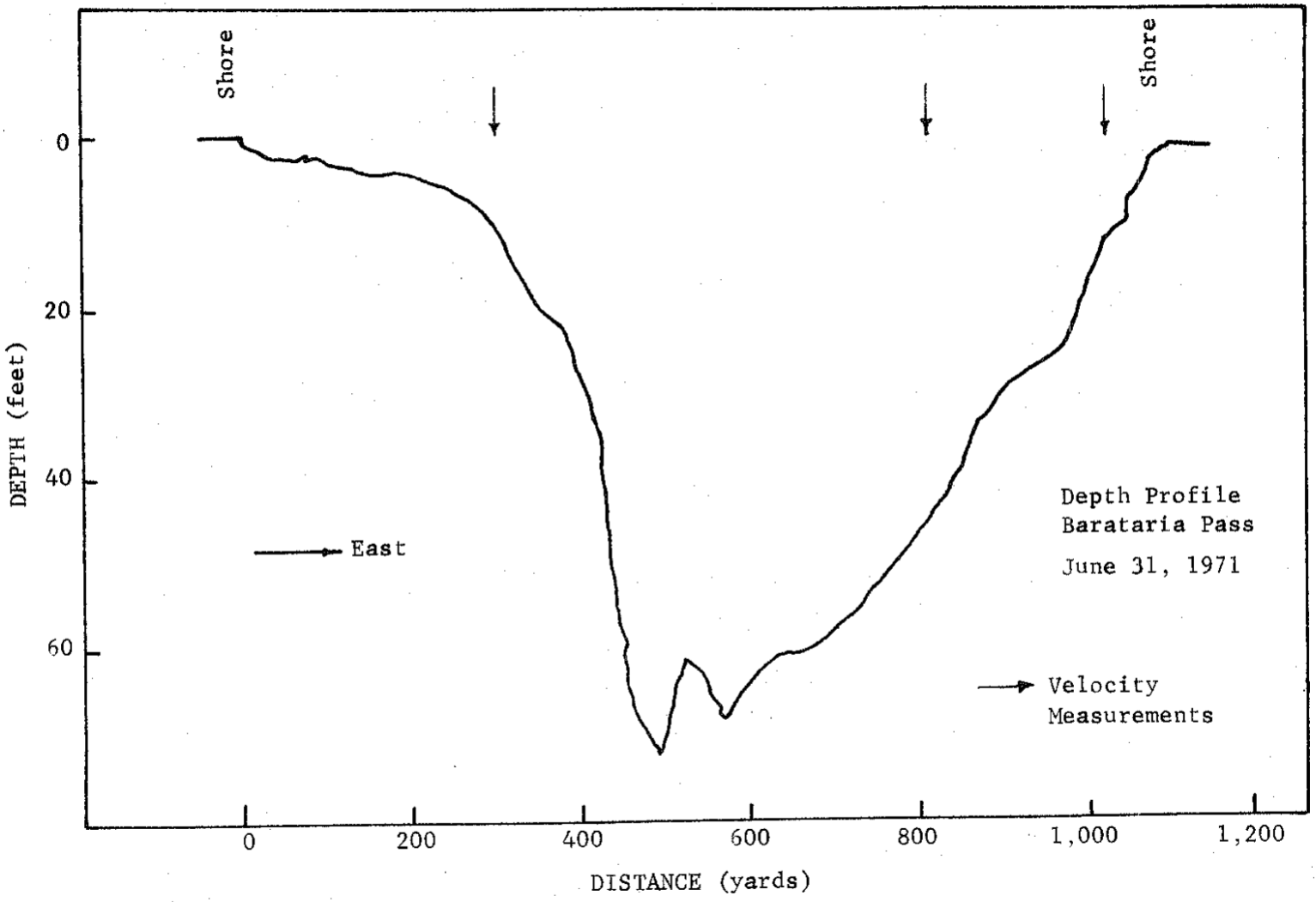

Figure B-4. Depth Profile of Barataria Pass

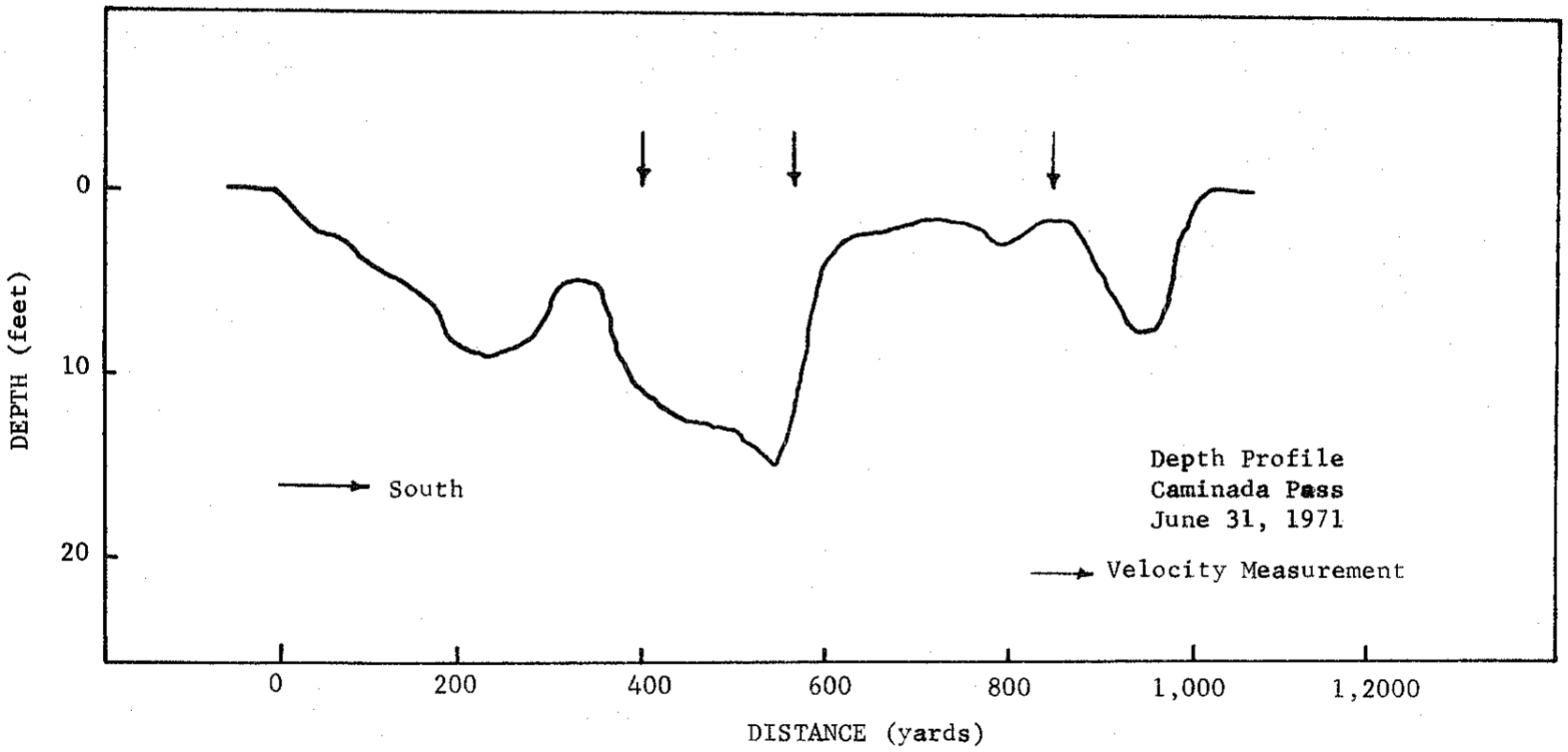

Figure B-5. Depth Profile of Caminada Pass

TABLE B-1

INSTRUMENTATION
USED

Parameter Measured	Instrument	Manufacturer
Velocity	B-10 Ducted Current Meter	Bendix Marine Advisers, Inc. 430s Cedros Ave. Soloma Beach, Calif. 92075
Salinity	Refractometer T/C	American Optical Corp. Scientific Instrument Div. Buffalo, N.Y. 14215
	Van Dorn Bottle	Rodney Adams Sea Grant Program, LSU Baton Rouge, La. 70803
	Mark I Water Quality Monitoring System	Martek Instruments, Inc. 879 West 16th St. Newport Beach, Calif. 92660
Temperature	Tele-Thermometer	Yellow Springs Instrument Co., Inc. Yellow Springs, Ohio
Depth	Raytheon Depthfinder DE-736	Raytheon Corp. South San Francisco, Ca.

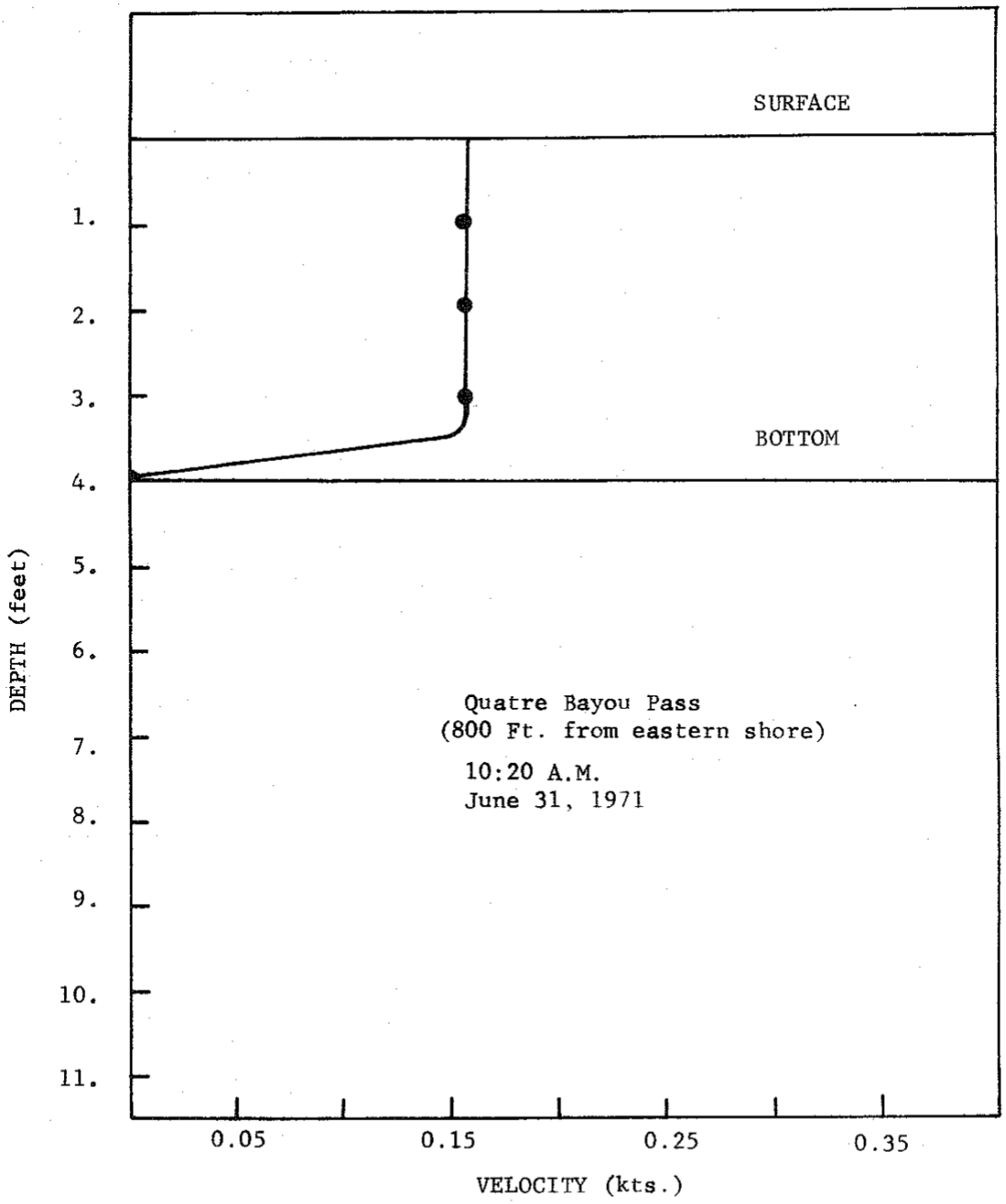

Figure B-6. Velocity Profile at Quatre Bayou Pass

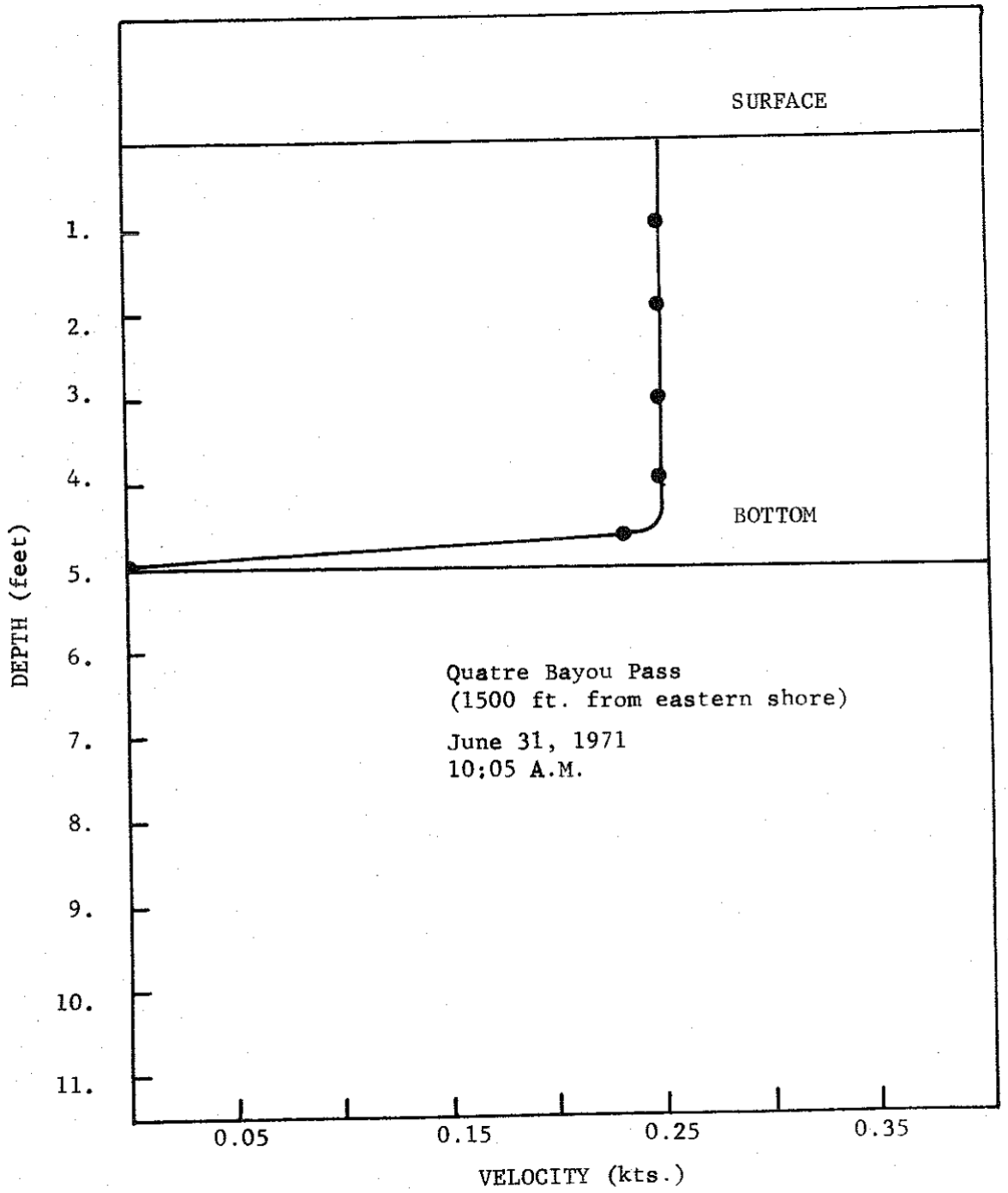

Figure B-7. Velocity Profile at Quatre Bayou Pass

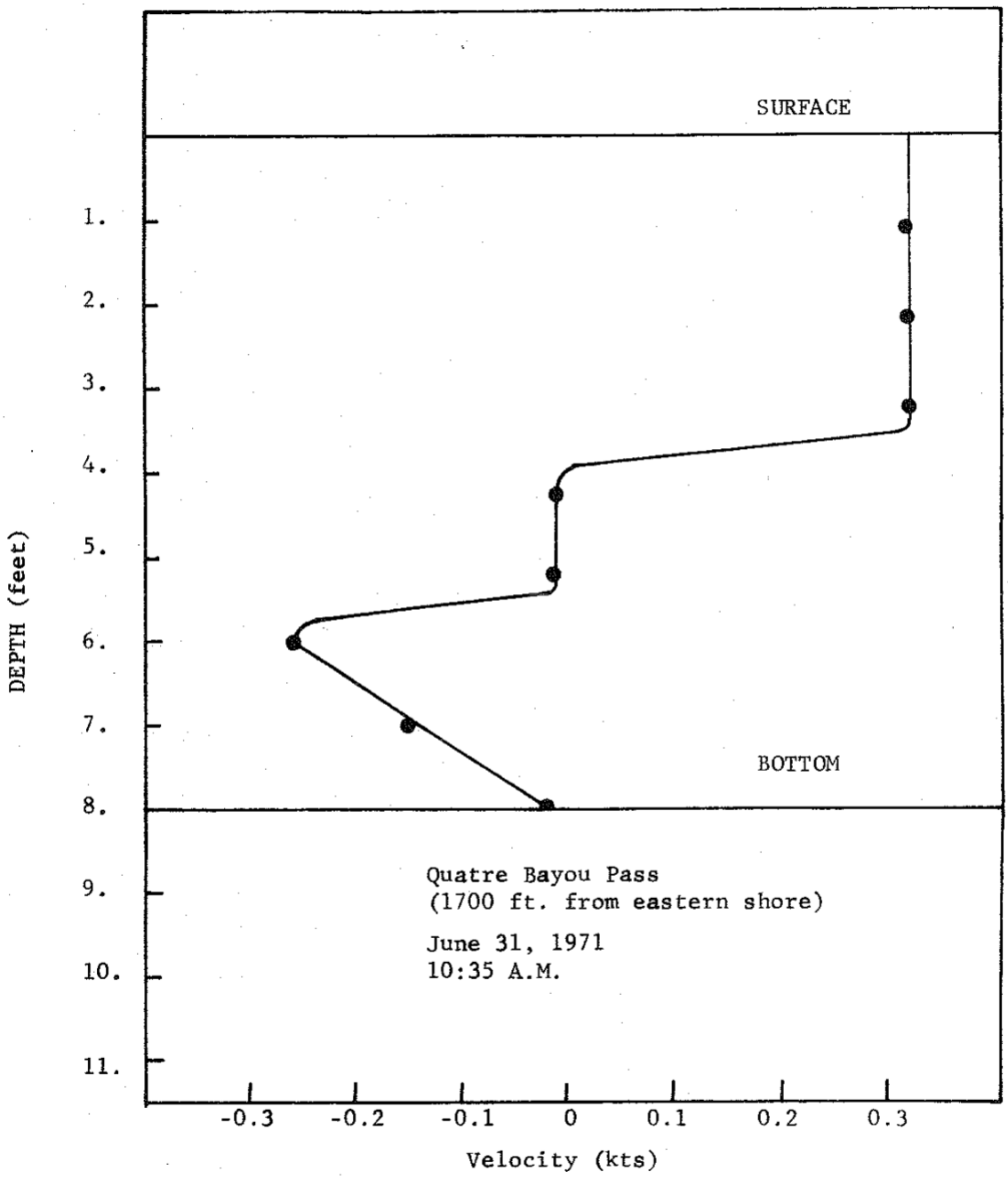

Figure B-8. Velocity Profile at Quatre Bayou Pass

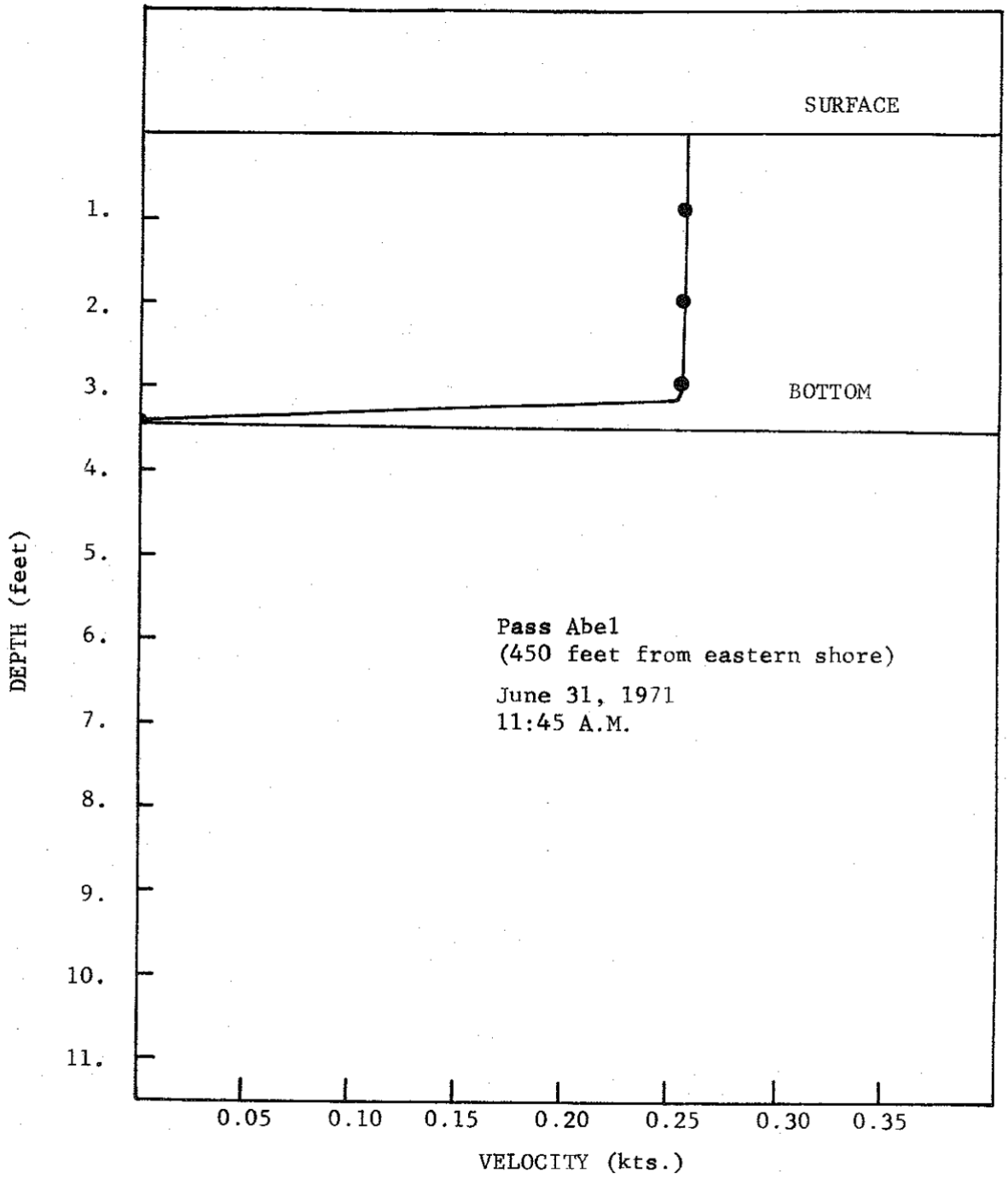

Figure B-9. Velocity Profile at Pass Abel

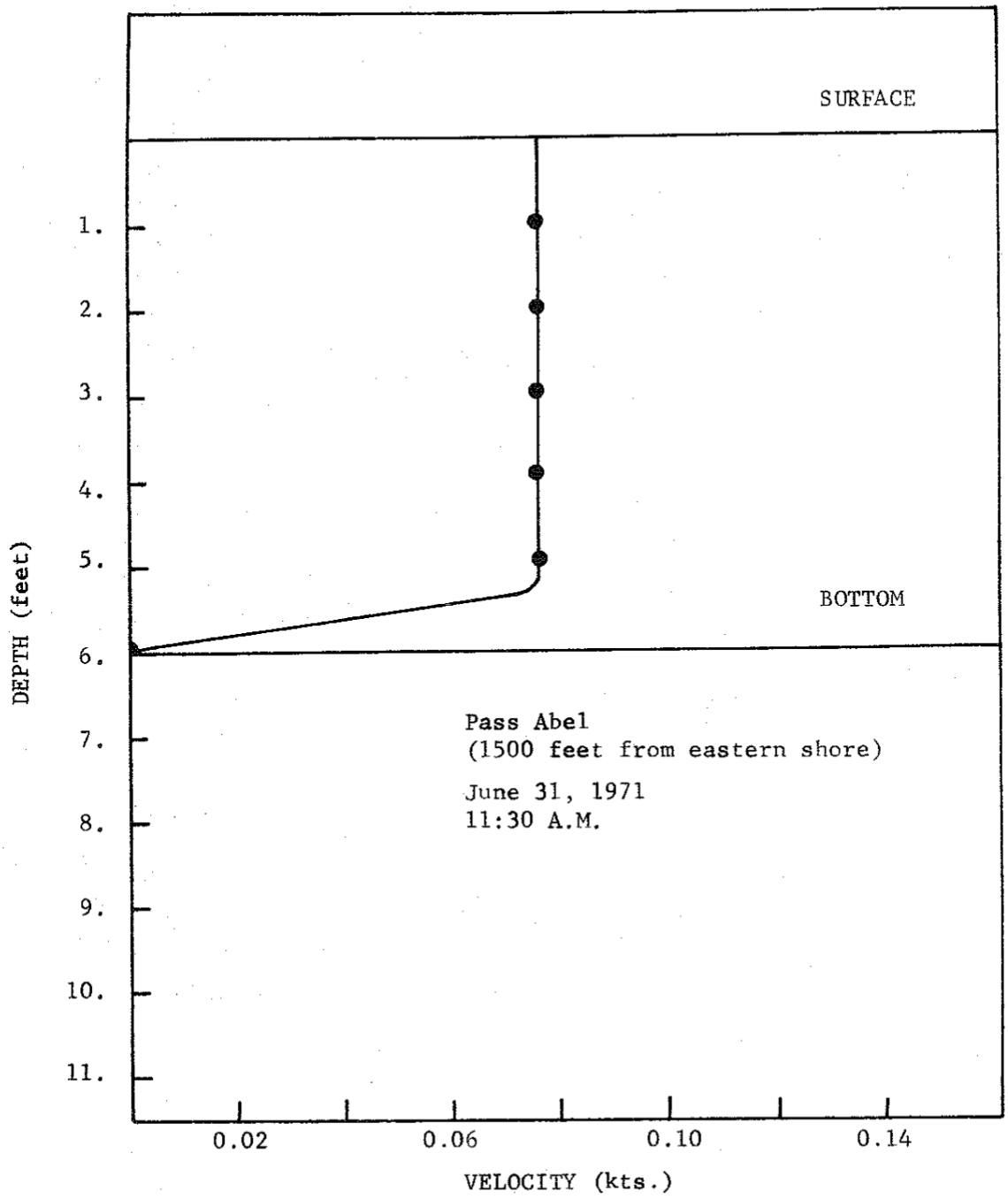

Figure B-10. Velocity Profile at Pass Abel

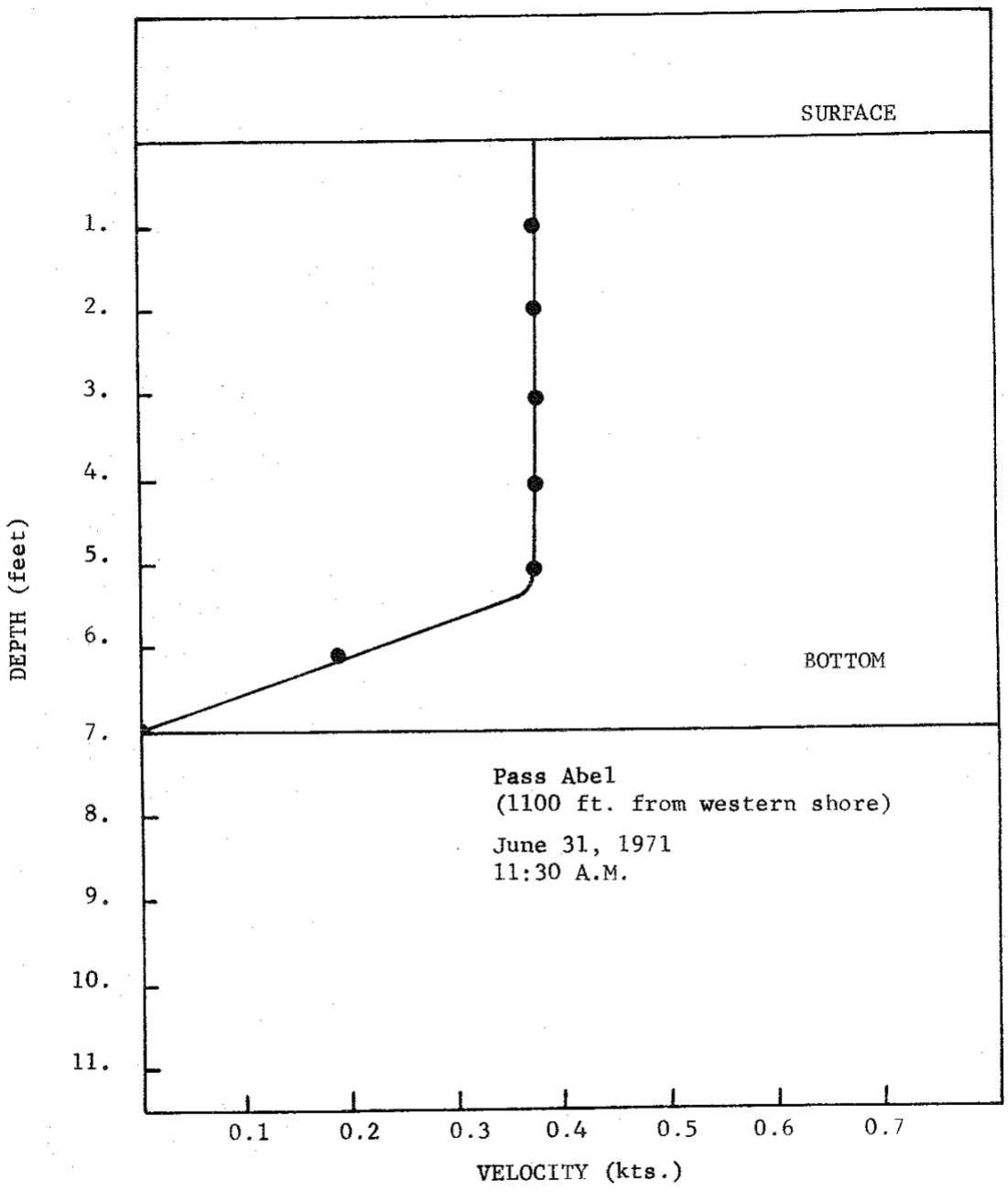

Figure B-11. Velocity Profile at Pass Abel

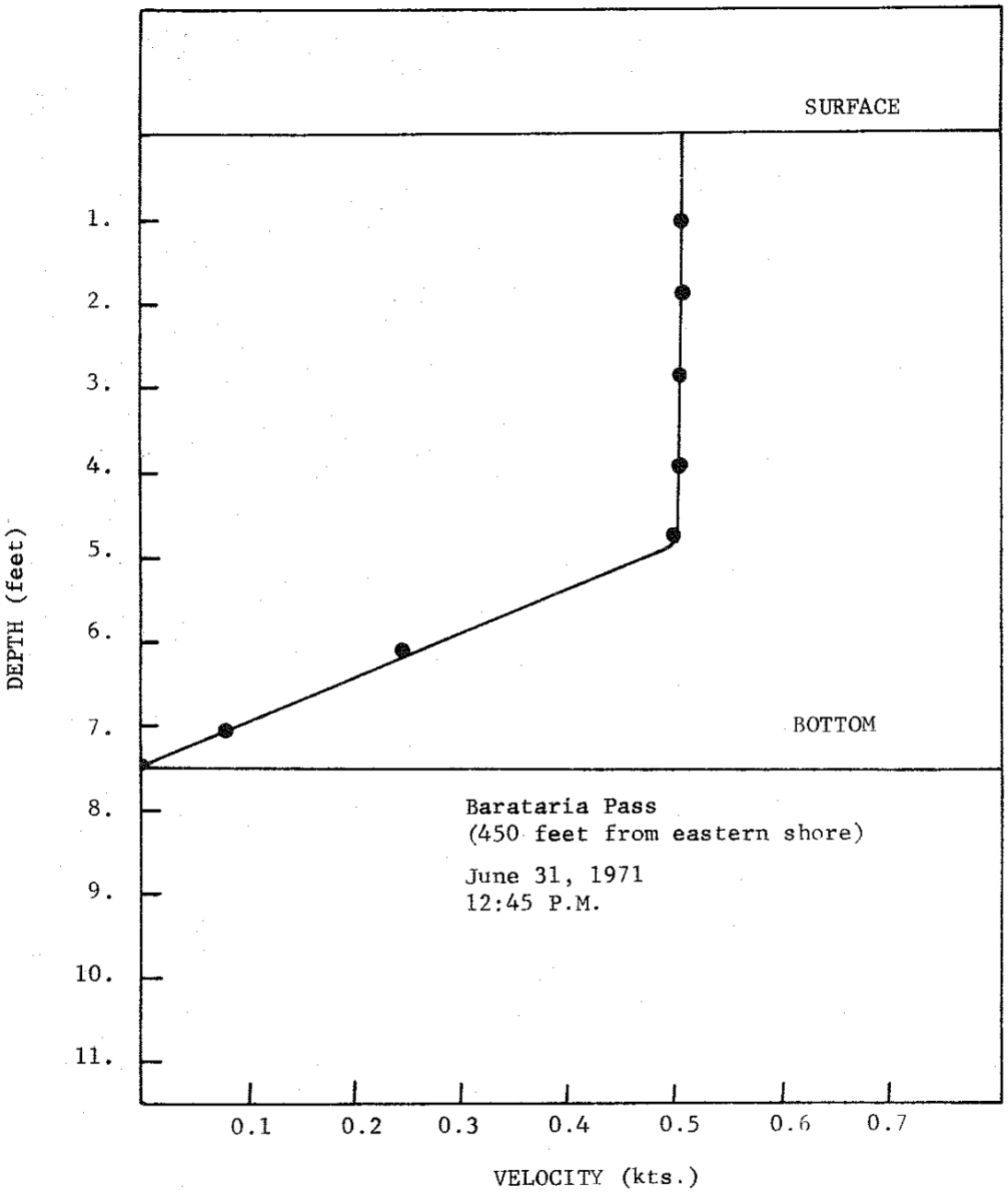

Figure B-12. Velocity Profile at Barataria Pass

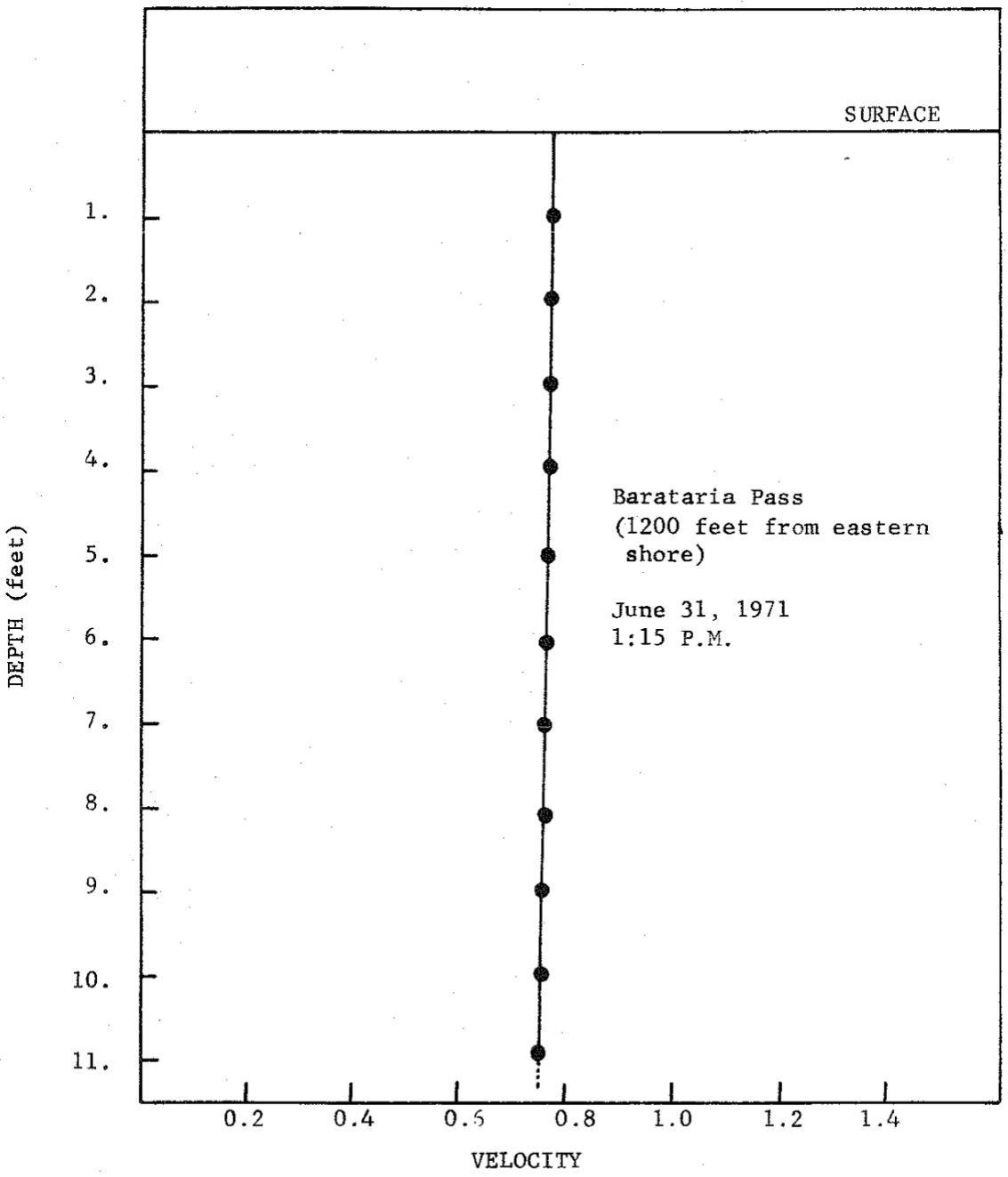

Figure B-13. Velocity Profile at Barataria Pass

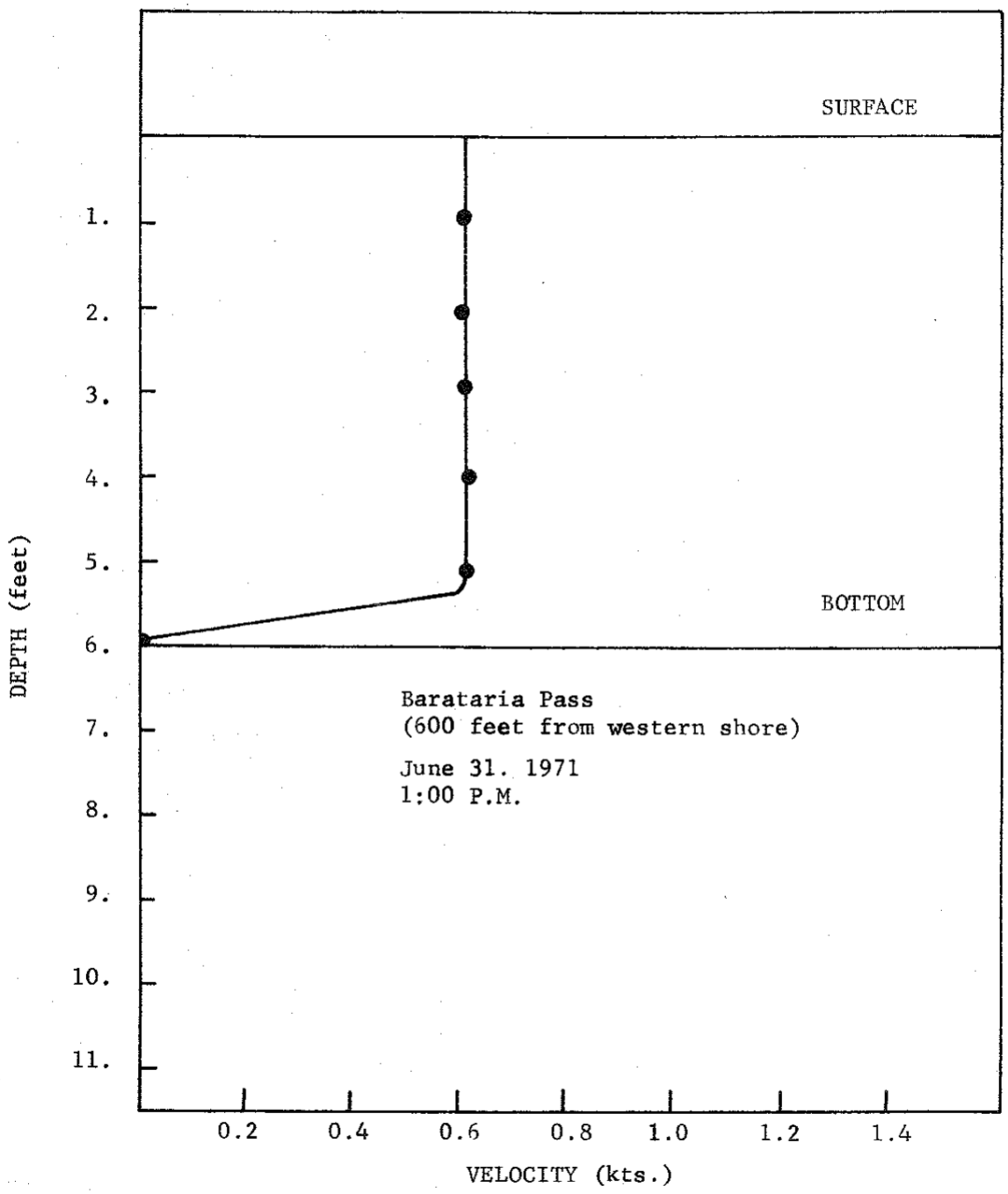

Figure B-14. Velocity Profile at Barataria Pass

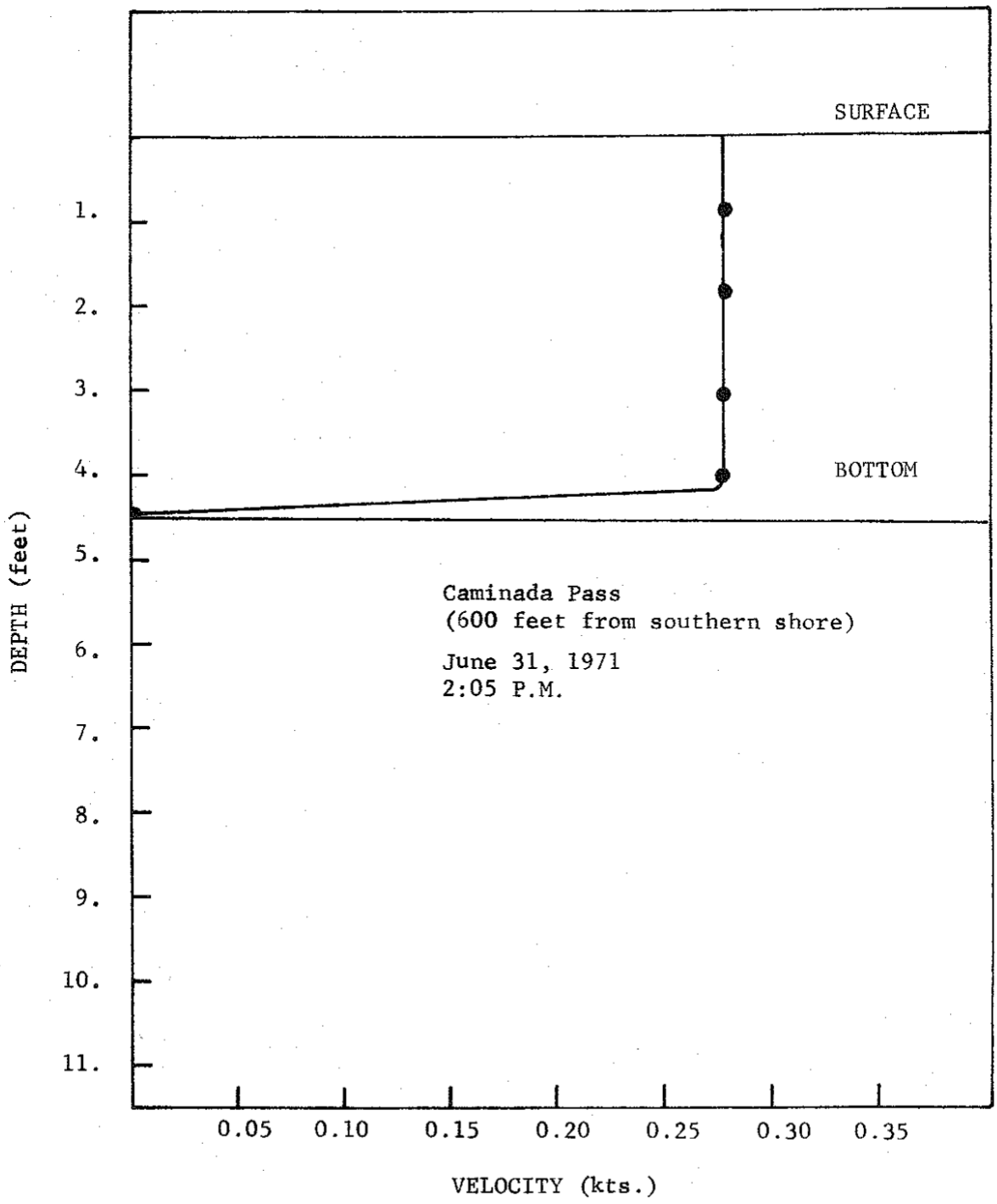

Figure B-15. Velocity Profile at Caminada Pass

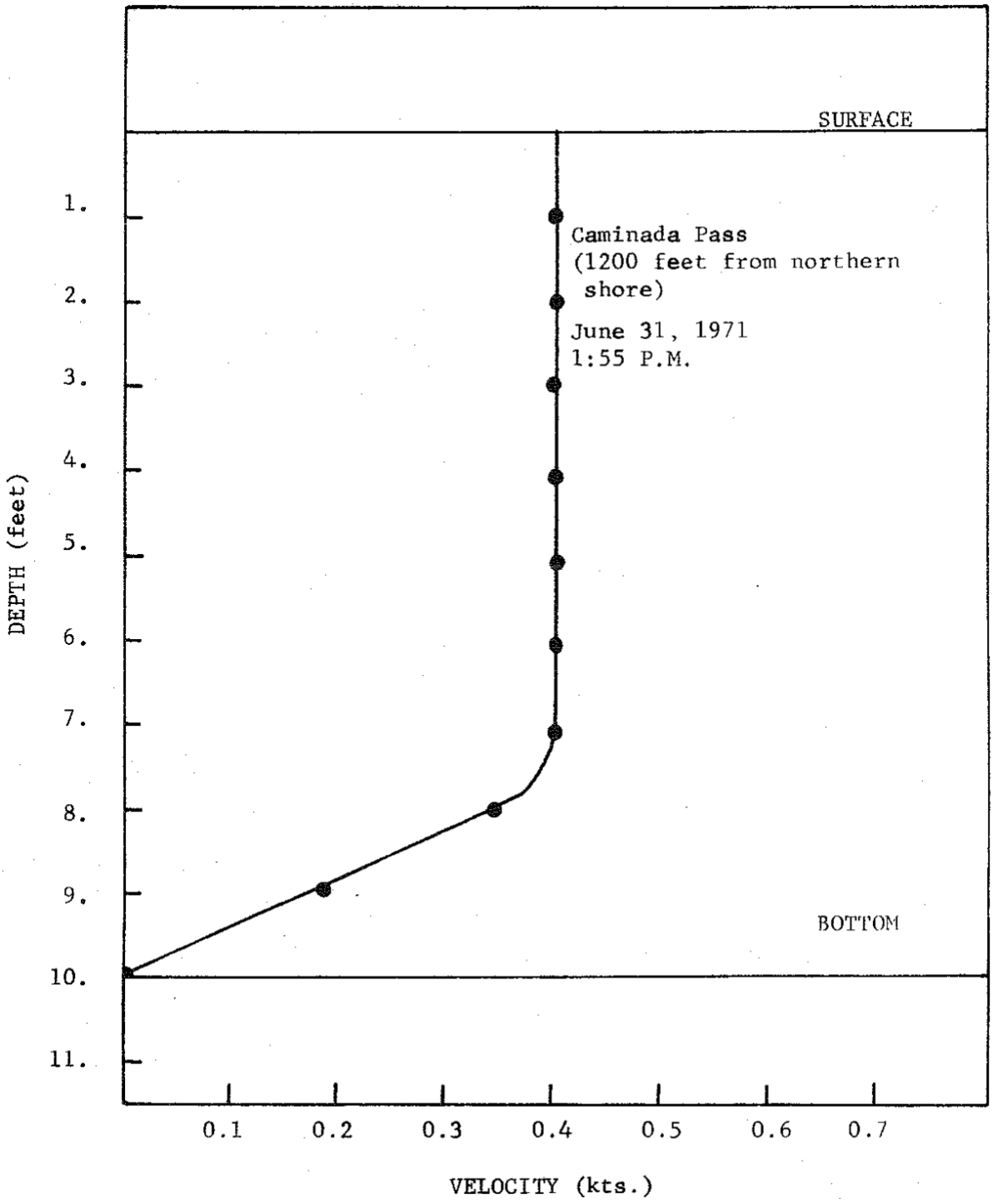

Figure B-12. Velocity Profile at Caminada Pass

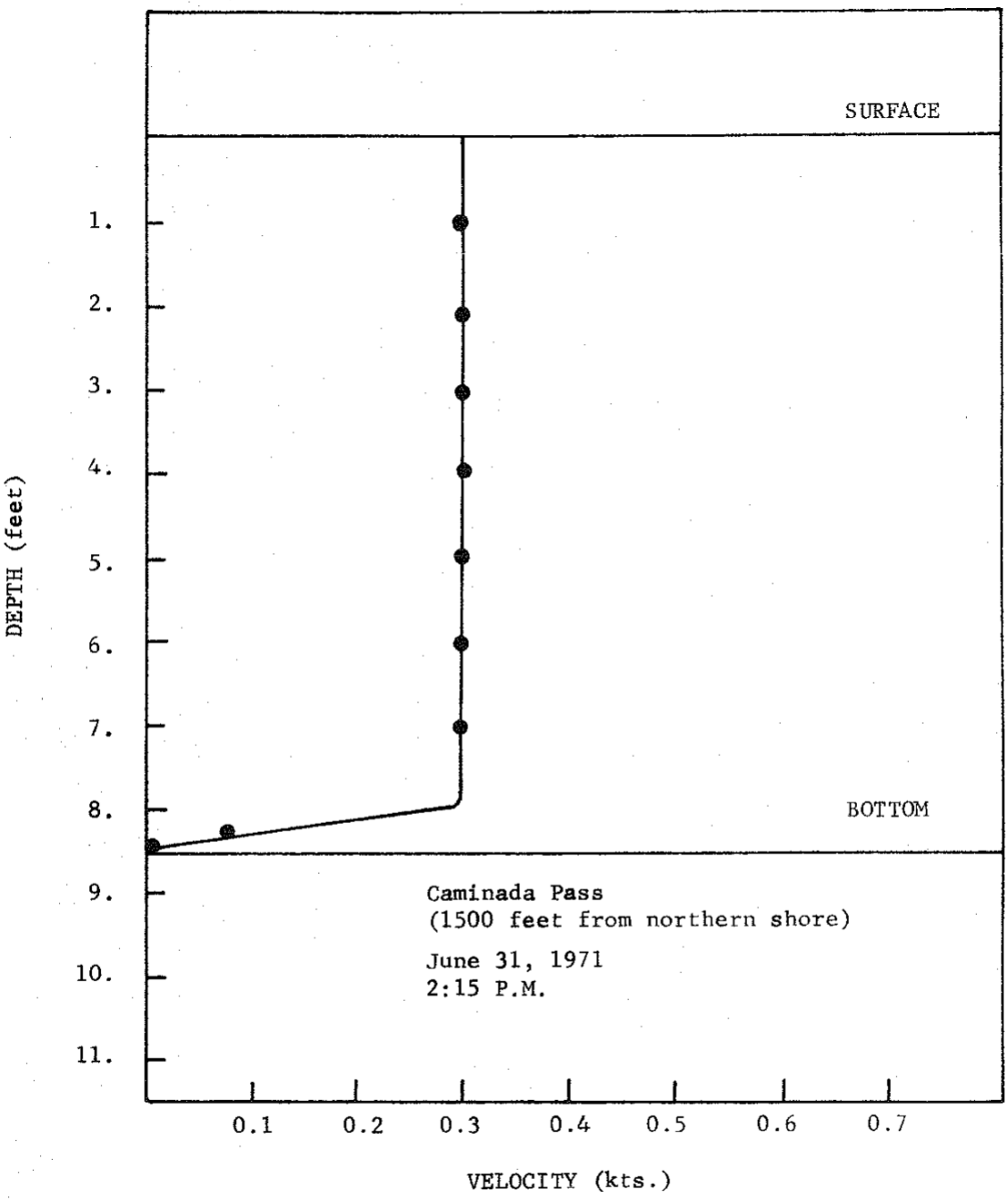

Figure B-17. Velocity Profile at Caminada Pass

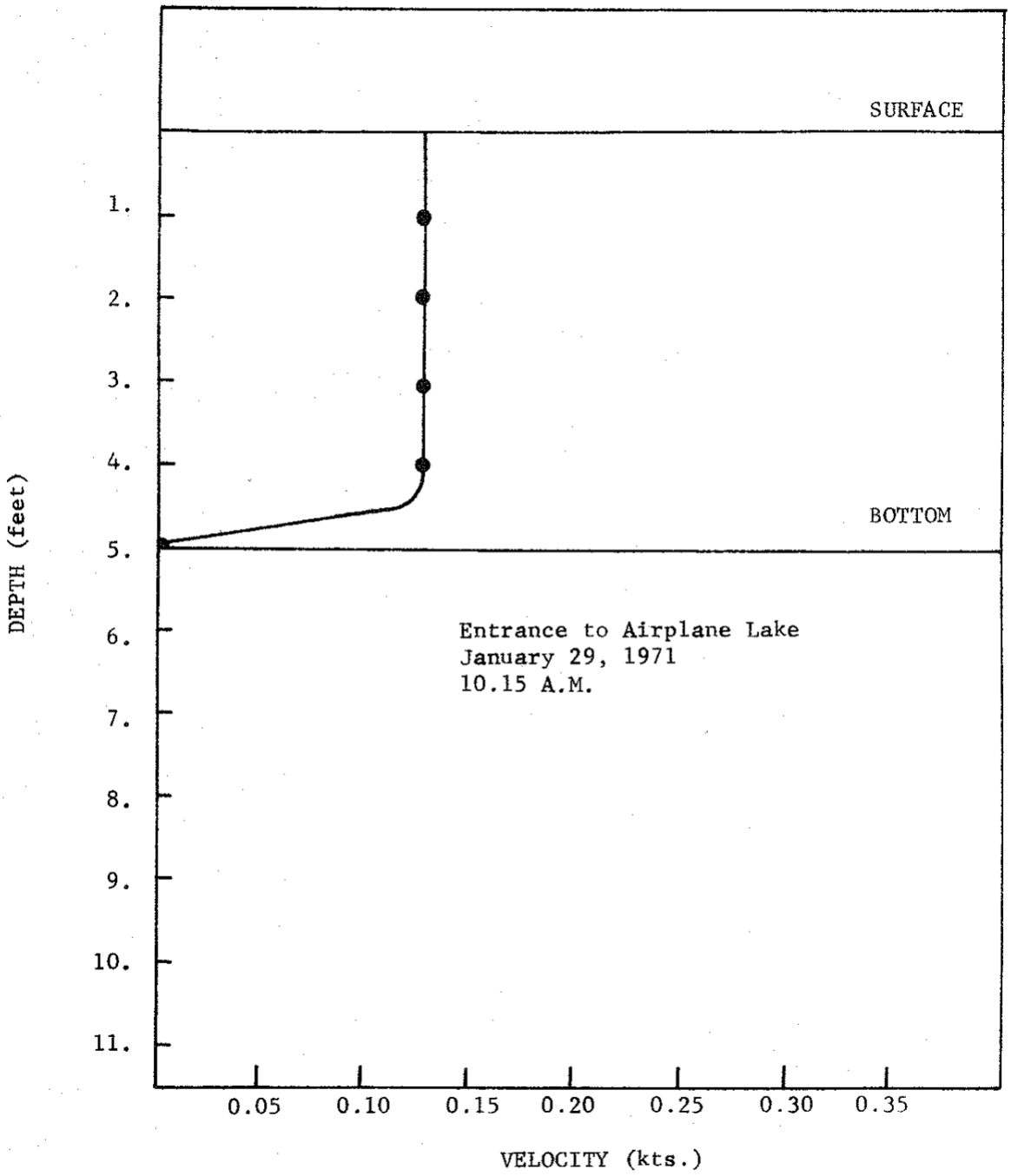

Figure B-18. Velocity Profile at Airplane Lake Entrance

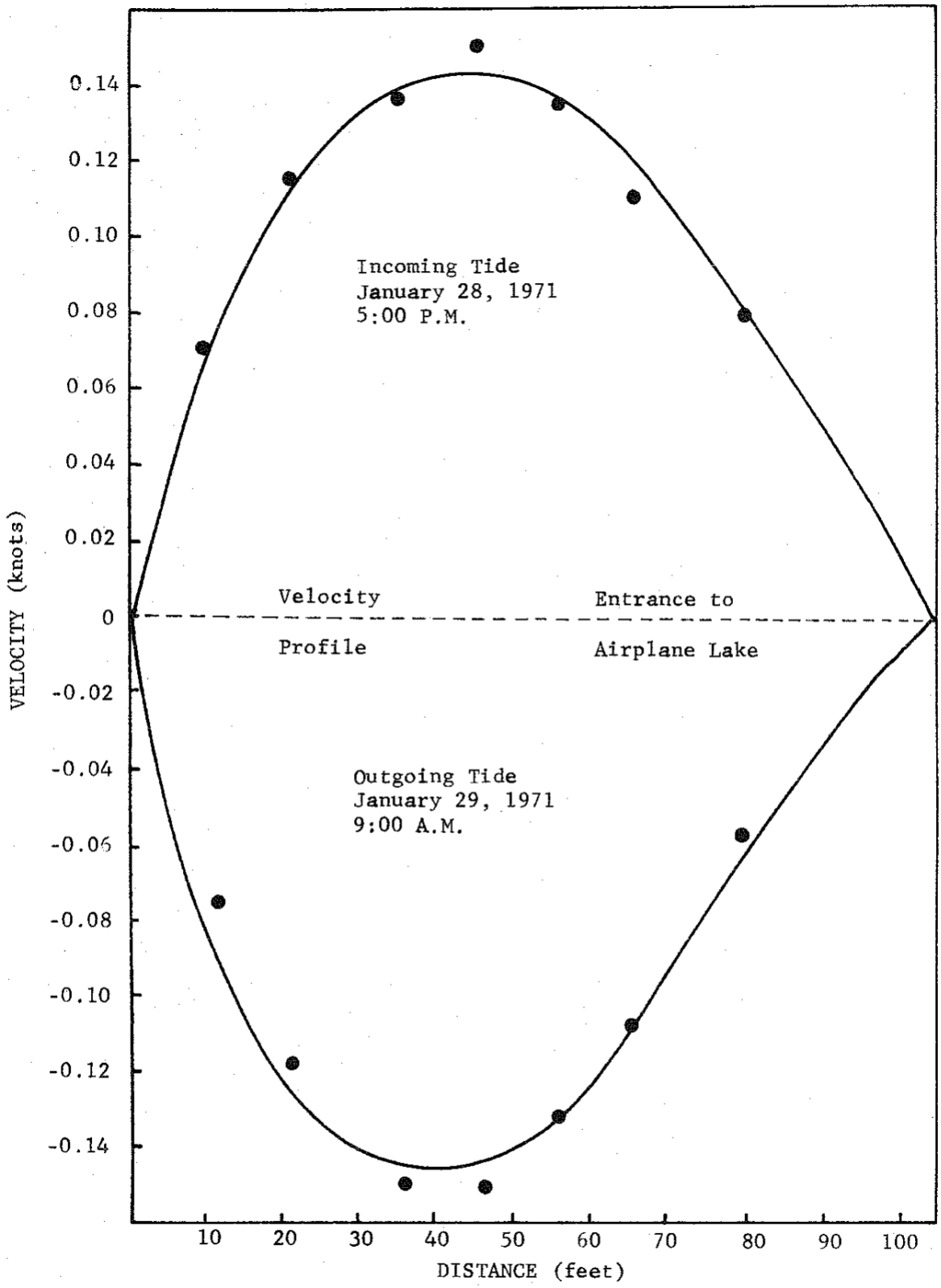

Figure B-19. Horizontal Velocity Profiles at Entrance to Airplane Lake

TABLE B-2

FLOW, TEMPERATURE, AND SALINITY MEASUREMENTS
OF SOME OF THE FRESH WATER INLETS TO
BARATARIA BAY

Location and date	velocity	canal depth	canal width	temperature	salinity
Barataria Waterway north of Laffite Aug. 13, 1971 10:47 A.M.	0.04 knots	3 yds	100 yds	28.5°C	1.25°/oo
Bayou Perot South of Intercoastal Canal, Aug. 13, 1971, 12:00	0.028 knots	7 yds	150 yds	28.5°C	1.5°/oo
Cutoff Scully Canal, Aug. 13, 1971, 2:05 P.M.	0.05 knots	1 yd	10 yds	29.2°C	0.5°/oo
North of Galiano Canal Aug. 13, 1971 2:05 P.M.	0.07 knots	1.5 yd	15 yds	28.8°C	0.5°/oo
Golden Meadow Yankee Canal Aug. 13, 1971 3:00 P.M.	0.2 knots	1 yd	15 yds	28.6°C	0.6°/oo
South Golden Meadow Canal Aug. 13, 1971 3:15 P.M.	0.16 knots	3 yds	40 yds	29°C	13°/oo
S. W. La. Canal @ Bayou Lafourche Aug. 13, 1971 4:50 P.M.	1.2 knots	3.5 yds	100 yds	29.5°C	18°/oo

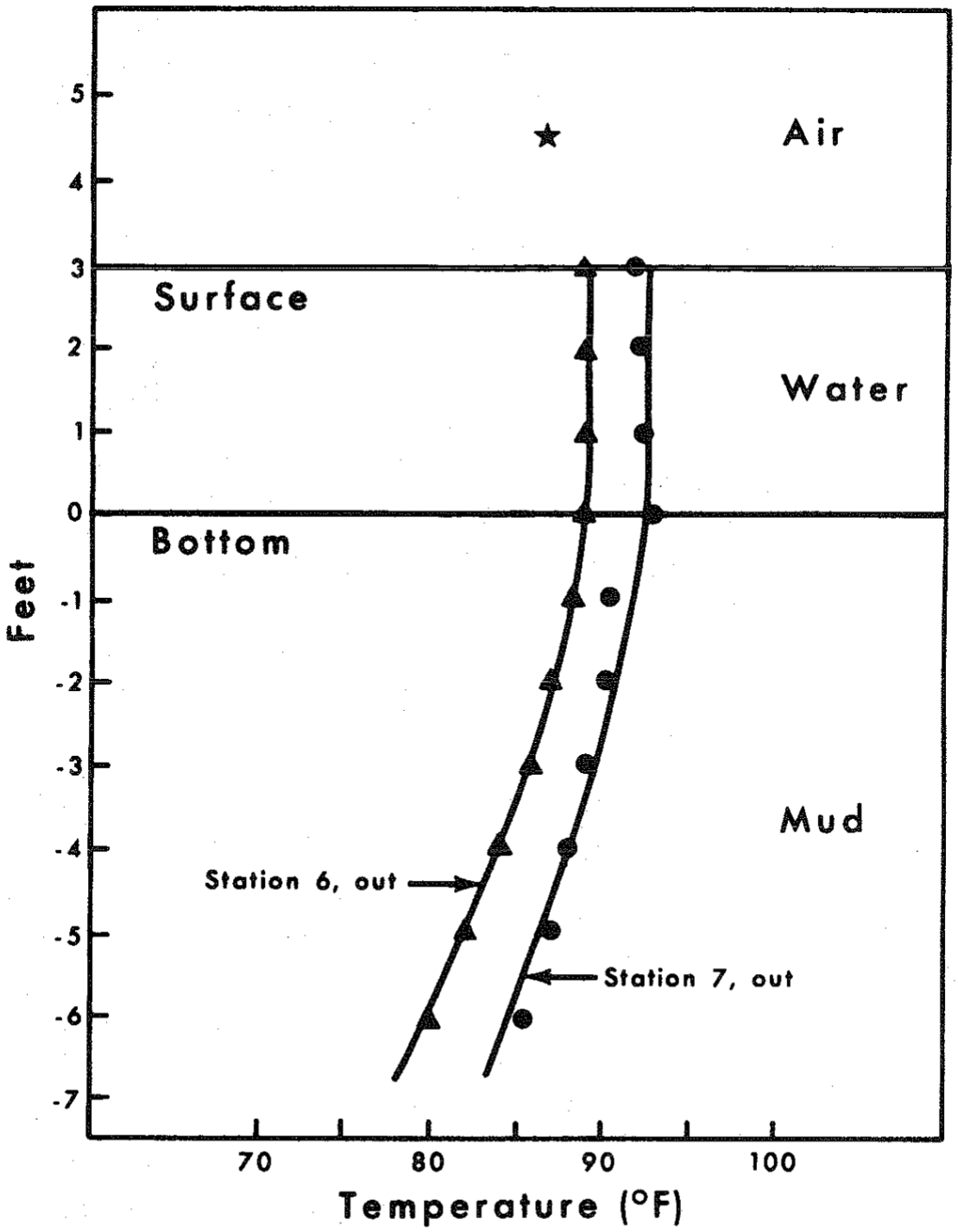

★ = air temperature = 87°F Wet bulb temperature = 82°F

Data taken at Airplane Lake, Sept. 11, 1970, at noon.

Figure B-20. Temperature Profiles in Bottom of Airplane Lake

1.25° F/ft. The bottom of a typical estuarine body of water is a mixture of silt, decomposing cellulose, and water. An approximate value the thermal conductivity of this mixture is 0.7 BTU/(hr)(ft)(°F). The temperature gradient at the water-bottom interface will change as conditions vary, but its absolute value will not be much larger than the one determined experimentally. These values can be used to obtain an-upper limit for the heat flow caused by conduction at the bottom. This value is compared with the upper-limit values of some of the surface heat flows in Table B-3. It can be seen from this table that heat flow at the bottom of a typical estuarine body of water is two orders of magnitude less than the maximum heat flow from solar radiation and 30 times smaller than the convective rate at the surface.

Salinity Measurements

A boundary condition was needed for the time variation of salinity in the Gulf water entering the bay during incoming tide. The salinity varies between the salinity of bay water going out to sea during the outgoing tide and the salinity of the open sea. The mass of water that leaves the bay mixes with the sea, and as the tide shifts, the salinity of the incoming water will increase from the value of the salinity of the outgoing water to the value of salinity of the open sea. Measurements were made of the time variation of salinity in Barataria Pass using a Van Dorn bottle, a refractometer, and the Mark I System (See Table B-l). Temperature was found not to vary as both sea temperature and bay temperature were equal. Salinity data is shown if Fig. B-21. With this data, the variation of salinity with time of the incoming tide was modeled, as described in Chapter IV.

Instrumentation and Other Data

Instruments used to obtain the data shown in this chapter are tabulated in Table B-l.

Besides the data shown in this chapter, other data was available from other investigators in the Sea Grant Program at LSU and the Louisiana Wild Life and Fisheries Commission.

TABLE B-3

UPPER LIMIT VALUE FOR SOME HEAT FLUXES

	Type	Symbol	Upper Limiting Value (cal/cm^2-min.)
Surface Heat Fluxes	Heat Flux Due to Solar Radiation	$q_{solar\ radiation}$	2.0 (Ref. B-1)
	Heat Flux Due to Surface Radiation	q_w	0.973×10^{-2} (Ref. B-1)
	Heat Flux Due to Convection	q_c	0.122 (Ref. B-1)
	Heat Flux Due to Reflection	q_{ref}	0.60 (Ref. B-1)
Bottom Heat Fluxes	Heat Flux Due to Conduction	$q_{(Z_b)}$	0.400×10^{-2}

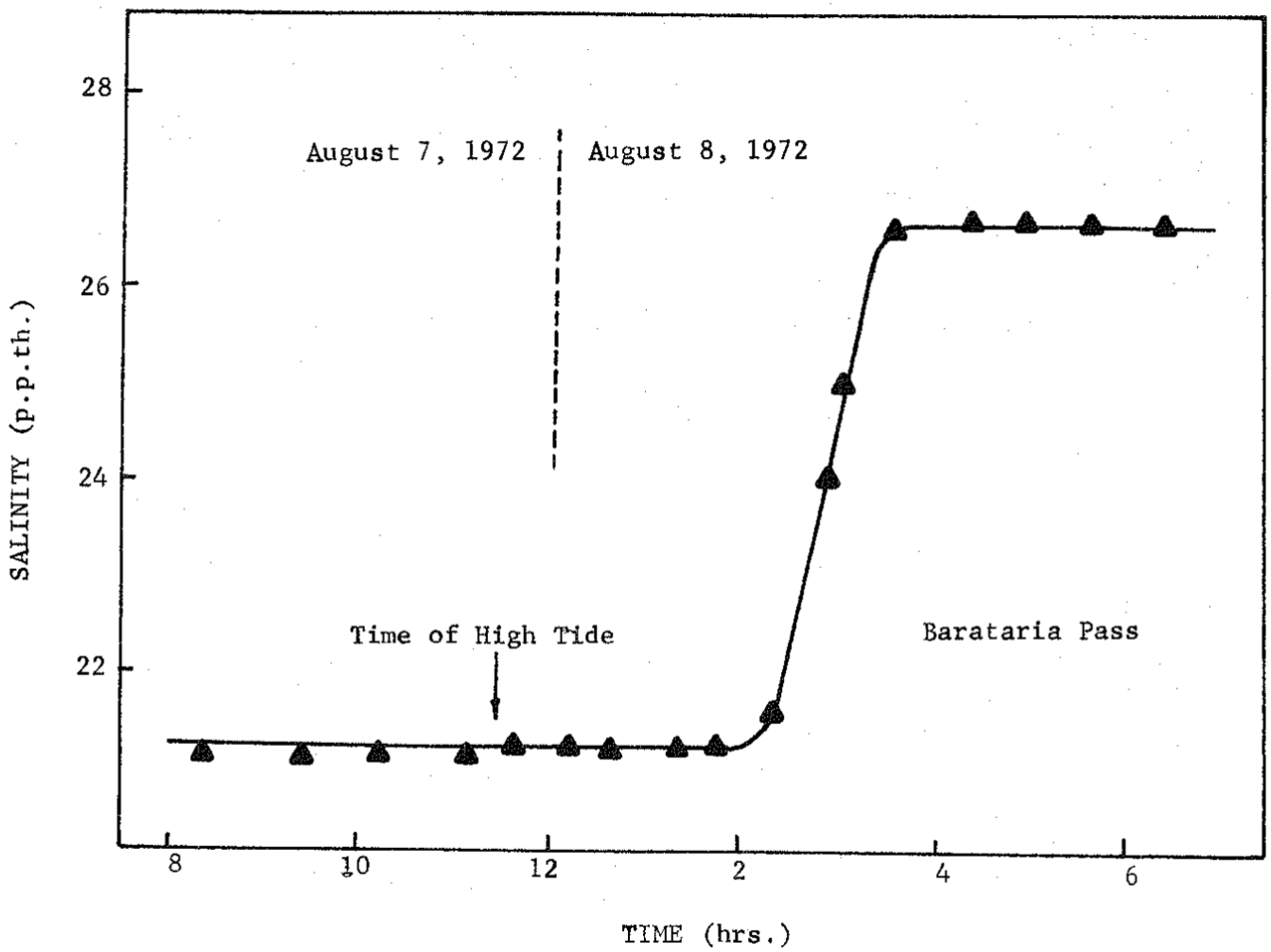

Figure B-21. Salinity as a Function of Time in Barataria Pass

REFERENCES

B-1 Neumann, Gerhard, and W.J. Pierson, Jr., Principles of Physical Oceanography, Prentice-Hall, Inc., Englewood Cliffs, N.J. c 1966, pp. 234-43, 253-6.

APPENDIX C

TIME INTEGRATION OF THE TRANSPORT PHENOMENA EQUATION FOR A SHALLOW ESTUARINE BAY

A time-averaged model is one in which the equations have been integrated over a time period t. Thus, a time-averaged model has the advantage of allowing large time steps, making long term solutions feasible with respect to computation costs. To produce a time-averaged model, the transport phenomena equations for a shallow estuarine bay must be integrated over a given time period. This time period becomes the independent variable in the equations.

The difficulties that this method generates are shown in the time integration performed in this appendix. Extra terms, similar to Reynold's stresses in turbulent flow, appear in the equations. These extra terms must be evaluated in order to be able to solve the time-averaged equations. At present, no empirical methods have been developed to evaluate these terms, and this appears to be an area for fruitful research.

Integration of the Hydrodynamic Model

The equations of the Hydrodynamic Model can be integrated over a time period t which could correspond to a 24 hour period or a tidal cycle. The result will be a time-averaged set of partial differential equations which could be applied to the area of interest in a model that can take large steps in time. In this section, this time integration will be performed.

Continuity Equation

The Continuity Equation is:

$$\frac{\partial Qx}{\partial x} + \frac{\partial Qy}{\partial y} + \frac{\partial L}{\partial t} = R - E_v \qquad (3.17)$$

and integrating over a time period, t, gives:

$$\frac{1}{t}\int_o^t \left[\frac{\partial Qx}{\partial x} + \frac{\partial Qy}{\partial y} + \frac{\partial L}{\partial t} \right] dt = \frac{1}{t}\int_o^t [R - E_v]\, dt \qquad (C\text{-}1)$$

Defining the following time averaged variables as

$$Qx \equiv \bar{Q}x + Qx' \tag{C-2}$$

where:

$$\bar{Q}x \equiv \frac{1}{t}\int_o^t Qx\,dt \tag{C-3}$$

and similarly:

$$Qy = \bar{Q}y + Qy' \tag{C-4}$$

$$L = \bar{L} + L' \tag{C-5}$$

$$R = \bar{R} + R' \tag{C-6}$$

$$E_v = \bar{E}_v + E_v' \tag{C-7}$$

The bar ($\bar{}$) indicates the average over the period and the prime (') indicates the instantaneous deviation from the average. Thus, Eq. (C-l) can be written as:

$$\frac{1}{t}\int_o^t \left[\frac{\partial(\bar{Q}x + Qx')}{\partial x} + \frac{\partial(\bar{Q}y + Qy')}{\partial y} + \frac{\partial(\bar{L} + L')}{\partial t} \right] dt =$$

$$\frac{1}{t}\int_o^t \left[\bar{R} + R' - \bar{E}_v - E_v' \right] dt \tag{C-8}$$

Evaluating each term separately:

$$\int_o^t \frac{\partial \bar{Q}x}{\partial x}\,dt = \frac{\partial}{\partial x}\int_o^t \bar{Q}x\,dt - \bar{Q}x\Big|_{t_f}\frac{\partial t_f}{\partial t} + \bar{Q}x\Big|_{t_o}\frac{\partial t_o}{\partial t} = \frac{\partial \bar{Q}x}{\partial x}\,t \tag{C-9}$$

$$\int_o^t \frac{\partial Qx'}{\partial x}\,dt = \frac{\partial}{\partial x}\int_o^t Qx'\,dt - Qx'\Big|_{t_f}\frac{\partial t_f}{\partial t} + Qx'\Big|_{t_o}\frac{\partial t_o}{\partial t} = 0 \tag{C-10}$$

since by definition the time average of the fluctuation, Qx', is zero.

$$\int_o^t \frac{\partial \bar{Q}y}{\partial y}\, dt = \frac{\partial \bar{Q}y}{\partial y}\, t \qquad \text{(C-11)}$$

$$\int_o^t \frac{\partial Q'y}{\partial y}\, dt = 0 \qquad \text{(C-12)}$$

$$\int_o^t \frac{\partial \bar{L}}{\partial t}\, dt = \frac{\partial \bar{L}}{\partial t}\, t \qquad \text{(C-13)}$$

$$\int_o^t \frac{\partial L'}{\partial t}\, dt = 0 \qquad \text{(C-14)}$$

$$\int_o^t \bar{R}dt = \bar{R}t \qquad \text{(C-15)}$$

$$\int_o^t R'dt = 0 \qquad \text{(C-16)}$$

$$\int_o^t \overline{Ev}dt = \overline{Evt} \qquad \text{(C-17)}$$

$$\int_o^t E\acute{v}dt = 0 \qquad \text{(C-18)}$$

Substituting Eqs. (C-8) through (C-17) into Eq. (C-7) results in the time-averaged continuity equation:

$$\frac{\partial \bar{Q}x}{\partial x} + \frac{\partial \bar{Q}y}{\partial y} + \frac{\partial \bar{L}}{\partial t} = \bar{R} - \overline{Ev} \qquad \text{(C-19)}$$

X-component of the Momentum Equation

The momentum equation in the x-direction is:

$$\frac{\partial U}{\partial t} + U\frac{\partial U}{\partial x} + V\frac{\partial U}{\partial y} - FV + g\frac{\partial L}{\partial x} = \tau_x^{\,s} - \tau_x^{\,b} \qquad (3.59)$$

Integrating over a time period, t, gives:

$$\frac{1}{t}\int_o^t \left[\frac{\partial U}{\partial t} + U\frac{\partial U}{\partial x} + V\frac{\partial U}{\partial y} - FV + g\frac{\partial L}{\partial x} \right] dt =$$

$$\frac{1}{t}\int_o^t \left[\tau_x^{\,s} - \tau_x^{\,b} \right] dt \qquad \text{(C-20)}$$

and defining:

$$U = \bar{U} + U' \qquad \text{(C-21)}$$

$$V = \bar{V} + V' \qquad \text{(C-22)}$$

$$D = \bar{D} + D' \qquad \text{(C-23)}$$

$$\tau^s = \bar{\tau}^s + \tau^{s\prime} \qquad \text{(C-24)}$$

$$\tau^b = \bar{\tau}^b - \tau^{b\prime} \qquad \text{(C-25)}$$

Eq. (C-19) can now be written as:

$$\frac{1}{t}\int_o^t \left[\frac{\partial(\bar{U} + U')}{\partial t} + (\bar{U} + U')\frac{\partial(\bar{U} + U')}{\partial x} + (\bar{V} + V')\right.$$

$$\left.\frac{\partial(\bar{U} + U')}{\partial y} - F(\bar{V} + V') + g\frac{\partial(\bar{L} + L')}{\partial x} \right] dt = \frac{1}{t}\int_o^t \left[(\bar{\tau}_x^{\,s} + \tau_x^{\prime s}) \right.$$

$$\left. - (\bar{\tau}_x^{\,b} + \tau_x^{\,b\prime}) \right] dt \qquad \text{(C-26)}$$

Evaluating each term separately:

$$\int_o^t \frac{\partial \bar{U}}{\partial t}\, dt = \frac{\partial \bar{U}}{\partial t}\, t \qquad \text{(C-27)}$$

$$\int_o^t \frac{\partial U'}{\partial t}\, dt = 0 \qquad \text{(C-28)}$$

$$\int_o^t \bar{U}\, \frac{\partial \bar{U}}{\partial x}\, dt = \bar{U} \int_o^t \frac{\partial \bar{U}}{\partial x}\, dt = \bar{U}\, \frac{\partial \bar{U}}{\partial x}\, t \qquad \text{(C-29)}$$

$$\int_o^t \bar{U}\, \frac{\partial U'}{\partial x}\, dt = \bar{U} \int_o^t \frac{\partial U'}{\partial x}\, dt = 0 \qquad \text{(C-30)}$$

$$\int_o^t U'\, \frac{\partial U'}{\partial x}\, dt = \int_o^t U'\, \frac{\partial U'}{\partial x}\, dt \qquad \text{(C-31)}$$

$$\int_o^t U'\, \frac{\partial \bar{U}}{\partial x}\, dt = 0 \qquad \text{(C-32)}$$

$$\int_o^t \bar{V}\, \frac{\partial \bar{U}}{\partial y} = \bar{V}\, \frac{\partial \bar{U}}{\partial y}\, t \qquad \text{(C-33)}$$

$$\int_o^t V'\, \frac{\partial \bar{U}}{\partial y} = 0 \qquad \text{(C-34)}$$

$$\int_o^t V'\, \frac{\partial \bar{U}}{\partial y}\, dt = 0 \qquad \text{(C-35)}$$

$$\int_o^t V'\, \frac{\partial U'}{\partial y}\, dt = \int_o^t V'\, \frac{\partial U'}{\partial y}\, dt \qquad \text{(C-36)}$$

$$\int_o^t F\bar{V}\, dt = F\bar{V}t \qquad \text{(C-37)}$$

$$\int_o^t FV'dt = 0 \qquad \text{(C-38)}$$

$$\int_o^t g\, \frac{\partial \bar{L}}{\partial x}\, dt = g\, \frac{\partial \bar{L}}{\partial x}\, t \qquad \text{(C-29)}$$

$$\int_o^t g\, \frac{\partial L'}{\partial x}\, dt = 0 \qquad \text{(C-40)}$$

$$\int_o^t \bar{\tau}_x^{\,b}\, dt = \bar{\tau}_x^{\,b}\, t \qquad \text{(C-41)}$$

$$\int_o^t \tau_x^{\,b\prime}\, dt = 0 \qquad \text{(C-42)}$$

$$\int_o^t \bar{\tau}_x^{\,s}\, dt = \bar{\tau}_x^{\,s}\, t \qquad \text{(C-43)}$$

$$\int_o^t \tau_x^{\,s\prime} dt = 0 \qquad \text{(C-44)}$$

Substituting Eqs. (C-27) through (C-44) into Eq. (C-26) gives the x-component of the time averaged equation of motion:

$$\frac{1}{t}\left[\frac{\partial \bar{U}}{\partial t} t + \bar{U} \frac{\partial \bar{U}}{\partial x} t + \int_o^t U' \frac{\partial U'}{\partial x} dt + \bar{V} \frac{\partial \bar{U}}{\partial y} t \right.$$

$$\left. + \int_o^t V' \frac{\partial U'}{\partial y} dt - F\bar{V}t + g \frac{\partial \bar{L}}{\partial x} t \right] = \frac{1}{t}\left[\bar{\tau}_x^{\,s} t - \bar{\tau}_x^{\,b} t \right] \qquad \text{(C-45)}$$

Rearranging:

$$\frac{\partial \bar{U}}{\partial t} + \bar{U} \frac{\partial \bar{U}}{\partial x} + \int_o^t U' \frac{\partial U'}{\partial x} dt + \bar{V} \frac{\partial \bar{U}}{\partial y} + \int_o^t V' \frac{\partial U'}{\partial y} dt$$

$$- F\bar{V} + g \frac{\partial \bar{L}}{\partial x} = \bar{\tau}_x^{\,s} - \bar{\tau}_x^{\,b} \qquad \text{(C-46)}$$

The y-component of the equation of motion can be similarly derived:

$$\frac{\partial \bar{V}}{\partial t} + \bar{V}\frac{\partial \bar{V}}{\partial y} + \int_o^t V' \frac{\partial V'}{\partial y}\,dt + \bar{U}\frac{\partial \bar{V}}{\partial x} + \int_o^t U' \frac{\partial V'}{\partial x}\,dt$$

$$+ F\bar{U} + g\frac{\partial \bar{L}}{\partial y} = \bar{\tau}_y^{\,s} - \bar{\tau}_y^{\,b} \qquad \text{(C-47)}$$

Integration of the Energy Transport and Mass Transport Models

The same reasoning used for the time-integration of the Hydrodynamic Model is used for these models. As both equations are similar, a generalized form will be used to obtain the time averaged equation. This generalized form is:

$$\frac{\partial(DS)}{\partial t} + \frac{\partial(UDS)}{\partial x} + \frac{\partial(VDS)}{\partial y} -$$

$$\frac{\partial}{\partial x}\left(D\text{Ð}x \frac{\partial S}{\partial x}\right) - \frac{\partial}{\partial y}\left(D\text{Ð}y \frac{\partial S}{\partial y}\right) - SS = 0 \qquad \text{(C-48)}$$

Eq. (C-48) can be time integrated as:

$$\frac{1}{t}\int_o^t \left[\frac{\partial(DS)}{\partial t} + \frac{\partial(UDS)}{\partial x} + \frac{\partial(VDS)}{\partial y} - \right.$$

$$\left. \frac{\partial}{\partial x}\left(D\text{Ð}x \frac{\partial S}{\partial x}\right) - \frac{\partial}{\partial y}\left(D\text{Ð}y \frac{\partial S}{\partial y}\right) - SS \right] dt = 0 \qquad \text{(C-49)}$$

in which:

$$SS = \overline{SS} + SS' \qquad \text{(C-50)}$$

$$S = \bar{S} + S' \qquad \text{(C-51)}$$

evaluating each term of Eq. (C-49) individually

$$\int_o^t \frac{\partial}{\partial t} (\overline{DS})\, dt = \frac{\partial(\overline{DS})}{\partial t}\, t \qquad \text{(C-52)}$$

$$\int_o^t \frac{\partial}{\partial t} (\overline{D}S')\, dt = 0 \qquad \text{(C-53)}$$

$$\int_o^t \frac{\partial}{\partial t} (D'\overline{S})\, dt = 0 \qquad \text{(C-54)}$$

$$\int_o^t \frac{\partial}{\partial t} (D'S')\, dt = \int_o^t \frac{\partial(D'S')}{\partial t}\, dt \qquad \text{(C-55)}$$

$$\int_o^t \frac{\partial}{\partial x} (\overline{DUS})\, dt = \frac{\partial(\overline{DUS})}{\partial x}\, t \qquad \text{(C-56)}$$

$$\int_o^t \frac{\partial}{\partial x} (\overline{DU}S')\, dt = \frac{\partial}{\partial x}\, \overline{DU} \int_o^t s'dt = 0 \qquad \text{(C-57)}$$

$$\int_o^t \frac{\partial}{\partial x} (\overline{D}U'\overline{S})\, dt = 0 \qquad \text{(C-58)}$$

$$\int_o^t \frac{\partial}{\partial x} (D'\overline{US})dt = 0 \qquad \text{(C-59)}$$

$$\int_o^t \frac{\partial}{\partial x} (D'U'\overline{S})\, dt = \frac{\partial}{\partial x}\, \overline{S} \int_o^t D'U'dt \qquad \text{(C-60)}$$

$$\int_o^t \frac{\partial}{\partial x} (\overline{D}U'S')dt = \frac{\partial}{\partial x}\, \overline{D} \int_o^t U'S'dt \qquad \text{(C-61)}$$

$$\int_o^t \frac{\partial}{\partial x} (D'\overline{U}S')\, dt = \frac{\partial}{\partial x}\, \overline{U} \int_o^t D'S'dt \qquad \text{(C-62)}$$

$$\int_o^t \frac{\partial}{\partial x} (D'U'S')\, dt = \frac{\partial}{\partial x} \int_o^t D'U'S'dt \qquad \text{(C-63)}$$

$$\int_o^t \frac{\partial}{\partial y} (\overline{DVS})dt = \frac{\partial}{\partial y} (\overline{DVS})\, t \qquad \text{(C-64)}$$

$$\int_o^t \frac{\partial}{\partial y} (\overline{DV}S')dt = 0 \qquad \text{(C-65)}$$

$$\int_o^t \frac{\partial}{\partial y} (\overline{D}V'\overline{S})\, dt = 0 \qquad \text{(C-66)}$$

$$\int_o^t \frac{\partial}{\partial y} (D'\overline{VS})\, dt = 0 \qquad \text{(C-67)}$$

$$\int_o^t \frac{\partial}{\partial y} (\overline{D}V'S')dt = \frac{\partial}{\partial y}\, \overline{D} \int_o^t V'S'dt \qquad \text{(C-68)}$$

$$\int_o^t \frac{\partial}{\partial y} (D'\overline{V}S')\, dt = \frac{\partial}{\partial y}\, \overline{V} \int_o^t D'S'dt \qquad \text{(C-69)}$$

$$\int_o^t \frac{\partial}{\partial y} (D'V'\overline{S})\, dt = \frac{\partial}{\partial y}\, \overline{S} \int_o^t D'V'dt \qquad \text{(C-70)}$$

$$\int_o^t \frac{\partial}{\partial y} (D'V'S')\, dt = \frac{\partial}{\partial y} \int_o^t D'V'S'dt \qquad (C\text{-}71)$$

$$\int_o^t \frac{\partial}{\partial x} (\bar{D}\text{Đ}_x \frac{\partial \bar{S}}{\partial x})\, dt = t \frac{\partial}{\partial x} \bar{D}\text{Đ}_x \frac{\partial \bar{S}}{\partial x} \qquad (C\text{-}72)$$

$$\int_o^t \frac{\partial}{\partial x} (\bar{D}\text{Đ}_x \frac{\partial S'}{\partial x})\, dt = \frac{\partial}{\partial x} \bar{D}\text{Đ}_x \int_o^t \frac{\partial S'}{\partial x} dt = 0 \qquad (C\text{-}73)$$

$$\int_o^t \frac{\partial}{\partial x} (D'\text{Đ}_x \frac{\partial \bar{S}}{\partial x})\, dt = 0 \qquad (C\text{-}74)$$

$$\int_o^t \frac{\partial}{\partial x} (D'\text{Đ}_x \frac{\partial S'}{\partial x})\, dt = \frac{\partial}{\partial x} \text{Đ}_x \int_o^t D' \frac{\partial S'}{\partial x} dt \qquad (C\text{-}75)$$

$$\int_o^t \frac{\partial}{\partial y} (\bar{D}\text{Đ}_y \frac{\partial \bar{S}}{\partial y})\, dt = t \frac{\partial}{\partial y} \bar{D}\text{Đ}_y \frac{\partial \bar{S}}{\partial y} \qquad (C\text{-}76)$$

$$\int_o^t \frac{\partial}{\partial y} (\bar{D}\text{Đ}_y \frac{\partial S'}{\partial y})\, dt = 0 \qquad (C\text{-}77)$$

$$\int_o^t \frac{\partial}{\partial y} (D'\text{Đ}_y \frac{\partial \bar{S}}{\partial y})\, dt = 0 \qquad (C\text{-}78)$$

$$\int_o^t \frac{\partial}{\partial y} (D'\text{Đ}_y \frac{\partial S'}{\partial y})\, dt = \frac{\partial}{\partial y} \text{Đ}_y \int_o^t D' \frac{\partial S'}{\partial y} dt \qquad (C\text{-}79)$$

$$\int_o^t \overline{SS}\, dt = \overline{SS}\, t \qquad (C\text{-}80)$$

Substituting Eqs. (C-52) through (C-80) into Eq. (C-49) gives the time integrated Species Transport Model:

$$\frac{\partial(\overline{DS})}{\partial t} + \int_o^t \frac{\partial(D'S')}{\partial t}\,dt + \frac{\partial(\overline{DUS})}{\partial x} + \frac{\partial}{\partial x}\overline{S}\int_o^t D'U'dt$$

$$+ \frac{\partial}{\partial x}\overline{D}\int_o^t S'U'dt + \frac{\partial}{\partial x}\overline{U}\int_o^t D'S'dt + \frac{\partial}{\partial x}\int_o^t D'U'S'dt$$

$$+ \frac{\partial(\overline{DVS})}{\partial y} + \frac{\partial}{\partial y}\overline{D}\int_o^t V'S'dt + \frac{\partial}{\partial y}\overline{V}\int_o^t D'S'dt$$

$$+ \frac{\partial}{\partial y}\overline{S}\int_o^t D'V'dt + \frac{\partial}{\partial y}\int_o^t D'V'S'dt - \frac{\partial}{\partial x}\left(\text{Þ}_x\overline{D}\frac{\partial\overline{S}}{\partial x}\right)$$

$$- \frac{\partial}{\partial x}\text{Þ}_x\int_o^t D'\frac{\partial S'}{\partial x}\,dt - \frac{\partial}{\partial y}\left(\text{Þ}_y\overline{D}\frac{\partial\overline{S}}{\partial y}\right) - \frac{\partial}{\partial y}\text{Þ}_y\int_o^t D'\frac{\partial S'}{\partial y}\,dt$$

$$- \overline{SS} = 0 \qquad \text{(C-81)}$$

As can be seen, the extra terms originated by the time integration are many and complex. Empirical and or theoretical relations are needed in order to evaluate these terms and be able to apply the time-averaged model.